Ocean colour satellite remote sensing of phytoplankton standing stock, surface hydrography processes as well as spatial and temporal variability of primary production in the western Black Sea

Dissertation
zur Erlangung des Doktorgrades
der Mathematischen-Naturwissenschaftlichen Fakultät
der Christian-Albrechts-Universität zu Kiel

vorgelegt on
Alexander Davidov

Kiel, Mai 2007

Referentin: Prof. Dr. Karin Lochte

Korreferent: Prof. Dr. Andreas Oschlies

Tag der mündlichen Prüfung: 10. Juli 2007

Zum Druck genehmigt: Kiel, den 18. Juli 2007

Prof. Dr. J. Grotemeyer

Der Dekan

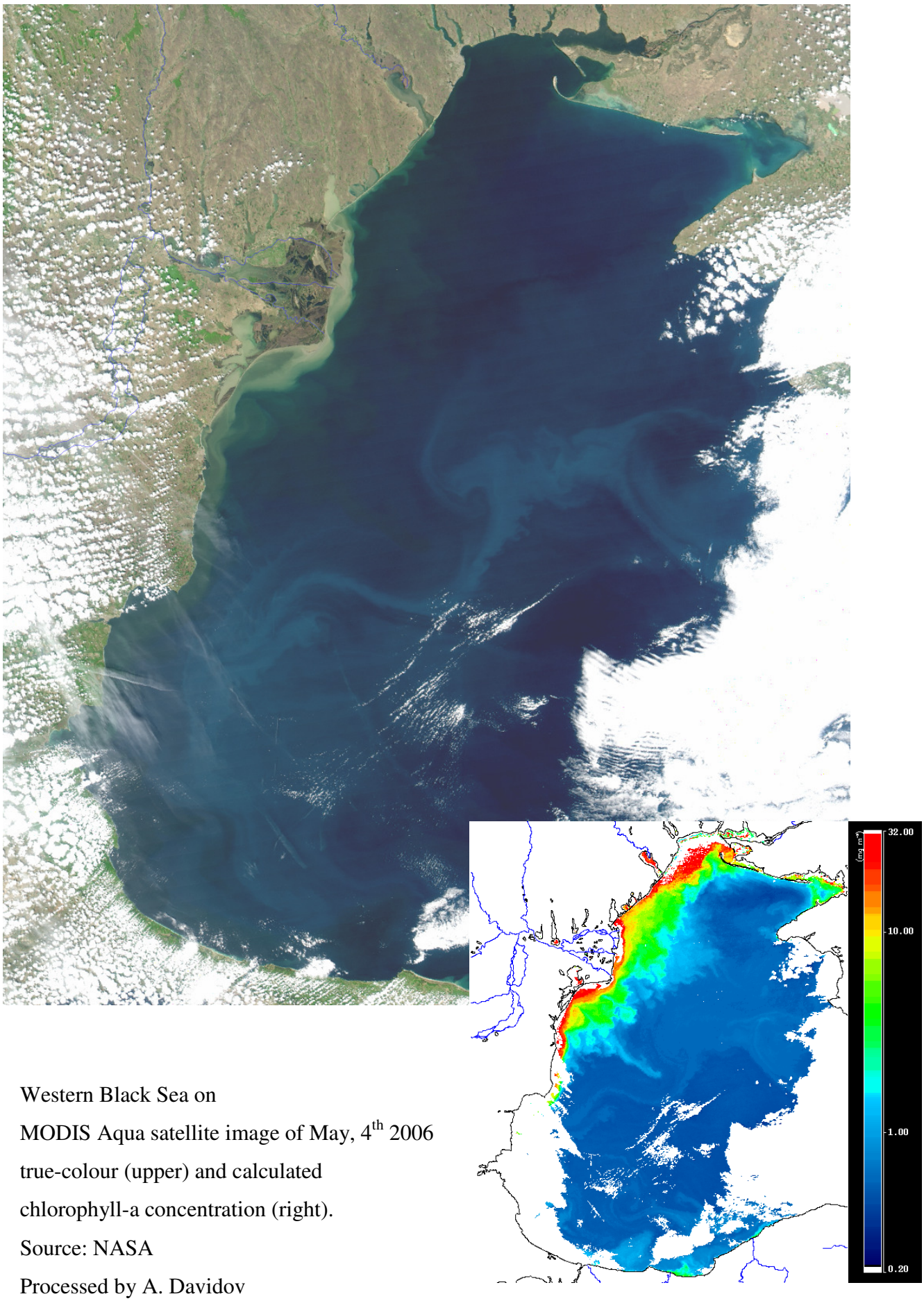

Western Black Sea on
MODIS Aqua satellite image of May, 4th 2006
true-colour (upper) and calculated
chlorophyll-a concentration (right).
Source: NASA
Processed by A. Davidov

TABLE OF CONTENTS

Abstract

The following cumulative study investigates the phytoplankton standing stock, its advection and variability by means of satellite remote sensing of ocean colour in the western Black Sea between 1997 and 2006.

One of the main aims of this study is to estimate the quality of the ocean colour data from the different seasons and different regions of the western Black Sea area. Furthermore, the performance of the atmospheric correction algorithms as well as the bio-optical algorithms for the retrieval of chlorophyll-a in the western Black Sea area are assessed. The spatial and temporal variability of the chlorophyll-a concentration in the surface layer of the western Black Sea and an estimation of the controlling mechanisms are described.

The potential of the use of optical remote sensing data for studying geophysical interactions in near-coastal areas of the Black Sea is demonstrated in Chapter I. The results in Chapter II show that in spite of some limitations, the existing atmospheric correction and bio-optical algorithms can determine and monitor the phytoplankton standing stock in the surface layer of the western Black Sea quite well.

The description of the spatial distribution of chlorophyll-a concentration and its temporal variability in the western Black Sea by ocean colour remote sensing in Chapter III suggests a separation of the sea into four regions with characteristic patterns. The analysis of the spatial pattern of satellite-derived chlorophyll-a shows that a considerable part of the western Black Sea is covered by eutrophied waters throughout the year.

The results show that there are differences in the variability of the satellite-derived chlorophyll-a concentration in the different regions, which at relatively constant seasonal forcing possibly reflect the different mechanisms of nutrient supply. Furthermore, the results demonstrate on the one hand the potential of the statistical analysis of time series in the western Black Sea and on the other hand the complexity of the investigated processes. Also the net primary production calculated with the Behrenfeld-Falkowski vertically generalized production model from the satellite remote sensing data appears to resolve the spatial and temporal variability in the western Black Sea well despite neglecting the nutrient limitation by this approach. However, it remains unclear whether the observed general reduction in the satellite-derived chlorophyll-a concentration for the period 1997-2006 is part of a long-term trend rather than a minimum and thus a turning point of oscillation.

The results in Chapter IV show that the model simulated chlorophyll-a patterns present good agreement compared to the satellite-derived chlorophyll-a images. The most noticeable differences are observed in the open sea area, consisting of an overestimation during spring

and an underestimation during autumn periods. However, good agreement exists between the model and the observations in the coastal areas that are the focus of this study.

Zusammenfassung

In der folgenden kumulativen Studie wird mittels Satellitenfernerkundung der Ozeanfarben Phytoplanktonbestand und Variabilität im westlichen Schwarzen Meer zwischen 1997 und 2006 untersucht.

Eines der Hauptziele der vorliegenden Arbeit ist die Bewertung der Qualität der Fernerkundungsdaten in den verschiedenen Jahreszeiten und Regionen des westlichen Schwarzen Meeres. Des Weiteren wird eine Schätzung der Algorithmen für die Korrektur der atmosphärischen Einflüsse sowie der bio-optischen Algorithmen zur Berechnung der Chlorophyll-a Konzentration abgegeben.

Ein weiteres Ziel ist die Beschreibung der räumlichen und zeitlichen Variabilität der Chlorophyll-a Konzentration im Oberflächenwasser des westlichen Schwarzen Meeres und die Erkennung der kontrollierenden Mechanismen.

Das Potenzial der Nutzung von Fernerkundungsdaten zur Untersuchung der geophysikalischen Wechselwirkungen in den küstennahen Gebieten des Schwarzen Meeres wird in Kapitel I demonstriert.

Die Ergebnisse in Kapitel II zeigen, dass mit den bereits existierenden bio-optischen Algorithmen sowie jenen zur atmosphärischen Korrektur trotz einiger Einschränkungen der Phytoplanktonbestand im Oberflächenwasser des westlichen Schwarzen Meeres genau bestimmt und überwacht werden kann.

Die Beschreibung der räumlichen Verteilung der Chlorophyll-a Konzentration und deren zeitliche Variabilität im westlichen Schwarzen Meer durch Satelliten Fernerkundung in Kapitel III legen eine Aufteilung des Gebietes in vier Regionen mit charakteristischen Eigenschaften nahe.

Die Analyse der räumlichen Verteilung der durch Satellitendaten ermittelten Chlorophyll-a Konzentration lässt erkennen, dass ein bedeutender Teil des westlichen Schwarzen Meeres das gesamte Jahr hindurch eutrophiert ist.

Die Ergebnisse zeigen, dass es Unterschiede in der Variabilität der durch Satellitendaten ermittelten Chlorophyll-a Konzentration in den verschiedenen Regionen gibt, die bei vergleichbaren klimatischen Bedingungen wahrscheinlich die verschiedenen Mechanismen der Nährstoffzufuhr aufzeigen.

Außerdem zeigen die Ergebnisse einerseits das Potenzial der statistischen Analyse von Zeitserien im westlichen Schwarzen Meer und andererseits die Komplexität der untersuchten Prozesse.

Die mit Hilfe des Behrenfeld-Falkowski Modells und anhand der Satellitendaten errechnete Primärproduktion bietet trotz fehlender Nährstoffkomponente eine gute Darstellung der räumlichen und zeitlichen Variabilität im westlichen Schwarzen Meer.

Dennoch bleibt offen, ob der beobachtete generelle Rückgang der durch Satellitendaten ermittelten Chlorophyll-a Konzentration innerhalb des Zeitraums 1997- 2006 einen lang anhaltenden Trend oder eher den Tief- bzw. Umkehrpunkt einer Oszillation darstellt.

Die Ergebnisse des Kapitels IV zeigen, dass die durch Modelle simulierte Chlorophyll-a Konzentration gut mit der durch Satellitendaten ermittelten Chlorophyll-a Konzentration übereinstimmt. Wesentliche Unterschiede wurden im Bereich des offenen Meeres beobachtet und resultieren aus einer Überschätzung im Frühjahr und einer Unterschätzung im Sommer.

Die Übereinstimmung zwischen den Modell- und Satellitendaten in den küstennahen Gebieten, die das Untersuchungsgebiet der vorliegenden Arbeit darstellen, ist dagegen hoch.

1. Introduction

During the 1980s and early 1990s, the Black Sea ecosystem was in a catastrophic condition (Mee 1992, Zeitzev and Mamaev 1997, Sorokin 2002, Lancelot et a. 2002). The deterioration of this ecosystem was mainly the result of eutrophication as well as of the invasion by the comb jelly "alien" species *Mnemiopsis leydyi.* The process of deterioration was also exacerbated by pollution (Cociasu et al. 1997), overfishing (Gücu 2002) and climate changes (Oguz 1995). Remarkably, since the mid-1990s, the impact of eutrophication has declined and first signs of recovery of the ecosystem were detected (Lancelot et al. 2002, Kideys 2002) suggesting that the state of the Black Sea is improving.

1.1. The Black Sea

The Black Sea, with a surface area of 423 000 km^2, is approximately one-fifth of the surface area of the Mediterranean Sea. It has a total volume of 547 000 km^3 and a maximum depth of around 2200 m (Figure 1.). The shelf of the Black Sea is generally narrow with the exception of the north-western part, which accounts for about 65% of the shelf and 23 % of the total Black Sea area. Three major European rivers: Danube (200 km^3 y^{-1}; about 60 % of the total river discharge into the Black Sea), Dnieper (43 km^3 y^{-1}) and Dniester (9.1 km^3 y^{-1}) enter its north-western part (Jaoshvili 2002). The catchment area of the Black Sea is about 1 800 000 km^2 (or about 4 times as large as its own area) (Figure 2.). The only connection of the Black Sea with the eastern Mediterranean Sea is the strait of Bosporus, which links the Black Sea with the Marmara Sea and further through the strait of the Dardanelles with the Aegean Sea

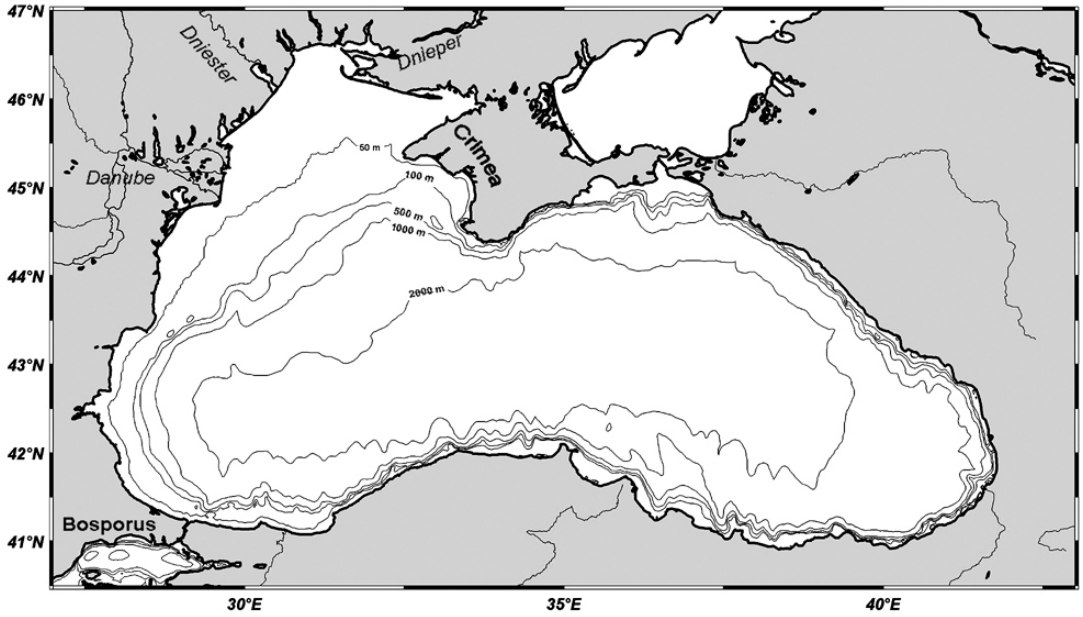

Figure 1. Black Sea bathymetry.

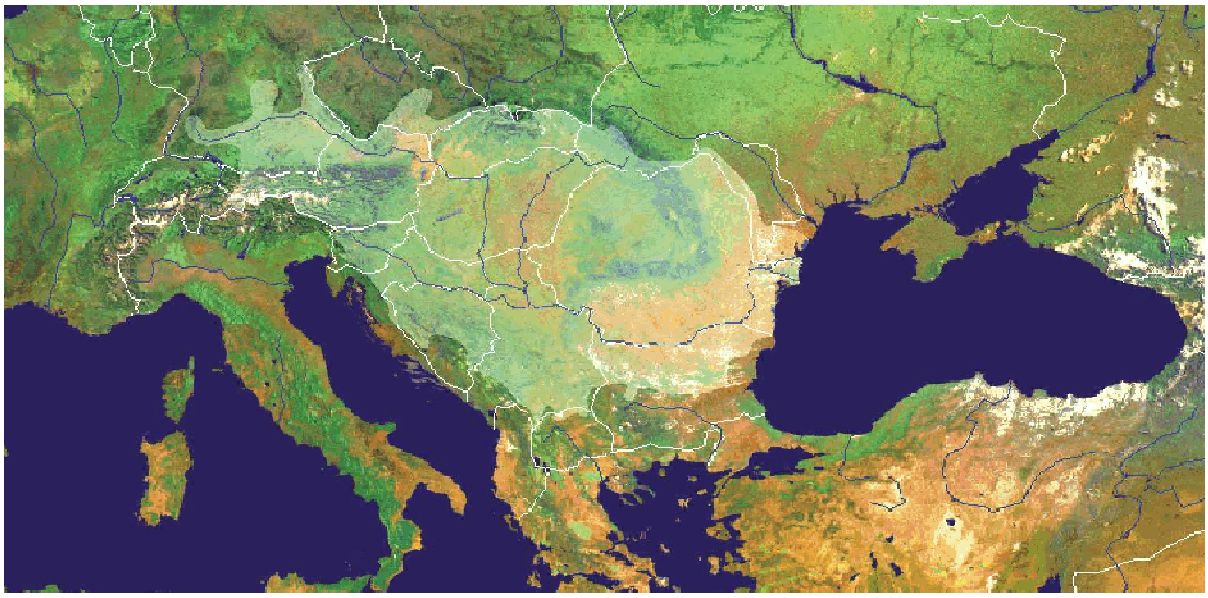

Figure 2. Map of the Black Sea and the Danube river catchment area.

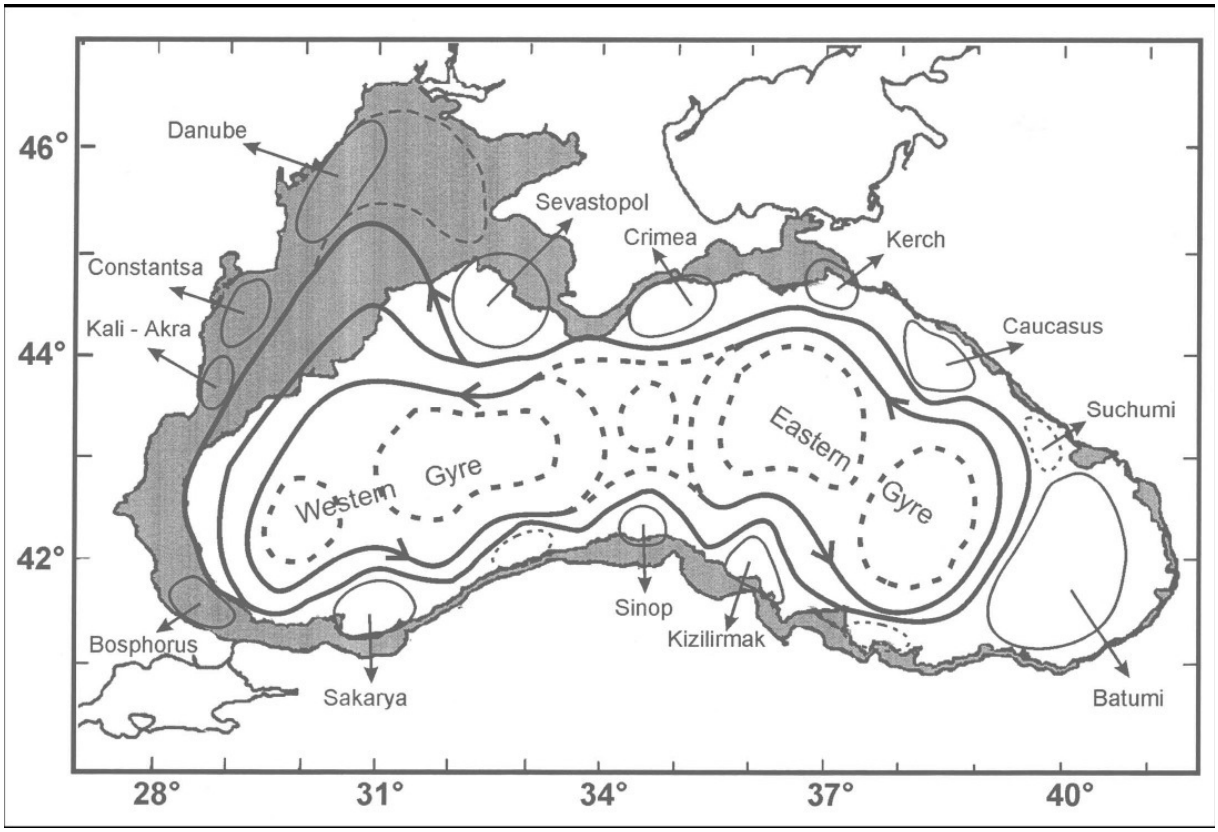

Figure 3. Schematic diagram showing major quasi-permanent/recurrent features of the upper layer circulation identified by synthesis of hydrographic studies and analysis of the Topex-Poseidon and ERS-I,II altimeter data. The cyclonic Western Gyre (Rim current) and the anticyclonic eddies (in front of Sevastopol, Danube delta, Constanta, Kali-Akra etc.) (after Oguz et al. 2004).

Considering the topography and its surface current system the Black Sea can be divided into an eastern and a western part. The circulation in the western Black Sea is dominated by the Rim Current, which is a cyclonic system with baroclinic and frontal instabilities, generating considerable short-term variability as well as seasonally varying mesoscale hydrographic structures (Oguz & Besiktepe 1999) (Figure 3.). The basic mechanism, which controls the flow structure in the surface layer of the north-western shelf, is the spreading of the Danube outflow. Wind stress and the Rim Current structure along the offshore side of the shelf are additional modifiers of this system. An anticyclonic circulation system with small-scale structures is observed over the north-western shelf (Oguz et al., 1995). The water exchange between shallow regions and the central deep part of the western Black Sea is complex mainly due to the instabilities of the frontal zone of the meandering Rim Current (Oguz at al. 1993).

The positive water balance of the Black Sea (i.e. the fresh water input exceeds evaporation) as well as the limited seawater exchange through the comparatively narrow and shallow (33 m sill depth) Bosporus, leads to strong vertical stratification (halocline). The seasonal mixing of the water column during winter is limited to this halocline density barrier. The Black Sea is considered to be the largest anoxic water body on Earth and the intermediate and deep water masses below a permanent halocline at depths of 100–150 m possess almost vertically uniform characteristics defined by absence of oxygen, a temperature of 9 °C and a salinity of 22 psu (Murray et al. 1991). With exception of some type of prokaryotes (sulphate reducing bacteria, methane oxidizing bacteria, archaea), no forms of planktonic and benthic animals or plants exist there.

The upper layer is characterized by active planktonic processes, relatively high oxygen concentrations as well as seasonally varying nutrient concentrations supplied laterally from rivers and vertically from sub-surface levels through vertical mixing (Oguz et al. 2004).

1.2. Changes of the Black Sea ecosystem

This Black Sea ecosystem was highly productive up to the 1960s and harboured a rich and diverse plant and animal community (Sorokin 2002). Due to intensification of agriculture and industry, the use of phosphate-containing washing agents and insufficient sewage treatment between the 1960s and until the late 1980s, riverine nitrogen and phosphorus inputs to the north-western Black Sea increased by a factor of 5 and 3, respectively, resulting in increased eutrophication of the ecosystem especially over the shallow shelf of the western Black Sea (Tolmazin 1985, Mee 1992, Cociasu at al. 1997). The effects of eutrophication in the north-western Black Sea shallow waters were severe. The phytoplankton biomass in this region

increased significantly in the 1970s and 1980s (Zaitzev and Mamaev 1997). The normal phytoplankton species succession changed from the dominance of diatoms towards mixotrophic dinoflagellates and cyanobacteria (Sorokin 2002). The peak of phytoplankton blooms moved from spring and autumn to a summer maximum when the vertical water stratification is more pronounced and oxygen supply to the bottom layers is reduced. The biomass in the blooms increased by a factor of 20-30 (Sorokin 2002, Bodeanu 1992). As a consequence, hypoxia developed in the north-western Black Sea shallow waters, which has been referred to as "the ecological catastrophe of the Black Sea" (Mee 1992) and "the ultimate example of deterioration of the marine environment in Europe" (Lancelot et al. 2002). In the 1980s hypoxia drastically reduced most of the benthic life, including epibenthic filter-feeders like *Mytilus galloprovincialis*, which before the 1970s occupied the north-western shelf in dense populations to a depth of 40 meter (Sorokin 2002).

An increase in the chlorophyll-a concentration became also obvious in the offshore regions of the Black Sea at the end of the 1970s (Mikaelyan 1997). Vladimirov *et al.* (1997) report that the water transparency (Secchi disc depth) in the central part of the Black Sea decreased by a factor of three (from 20 to 6.2 m) between the 1970s and 1992. The outburst of the population of introduced comb jelly *Mnemiopsis leydyi* caused a significant reduction in the biomass of the mesozooplankton community as well as fish eggs and larvae during the late 1980s (Shushkina *et al.* 1998). This effect, together with overfishing, ultimately caused a collapse of commercial fish stocks (anchovy, sprat and horse-mackerel) during the early 1990s (Rass, 1992).

Since the early 1990s riverine phosphate input and consequently eutrophication in the western Black Sea have decreased considerably (Cociasu *et al.* 1997, Horstmann *et al.* 2003). The phosphorus discharge by the Danube river between 1992 and 2002 shows a decline of a factor >2. Due to buffering function of the soil/ ground waters there is a delay in the transfer of agricultural nitrogen (years to decades from the fields to river systems) (Behrendt *et al.* 2003) which suggests an additional decrease of the nitrogen-loads of the Danube river in future years. The decrease of the nutrient river loads during the 1990s was due to improved sewage treatment in the Danubian countries and to the economic collapse of the Eastern European countries in the Danube catchment area reducing the industrial activities and the use of fertilizer in agriculture.

Regime shifts as temperature cycles related to the North Atlantic Oscillation (Bilio and Niermann 2004) in the 1990s apparently have resulted in an increase of winter temperatures of the Black Sea by 2 °C (Oguz *et al.* 2005). Consequently reduction of

convection and vertical nutrient transport has decreased phytoplankton primary productivity and may have contributed to the decrease of eutrophication in the Black Sea.

First signs of the coastal ecosystem recovery where obtained in 1995 (Lancelot et al. 2002), when river-borne nutrient discharges decreased and when the near bottom oxygen saturation improved. In the mid 1990s, the water transparency increased again to 14 m in the central western Black Sea (Vladimirov *et al.* 1997). However, different from the shallow water benthic ecosystem, the pelagic food web of the Black Sea shows retardation in recovery (Daskalov 2002). To date, the medusa *Aurelia aurita,* as well as the newly introduced Ctenophore *Mnemiopsis leydyi*, dominate the macrozooplankton community (Niermann pers. comm.). These gelatinous species still outcompete small pelagic fish (Anchovy) in predation of mesozooplankton' (Bilio and Niermann 2004, Gücu 2002), which apparently does not allow the carnivorous fish stocks to recover.

Despite of the implementation of international ocean research programs in recent years [NATO Science for Peace Program, EROS 2000/21, Nutrient Management in the Danube Basin and its Impact on the Black Sea (DANUBS)], *in situ* investigations and monitoring activities in the western Black Sea were reduced considerably in the 1990s, due to the economical collapse in the Black Sea countries (except Turkey). Especially in the central part of the Black Sea, data of *in situ* measurements from the last 17 years are very limited.

1.3. Basic principles of the passive remote sensing of ocean colour

A passive system for remote sensing of ocean colour makes use of a sensor with a narrow field of view, capable of monitoring the radiometric flux reaching the sensor at several selected wavelengths (spectral bands – 8 in SeaWiFS and 36 in MODIS) in the visible and near-infrared domains of the electromagnetic spectrum. The sensor, mounted on a satellite is targeted at a point on the surface of the earth. The sensors operate during daylight hours, and the ultimate source of light reaching the sensor is the sun. However, the photons from the sun can follow different pathways before they reach the remote detector. Photons can be scattered by the atmosphere, sunlight reflected at the sea surface and light is upwelled from the sea surface after back-scattering in water. The light upwelling from the sea surface is attenuated on its journey from the sea surface to the sensor, due to absorption and scattering by the intervening atmosphere.

It is only the upwelling light from the sea surface that carries any useful information on the water body. The atmospheric contributions (more than 80% of the light reaching the sensor) and the reflection at the sea surface constitute noise in this context, and have to be corrected for (Morel, 1980). Small errors in estimating the atmospheric contribution can cause

considerable biases in the estimation of the water component. Furthermore, the upwelling component from the water has to be processed to evaluate what the water-leaving component would have been, if there were no atmosphere in-between the sensor and the water body. Techniques for atmospheric correction (atmospheric correction algorithms) therefore form a very important component of remote sensing of ocean colour (Gordon and Morel, 1983; Gordon and Wang, 1994).

The water-leaving signal is influenced by several factors (Fig. 4). Direct sun light and scattered sky light that penetrates the sea surface may be absorbed or scattered by the water molecules, or by the various suspended and dissolved materials present in the water. Remote sensing involves analyses of the variations in magnitude and spectral quality of the water-leaving radiation to derive quantitative information on the type of substances present in the water and their concentrations.

In addition to pure water there are three main optical active components: phytoplankton, suspended material (inorganic) and yellow substances (coloured, dissolved organic matter, "gelbstoff").

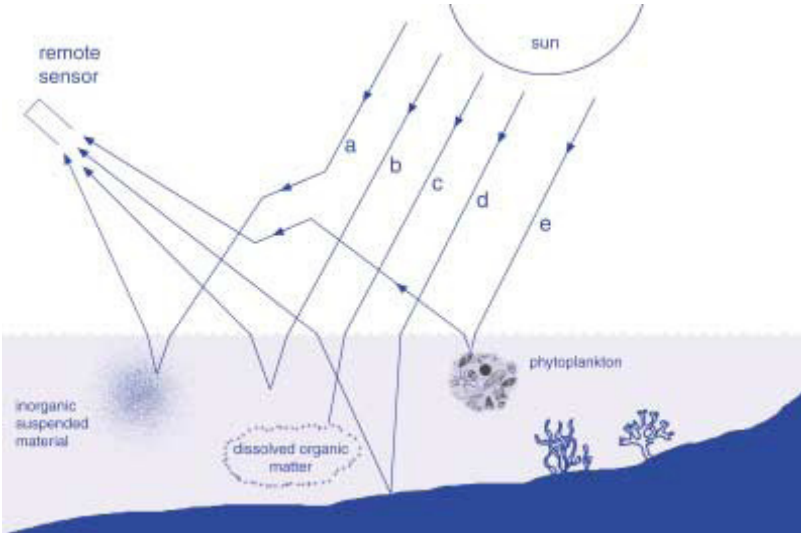

Figure 4. Factors that influence upwelling light leaving the sea surface. (a) upward scattering by inorganic suspended material; (b) upward scattering from water molecules; (c) absorption by the yellow-substances component; (d) reflection of the bottom; and (e) upward scattering from the phytoplankton component. Light leaving the water may be scattered away from, or towards the remote sensor by the atmosphere (after IOCCG, 2000).

A classification scheme, according to which oceanic waters are partitioned into Case 1 or Case 2 waters, was introduced by Morel and Prieur (1977) and later improved by Gordon and Morel (1983). By definition, Case 1 waters are those waters in which phytoplankton (with their accompanying and covarying retinue of material of biological origin) are the principal

agents responsible for variations in optical properties of the water. In Case 2 waters, other particulate matter or yellow substances (or both these types of substances) may make a significant contribution to the optical properties. Furthermore, these contributions are not linked to the concentration of phytoplankton but have to be treated as independent variables instead.

The colour of water is determined by scattering and absorption of visible light by pure water itself, as well as by the inorganic and organic, particulate and dissolved material present in the water. Phytoplankton are composed of pigments, the most dominant being chlorophyll-a. Factors which can affect the shape of the absorption spectra due to phytoplankton are: pigment composition and concentration, shape and size of cells, light adaptation and the physiological state of cells. However, the basic shape of the absorption spectra of any algal group is a reflection of its pigment composition (Fig 5). Pigments *in vivo* are in complex with proteins, which cause a shift in the absorption maxima.

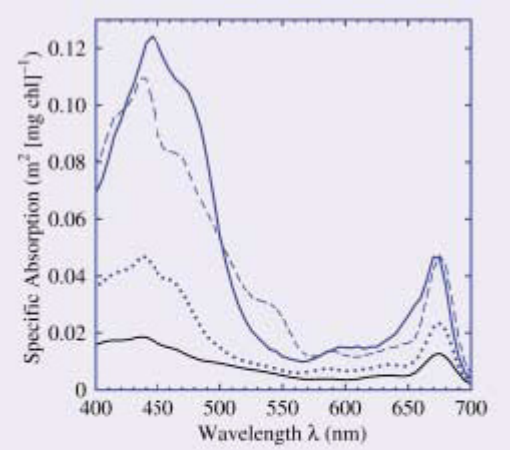

Species	Location	Z (m)	Chl (mg m^{-3})
Prochlorophytes	Off Chile	105	0.2
Cyanobacteria	Arabian Sea	20	1.1
Phaeocystis sp.	Labrador Sea	10	3.4
Diatoms	Labrador Sea	20	10.0

Figure5. Some examples of specific absorption spectra of natural phytoplankton populations from various marine environments. The dominant phytoplankton group or species (identified on the basis of HPLC analysis and microscopic examination) in each sample is indicated. The ambient chlorophyll-a concentration at the time of sampling is also shown. Unpublished data from the Biological Oceanography Group at the Bedford Institute of Oceanography, Canada (in IOCCG, 2000).

The intrinsic colour of the ocean in the context of remote sensing is defined by spectral variations in remote-sensing reflectance (R_{rs}) at the sea surface (z=0). R_{rs} is defined as:

$$R_{rs}(\theta,\phi,\lambda,0) = \frac{L(\theta,\phi,\lambda,0)}{E_d(\lambda,0)} \qquad (1)$$

where $L(\theta, \varphi, \lambda, 0)$ is the upwelling radiance and $Ed(\lambda, 0)$ is the irradiance in all downward directions, or the downwelling irradiance, at the same wavelength. All optical properties of ocean waters are wavelength dependent. Remote-sensing reflectance R_{rs} e has dimensions of [steradian^{-1} – unit for solid 3D angle]. The arguments θ and φ on the radiance indicate that the water-leaving radiance can vary with the viewing angle at the surface. Water-air interface effects (transmittance, internal reflection and refraction) have to be suitably accounted for, before R_{rs} below the surface of the water can be compared with the remotely-sensed signal. The aim of remote-sensing of ocean colour is to derive quantitative information on the types of substances present in the water and on their concentrations, from variations in the spectral form and magnitude of the ocean-colour signal.

The empirical bio-optical algorithms are based on direct regression of the ratio of R_{rs} at two or more wavelengths to chlorophyll-a concentration (Chl_{sat}). The accuracy, precision, and utility of an empirical ocean colour algorithm for estimating chlorophyll-a distribution depends on the characteristics of the algorithm and the *in situ* observation used to develop it. The data set of more than 2800 *in situ* (chlorophyll as well as radiometric) observations, representing a large diversity of bio-optical provinces was used for calibration and validation of the OC4v4 algorithm (O'Reilly et al. 2000). The *in situ* chlorophyll-a concentration ranges from 0.008 to 90.0 mg m^{-3} and was determined from HPLC and fluorometric measurements.

The fourth order polynomial equation for OC4v4 is:

$$Chl_{sat} = 10.0^{(0.366 - 3.067R_{rs} + 1.930R_{rs}^2 + 0.649R_{rs}^3 - 1.532R_{rs}^4)} \qquad (2)$$

where $R_{rs} = \log_{10}(R_{555}^{443} > R_{555}^{490} > R_{555}^{510})$, where the argument of the logarithm is a shorthand representation for the maximum value of the three ratios.

Calibration and validation of the remote sensing data with *in situ* radiometric measurements and chlrophyll measurements follow the procedures and protocols as described in Ocean Optics Protocols for Satellite Ocean Color Sensor Validation (Mueller *et al.* 2003: Rev. 4).

1.4. Satellite ocean colour remote sensing in the western Black Sea

The evaluation of available satellite remote sensing data of ocean colour in combination with the limited ground-truth data and modelling may help to alleviate the limitation posed by lack of in situ data. It can be used to improve considerably the understanding of the basic physical and biogeochemical processes as well as the eutrophication in the western Black Sea.

The ocean colour satellite sensor Coastal Zone Colour Sensor (CZCS: Hovis et al. 1980) provided first synoptic datasets of the phytoplankton distribution in the western Black Sea between 1978 and 1986. Nezlin et al. (1999) found that the annual succession of total

phytoplankton pigments in the central Black Sea as derived from CZCS for the period between 1978 and 1986 agrees well with the *in situ* measurements for this period. The observation of the near-coastal features from the CZCS time series provides information on frontal dynamics and potential correlations with nutrient enrichment or pollution (Barale & Murray 1995). Kopelevich et al. (2002) proposed an algorithm for the determination for the "true" values of chlorophyll-*a* concentration derived from CZSC based on retrospective joint analysis of satellite and *in situ* data of the Black Sea.

The Modular Optoelectronic Scanner (MOS: Zimmermann & Neumann 1997) (1995 - 2004) provided information on the water constituents (chlorophyll-a, yellow substances, sediments) of the western Black Sea. An algorithm for calculation of chlorophyll-*a* concentration from MOS in the western Black Sea based on *in situ* measurements was proposed by Barale et al. (2002). This algorithm was based on the analysis of satellite data and coincident *in situ* data, measured during the EROS 2000/21 projects (Lancelot et al. 2002). However due to the small swath width and large time intervals between two overflights of the satellite it was not possible to analyse the successional processes in the surface waters from MOS.

In 1997 Sea Wide-Field-of-view Sensor (SeaWiFS: McClain et al. 2004), in 2000 (Terra) and in 2002 (Aqua) Moderate Resolution Imaging Spectroradiometer (MODIS: Esaias *et al.* 1998) ocean colour satellite sensors were taken into operation and provide synoptical data from the Black Sea area on a daily basis. All three sensors have a spatial resolution of about 1.1 km at nadir and each records images from the Black Sea once or twice per day. The full-resolution, ocean colour and sea surface temperature (MODIS) data are distributed to the scientific community through the Ocean Colour Web of Goddard Space Flight Center at NASA (Feldman and McClain 2006).

By means of satellite remote sensing of the ocean colour is not possible to measure directly the changes of the nutrient concentration, oxygen depletion or food-web changes. However, from the frequent observation of the changes in the chlorophyll-a concentration, which is an indicator for the biomass and primary productivity in the surface layer, we have a reliable information on the eutrophication and the deterioration of the Black Sea ecosystem. For instance, the extensive blooms of phytoplankton detected by the satellite remote sensing over the shallow shelf at the time of stable vertical water stratification and low wind stress (stagnation) lead after sinking and decomposition of the biomass to oxygen depletion in the bottom layer and possible mass mortality of the benthos organisms.

The temporal and spatial pattern of satellite-derived chlorophyll-a give an information of the nutrient supply and primary productivity as well as on the advection of the nutrient-rich river

water in the western Black Sea. The satellite remote sensing data of ocean colour are easy to access and useful tool for synchronous and frequent monitoring of the western Black Sea area.

1.5. Aims of the study and the contribution of the single chapters

The aims of the study are:

To estimate the availability and the quality of the ocean colour data from the different seasons and different regions of the western Black Sea area.

To assess the performance of the atmospheric correction algorithms as well as the bio-optical algorithms for the retrieval of chlorophyll-a in the western Black Sea area and furthermore to detect the limitation of this approach.

To describe the spatial and temporal variability of the chlorophyll-a concentration in the surface layer of the western Black Sea and to make an estimation of the factors which control this variability.

To examine the potential of the satellite ocean colour data for validation of the biogeochemical models in the western Black Sea.

To make an assessment of the current state of the western Black Sea ecosystem and to examine how satellite remote sensing of ocean colour can contribute to the understanding of the processes of eutrophication and primary productivity there.

The contribution of the four Chapters (paper/manuscripts) to achieve these aims is described below.

In *Chapter I* the satellite-based optical observations of surface waters have been used to assess the main environmental interactions in the north-western Black Sea. The analysis of historical CZCS (1978-1986) and more recent MOS (May 1996 – April 1998) ocean colour data were used for evaluations of the presence and abundance of water constituents (primarily phytoplankton pigments) and for providing essential information on the processes which take place in the area and on their spatial and temporal scales. The suitability of the MOS sensor concerning its coverage, spatial resolution and spectral characteristics for regional studies of coastal zone processes is discussed. Furthermore, the methods used for data processing are described in some detail, starting from the novel atmospheric corrections processing scheme developed especially for MOS and continuing with the creation of local bio-optical algorithms derived from the combined analysis of *in situ* measurements and MOS water-leaving radiances. The results obtained applying these algorithms to a multi-seasonal series of MOS images are discussed in light of the main oceanographic features of the Black Sea.

In *Chapter II* the performance of the operational SeaWiFS atmospheric correction algorithm and bio-optical algorithms in the western Black Sea area was evaluated by comparing satellite data with concurrent *in situ* radiometric measurements and four different data sets of *in situ* chlorophyll-a. For these purposes *in situ* measured exact normalized water-leaving radiance was compared to satellite retrieved exact normalized water-leaving radiance. Furthermore, *in situ* measured mean optically weighted chlorophyll *a* concentration in the remotely sensed depth was compared to the results of three empirical, one semi-empirical and two regional bio-optical algorithms. In addition, the satellite derived vertical attenuation coefficient was compared to 42 measurements of the Secchi disc depth. The share of possible sources of inaccuracy such as: in-situ chlorophyll-a concentration with and without consideration of the subsurface concentrations; full-resolution satellite images vs. global area coverage data were estimated and discussed.

The results show that among the five different atmospheric correction algorithms tested, the multi-scattering mode with fixed aerosol model type 'coastal with 70% humidity' showed the best coincidence of *in situ* and satellite derived data. Furthermore, it was found that the OC4v4 bio-optical algorithm produced best results with a mean systematic error of 30% and a random error of 77% in the high-chlorophyll, partly turbid and coloured dissolved organic matter rich waters of the western Black Sea. It is demonstrated that with present SeaWiFS operational algorithms it is possible to monitor phytoplankton standing stock and its temporal succession in the western Black Sea with an acceptable accuracy using ocean colour remote sensing data.

In *Chapter III* nine years (1997 –2006) of SeaWiFS and MODIS ocean colour data are used to study the near-surface chlorophyll-variability on seasonal and interannual timescales in the western Black Sea. In this study the spatial pattern as well as the annual and the interannual variability of the surface chlorophyll-a between 1997 and 2006 in the western Black Sea are described and its relation to the physical factors like sea surface temperature, light availability, surface winds and Danube river water discharge as well as the North Atlantic Oscillation index are examined. Furthermore, the primary productivity of the western Black Sea as derived from satellite data and models, its magnitude and variability is described. Time-series of satellite-derived chlorophyll-a, wind stress, sea surface temperature, photosynthetic available radiation, North-Atlantic Oscillation index and net primary production in the four regions of the western Black Sea are analysed by means of two basic statistical approaches (multiple linear correlation and empirical orthogonal function).

The results suggest a classification of the western Black Sea into four different regions according to the amount and the variability of the surface chlorophyll *a*: (1) waters directly influenced by the Danube river, (2) the north-western shelf, (3) the western and south-western shelf area and (4) the central part of the western Black Sea. Furthermore it is shown that between 26% and 65% of the entire western Black Sea area - depending on the season and river water discharge - can be considered as chlorophyll-rich waters (>1 mg m^{-3}). The results demonstrate also a high temporal and spatial variability of satellite derived chlorophyll-a in all parts of the western Black Sea. Comparisons of the temporal pattern of chlorophyll-a to those of wind stress, sea surface temperature, photosynthetic available radiation and North-Atlantic Oscillation index anomalies display distinct seasonal signal but also a significant amount of independent variability. Furthermore, the results suggest that the interannual variability of chlorophyll-a is not related to a single factor, but to a bundle of factors with varying impact in the different regions of the western Black Sea.

In *Chapter IV* the main physical and biological processes that control the seasonal cycle of the plankton dynamics over the Western Black Sea are investigated by means of a three-dimensional, low trophic level, coupled biophysical model. The model ability to reproduce the observed seasonal primary production variation over the western Black Sea was improved and assessed by using a series of 8-day SeaWiFS satellite-derived chlorophyll-a data. Over the entire year 2003 period, the model parameterizations and the calibration of the biological parameters was improved by the satellite data.

The results show that despite the model's simplicity, the simulated chlorophyll-a patterns are in a good agreement to the SeaWiFS derived chlorophyll-a. However, the limiting nutrients showed significant deviations from the observed concentrations, which suggests that certain processes need to be improved in the biological model, such as remineralization and grazing pressure.

References

1. Barale, V. & Murray, C. N. 1995 The surface color field of enclosed marine basins: pigment patterns of the Black Sea. *Remote Sensing Reviews* 12, 61–82.
2. Barale, V., P. Cipollini, A. Davidov and F. Melin. Water Constituents in the North-western Black Sea from Optical Remote Sensing and *In situ* Data. *Estuarine, Coastal and Shelf Science* (2002) 54, 309–320.
3. Behrendt, H., Constantinescu, L.T., Cvitanic, I., Drumea, D., Jabucar, D., Juran, S., Pataki, B., Schreiber, H., Snishko, S. and Zessner, M., 2003. Nutrient inputs and loads in the Danube river system - Results of a river system oriented model analysis. *Österr. Wasser-und Abfallwirtschaft*, Heft 9-10, 55.
4. Bilio M. and U. Niermann, 2004. Is the comb jelly really to blame for it all? *Mnemiopsis leidyi* and the ecological concerns about the Caspian Sea. *Mar Ecol Prog Ser*., 269, 173–183.
5. Bodeanu N., 1992. Algal blooms and development of the main phytoplanktonic species in the Romanian Black Sea littoral. *Sci. Total Environ.* (suppl.), Elsevier. Amsterdam 891-906.
6. Cociasu, A., Diaconu, V., Popa, L., Buga, L., Nae, I., Dorogan, L. and Malciu V., 1997. The nutrient stock of the Romanian shelf of the Black Sea during the last three decades. In: Sensitivity to Change: Black Sea, Baltic Sea and North Sea, E. Özsoy and A. Mikaelyan (eds.), pp. 49-63.
7. Daslalov G.M., 2002. Long-term changes in fish abundance and environmental indices in the Black Sea. *Mar. Ecol. Prog. Ser.*, 255, 259-270.
8. Esaias, W.E., Abbott, M.R., Barton, I., Brown, O.B., Campbell, J.W., Carder, K.L., Clark, D.K., Evans, R.H., Hoge, F.E., Gordon, H.R., Balch, W.M., Letelier, R., and Minnett, P.J. (1998), An overview of MODIS capabilities for ocean science observations. *IEEE Transactions on Geoscience and Remote Sensing*, 36, 1250-1265.
9. Feldman, G. C., C. R. McClain, Ocean Color Web, SeaWiFS and MODIS Aqua data, NASA Goddard Space Flight Center. Eds. Kuring, N., Bailey, S. W., Decenber 2006. http://oceancolor.gsfc.nasa.gov/
10. Gordon, H. R. and Morel, A., 1983. Remote Assessment of Ocean Color for Interpretation of Satellite Visible Imagery. A Review, Lecture Notes on Coastal and Estuarine Studies, R. T. Barber, N. K. Mooers, M. J. Bowman and B. Zeitzschel (eds.), Springer-Verlag, New York, 114 p.

11. Gordon, H. R. and Wang, M.,1994. Retrieval of water-leaving radiance and aerosol optical thickness over the oceans with SeaWiFS: A preliminary algorithm. Appl. Optics 33: 443-452.

12. Gucu, A.C., 2002. Can Overfishing be Responsible for the Successful Establishment of Mnemiopsis leidyi in the Black Sea? *Estuar. Coast. Shelf Sci*., 54, 3, 439-451.

13. Horstmann, U., Davidov, A., Cociasu, A., Velikova, V., 2003. Der Einfluss verringerter Nährstofffrachten der Donau auf das Schwarze Meer. Österreichische Wasser- und Abfallwirtschaft. 55(11-12):205-211.

14. Hovis, W. A., Clark, D. K., Anderson, F., Austin, R. W., Wilson, W. H., Baker, E. T., Ball, D., Gordon, H. R., Mueller, J. L., El-Sayed, S. Z., Sturm, B., Wrigley, R. C. & Yentsch, C. S. 1980 Nimbus-7 Coastal Zone Color Scanner system description and initial imagery. *Science* 210, 60–63.

15. IOCCG, 2000. Remote Sensing of Ocean Colour in Coastal, and Other Optically-Complex,Waters. Sathyendranath, S. (ed.)*, Reports of the International Ocean-Colour Coordinating Group, No. 3, IOCCG, Dartmouth, Canada.*

16. Jaoshvili, S., 2002. The rivers of the Black Sea. European Environmental Agency. Technical Report No.71.
(http://reports.eea.eu.int/technical_report_2002_71/en/tab_content_RLR)

17. Kideys, A.E., 2002. Enhanced: Fall and Rise of the Black Sea Ecosystem. *Science*, 297(5586): 1482-1484.

18. Kopelevich, O.V., Sheberstov, S.V., Yunev, O., Basturk, O., Finenko, Z.Z., Nikonov, S. and Vedernikov, V.I., 2002. Surface chlorophyll in the Black Sea over 1978-1986 derived from satellite and in situ data. J. Mar. Syst. 36(3-4):145-160

19. Lancelot, C., J.-M. Martin, N. Panin and Y. Zaitsev, 2002. The North -western Black Sea: A Pilot Site to Understand the complex Interaction between Human Activities and the Coastal Environment. *Estuar. Coast. Shelf Sci*., 54, 279-283.

20. McClain, C.R., Feldman, G.C. and Hooker, S.B., 2004. An overview of the SeaWiFS project and strategies for producing a climate research quality global ocean bio-optical time series Deep Sea Res. (II Top. Stud. Oceanogr.) 51(1-3):5-42.

21. Mee, L.B., 1992. The Black Sea in crisis. *Ambio,* 21, 278-286.

22. Mikaelyan A (1997) Long-term variability of phytoplankton communities in open Black Sea in relation to environmental changes. In: Sensitivity to Change: Black sea, Baltic Sea and North Sea. Özsoy & Mikaelyan (eds.), Kluwer Acad. Publ., pp 105-116.

23. Morel, A. and Prieur, L., 1977. Analysis of variations in ocean color. Limnol. Oceanogr. 22: 709-722.

24. Morel, A., 1980. In-water and remote measurement of ocean color. Boundary-Layer Meteorol. 18: 177-201.

25. Mueller, J.L., Fargion G.S. and McClain, C.R. (eds.), 2003, Ocean Optics Protocols for Satellite Sensor Validation, Revision 4, NASA/TM-2003-211621.

26. Murray, J. W., Z. Top, and E. Ozsoy, 1991. Hydrographic properties and ventilation of the Black Sea. Deep-Sea Res., 38, Suppl.2A, S663–690.

27. Nezlin, N.P., Kostianoy, A.G. and Gregoire, M., 1999. Patterns of seasonal and interannual changes of surface chlorophyll concentration in the Black Sea revealed from remote sensed data. Remote Sens. Environ., 69:43-55.

28. O'Reilly, J.E., Maritorena, S., O'Brien, M.C., Siegal, D.A., Toole, D., Menzies, D., Smith, R.C., Mueller, J.L., MitchellL, B.G., Kahru, M., Chavez, F.P., Strutton, P., Cota, G.F., Hooker, S.B., Mcclain, C.R., Carder, K.L., Muller-Karger, F., Harding, L., Magnuson, A., Phinney, D., Moore, G.F., Aiken, J., Arrigo, K.R., LeTelier, R. and Culver, M., 2000. Ocean Color Chlorophyll-a algorithms for SeaWiFS, OC2 and OC4: Verison 4. In: SeaWiFS postlaunch calibration and validation analyses, part 3. SeaWiFS postlaunch technical report series. S.B. Hooker and E.R. Firestone (eds). NASA/TM-2000-206892, 11, pp. 9-23.

29. Oguz, T. and Besiktepe, S., 1999, Observation on the Rim Current structure, CIW formation and transport in the western Black Sea. Deep-Sea Research I 46:1733-1753.

30. Oguz, T., Latun, M., Latif, M.A., Vladimirov, V.V., Sur, H.I., Markov, A.A., Ozsoy, E., Kotovshchikov, B.B., Eremeev, V.V. and Unluata, U., 1993. Circulation in the surface and intermediate layers of the Black Sea. Deep-Sea Research, 40(8):1597-1612.

31. Oguz, T., P., Malanotte-Rizzoli, D., Aubrey, 1995. Wind and thermohaline circulation of the Black Sea driven by yearly mean climatological forcing. J. Geophys. Res., 100, 6846–6865.

32. Oguz, T., Turgul, S., Kideys, A., Ediger, V. and Kublay N., 2004. Chapter 33. Physical and biochemical characteristics of the Black Sea. In: *The Sea*, Robinson, A. and Brink, K. (eds.),Harvard, 14:1331-1369.

33. Rass, T.S., 1992. Changes in the fish resources of the Black Sea. Oceanology (Eng. Trans.), 32, 197–153.

34. Shushkina, E.A., M.E. Vinogradov, L.P. Lebedeva, T. Oguz, N.P. Nezlin, V. Yu. Dyakonov, and L.L. Anokhina, 1998. Studies of structural parameters of planktonic

communities of the open part of the Black Sea relevant to ecosystem modeling. In: Ecosystem Modeling as a Management Tool for the Black Sea, vol. 1, NATO Sci. Partnership Sub-ser., 2, vol. 47, L.I. Ivanov, and T. Oguz, eds. Kluwer Acad., Norwell, Mass., pp. 311–326.

35. Sorokin, Y.I., 2002. The Black Sea, Ecology and Oceanography. Backhuys Publishers, Leiden, The Netherlands, 875.
36. Vladimirov, V.L., Mankovsky, V.I., Solov'ev, M.V. and Mishonov, A.V., 1997. Seasonal and long-term variability of the Black Sea optical parameters. In: Sensitivity to Change: Black Sea, Baltic Sea and North Sea, E. Özsoy and A. Mikaelyan (eds.), pp. 33-48.
37. Zaitsev Y.P. and Mamaev V., 1997. Marine biological diversity in the Black Sea. Black Sea Environmental Series, Vo.3, UNDP New York, 207.
38. Zimmermann, G. & Neumann, A. 1997 The space-borne imaging spectrometer MOS for ocean remote sensing. Proceedings of the 1st International Workshop on MOS-IRS and Ocean Colour, Berlin, 28–30 April 1997, ed. by Institute of Space Sensor Technology, DLR, pp. 21–29.

2. Chapters

2.1. List of chapters

This doctoral thesis is based on the following publications/manuscripts:

Chapter I Barale, V., P. Cipollini, A. Davidov and F. Melin. Water Constituents in the North-western Black Sea from Optical Remote Sensing and *In situ* Data. *Estuarine, Coastal and Shelf Science* (2002) 54, 309–320.

Chapter II Davidov A., Assessment of algorithms for atmospheric correction and chlorophyll a retrieval from SeaWiFS satellite data in the western Black Sea area. *Submitted to International Journal of Remote Sensing in April 2006*

Chapter III Davidov A., Temporal and spatial variability of satellite-derived chlorophyll-a and primary production and their relation to physical factors in the western Black Sea. *To be submitted to Marine Ecology Progress Series in June 2007.*

Chapter IV Tsiaras, K. P., V.H. Kourafalou, A. Davidov and J. Staneva, Black Sea plankton dynamics: seasonal variability and comparison to SeaWiFS data. *Submitted to Journal of Geophysical Research in November 2006.*

2.2. Statement on my contribution to the publications/manuscripts

Chapter I. The contribution of the PhD candidate in this study was the collection, the selection and the processing of the MOS satellite data as well as the preparation of the in situ data for regression analysis.

Chapter II. The concept for this manuscript was derived by the PhD candidate. The in situ measurements (unless other referred in text), data processing as well as data analysis were planned and conducted by the PhD candidate. The paper was written entirely by the PhD candidate.

Chapter III. The concept for this manuscript was derived by the PhD candidate. The data processing (unless other referred in text) and analysis were planned and conducted by the PhD candidate. The paper was written entirely by the PhD candidate.

Chapter IV. The contribution of the PhD candidate to this study was the processing of the SeaWiFS ocean colour data and their preparation for the model validation.

Chapter I

Water Constituents in the North-western Black Sea from Optical Remote Sensing and *In situ* Data

V. Barale[a], P. Cipollini[b], A. Davidov[c] and F. Melin[a]

[a]Institute for Environment and Sustainability, Joint Research Centre of the EC, 21020 Ispra (VA), Italy

[b]Southampton Oceanography Centre, Southampton, U.K.

[c]Institut fur Meereskunde an der Universitat Kiel, Kiel, Germany

Printed in: *Estuarine, Coastal and Shelf Science* (2002) **54,** 309–320

Estuarine, Coastal and Shelf Science (2002) **54,** 309–320
doi:10.1006/ecss.2000.0649, available online at http://www.idealibrary.com on IDEAL®

Water Constituents in the North-western Black Sea from Optical Remote Sensing and *In situ* Data

V. Barale[a,d], P. Cipollini[b], A. Davidov[c] and F. Melin[a]

[a]*Institute for Environment and Sustainability, Joint Research Centre of the EC, 21020 Ispra (VA), Italy*
[b]*Southampton Oceanography Centre, Southampton, U.K.*
[c]*Institut fur Meereskunde an der Universitat Kiel, Kiel, Germany*

Received September 1998 and accepted in revised form September 1999

Satellite-based optical observations of surface waters have been used to assess the main environmental interactions in the north-western Black Sea, as a contribution to the EROS 21 project. Such observations allow evaluations of the presence and abundance of water constituents (primarily phytoplankton pigments), providing essential information on the processes which are taking place in the area and on their spatial and temporal scales. An analysis of ocean colour imagery was performed, using historical data collected by the CZCS (1978–1986), and by the MOS before, during and after the EROS 21 oceanographic cruise which took place in April/May 1997. The time series of CZCS-derived parameters (i.e. chlorophyll-like pigment concentration) originates from the archive generated by the OCEAN project. The MOS data were processed to apply sensor calibration, to correct for atmospheric contamination so as to assess water-leaving radiances for each visible channel, and to estimate geophysical parameters such as pigment concentration and in-water optical depth, which is correlated to suspended matter concentration. The atmospheric correction was performed with a novel algorithm developed especially for MOS application. The bio-optical algorithms used to derive in-water parameters were obtained by comparison with the concurrent *in situ* measurements of optically active parameters collected in the north-western Black Sea in the framework of the EROS 21 project. The multi-satellite data set highlights the differences between western and eastern sub-basins, inshore and offshore domains, northern and southern near-coastal areas. In the Danube delta area, the water constituents trace complex interactions of near-coastal and basin-wide features of the Black Sea.

Keywords: water constituents; optical remote sensing; Black Sea

Introduction

The almost totally landlocked Black Sea (Figure 1), draining most of north-eastern Europe through a number of major rivers, can be taken as the ultimate representative of an environmentally-stressed enclosed sea. Among large marine water bodies, the Black Sea has a significantly high ratio of drainage basin to water basin area, accompanied by a high population density in the catchment area itself. As a consequence, it is subject to a considerable anthropogenic impact. In recent years, severe changes have been documented in the ecosystem of the Black Sea (Murray, 1991). Examples of ecological collapse include loss of vast areas of sea-grass meadows; nearly total disappearance of benthos over broad regions of the shelf; dramatic decline of fisheries; loss of diversity in phytoplankton with blooms becoming monospecific as well as more frequent and intense. This biological upheaval, according to Unluata *et al.* (1993), mirrors changes in the ecosystem bio-geochemitry i.e. an increased influx of nutrients, heavy metals, pesticides and hydrocarbons, contributing to massive eutrophication and toxicity, particularly along coastal boundaries and on the north-western shelf directly impacted by fluvial runoff.

The work presented here concerns the use of satellite-based optical observations of surface waters to assess the main environmental interactions in the north-western Black Sea, as a contribution to the European River-Ocean System 21 (EROS 21) Project. The EROS 21 activities have been conducted as a collaboration between scientists from the European Union and from the riparian countries of the Danubian region, with the aim of investigating the conditions that have led to the destabilization of the Black Sea ecosystem during recent decades (see Van Eeckhout & Lancelot, 1997, and other authors in the same volume). Satellite observations were introduced among project activities to contribute an assessment of the presence and abundance of water constituents (primarily phytoplankton pigments),

[d]Corresponding author. E-mail: vittorio.barale@jrc.it

0272–7714/02/030309+12 $35.00/0

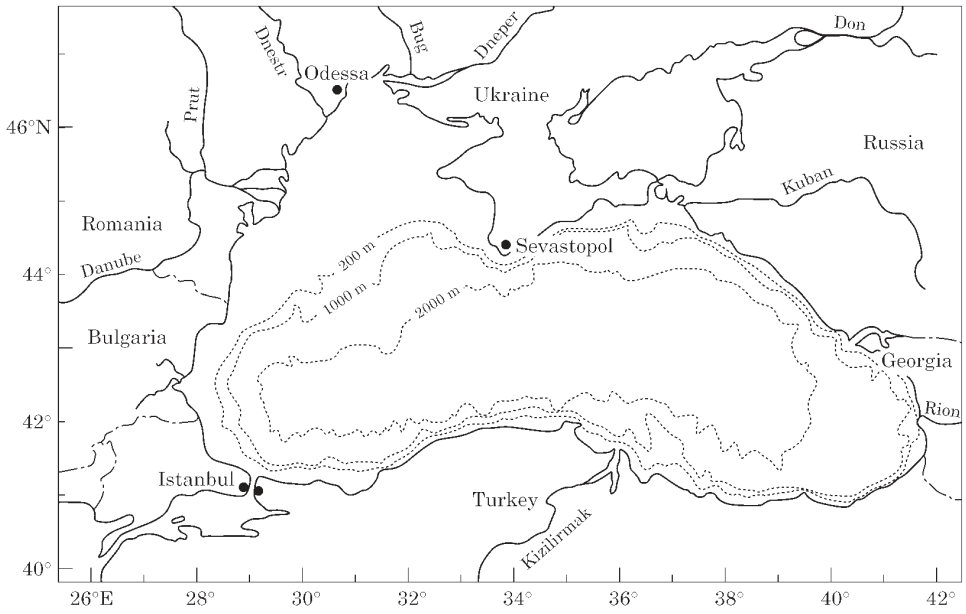

FIGURE 1. The Black Sea: geographic setting, main rivers and bathimetric features.

providing information on the processes which take place in the area, and on their spatial and temporal scales. In the Mediterranean region, optical remote sensing has been applied before to the investigation of processes due to physical and bio-geo-chemical interactions—in particular of those related to the environmental impact of coastal and fluvial runoff, coupled to water circulation patterns (Barale & Larkin, 1998). These processes are quite evident for an enclosed basin such as the Black Sea, which presents relatively clear, mesotrophic waters in the pelagic region, and highly turbid, possibly eutrophic, near-coastal areas.

Data collected by the Coastal Zone Color Scanner (CZCS), on board the NIMBUS-7 satellite (Hovis *et al.*, 1980), in the 1978–1986 period, have been used to explore the surface water optical conditions in the historical framework, and in the Mediterranean basin context (Figure 2). In the available CZCS imagery, all major rivers—the Danube, Dnestr and Dnepr, and the Don in the Sea of Azov, as well as other minor effluents, mostly along the western and southern coast—produce distinct plumes interacting with the marine environment. Within the range of the plumes, as with coastal runoff in general, it is often impossible for a limited optical sensor like the CZCS to distinguish the signature of biogenic pigments from that of the total load of dissolved and suspended materials present in the water. Also, concurrent *in situ* measurements performed at the time of satellite overpasses were only rarely available, at the time of the CZCS, so that the statistics on historical concentrations should be taken with caution. However, the observation of near-coastal features in the CZCS time series provides important clues on frontal dynamics and potential correlations with nutrient enrichment or pollution (Barale & Murray, 1995).

In order to assess the current status of the pigment field in the Black Sea, the historical data were compared with data collected by the Modular Optoelectronic Scanner (MOS), on board the IRS-P3 satellite (Zimmermann & Neumann, 1997), before, during and after the EROS 21 oceanographic cruise which took place in April/May 1997. The coverage, spatial resolution and spectral characteristics provided by the MOS (respectively 200 km swath width, 520 m pixels at nadir, and 13 spectral channel, 20 nm wide, between 408 and 1010 nm, in the MOS-B configuration) are particularly suited for regional studies of coastal zone processes, such as the development and impact of river plumes. In the present case, MOS data have been used primarily to evaluate the concentration of water constituents as determined in the north-western basin by fluvial discharges from the Danube delta area. The availability of field data collected in the framework of the EROS 21 Project, at a time when it was possible to retrieve concurrent, or quasi-concurrent, MOS imagery, provided the means to use advanced spectrometry from space in the assessment of bio-geo-chemical properties in a major

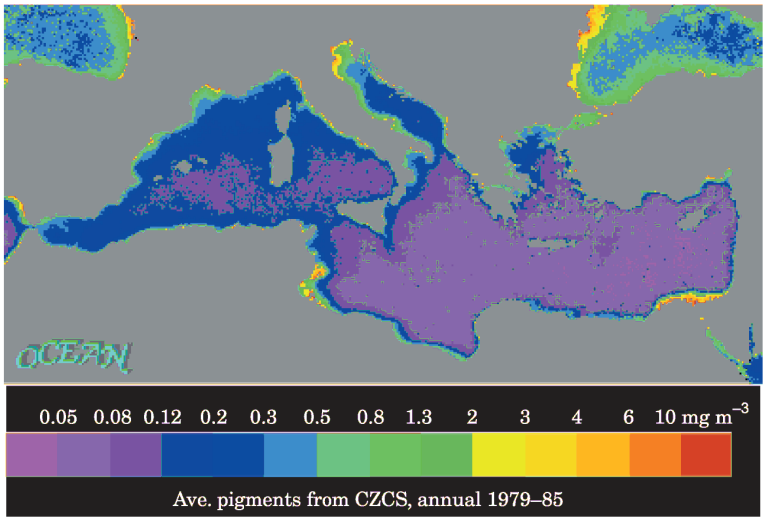

FIGURE 2. Water constituents concentration of the Black Sea, as compared to those of the other Mediterranean sub-basins. The image is a CZCS multi-annual composite of the Mediterranean basin, derived from 2095 images collected in the 1979–1985 period. The original data were processed to derive chlorophyll-like pigment concentration (shown by the colour coding as mg m^{-3}), remapped to the same equal area geographical projection, with 1 km^2 pixels, and composited by averaging on a pixel by pixel basis. The image highlights differences between the various Mediterranean sub-basins: note that the main feature of the Black Sea is the higher pigment concentration, with respect to the oligotrophic waters of the open (eastern) Mediterranean.

river plume. In the following, methods used for data processing will be described in some detail, starting from the processing scheme implemented to perform atmospheric corrections, and continuing with the bio-optical algorithms derived from the combined analysis of *in situ* measurements and MOS water-leaving radiances. Further, the results obtained applying these algorithms to a multi-seasonal series of MOS images will be discussed in light of the main oceanographic features of the Black Sea.

Optical remote sensing data

The historical archive of optical remote sensing data used in the present study originates from the activities of the Ocean Colour European Archive Network (OCEAN) project (see Barale & Zibordi, 1994, and references therein), which assembled a data base of CZCS data for the European enclosed and marginal seas collected between 1978 and 1986. The raw data (2095 original images for the whole Mediterranean region, of which 257 covering the Black Sea itself) were processed to apply sensor calibration algorithms, to correct for atmospheric contamination, and to derive chlorophyll-like pigment concentration. Single images were generated for each available day, co-registered using the same geographic equal-area projection and resolution, with a 1-km pixel size, and then averaged pixel by pixel, to compute annual and monthly composites (Figure 3). The composite images retain only persistent features of the pigment field, and were used to explore the main bio-optical features appearing in the surface waters of the Black Sea (see Appendix 1).

The time series of historical data was complemented by a set of images collected by the MOS (30 cloud-free or partially cloud-free scenes between May 1996 and April 1998). The original (level 1b) MOS images were pre-processed for geo-location using standard procedures provided by the data supplying agency (C. Tschentscher, pers. comm.). Residual geo-location uncertainties, mainly due to errors in the satellite attitude, were minimized by navigating each image—that is by adjusting the satellite roll, pitch and yaw and the scene acquisition time in order to achieve the optimum match between a digital model of the coastline and the image itself. Once the geometry had been corrected and the sun and satellite angles had been properly estimated, an atmospheric correction scheme (Sturm, 1998) was applied to the top-of-the-atmosphere signal recorded by the sensor. The output of the atmospheric correction is the water-leaving radiance L_{wi} in each of the visible MOS channels i, which is registered onto the standard geographical grid created for the area of study.

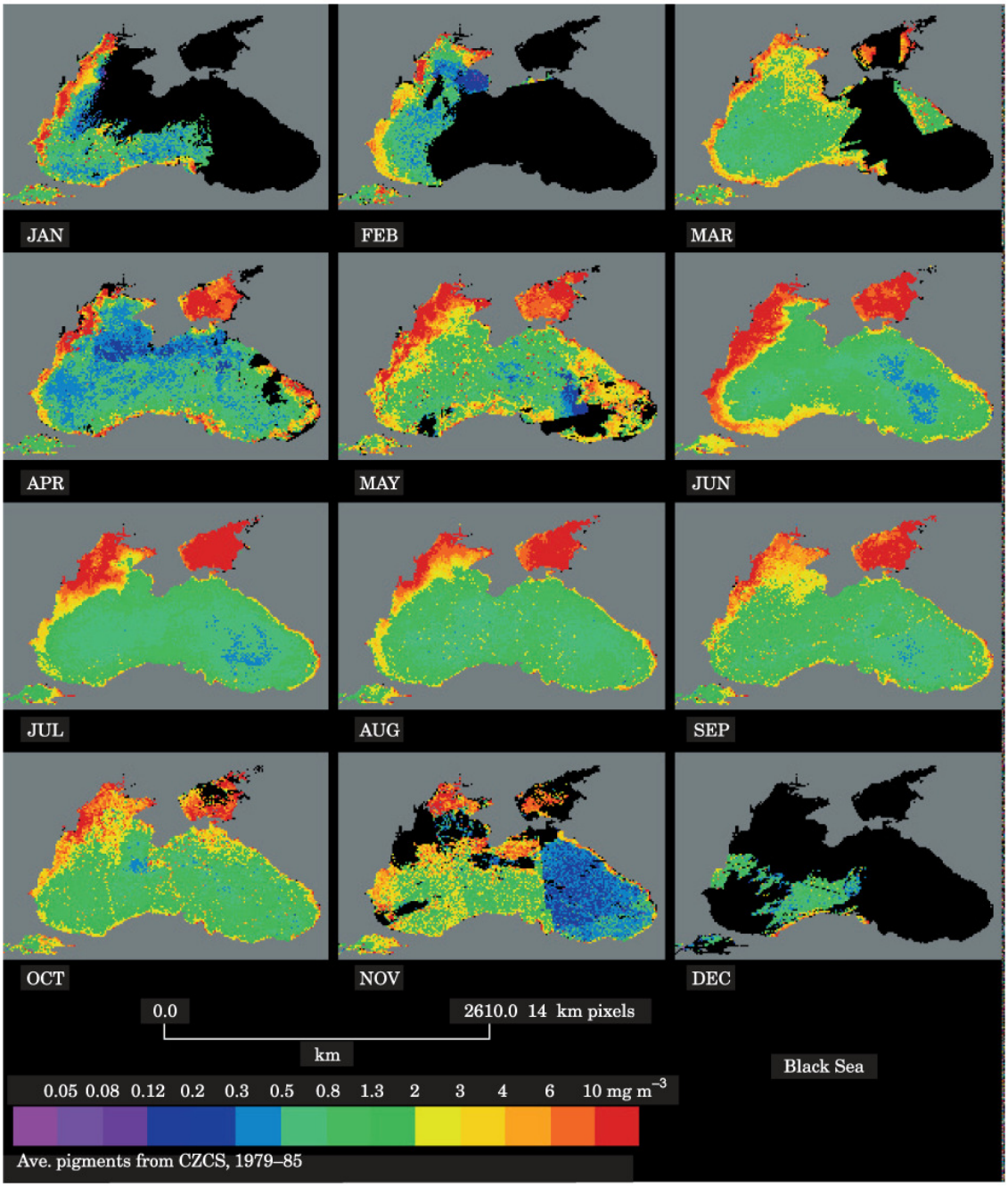

FIGURE 3. Water constituents concentration in the Black Sea, evaluated on a monthly basis, showing the variability of surface features over the annual cycle. The images are mean CZCS monthly composites, over the period 1979–1985. Processing, compositing and colour coding as in Figure 2. The black color coding represents areas where valid data have never been collected during the CZCS lifetime, mostly due to persistent cloud cover (coupled to limited satellite coverage and lack of local receiving stations).

The L_{wi} values can be used in standard bio-optical algorithms to retrieve maps of geophysical parameters, such as the concentration of water constituents. However, in this particular application, quasi-simultaneous MOS images and *in situ* data were available, therefore a regression analysis of MOS

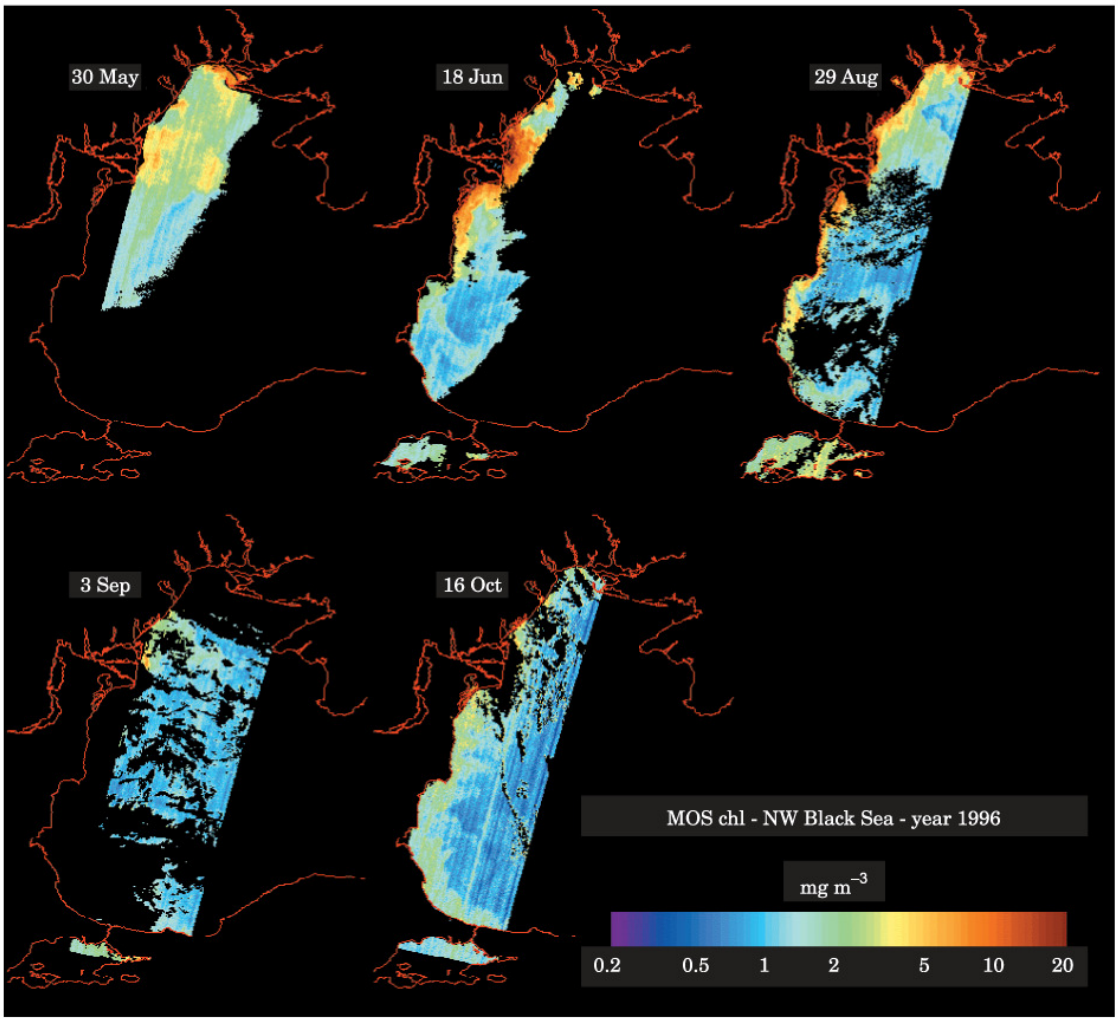

FIGURE 4. Chlorophyll-like pigments maps, derived from MOS data, for 1996. The colour coding indicates concentrations C in mg m^{-3}.

water-leaving radiances and concurrent *in situ* measurements of optically active parameters (chlorophyll-like pigments, in particular) was performed to derive specific bio-optical algorithms for the north-western Black Sea region. The *in situ* measurements were gathered in April–May 1997, during the EROS 21 cruise in the region of the Danube delta (Lancelot & Esorov, 1997). During the cruise period, there were two reasonably cloud-free MOS overpasses on 26 April 1997 (Julian day 116, take 46) and on 1 May 1997 (Julian day 121, take 47). Thus, special attention was given to the correction of these two images and the extraction of radiance values at the locations corresponding to the oceanographic stations.

In the atmospheric correction scheme, it is possible either to select for an entire scene a constant value of the Ångstrøm exponent v, which links radiance ratios to simple wavelengths ratios (Ångstrøm, 1961; Sturm, 1983), or to compute this parameter on a pixel-by-pixel basis by using the MOS channels in the near infrared. Various tests have been carried out on the two MOS images with $v=1$, $v=0$, $v=-1$ and with a pixel-by-pixel computed v. The latter resulted in values of v far too variable over a single scene, too noisy and often unrealistic ($>+2$). This is mainly due to two reasons: (*i*) the uncertainty in the absolute calibration of the near infrared bands of the sensor and (*ii*) the striping noise. This noise results from the non-uniform response of the single elements in the

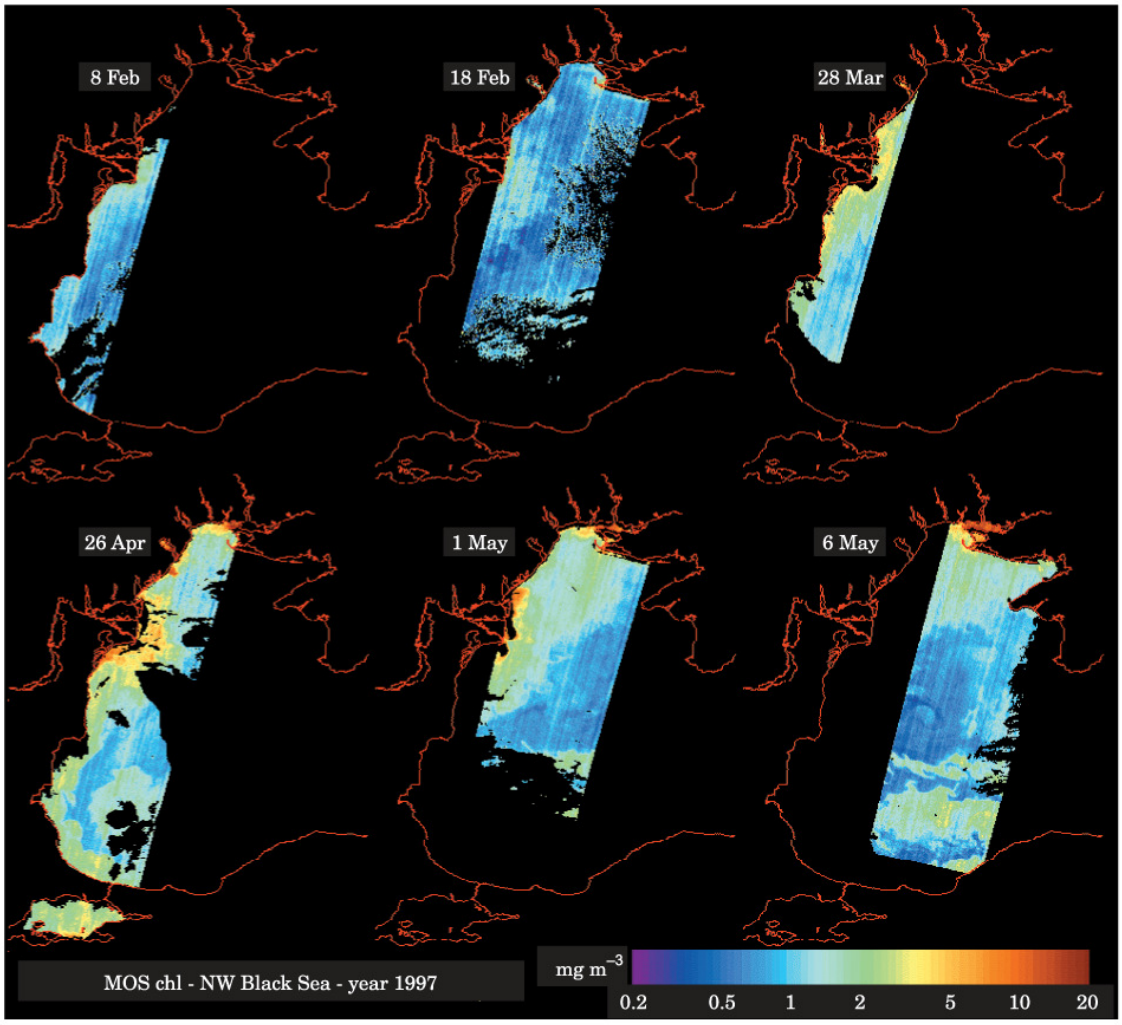

FIGURE 5. (a) Chlorophyll-like pigments map, derived from MOS data, for 1997. The color coding indicates C in mg m^{-3}.

detector array and affects all the channels, as evident from the maps presented in the following sections. Its correction will constitute a major improvement in the quality of MOS-derived water constituent maps (see Corsini *et al.*, 1998). With $v=1$, radiance values in many channels over a number of stations were zero, while with $v=0$ the radiance values seemed plausible but the subsequent bio-optical algorithms yielded an excessive and unrealistic variation of chlorophyll concentration over the basin. Conversely, $v=-1$ gave both realistic values of radiance and concentrations of chlorophyll consistent with the known CZCS climatology. Thus, it was decided to assume this value of the Ångstrøm exponent to process the entire 1996–1998 MOS time series.

In trying to retrieve the bio-optical algorithms from the comparison between *in situ* measurements and atmospherically corrected water-leaving radiances, some factors had to be taken into account:

- all stations were in the area of the Danube river plume, i.e. in case 2 waters (waters optically dominated by a combination of constituents, including plankton, dissolved organic matter and suspended sediments—and not by phytoplankton pigments alone, as in case 1 waters; see Morel & Prieur, 1977), as confirmed by the measurements themselves. This implies that the algorithm to estimate pigment concentration had to account also for the effects of diverse water constituents.
- due to the time needed to move from a station to the subsequent one, and to the inherent time needed for performing the measurements at each station, no more than 2–3 stations *per* day could be sampled. This implies that stations sampled before and after

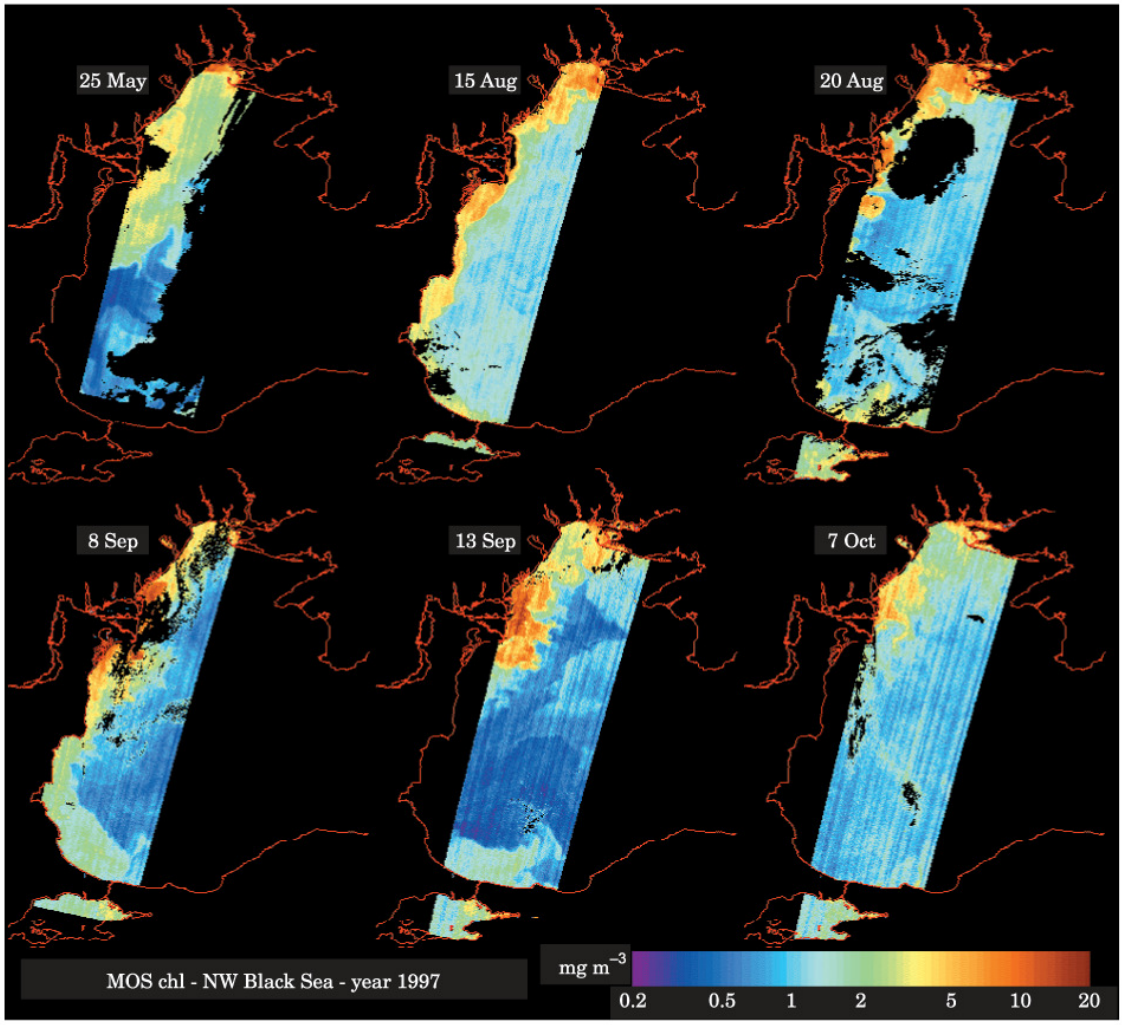

FIGURE 5b. Chlorophyll-like pigments maps, derived from MOS data, for 1997. The colour coding indicates concentrations C in mg m^{-3}.

the day of the two overpasses had to be included in the analysis in order to have a significant number N of samples for the regressions.

- even after navigation, the two MOS images on Julian day 116 and 121 present a small residual geo-location error (of the order of 2–3 pixels) which is detrimental to the accuracy in the location of the values corresponding to each station. To reduce this problem, a 7 × 7 pixel cluster, centred in the nominal position of the station, was considered to determine the MOS-derived geophysical parameter value.
- in both images, the area of the cruise is affected by sparse clouds, so that remnant cloud contamination is a potential reducing factor for the correlation. This was tackled by taking the median instead of the mean value in the 7 × 7 pixel cluster.
- data from MOS channel 7 (650 nm) could not be used in the analysis, owing to the large uncertainty in its calibration.

An algorithm for the estimation of the concentration of phytoplankton chlorophyll-like pigments C (mg m^{-3}) can be built by taking into account some well-known optical properties of the water constituents. The approach by Tassan (1994), adopted also by Chauhan *et al.* (1997), was followed. This relation uses a ' sensitivity ' term, the ratio of radiances in the maximum and minimum absorption of chlorophyll (corresponding to MOS channel 2, at 443 nm, and MOS channel 5, at 570 nm), and a ' compensating ' term, the ratio of radiances in MOS channel 1, at 408 nm, and MOS channel 3, at 485 nm, which is less dependent on C and more sensitive to sediments and

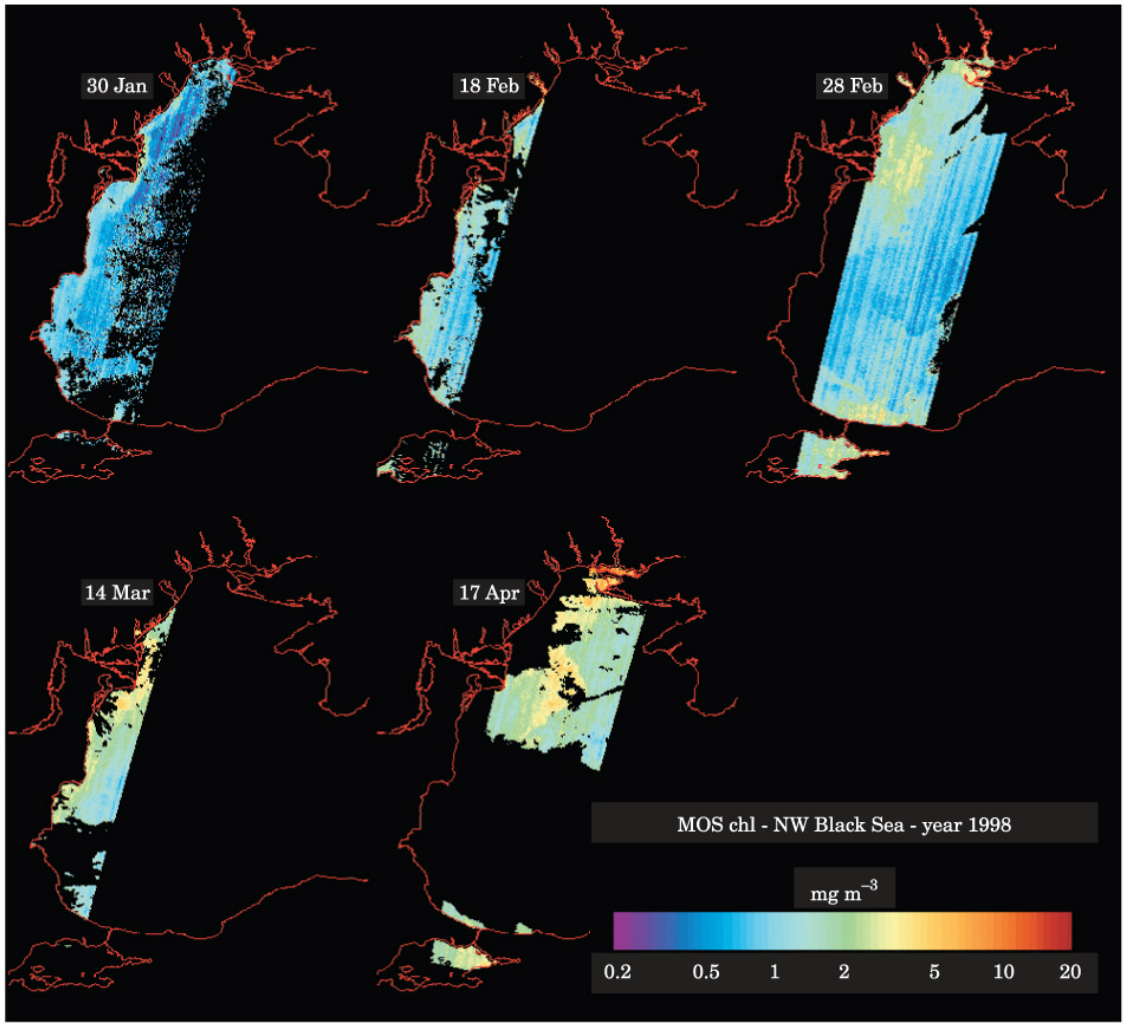

FIGURE 6. Chlorophyll-like pigments maps, derived from MOS data, for 1998. The colour coding indicates concentrations C in mg m^{-3}.

dissolved organic matter. Rather than combining the two ratios into a single regression variable, they have been used here as two separate variables. The regression over the set of stations gave the following algorithm:

$$\log(C) = 0{\cdot}12 - 3{\cdot}43 \log (L_{w2}/L_{w5}) + 4{\cdot}02 \log (L_{w1}/L_{w3}) \quad (1)$$

with $N=12$ and a correlation coefficient $r=0{\cdot}56$. This algorithm, when applied to the images, gave maps of C with realistic values and structures, and consistent with the known CZCS climatology, even in the case 1 areas not covered by the cruises.

Another parameter measured during the EROS 21 campaign was the in-water optical depth (or Secchi disk depth) *tau* (m), which is well correlated with the total concentration of suspended sediments in the water body. The channels which have to be used for the estimation of this parameter are those only weakly sensitive to C, that is 4 (520 nm), 5 (570 nm) and 6 (615 nm). In the present case, it was observed that the use of channel 6 resulted in an increase of the noise on the final maps, thus only channels 4 and 5 were used in the regression. The algorithm is:

$$\log (tau) = 0{\cdot}48 + 5{\cdot}92 \log (L_{w4}) - 5{\cdot}83 \log (L_{w5}) \quad (2)$$

with $N=12$ and a correlation coefficient $r=0{\cdot}86$. Algorithms (1) and (2) were finally applied to the whole time series of MOS images. Figures 4, 5 and 6 show a selection of the pigment maps obtained for

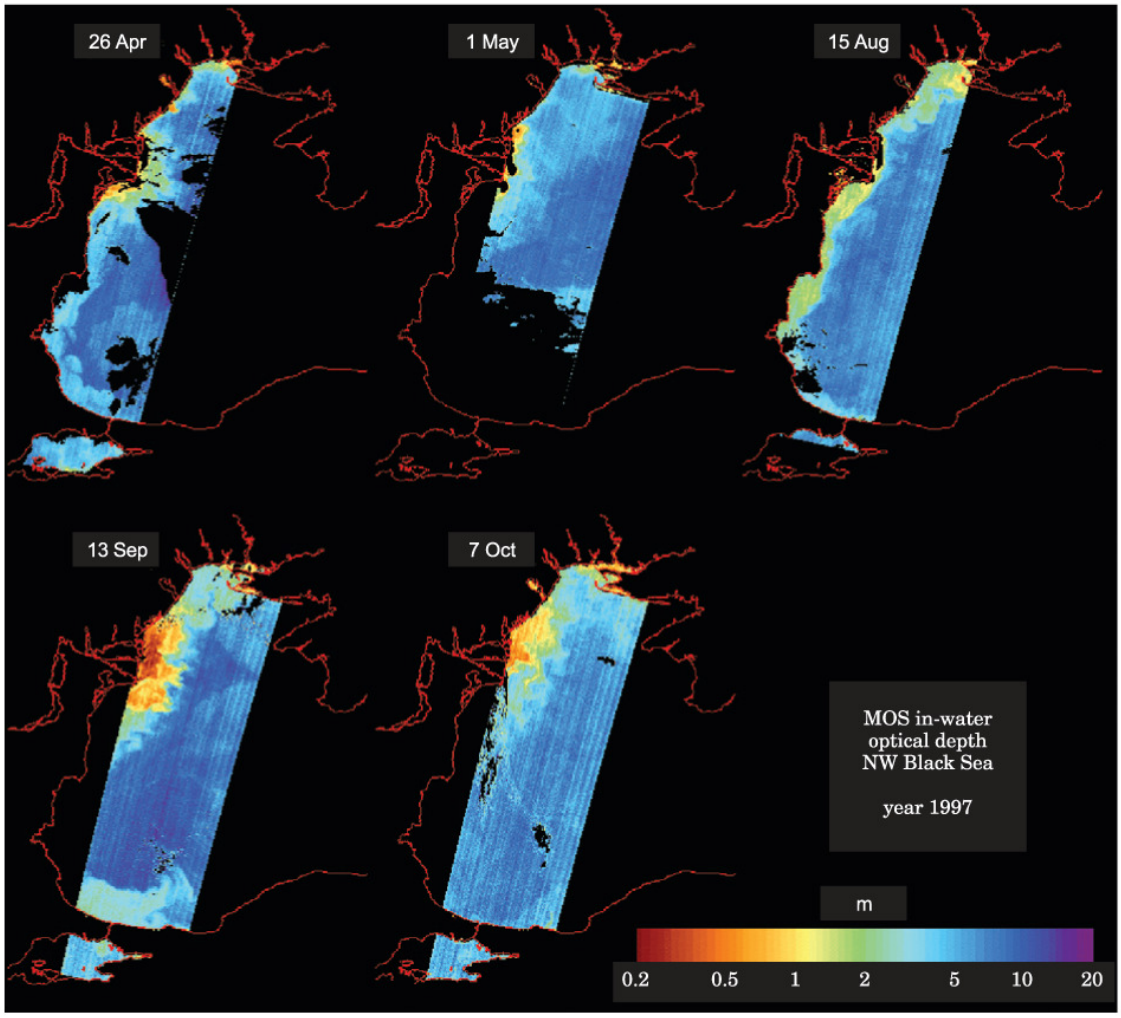

FIGURE 7. In-water optical depth (or Secchi disk depth) maps obtained for some of the best (cloud-free) images in the MOS 1997 image series. The colour coding indicates *tau* in m).

1996, 1997 and 1998, respectively. Figure 7 shows the corresponding *tau* maps for some of the best (cloud-free) images in the 1997 series.

Water constituents patterns

The main feature of the Black Sea emerging from the analysis of historical data is the higher pigment concentration with respect to the other basins of the Mediterranean region. Even though the Black Sea is located in a semi-arid climatic zone, precipitation is very high in the south-eastern part, with the result that, on average, evaporation only slightly exceeds precipitation. However, the principle catchment area of the basin is in a humid climatic zone, and it is this fact that leads to the excess input of fresh water. The massive riverine water inflow is coupled to a high input of water constituents, which provides the Black Sea with its higher pigment concentrations. Therefore, these high values can be interpreted as being related to the combined effect that (*i*) coastal (fluvial) runoff, (*ii*) strong vertical stratification, and (*iii*) surface circulation features in general, have on the presence and abundance of suspended and dissolved matter in the surface layer of the basin.

The impact of river discharges, from the Danube, Dnestr and Dnepr in particular, along the western coast can be readily evaluated from the CZCS images (Figure 3). The river plume system (defined by estimated values of $C>10$ mg m^{-3} — although it

must be remembered that these values are altered in a non-quantifiable manner by the presence of different water constituents) is connected to a band of coastal-type waters (with approximately $2<C<10$ mg m^{-3}) which occupies most of the north-western shelf area. This type of water also appears to be entrained in the large scale surface circulation pattern of the Black Sea, tracing the western component of the basin-wide gyre, or the westernmost of the two cyclonic gyres that occur in the western and eastern sub-basins. A double-vortex feature is seen developing at times in the high shear zone between the two main cyclonic components of this basin-wide pattern. The lower pigments of the eastern part of the basin (C values between 0·2 and 0·8 mg m^{-3}) might be generally linked to a reduced water constituent input of coastal origin. Actually, low pigment concentrations, associated with the interior of the cyclonic gyre(s) of the surface circulation, appear at times in the western sub-basin too, and may therefore be a recurrent feature of the open Black Sea.

Hints of the water exchange at the Bosphorus Strait can also be observed in the CZCS images. A two-layer flow regime exists in the Strait, with an upper layer flowing from the Black Sea towards the Sea of Marmara, and a lower layer of Mediterranean origin flowing in the opposite direction (Latif *et al.*, 1991). The plume of high pigment waters extending from the Bosphorus seems to trace the Black Sea outflow into the Sea of Marmara, in most of the images where this area is covered.

The patterns appearing in the MOS-derived pigment concentration data (although the imagery is of rather difficult interpretation, due to the reduced spatial coverage of the remote sensor, for any given satellite pass, in comparison to that of the CZCS) describe an analogous situation (Figures 4, 5, 6). High pigment levels (in the range between 1 and 10 mg m^{-3}) are recurrent in the coastal zone, in particular near the Danube delta area, along the wider north-western shelf area, in front of the Dnestr and Dneper river mouths, and in a narrower band along the south-western littoral. In most MOS images, the coastal zone impacted by river discharges seems to have a scale smaller than that seen in the historical imagery. Further, it appears to be separated from the open sea core of the western gyre by an area of small- to meso-scale turbulence. Much lower pigment values (less than 1 mg m^{-3}) are recurrent in the open sea zone. The in-water optical depth (or Secchi disk depth), shown in Figure 7, confirms the quasi-oceanic type of the offshore waters, characterized by transparencies similar to those of other Mediterranean sub-basins.

As for the time domain, the historical record seems to suggest recurrent maxima, in both pigment concentration values and size of coastal plumes, in the summer period. The current MOS-derived imagery also present minima in concentrations and surface features in the winter period (see e.g. the 18.02.97 image in Figure 5, or the 28.02.98 image in Figure 6), and maxima in the spring-summer period (see e.g. the 30.05.96 and 18.06.96 images in Figure 4, as well as the 26.04.97, 15.08.97 and 13.09.97 images in Figure 5). However, the general trend in the MOS data seems to be that of quite variable conditions, possibly driven by single episodes of anomalous run-off and mixing and linked to specific meteorological conditions.

Conclusions

The use of optical remote sensing data can provide substantial support to the study of geophysical interactions in marginal basins and near-coastal areas such as those of interest here. The main feature of the north-western Black Sea appearing in the historical and current imagery is the higher concentration of water constituents linked to the outflow from the Danube delta, and to other river (Dnper, Dnester) runoff or resuspension processes in the north-western part of the basin. The impact of fluvial discharges (both a direct effect due to the sediment load and an indirect one induced on the planktonic flora by the associated nutrient load) can be readily evaluated from the comparison of inshore and offshore optical characteristics appearing in the optical remote sensing data, both historical (CZCS) and current (MOS). The resulting coastal-type waters are entrained in the surface circulation pattern of the Black Sea, tracing a number of mesoscale features connected with river plumes, which are visible towards the central and southern parts of the basin, especially in the in-water optical depth maps. The analysis of an ever longer time series of satellite data, and the derivation of bio-optical algorithms with sounder statistical foundations (the present experiment being somewhat limited by the scarcity of matching *in situ* and remote measurements) will allow the exploration of such features in more detail, and in particular the definition of their evolution in both the spatial and temporal domains.

Acknowledgements

The present paper reports the activities conducted at the Marine Environment Unit of the Space

Applications Institute (SAI) Joint Research Centre (JRC) of the European Commission (EC), in the framework of the Project "Bio-Geo-Chemical Interactions between the Danube River and the North Western Black Sea", European River-Ocean System 21 (EROS 21), under EC Contract 12062-96-07 A2FP ISP B. This work has been carried out, in part, while P. Cipollini was at SAI/JRC as a Visiting Scientist from the Southampton Oceanography Centre (JRC contract P0125/6027/97), and A. Davidov was visiting SAI/JRC as a trainee from the University of Kiel (JRC contract P0125/2139/98). The authors wish to thank C. Lancelot, Universite Libre de Bruxelles, Bruxelles (Belgium), for her support in the framework of the EROS 21 Project, and for the *in situ* data used in the present work; S. Moncheva, Institute of Oceanography, Varna (Bulgaria), who collected and analysed the *in situ* measurements; V. Suetin for helpful discussions. This is publication No. 175 of the EU-ELOISE initiative.

References

Ångstrøm, A. 1961 Techniques of determining the turbidity of the atmosphere. *Tellus* **13,** 214–223.

Barale, V. & Larkin, D. 1998 Optical remote sensing of coastal plumes and run-off in the Mediterranean region. *Journal of Coastal Conservation* **4,** 51–68.

Barale, V. & Murray, C. N. 1995 The surface color field of enclosed marine basins: pigment patterns of the Black Sea. *Remote Sensing Reviews* **12,** 61–82.

Barale, V. & Zibordi, G. 1994 Trends in the surface colour field of the European marginal seas. *Proceedings of the Second Thematic Conference on Remote Sensing for Marine and Coastal Environments*, New Orleans (U.S.A.), 31 Jan–2 Feb 1994, vol. II, pp. 567–576.

Chauhan, P., Dwivedi, R. M., Solanki, H. U., Raman, M., Chauhan, H. B., Kumari, B., Mohan, M., Nayak, S. R., Kurien, J., Bhattatri, P. M. A. & Sathe, P. V. 1997 Preliminary results of IRS-P3 MOS data analysis for ocean colour application over Arabian Sea, India. *Proceedings of the 1st International Workshop on MOS-IRS and Ocean Colour*, Berlin, 28–30 April 1997, ed. by Institute of Space Sensor Technology, DLR, pp. 131–152.

Corsini, G., Diani, M., Grasso, R., Rinaldi, R. & Walzel, T. 1998 A method for removing striping in MOS-B data. *Proceedings of the 2nd International Workshop on MOS-IRS and Ocean Colour*, Berlin, 10–12 June 1998, ed. by Institute of Space Sensor Technology, DLR, pp. 53–63.

Hovis, W. A., Clark, D. K., Anderson, F., Austin, R. W., Wilson, W. H., Baker, E. T., Ball, D., Gordon, H. R., Mueller, J. L., El-Sayed, S. Z., Sturm, B., Wrigley, R. C. & Yentsch, C. S. 1980 Nimbus-7 Coastal Zone Color Scanner system description and initial imagery. *Science* **210,** 60–63.

Lancelot, C. & Esorov, V. 1997 Cruise Report, EROS 21 Danube Black Sea Cruise, 1st leg, 9 April 65 May 1997. Report of the 49th cruise of RV *Professor Vodyanistky*.

Latif, M. A., Ozsoy, E., Oguz, T. & Unluata, U. 1991 Observations of the Mediterranean inflow into the Black Sea. *Deep-Sea Research* **38** (Supplement 2), S711–S723.

Morel, A. & Prieur, L. 1977 Analysis of variations in ocean colour. *Limnology and Oceanography* **22,** 709–722.

Murray, J. W., ed. 1991 Black Sea oceanography: results from the 1988 Black Sea Expedition. *Deep Sea Research,* **38** (Supplement 2), 1266.

Sturm, B. 1983 Selected topics of Coastal Zone Color Scanner data evaluation. In *Remote Sensing Applications in Marine Science and Technology,* (Cracknell, A. P., ed.). Riedel Publishing Company, Dordrecht, pp. 137–167.

Sturm, B. 1998 A simple atmospheric correction algorithm applied to contemporaneously taken SeaWiFS and MOS-B scenes. *Proceedings of the 2nd International Workshop on MOS-IRS and Ocean Colour*, Berlin, 10–12 June 1998, ed. by Institute of Space Sensor Technology, DLR, pp. 103–110.

Tassan, S. 1994 Local Algorithms using SeaWIFS data for the retrieval of phytoplankton pigments, suspended sediments and yellow substance in coastal waters. *Applied Optics* **33**, 2369–2378.

Unluata, U., Aubrey, D. G., Belberov, Z., Eremeev, V. & Vinogradov, M. 1993 International Program Investigates the Black Sea. *EOS Transactions, American Geophysical Union* **74**, 401, 407, 412.

Van Eeckhout, D. & Lancelot, C. 1997 Modelling the functioning of the north-western Black Sea ecosystem from 1960 to present. In: *Sensitivity to change: Black Sea, North Sea and Baltic Sea*, (Ozsoy, E. & Mikaelyan, A., eds.). NATO ASI Series Environment 2:27, Kluwer Academic Publishers, Dordrecht, pp. 455–468.

Zimmermann, G. & Neumann, A. 1997 The space-borne imaging spectrometer MOS for ocean remote sensing. *Proceedings of the 1st International Workshop on MOS-IRS and Ocean Colour*, Berlin, 28–30 April 1997, ed. by Institute of Space Sensor Technology, DLR, pp. 21–29.

Appendix 1

The OCEAN Project archives can be accessed via INTERNET, as level_3 data products (i.e. fully processed images remapped on a standard geographical grid)—with the capability of extracting full basins at reduced resolution, subsets at full resolution, numerical arrays, line tracts and time series, in both image and graphical form—at:

http://www.me.sai.jrc.it/

while level_1/2 data products (original images and processed images still in the original geographical set up) can be found—and ordered from a data catalogue—at:

http://earthnet.esrin.esa.it/

i.e. the WWW addresses maintained by the ME SAI, JRC/EC, and the ESA.

Black Sea CZCS value-added data products, browse products, and software specifically developed for the EROS 21 Project software are also available on a dedicated CD-ROM containing:

- OCEAN Primary and Composite products derived from the CZCS historical data set (1979–1985) for the Black Sea basin;
- a corresponding set of browse products, accompanied by a set of HTML files, which allow

the products to be easily visualized from a standard WWW browser;

- a command line standalone program, developed in C, to allow a user to establish the latitude and longitude of any pixel in the images;
- a set of C functions, assembled to allow a developer to program dedicated geo-referencing code.

Chapter II

Assessment of algorithms for atmospheric correction and chlorophyll a retrieval from SeaWiFS satellite data in the western Black Sea area

Alexander Davidov

Leibniz-Institute of Marine Sciences – IFM-Geomar, Kiel, Germany
Düsternbrooker Weg 20, 24105 Kiel, Germany
Email: adavidov@ifm-geomar.de

Submitted to International Journal of Remote Sensing

Assessment of algorithms for atmospheric correction and chlorophyll a retrieval from SeaWiFS satellite data in the western Black Sea area

Running Head: Assessment of SeaWiFS algorithms in the Black Sea

ALEXANDER DAVIDOV

Leibniz-Institute of Marine Sciences – IFM-Geomar, Kiel, Germany
Düsternbrooker Weg 20, 24105 Kiel, Germany
Email: adavidov@ifm-geomar.de

The performance of the operational SeaWiFS atmospheric correction algorithm and bio-optical algorithms in the western Black Sea area were evaluated by comparing satellite data with concurrent *in situ* radiometric measurements and four different data sets of *in situ* chlorophyll a. Among the five different atmospheric correction algorithms applied, the multi-scattering mode with fixed aerosol model type 'coastal with 70% humidity' showed the best coincidence of *in situ* and satellite derived data. The standard SeaWiFS multi-scattering correction with 765/865 nm model selection and near-infrared correction for non-zero normalized water-leaving radiance as well as four other fixed aerosol models were found to perform rather poorly and showed strong overestimation of the water-leaving radiance especially in the blue end of the spectra. In the high-chlorophyll, partly turbid and coloured dissolved organic matter rich waters of the western Black Sea the OC4v4 bio-optical algorithm produced best results with a mean systematic error of 30% and a random error of 77%. Also the semi-analytical algorithm GSM01 demonstrates good potential for chlorophyll *a* determination in these optically complex waters (systematic error of 11% and random error of 46%). An overestimation of chlorophyll *a* in the range of less than 1 mg m^{-3} and an underestimation in the range of more than 10 mg m^{-3} was found by applying the OC4v4 algorithm. The difference between *in situ* measured and satellite derived chlorophyll *a* is higher at the stations close to the shore than at the offshore stations. The results show that the vertical chlorophyll *a* distribution should be considered when validating satellite data of the Black Sea. Full-resolution satellite data are required for the validation of *in situ* data in areas with high-, meso- and smallscale surface variability like the western Black Sea. Considering the results of this study and the method's limitations it appears that even with present SeaWiFS operational algorithms it is possible to monitor phytoplankton standing stock and its

temporal succession in the western Black Sea with an acceptable accuracy using ocean colour remote sensing data.

Keywords: Black Sea; SeaWiFS; chlorophyll; algorithm; validation

1. Introduction

Algorithms for the retrieval of satellite derived chlorophyll *a* concentrations ($Chl_{sat,}$ [mg m^{-3}]) from Sea-viewing Wide Field-of-view Sensor (SeaWiFS*:* O'Reilly *et al*. 1998, 2000) ocean colour data are primarily designed for the conditions in the open ocean, where phytoplankton with its chlorophyll a is the predominant optically active factor in the water.

The Black Sea has productive waters [chlorophyll a concentrations up to 100 mg m^{-3} (Sorokin 2002)] and in some areas a high concentration of river-born suspended matter and coloured dissolved organic matter (CDOM). The aerosols over the almost completely land-locked Black Sea can differ considerably from marine aerosols over the open ocean.

The advection pattern in the western Black Sea is dominated by the Rim Current, which is a cyclonic system with baroclinic and frontal instabilities, generating considerable short-term variability as well as seasonally varying mesoscale hydrographic structures (Oguz and Besiktepe 1999). The water exchange between high-chlorophyll shallow regions and the deep, low-chlorophyll central part of the western Black Sea is generally reduced by the Rim current. However, instabilities like fronts and eddies along the continental slope positively influence the exchange of surface water masses.

Ocean colour satellite remote sensing is an important approach for monitoring the phytoplankton distribution, annual succession and also the estimation of the primary production in the Black Sea. However there is doubt and discussion about the accuracy of the current SeaWiFS operational algorithms for the western Black Sea. Suetin *et al.* (2001, 2002 and 2004) report uncertainties in the operational atmospheric correction over the Black Sea, which lead to numerous negative values of the water-leaving radiance [$L_w(\lambda)$, [mW μm^{-1} sr^{-1}]], especially in SeaWiFS bands 1, 2, 3 and 4. Burenkov *et al.* (2000) found considerable differences between satellite derived and *in situ* measured normalized water-leaving radiance [$L_{wn}(\lambda)$, [mW cm^2 μm^{-1} sr^{-1}]] at one single station*.* Sancak *et al.* (2005) compared *in situ* measurements of $L_w(\lambda)$ and surface chlorophyll *a* concentrations (Chl_{insitu}, [mg m^{-3}]) collected on nine stations in October 1999 in the south-western Black Sea with coincident SeaWiFS data. This comparison of the mean [3 x 3 km (9 km^2)] surface Chl_{insitu} with Chl_{sat} retrieved by the bio-optical maximum band ratio algorithms (OC4v4 and OC2v4) as

described by O'Reilly *et al*. (1998, 2000) suggest that these algorithms are generally overestimating Chl_{sat} in the Black Sea. The SeaWiFS data used by Sancak *et al.* (2005) however belong to the older SeaWiFS processing version 3, while in our study version 5 data were used. Suetin *et al.* (2001, 2004), Burenkov *et al.* (2000) and Kopelevich *et al.* (2004) stated also that the operational bio-optical algorithms did not retrieve correct Chl_{sat} in the Black Sea. Suetin *et al.* (2001) proposed a regional algorithm specifically for the Black Sea based on the band ratio between 555 nm and 510 nm (Clark 1981) but with new coefficients in the equation, based on *in situ* measurements on June 3-4, 1998. Burenkov *et al.* (2000) proposed another regional empirical algorithm validated at five stations in October 1997. Kopelevich *et al.* (2004) proposed an algorithm based also on the measurements used by Burenkov *et al.* (2000) completed with *in situ* measurements from two cruises in September 2000 and August 2001 in the eastern Black Sea. The Kopelevich *et al.* (2004) empirical algorithm is based on a regression analysis of 13 measurements using bands 510 nm and 555 nm from global area coverage (GAC) images with a spatial resolution of 4 x 4 km (16 km^2) pixel size. However, the validity of these 'regional' algorithms is usually limited to single datasets from which they are derived.

The aim of our study was to asses the quality of the satellite derived $L_w(\lambda)$ as well as of the Chl_{sat} in the western Black Sea derived by means of SeaWiFS operational algorithms and to estimate possible sources of inaccuracy.

For these purposes we compared *in situ* measured to satellite retrieved exact normalized water-leaving radiance [$^{ex}L_{wn}(\lambda)$, [mW cm^2 μm^{-1} sr^{-1}]]. Furthermore, *in situ* measured mean optically weighted chlorophyll *a* concentration in the remotely sensed depth ($\overline{\mathrm{Chl}}_{\mathrm{insitu}}$) was compared to the results of three empirical, one semi-empirical and two regional bio-optical algorithms. In addition, the satellite derived vertical attenuation coefficient [$K_{Lu}(\lambda)$, [m^{-1}]] was compared to 42 measurements of the Secchi disc depth.

The share of possible sources of inaccuracy such as: Chl_{insitu} with and without consideration of the subsurface concentrations; full-resolution satellite images vs. GAC data are estimated and discussed.

2. Data and Methodology

2.1 In situ measurements of downwelling irradiance and upwelling radiance

In September 2002 radiometric measurements with hyperspectral spectroradiometers TriOS (RAMSES ACC and ACR: 111 bands between 350 and 900 nm Heuermann *et al.* 2002), were undertaken on board of RV 'Aegaeo'. On September 9, 2002, almost synchronously to the SeaWiFS pass at 10:30 UTC, in situ measurements of incident irradiance and upwelling radiances (under and above the water surface) were obtained at 10:15 UTC on station CT1 (44.491° N; 28.932° E) and at 11:57 UTC on station DT1 (44.339° N; 28.734° E) (Fig. 1). Above-water downwelling irradiance [$E_s(0^+,\lambda)$, [mW cm^{-2} nm^{-1}]] was measured with the hyperspectral irradiance sensor fixed on the ship in zenith direction. In-water upwelling radiance [$L_u(z,\lambda)$, [mW μm^{-1} sr^{-1}]] was measured at depths 0.3, 1 and 2 m with the hyperspectral radiance sensor deployed on winch. Both devices were calibrated by the manufacturer shortly before the cruise. At each depth between 5 and 12 spectra were recorded successively and the mean and the standard deviation for each wavelength were calculated.

[insert figure1 about here]

2.2 Determination of in situ vertical attenuation coefficient and exact normalized water-leaving radiance

For the calculation of the $L_{wn}(\lambda)$ and further the ${}^{ex}L_{wn}(\lambda)$ from the in-water *in situ* radiometric measurements the procedures and protocols as described in Ocean Optics Protocols for Satellite Ocean Color Sensor Validation (Mueller *et al.* 2003: Rev. 4, Vol. III: Radiometric Measurements and Data Analysis Protocols) were applied.

For the determination of the upwelling radiance just below the surface $L_u(0^-,\lambda)$ and the $K_{Lu}(\lambda)$ the following equations were used:

$$K_{Lu}(z) = -\frac{d\ln[L_u(z)]}{dz}\bigg|_z \qquad (1)$$

The variables $K_{Lu}(2\text{-}1, \lambda)$ and $K_{Lu}(1\text{-}0.3, \lambda)$ were calculated from the differences between $L_u(z,\lambda)$ at three different depths and then the ${}^{mean}K_{Lu}(\lambda)$ was calculated.

The extrapolation of measured $L_u(1^-,\lambda)$ up to sea surface $L_u(0^-,\lambda)$, under the assumption that ${}^{mean}K_{Lu}(\lambda) \approx K_{Lu}(1^-, \lambda)$ was carried out using equation 2:

$$\mathrm{Lu}(0^-,\lambda)=\mathrm{Lu}(z_0,\lambda)e^{K_{Lu}(z_0,\lambda)\,z_0} \qquad (2)$$

For control purposes, $L_u(0^-,\lambda)$ was also determined by a traditional method described by Smith and Baker (1984, 1986): A regression function resulting from the natural logarithm of $L_u(0.3^-,\lambda)$, $L_u(1^-,\lambda)$ and $L_u(2^-,\lambda)$ for the depths 0.3, 1 and 2 m assuming that the light is decreasing logarithmically with depth was used. The $\ln[L_u(0^-,\lambda)]$ was determined as the intercept and $K_{Lu}(z)$ as the slope of the regression line.

An immersion correction for the glass-water interface for the TriOS radiometer, which is needed for additional calibration, was applied for $L_u(0^-,\lambda)$ at the SeaWiFS spectral bands according to Ohde and Siegel (2003).

Water-leaving radiance $L_w(\lambda)$ was calculated from $L_u(0^-,\lambda)$ by applying the upward radiance transmittance of the sea surface.

$$\mathrm{L_w}(\lambda)=\frac{(1-\rho)}{n^2}\mathrm{L_u}(0^-,\lambda)\text{ , where }\qquad \frac{(1-\rho)}{n^2}=0.543 \qquad (3)$$

[Fresnel reflectance (air-sea) ρ=0.025 and refractive index of sea water *n*=1.34]. Remote sensing reflectance [$R_{rs}(\lambda)$, [sr^{-1}]] was calculated as:

$$\mathrm{R_{rs}}(\lambda)=\frac{\mathrm{L_w}(\lambda)}{\mathrm{E_s}(\lambda)} \qquad \text{with calculated } L_w(\lambda) \text{ and measured } E_s(0^+,\lambda). \quad (4)$$

$L_{wn}(\lambda)$ as defined by Gordon and Clark (1980) was calculated as follows:

$$\mathrm{L_{wn}}(\lambda)=\frac{\mathrm{L_w}(\lambda)}{\mathrm{E_s}(\lambda)}F_0(\lambda) \qquad (5)$$

with extraterrestrial solar irradiation (F_0, [μW cm^{-2} nm^{-1}]) taken from Thuillier et al. (2003).

$^{ex}L_{wn}(\lambda)$, which includes $L_{wn}(\lambda)$ corrected for bidirectional reflectance, chlorophyll fluorescence and Raman scattering (Morel and Mueller 2003) were used for comparison between satellite derived and *in situ* measured data. *In situ* measured $^{ex}L_{wn}(\lambda)$ was calculated with pre-computed f, Q, and R-gothic functions (available in look-up tables of model based calculation at *ftp://oceane.obs-vlfr.fr*) as follows:

$$^{ex}L_{wn}(\lambda)=L_{wn}^{insitu}(\lambda)\frac{f_0(\lambda,\tau_a,Chl)}{Q_0(\lambda,\tau_a,Chl)}\left(\frac{f(\lambda,\theta_0,\tau_a,Chl)}{Q_n(\lambda,\theta_0,\tau_a,Chl)}\right)^{-1} \qquad (6)$$

2.3 Determination of satellite derived exact water-leaving radiance

The $L_{wn}(\lambda)$ from SeaWiFS as well as the $R_{rs}(\lambda)$ and the vertical attenuation coefficient at 490 nm [$K_d(490)$, [m^{-1}]] (Mueller 2000) were calculated by means of the SeaWiFS Data Analysis System version 4.6 software (SeaDAS: Baith *et al. 2001*). In SeaDAS several alternative atmospheric correction algorithms according to Gordon and Wang (1994), Wang (2000) and Franz *et al.* (2003) are implemented. A $L_{wn}(\lambda)$ was calculated with the operational SeaWiFS atmospheric correction considering multi-scattering with 765nm/865nm model selection and NIR correction for non-zero $L_{wn}(\lambda)$. Furthermore, $L_{wn}(\lambda)$ was also determined with the multi-scattering correction with fixed aerosol models, in which the following different models were used: 'coastal with 70% humidity' (coastal70), 'coastal with 99% humidity' (coastal99), 'marine with 70% humidity' (marine70) and 'tropospheric with 70% humidity' (tropospheric70). The satellite derived $^{ex}L_{wn}(\lambda)$ was produced using the routines in the SeaDAS software.

Near real-time ancillary data [atmospheric pressure, wind velocities and ozone load from the National Center for Environmental Prediction (NCEP) and the Total Ozone Mapping Spectrometer (TOMS)] were used for the atmospheric correction algorithm. Alternatively, for the operational SeaWiFS correction and the fixed 'coastal70' model an atmospheric correction with a climatological dataset of the ancillary data was performed.

2.4 In situ biogeochemical and bio-optical measurements and data analysis

Four datasets with 144 Chl_{insitu} measurements, obtained during the period 1998 - 2004 (Tab.1.) including data from the central, the north-western and the north-eastern part of the western Black Sea (Fig. 1) were used for the validation of the SeaWiFS algorithms for the Chl_{sat} calculation. Satellite and in situ data were considered as 'matching-up' when the time shift between satellite recording and in situ sampling did not exceed 48 hours. The analysis of the "matching up" data was based on the guidelines given by Bailey et al. (2000).

[insert table 1 about here]

Almost half of the *in situ* data (72 samples) were obtained in September mainly during two cruises in 2002 and 2004. From March to November the number of samples is equally distributed through the year and varies between four and 15 per

month (Tab.2). For the winter months only one sample from February 1998 exists, due to cloud coverage and limited availability of *in situ* data.

[insert table 2 about here]

Most of the stations were located across the north-western shelf (depth < 100 m). 11 stations were situated over the continental slope and 13 stations in the central deep part of the western Black Sea (> 2000 m). 40 stations were within 12 miles offshore or directly in front of the Danube river delta (Fig. 1).

2.4.1The in situ datasets from 2002 and 2004

During September 5^{th} – 9^{th}, 2002 the Chl_{insitu} and a number of chemical and physical parameters were measured at the surface as well as on the depth profile at 46 stations in front of the Danube delta and over the north-western shelf (Sep2002 dataset). During September 2^{nd} – 6^{th}, 2004, similar measurements were undertaken at 22 stations over the north-western shelf and off the Danube delta (Sep2004 dataset). The Chl_{insitu} in the water samples in the Sep2002 dataset was determined using a spectrophotometer according to the method described by Jeffrey and Humphrey (1975) at surface, 5, 10, 20 m and bottom. For the Sep2004 dataset, the Chl_{insitu} was determined using a fluorometer (Welschmeyer 1994, Trees *et al.* 2003). The comparison of the laboratory determined Chl_{insitu} by means of spectrophotometrical and fluorometrical methods in the Black Sea (Yunev *et al.* 2002) shows that the results of both methods are fully compatible and can be combined in a single dataset without further correction. Additionally, during both cruises continuous vertical profiles of the Chl_{insitu} were recorded by means of a fluorescence probe, which was mounted on the CTD profiler. Samples for Chl_{insitu} determination were collected continuously during day and night. The Sep2002 and Sep2004 datasets were primarily used for the validation of the Chl_{sat} because high-resolution depth profiles were available.

2.4.2 NIMRD dataset

Between March 2001 and November 2003, an overall of 55 Chl_{insitu} measurements at surface, 5 m and 10 m depth were obtained by the National Institute for Marine Research and Development – Constanta. The samples were taken at 15 stations, situated on five transects from the coast towards offshore regions in front of the Danube delta and south of the delta, here referred to as NIMRD dataset. The Chl_{insitu} was measured in discrete water samples at 0, 5, 10 m depth as well as near the

bottom. For the Chl_{insitu} of the NIMRD dataset no detailed description of the sampling procedures and of the analytical methods exist and all stations are located close to the coast in an area with very high mesoscale and smallscale variability (fronts and river plume) (EU DANUBS Project internal annual report 2004, pers. communication).

2.4.3 IBSS dataset

For the 22 stations in the western Black Sea (13 in the central part and nine in the north-eastern part) sampled between February 1998 and September 1999 Chl_{insitu} data were available (Fig. 1). The 22 samples were collected by ships of opportunity by the Institute for Biology of the Southern Seas branch Sevastopol and are here referred to as IBSS dataset. The water samples were taken at the very surface with a bucket and were stored in a cold (>0 °C), dark place. After eight to 12 hours the samples were filtered and Chl_{insitu} was measured spectrophotometrically (Berseneva *et al.* 2004).

2.5 Calculation of mean optically weighted chlorophyll a concentration

In order to compare the Chl_{insitu} to the Chl_{sat} detected by the satellite sensor, a calculation of the $\overline{\mathrm{Chl}}_{\mathrm{insitu}}$ was carried out (Gordon and Clark 1980). The depth profiles of Chl_{insitu} from the fluorescence probe (Sep2002 and Sep2004 datasets) were calibrated with Chl_{insitu} values from the water samples. For stations sampled during day time (7:00 - 20:00 h), the first three meters of the fluorescence profile were abandoned, because a sun-light inhibition of the chlorophyll *a* fluorescence was observed. The regression analysis between fluorescence probe and laboratory measured Chl_{insitu} for each cruise/station was implemented. The resulting linear regression equation was used for the calculation of the high-resolution depth profiles of the Chl_{insitu} from the fluorescence profiles. From the satellite derived $K_d(490)$ the remotely sensed depth for each station was calculated. The $\overline{\mathrm{Chl}}_{\mathrm{insitu}}$, which is virtually what the satellite sensor detects was calculated using equation 7.

$$\overline{Chl}_{sat} = \frac{\int_0^{z_{rs}} Chl(z)e^{-2Kd(490)}dz}{\int_0^{z_{rs}} e^{-2Kd(490)z}dz} \qquad (7)$$

The $\overline{\mathrm{Chl}}_{\mathrm{insitu}}$ is taking into consideration the vertical distribution as well as the self-shadowing of the chlorophyll *a*. On some stations in the Sep2002 dataset no

statistical significance in the vertical distribution of spectrophotometrically measured Chl_{insitu} and fluorescence probe Chl_{insitu} could be established. In this case as well as for the NIMRD dataset an interpolation of the Chl_{insitu} between measured depths was applied and the $\overline{\mathrm{Chl}}_{\mathrm{insitu}}$ was determined.

2.6 Satellite data and analysis

40 full-resolution SeaWiFS ocean colour images corresponding to *in situ* data between 1998 and 2004 were used. The SeaWiFS data of the western Black Sea were received at the ground-based station of Rome University and processed and distributed by the Goddard Space Flight Center (GSFC-DAAC) at NASA, USA. The satellite sensor has a spatial resolution of about 1.1 km and records images from the Black Sea at approximately 10:00 GMT (12:00 local time) once per day. Near real-time NCEP and TOMS ancillary data for the atmospheric correction were also obtained by NASA. The $L_{wn}(\lambda)$ and the $R_{rs}(\lambda)$ were calculated by means of an atmospheric correction algorithm (Gordon and Wang 1994, Wang 2000, Franz *et al.* 2003) considering the multi-scattering effects with fixed aerosol model type 'coastal70', which was found to perform best after analysis of the *in situ* measured radiance (see below). For the calculation of the Chl_{sat} from SeaWiFS four operational algorithms were used. Maximum band ratio OC4v4 and OC2v4, as well as Clark (Clark 1999) are empirical algorithms conditioned with extended datasets of *in situ* measurements, while GSM01 (Maritorena *et al.* 2002) is a semi-analytical algorithm, with more potential for case 2 waters, but still not sufficiently optimized for turbid waters. The $K_d(490)$ was calculated according to Mueller (2000), Signorini et al. (2003) and Smith and Baker (1981**).** The calculations were performed using the software package SeaDAS v4.6.

Two local algorithms for the Black Sea proposed by Suetin *et al.* (2001) and Kopelevich *et al.* (2004) with satellite derived $R_{rs}(\lambda)$ were applied on the stations CT1 and DT1 in addition to standard SeaWiFS algorithms OC4v4, OC2v4, Clark and GSM01. The OC4v4 algorithm was also executed with *in situ* measured $R_{rs}(\lambda)$ as input.

The quality of the SeaWiFS satellite data with respect to possible sources of errors in the region of investigation was reviewed from quasi true-colour images for detection of clouds, haze or radiometric outliers.

SeaWiFS satellite images were mapped to mercator projection with 1.1 km ground resolution prior to the extraction of the "matching up" values.For the purposes of the evaluation of the algorithm performance the mean normalized bias (MNB) as an indicator for the systematic error and normalized root mean square (RMS) as an indicator for the random error as used by Darecki and Stramski (2004) were calculated.

$$MNB = \frac{1}{n}\sum_{i=1}^{n}\left[\frac{\left(Chl_{sat_i} - \overline{Chl}_{insitu_i}\right)}{\overline{Chl}_{insitu\,i}}\right] * 100 \text{ and} \qquad (8)$$

$$RMS = stdev\left[\frac{\left(Chl_{sat} - \overline{Chl}_{insitu}\right)}{\overline{Chl}_{insitu}}\right] * 100 \qquad (9)$$

Because of the lognormal distribution of Chl_{sat} and Chl_{insitu} in the Black Sea, the RMS_{log} was calculated and used for the evaluation of the algorithm performance (Campbell et al. 1995).

$$RMS_{\log} = \sqrt{\frac{1}{n}\sum_{i=1}^{n}[\log_{10}(Chl_{sat\,i}) - \log_{10}(\overline{Chl}_{insitu\,i})]^2} \qquad (10)$$

The chlorophyll a data were $\log_{10}$ transformed prior to the calculation of slope, intercept, r^2 and r.

The remotely sensed depth derived from the satellite sensor, which by definition of Gordon and Clark (1980) is ¼ of the first optical depth (availability of 10% of the light on the sea surface),

$$\text{remote sensed depth} \approx \frac{4.6Kd(490)}{4} \qquad (11)$$

was compared to the Secchi disc depth measured from the ship. The chlorophyll *a* data were analysed with regards to spatial distribution as well as to time shift between the satellite and the *in situ* measurements.

3. Results

3.1 In situ measurements on stations CT1 and DT1

On the stations CT1 and DT1 high Chl_{insitu} (43.67 and 14.67 mg m^{-3}) were measured. The high turbidity observed and the depth profiles of the salinity suggest that the surface layer (5 m) is under strong influence of the Danube river waters. The total phytoplankton biomass measured on station CT1 was 228 mg m^{-3}, and consisted of Bacillaryophyceae (72%) and Dinophyceae (26%). The phytoplankton cell density was 6.4 billion cells per m^3 on station CT1. Both stations were located in near-shore waters, however station CT1 was situated closer to the Danube river delta than station DT1. During the *in situ* radiometric measurements the sky was clear, the sea surface was calm and the wind velocity was under 2 m s^{-1}.

3.2 Validation of the normalized water-leaving radiance using different atmospheric correction algorithms

The comparison of the $L_{wn}(\lambda)$ determined by means of equations 1 and 2 with the $L_{wn}(\lambda)$ determined for control purposes from the regression analysis of $L_u(z,\lambda)$ at different depths shows good agreement between the two methods (Fig. 2 A,B). A slight overestimation (r^2=0.99, n=6, intercept=0.03, slope=1.03) over the whole spectrum was found for the regression-based calculation at station CT1, while on the station DT1 the differences are negligible (r^2=0.99, n=6, intercept=-0.015, slope=1.02).

[insert figure 2 about here]

The comparison of *in situ* $^{ex}L_{wn}(\lambda)$ and satellite derived $^{ex}L_{wn}(\lambda)$ shows that the radiances computed with the atmospheric correction based on the fixed aerosol model 'coastal70' (Fig. 2 A,B) fits best (RMS=35%) in magnitude as well as in the spectral distribution. The SeaWiFS operational atmospheric correction as well as the models 'marine70' and 'coastal99' with higher humidity perform poorly (RMS of 140%, 94% and 134% respectivly) and neither the magnitude nor the spectral distribution resemble the *in situ* $^{ex}L_{wn}(\lambda)$ values. The 'tropospheric70' fixed model did not retrieve any valid radiances on stations CT1 and DT1 and therefore will not be analysed further. There is a general overestimation of $^{ex}L_{wn}(\lambda)$, which is especially high in the blue-green (412-510 nm) part of the spectrum. Although the 'coastal70' derived $^{ex}L_{wn}(\lambda)$ radiances are in the same order of magnitude (differences between

0.006 and 0.17) compared to *in situ* $^{ex}L_{wn}(\lambda)$, there is a noticeable difference in the spectral distribution, which leads to differences in the estimation of the Chl_{sat} when bio-optical algorithms are applied. In the blue-green part of the visible spectrum there is an overestimation in 1 (412 nm), 2 (443 nm), 3 (490 nm) and 4 (510 nm) SeaWiFS bands on station CT1, while on station DT1 only bands 1 and 2 are overestimated. On both stations the underestimation in band 5 (555nm) is more pronounced than the differences in bands 2, 3 and 4, which are also used in the bio-optical algorithms.

The general performance of the atmospheric correction algorithm applying the 'coastal70' fixed model compared to the SeaWiFS operational correction algorithm is significantly better in the western Black Sea (Tab. 3). 'Coastal70' delivered a negligible number of 66 pixels with negative values of $L_{wn}(\lambda)$ at 412 nm compared to 2308 pixels (2790 km^2) with SeaWiFS operational algorithm. Also the number of pixels with positive $L_{wn}(\lambda)$ values, which are used for the calculation of biogeochemical parameters is considerably higher.

[insert table 3 about here]

The differences in the Chl_{sat} compared to $\overline{Chl}_{insitu}$ are mainly due to the bio-optical algorithms but also could result from uncertainties of the atmospheric correction. The Chl_{sat} calculated with OC4v4 bio-optical algorithm for four different atmospheric correction models varied between 4.88 and 13.25 mg m^{-3} on station CT1 and between 1.87 and 5.42 mg m^{-3} on station DT1 (Fig. 3). Despite the significant understimation of $\overline{Chl}_{insitu}$ resulting from different atmospheric corrections, Chl_{sat} calculated with the aerosol model 'coastal70' was always closest to $\overline{Chl}_{insitu}$ (43.67 mg m^{-3} on CT1 and 14.67 mg m^{-3} on DT1). Therefore, in this study, the satellite data used for validation of the bio-optical algorithm in the western Black Sea were processed with the 'coastal70' atmospheric correction procedure.

[insert figure 3 about here]

A good agreement between the satellite derived remotely sensed depth and the *in situ* measured Secchi disc depth was found in the western Black Sea. A significant correlation ($r=0.89$, $r^2=0.79$, $n=42$, $p<0.05$) between these two parameters was found on 42 stations, on which Secchi disc depths were measured in Sep2002, Sep2004 and in NIMRD datasets (Fig. 4). The remotely sensed depth was calculated from

$K_d(490)$, which is also based on the normalised water-leaving radiances derived from the 'coastal70' atmospheric correction.

[insert figure 4 about here]

3.3 Validation of the bio-optical algorithm

Comparisons of the results of different bio-optical algorithms with $\overline{\mathrm{Chl}}_{\mathrm{insitu}}$ on stations CT1 (43.67 mg m^{-3}) and DT1 (14.67 mg m^{-3}) showed, that the concentrations calculated with the OC4v4 algorithm from *in sit*u measured $R_{rs}(\lambda)$ (29.78 mg.m^{-3} on CT1 and 6.95 mg.m^{-3} on DT1) are in better agreement with $\overline{\mathrm{Chl}}_{\mathrm{insitu}}$ than the same algorithm with satellite derived $R_{rs}(\lambda)$ (13.25 mg.m^{-3} on CT1 and 5.42 mg.m^{-3} on DT1). However, the OC4v4 derived Chl_{sat} values were still lower than the $\overline{\mathrm{Chl}}_{\mathrm{insitu}}$ (Fig. 5). The GSM01 algorithm (18.98 mg m^{-3}) performs better than the OC4v4 algorithm (13.25) with satellite retrieved $R_{rs}(\lambda)$ on station CT1, while OC2v4 and Clark derived Chl_{sat} showed even stronger underestimation of the $\overline{\mathrm{Chl}}_{\mathrm{insitu}}$. The Chl_{sat} calculated with two local algorithms from satellite derived $R_{rs}(\lambda)$ as proposed by Suetin *et al.* (2001) (7.29 and 3.16 mg m^{-3}) and Kopelevich *et al.* (2004) (2.55 and 1.45 mg m^{-3}) was also strongly underestimated at these two stations.

[insert figure 5 about here]

In the datasets Sep2002 and Sep2004 the $\overline{\mathrm{Chl}}_{\mathrm{insitu}}$ ranges between 0.24 and 43.67 mg m^{-3} representing different trophic conditions observed in the river water influenced western Black Sea. Oligo- and mesotrophic conditions (less than 2 mg.m^{-3}) were observed on 43 out of 68 stations, eutrophic (2 - 5 mg m^{-3}) on six and hypertrophic / bloom concentrations (over 5 mg m^{-3}) were measured on 19 stations. The remotely sensed depth varied between 2.26 and 12.61 m. Comparisons between $\overline{\mathrm{Chl}}_{\mathrm{insitu}}$ and Chl_{sat} as retrieved with 4 different algorithms show significant correlations in all four cases (Fig. 6, Tab. 4) with the following ranking: OC4v4, OC2v2, GSM01 and Clark. There is considerable overestimation in the areas, where the $\overline{\mathrm{Chl}}_{\mathrm{insitu}}$ is less than 1 mg m^{-3} and underestimation of $\overline{\mathrm{Chl}}_{\mathrm{insitu}}$ values in the chlorophyll-rich areas (> 10 mg m^{-3}) observed for all four algorithms. This over- and underestimation is less distinct on the GSM01 algorithm compared to OC4v4, OC2v4 and Clark algorithms (in the order of appearance). The range of $\overline{\mathrm{Chl}}_{\mathrm{insitu}}$ is also best covered by the GSM01 algorithm followed by the algorithms OC4v4, Clark and OC2v4.

[insert figure 6 about here]

[insert table 4 about here]

On 60 out of 68 stations the normalized bias between $\overline{\mathrm{Chl}}_{\mathrm{insitu}}$ and OC4v4 Chl_{sat} is less than 100%, while on the remaining eight stations it is higher (100-245%). On 63 out of 65 stations the normalized bias between $\overline{\mathrm{Chl}}_{\mathrm{insitu}}$ and GSM01 derived Chl_{sat} is less than 100%, while in the remaining two cases it is slightly higher.

In the IBSS dataset Chl_{insitu} (single sample at surface) ranges between 0.19 and 1.62 $mg.m^{-3}$, while the OC4v4 Chl_{sat} values lie between 0.18 and 3.18 $mg.m^{-3}$ (Fig. 7A). The remotely sensed depth varies between 2.1 and 30.1 m. The comparison of the time-synchronous measurements of Chl_{sat} and Chl_{insitu} shows a significant correlation for the western Black Sea ($r=0.57$ $r^2=0.32$, $n=22$, $RMS_{log}=0.32$). The MNB between Chl_{sat} and Chl_{insitu} was 62% and the RMS was 79%. For 17 out of 22 data pairs the normalized bias was less than 100% and in five cases the values calculated from SeaWiFS were higher than 100%. For three out of these five cases the Chl_{insitu} values were extremely low and the remotely sensed depth exceeded 11 m. In the remaining two cases both, Chl_{insitu} and Chl_{sat}, were high and the remotely sensed depths were extended (13 m and 16 m). The Chl_{insitu} values were generally lower than Chl_{sat}. On the stations with remotely sensed depth less than 8 m the MNB was less than 44%.

[insert figure 7 about here]

In the NIRMD dataset the $\overline{\mathrm{Chl}}_{\mathrm{insitu}}$ varied between 0.23 and 39.98 mg m^{-3} (Fig. 7B), while the Chl_{sat} was in the range of 0.57 – 44.15 mg m^{-3}. A comparison of the concurrent (within 12 hours) measurements of Chl_{sat} and $\overline{\mathrm{Chl}}_{\mathrm{insitu}}$ in the north-western part of the western Black Sea and in front of the Danube delta shows a significant correlation ($r=0.59$, $r^2=0.34$, $n=54$, $p<0.05$, $RMS_{log}=0.47$). The Chl_{sat} is overestimated over the whole range with exceptions between 1 and 6 mg m^{-3}, where a rather high variance was found. MNB and RMS are relatively high with 68% and 196% respectively. Regarding the spatial distribution, better covariance was found on transects outside of the Danube influenced area. All stations were located near the shore where high turbidity and CDOM loads are present at all seasons. No distinct trend of over- or underestimation during the course of the year was observed.

[insert figure 8 about here]

The comparison between four datasets with Chl_{insitu} and OC4v4 Chl_{sat} shows that there is an overestimation on the low-chlorophyll a (<1 mg m^{-3}) stations, high variance in the middle range (1-10 mg m^{-3}) and rather underestimation in the chlorophyll-rich waters (Fig. 8A). The Chl_{sat} does not resolve well the whole range of the Chl_{insitu}. However, the calculated median values from both methods show good coincidence: 1.39 mg m^{-3} for Chl_{insitu} vs. 1.51 mg m^{-3} for Chl_{sat} for 144 stations (Fig. 8B). The overall correlation of the Chl_{insitu} and Chl_{sat} is statistically significant ($r=0.8$, $r^2=0.65$, $n=144$, $RMS_{log}=0.38$).

3.4 Temporal, spatial and vertical variability of Chl_{sat}

About 60% of the analysed pair measurements were made within 12 hours between *in situ* sampling and the satellite overpass, 32% within 24 hours and 8% within 48 hours. The measurements with smaller time shift, show better agreement except for the near shore area (NIMRD dataset), where high variation was found even for a 12 hours timeshift.

The comparison between OC4v4 Chl_{sat} obtained from full-resolution data (1 km^2) with Chl_{sat} obtained from GAC data (pixel area of 16 km^2) shows high variance with a MNB of 56%, a RMS of 94% and a RMS_{log} of 0.23 (Fig. 9).

[insert figure 9 about here]

The comparison of the surface Chl_{insitu} to the $\overline{Chl}_{insitu}$, shows that there is a considerable variance with a RMS of 40%, a MNB of 3% and RMS_{log} of 0.11 (Fig. 10). A very high overestimation of the Chl_{sat} was found on the stations in the central western Black Sea, where the satellite retrieved remote sensing depth reached up to 30 m.

[insert figure 10 about here]

4. Discussion

4.1 Validation of the atmospheric correction

For the evaluation of the performance of four different atmospheric correction algorithms *in situ* radiometric measurements on two near-shore stations with high Chl_{insitu} and high turbidity in the surface layer and strong vertical stratification were used. The atmospheric correction is known to be one of the main reasons for uncertainties of the $L_w(\lambda)$ and Chl_{sat} over waters with high turbidity (Lavender *et al.* 2005), where concentrations of Chl_{insitu} exceed 2 mg m^{-3} (Siegel *et al.* 2003) and where CDOM concentrations are high (HELCOM 2004). Station CT1 lies closer to the Danube delta than station DT1 and was influenced more strongly by the river waters resulting in a higher Chl_{insitu}, turbidity and CDOM concentrations. Therefore, as expected, in the comparison between *in situ* measured and satellite derived $^{ex}L_{wn}(\lambda)$ the 'coastal70' model has shown better results for the station DT1 (Fig. 2D). The high deviation in the blue-green part of the spectrum found on both stations is probably due to wrong assumption of zero $L_{wn}(\lambda)$ in the NIR spectral bands of SeaWiFS. The extrapolation from NIR towards the blue end with initially false values would thus magnify the error for the bands in the blue part of the spectrum. This is especially valid for the operational SeaWiFS atmospheric correction but also for the fixed models 'marine70' and 'coastal99'. We found an overestimation of the $L_{wn}(\lambda)$ in the blue bands, which is in contradiction to the underestimation of the $L_{wn}(\lambda)$ in the blue bands of the spectrum reported by Suetin *et al.* (2002, 2004) as a result of overcorrection over the Black Sea. An explanation for this disagreement could be the fact that stations CT1 and DT1 are located close to the river plume and that the absorption by high concentration of CDOM can considerably decrease the accuracy of the retrieval of the absolute water leaving radiance in the blue end of the spectrum as reported for the Baltic Sea (HELCOM, 2004). Overestimation in the blue spectrum and underestimation in the green band (555 nm) of $L_{wn}(\lambda)$, which were found for the 'coastal70' model (Fig. 2AB) result in higher band ratios and consequently in lower values of Chl_{sat}. However, the underestimation of Chl_{sat} applying 'coastal70' is not as high as for the four other atmospheric corrections applied. The discrepancy in the $^{ex}L_{wn}(\lambda)$ found in band 6 (670 nm) is not relevant for the determination of Chl_{sat}, because this band is not used in the bio-optical algorithms applied.

Very few pixels with negative radiance values were produced using the 'coastal70' atmospheric correction (Tab. 3). The appearance of negative pixels was reported by Suetin *et al.* (2001, 2004) *and* Burenkov *et al.* (2000) to have been one of main problems in the performance of the previous atmospheric correction algorithms over the Black Sea. Even the operational SeaWiFS atmospheric correction retrieved considerably fewer negative values than these reported by Suetin *et al.* 2001. This can probably be attributed to the improvements of the operational SeaWiFS algorithms that were undertaken in the 5th reprocessing of the SeaWiFS data (Patt *et al*. 2003). The 'coastal70' produces more pixels with radiances greater than zero than the operational SeaWiFS correction and thus provides more pixels with calculated Chl_{sat} for the analysis.

4.2 Chlorophyll a concentration as depending of the quality of the atmospheric correction

For the retrieval of the Chl_{sat}, band ratios instead of single bands were used. Therefore, the order of magnitude of the measured radiances can not be a criterion for the correctness of the Chl_{sat} on its own. The spectral distribution of the measured $L_{wn}(\lambda)$ plays a major role with respect to the determination of the Chl_{sat}. Also in this aspect the 'coastal70' performs considerably better than the remaining three corrections (Fig. 3).

4.3 Validation of bio-optical algorithms for stations CT1 and DT1

The validation of the Chl_{sat} retrieved by means of different bio-optical algorithms with the $\overline{Chl}_{insitu}$ on stations CT1 and DT1 shows a strong underestimation of the Chl_{sat} (Fig. 5). The difference between $\overline{Chl}_{insitu}$ (43.7 and 14.7 mg m^{-3}) and Chl_{sat} (OC4v4) (13.3 and 5.4 mg m^{-3}) can be attributed to both, atmospheric correction and bio-optical limitations. The differences between $\overline{Chl}_{insitu}$ and OC4v4 Chl_{sat} (29.8 and 6.9 mg m^{-3}) calculated from *in situ* measured $R_{rs}(\lambda)$ are resulting from the limitations of the OC4v4 bio-optical algorithm alone. This suggests an underestimation of the Chl_{sat} by this algorithm in chlorophyll-rich waters of the western Black Sea with high turbidity and high loads of CDOM from the Danube river plume. The OC2v4 and Clark algorithms did not perform better, as they are also primarily designed for case 1 waters. The GSM01 algorithm performs better than OC4v4 on station CT1 but worse on station DT1, probably due to the differences in the ratio between turbidity and CDOM on both stations. This shows the potential of the GSM01 algorithm for western

Black Sea waters with more than one non-covarying optically active constituent. However, this algorithm is not yet optimized for all types of turbid waters with high CDOM load as demonstrated by its overall performance.

A very strong underestimation of the Chl_{sat} was found when applying the regional Black Sea algorithms proposed by Suetin *et al.* (2001) and Kopelevich *et al.* (2004). This is probably due to the fact that these algorithms were proposed for the central part of the Black sea and that the algorithms were created from very limited $\overline{Chl}_{insitu}$ data and satellite $L_w(\lambda)$ retrieved from early SeaWiFS reprocessing versions, in which the inaccuracy of the atmospheric correction was significantly higher.

4.4 Assessment of bio-optical algorithms for Sep2002 and Sep2004 datasets

The comparison of the four SeaWiFS bio-optical algorithms with Chl_{insitu} data has shown that the GSM01 represents best the range of Chl_{insitu} and reduces its over- and underestimation (Fig. 6). However, there is larger scattering in the Chl_{sat} retrieved by the GSM01 algorithm compared to OC4v4 and outliers were found on single stations, which are difficult to account for. We expect that after some adjustment of the GSM01 algorithm for case 2 waters, there is a high potential to retrieve more realistically Chl_{sat} in the western Black Sea. However, at present a more significant correlation was found between the OC4v4 Chl_{sat} and the Chl_{insitu}. A systematic error of 30% and a random error of 77% can be considered as acceptable for the estimation of phytoplankton standing stock in the surface layer of the western Black Sea. This is especially valuable as the satellite derived data are synoptical observations over a large sea area, while *in situ* data represent only single points.

4.5 Assessment of the bio-optical algorithms for all datasets

The lognormal distribution of the Chl_{sat} in the western Black Sea, which represents also the satellite intra-pixel variability leads to general underestimation of the Chl_{sat} as shown in Campbell (1995). Consequently, a correlation of the logarithm of the chlorophyll a concentration should be used for the evaluation of the algorithm performance as reported in Campbell et al. (1995) and Darecki and Stramski (2005). A confidence interval should also be considered for the overestimation found at lower values and the underestimation in the high chlorophyll a waters of the western Black Sea.

4.6 Possible sources of inaccuracy

4.6.1 Spatial variability

The overall values for the systematic error MNB (49%) as well as the random error RMS (196%) and RMS_{log} (0.38) in the western Black Sea are relatively high, however there are several limitations with respect to the *in situ* datasets used, which could not be avoided completely. The stations on which the MNB was found to be higher than 100% are located in or at the edge of the Danube river plume as detected from surface salinity measurements. The area influenced by Danube river waters is characterized by high horizontal and vertical gradients of the biochemical parameters and rapid changes in its advection pattern. Despite the significant correlation, a high variance was observed between Chl_{sat} and $\overline{Chl}_{insitu}$ from the NIMRD dataset, which is located in this area (Fig. 1, Fig. 7B). This shows that the comparison of the $\overline{Chl}_{insitu}$ on a single point of observation with satellite mean Chl_{sat} within an area of 1 km^2 can be a considerable source of inaccuracy (Fig. 9). Therefore, a validation with 9 km^2 data (Sancak *et al.* 2005), GAC data (16 km^2) (Kopelevich *et al.* 2004, Stanichny *et al.* 2004), or even lower-resolution data (3025 km^2) (Suetin *et al.* 2001) is of limited relevance for the Black Sea.

4.6.2 Vertical distribution of chlorophyll a

The IBSS dataset has an MNB of 62% and an RMS of 79% but this includes only the Chl_{insitu} from the very surface. The explanation for the overestimation of the Chl_{sat} over the whole range found in the IBSS dataset (Fig. 7A) is obviously the considerable variance found when comparing Chl_{insitu} to $\overline{Chl}_{insitu}$ (Fig. 10). If the $\overline{Chl}_{insitu}$ is not considered, a strong overestimation on stations with deep chlorophyll maxima and high remote sensing depth as well as an underestimation on stations with surface maxima and high remote sensing depth occurs. Investigations by Demidov (1999) and Sorokin (2002) have shown that quite often a non-uniform vertical distribution of the Chl_{insitu} with a chlorophyll maximum of up to 40 m in the western Black Sea exists.

5. Conclusions

The results of this study show that in spite of some limitations, the existing atmospheric correction and bio-optical algorithms can quite well determine and monitor the phytoplankton standing stock in the surface layer of the western Black Sea. However, further validation and calibration of the satellite remote sensing data with coincident *in situ* measurements are required to improve the quality of the existing atmospheric correction algorithm and the bio-optical algorithms for the Black Sea. Special attention should be paid to the parameterisation of the bio-optical algorithms taking into account the spatial and temporal variability of suspended matter and CDOM. Furthermore better representation of the *in situ* data from the central part of the Black Sea as well as measurements during winter should be included into the validation.

Acknowledgments

The satellite data used in this study were acquired as part of the NASA's Earth-Sun System Division and archived and distributed by the Goddard Earth Sciences (GES) Data and Information Services Center (DISC) Distributed Active Archive Center (DAAC). Some of the *in situ* data used in this study were collected in the frame of the project "Nutrient Management in the Danube Basin its Impact on the Black Sea" (daNUbs) supported under contract EVK1-CT-2000-00051 by the Energy, Environment and Sustainable Development (EESD) Programme of the 5th EU Framework Programme.

References

1. BAITH, K. S., LINDSAY, R., FU, G. and MCCLAIN, C. R., 2001, SeaDAS: Data Analysis System developed for Ocean Color Satellite Sensors. *EOS*, *Trans. Am. Geophys. Union*, **82**, p. 202.

2. BAILEY, S.W., MCCLAIN, C.R., WERDELL, P.J., AND SCHIEBER, B.D., 2000, Normalized Water-Leaving Radiance and Chlorophyll *a* Match-up Analyses. In: MCCLAIN, C.R., BARNES, R.A., EPLEE, JR., R.E., FRANZ, B.A., HSU, N.C., PATT, F.S., PIETRAS, C.M., ROBINSON, W.D., SCHIEBER, B.D., SCHMIDT, G.M., WANG, M., BAILEY, S.W., AND WERDELL, P.J., 2000, SeaWiFS Postlaunch Calibration and Validation Analyses, Part 2. NASA Tech. Memo. 2000-206892, Vol. **10**, S.B. Hooker and E.R. Firestone, Eds., NASA Goddard Space Flight Center, 57 pp.

3. BERSENEVA, G.P., CHURILOVA, T.Y. and GEORGIEVA, L.B., 2004, Seasonal variability of chlorophyll and phytoplankton biomass in the western part of the Black Sea. *Oceanology*, **44**, pp. 211-219, (in Russian).

4. BURENKOV, V.I., KOPELEVICH, O.V., SHEBERSTOV, S.V. and VEDERNIKOV, V.I., 2000, Se-truth measurement of the ocean color: Validation of the SeaWiFS satellite scanner data. *Oceanology*, **40**, pp. 329-334.

5. CAMPBELL, J.W., 1995, The lognormal distribution as a model for bio-optical variability in the sea. *J. Geophys. Res.*, **100**, pp. 13237-13254.

6. CAMPBELL, J.W., BLAISDELL, J.M. AND DARZI, M., 1995, Level-3 SeaWiFS data products: spatial and temporal binning algorithms. *SeaWiFS Technical Report Series, NASA Technical Memo.* 104566, Vol. **32**. Goddard Space Flight Center, Greenbelt, Maryland.

7. CLARK, D.K., 1981, Phytoplankton pigment algorithms for the NIMBUS-7 CZCS. In: Oceanography from Space. Gower, J.F.R. (ed.) Plenum Press, New York, pp. 227-237.

8. CLARK, D.K., 1999. MODIS Algorithm Theoretical Basis Document for Bio-Optical Algorithms - Case 1 Waters, version 1.2, *ATBD-MOD-18*, p. 36.

9. DEMIDOV, A.B., 1999, Spatial and temporal variability of chlorophyll *a* in the Black Sea during the winter-spring period. *Oceanology*, **39**, pp. 688-700.

10. FRANZ, B.A., EPLEE, R.E., BAILEY, S.W. and WANG, M., 2000, Changes to the atmospheric correction algorithm and retrieval of oceanic optical properties. In: Algorithm updates for the fourth SeaWiFS data reprocessing. SeaWiFS postlaunch technical report series. S.B. Hooker and E.R. Firestone (eds). NASA/TM-2003-206892, **22**, pp. 29-33.

11. GORDON, H.R. and CLARK, D.K., 1980, Remote sensing optical properties of a stratified ocean: an improved interpretation. *Appl. Opt.*, **19**, pp. 3428-3430.

12. GORDON, H.R. and CLARK, D.K., 1981, Clear water radiances for atmospheric correction of Coastal Zone Color Scanner imagery. *Appl. Opt.*, **20**, pp. 4174-4180.

13. GORDON, H.R. and WANG, M., 1994, Retrieval of water-leaving radiance and aerosol optical thickness over the oceans with SeaWiFS: a preliminary algorithm. *Appl. Opt.,* **33,** pp. 443-452.

14. HELCOM, 2004, Thematic report on validation of algorithms for chlorophyll a retrieval from satellite data of the Baltic Sea area. *Baltic Sea Environ. Proc.* **94**. Schrimpf, W. (ed.), p 44.

15. HEUERMANN, R, REUTER R. and WILLKOMM R., 2002, RAMSES - A modular multispectral radiometer for light measurements in the UV and VIS. *Internal report TRIOS*. http://www.trios.de.

16. JEFFREY, S.W, and HUMPHREY, G.F., 1975, New spectrophotometric equation for determining chlorophyll a, b, c1 and c2. *Biochem. Physiol. Pflanz.*, **167**, pp. 194-204.

17. KOPELEVICH, O.V., BURENKOV, V.I., ERSHOVA, S.V., SHEBERSTOV, S.V. and EVDOSHENKO, M.A., 2004, Application of SeaWiFS data for studying variability of bio-optical characteristics in the Barents, Black and Caspian Seas. *Deep Sea Research,* **51**, pp. 1063-1091.

18. LAVENDER, S.J., PINKERTON, M.H., MOORE, G.F., AIKEN, J. and BLONDEAU-PATISSIER, D., 2005, Modification to the atmospheric correction of SeaWiFS ocean colour images over turbid waters. *Continental Shelf Research*, **25**, pp. 539-555.

19. MARITORENA, S., SIEGEL, D.A., and PETERSON, A.R., 2002, Optimization of a semianalytical ocean color model for global-scale application. *Appl. Opt.*, **41**, pp. 2705-2714.

20. MOREL, A. and MUELLER, J.L., 2003, Normalized water living radiance and remote sensing reflectance: Bidirectional reflectance and other factors. In: Ocean Optics Protocols for Satellite Sensor Validation, Revision 4, Volume III: Radiometric Measurements and Data Analysis Protocols. Mueller, J.L., Fargion G.S. and McClain, C.R. (eds.), NASA/TM-2003-211621, pp. 32-59.

21. MUELLER, J.L., 2000. SeaWiFS Algorithm for the diffuse attenuation coefficient, K(490), usung water-leaving radiances at 490 and 555 nm. In: SeaWiFS postlaunch calibration and validation analyses, part 3. SeaWiFS postlaunch technical report series. Hooker, S.B. and Firestone, E.R. (eds). NASA/TM-2000-206892, **11**, pp. 24-27.

22. MUELLER, J.L., 2003, In-water radiometric profile measurements and data analysis protocols. In: Ocean Optics Protocols for Satellite Sensor Validation, Revision 4, Volume III: Radiometric Measurements and Data Analysis Protocols. Mueller, J.L., Fargion G.S. and McClain, C.R. (eds.), NASA/TM-2003-211621, pp. 7-20.

23. MUELLER, J.L., FARGION, GS. and MCCLAIN, C.R., (eds.), 2003, Ocean Optics Protocols for Satellite Sensor Validation, Revision 4, Volume III: Radiometric Measurements and Data Analysis Protocols. NASA/TM-2003-211621.

24. OHDE, T. and SIEGEL, H., 2003, Derivation of immersion factors for the hyperspectral TriOS radiance sensor. *J. Opt. A: Pure Appl. Opt.*, **5**, pp. L12-L14.

25. O'REILLY, J.E., MARITORENA, S., MITCHELL, B.G., SIEGEL, D.A., CARDER, K.L., GARVER, S.A., KAHRU, M. and MCCLAIN, C., 1998, Ocean Colour Chlorophyll Algorithms for SeaWiFS. *J. Geophys. Res.*, **103**, pp. 24937-24953.

26. O'REILLY, J.E., MARITORENA, S., O'BRIEN, M.C., SIEGAL, D.A., TOOLE, D., MENZIES, D., SMITH, R.C., MUELLER, J.L., MITCHELLL, B.G., KAHRU, M., CHAVEZ, F.P., STRUTTON, P., COTA, G.F., HOOKER, S.B., MCCLAIN, C.R., CARDER, K.L., MULLER-KARGER, F., HARDING, L., MAGNUSON, A., PHINNEY, D., MOORE, G.F.,

AIKEN, J., ARRIGO, K.R., LETELIER, R. and CULVER, M., 2000, Ocean Color Chlorophyll a algorithms for SeaWiFS, OC2 and OC4: Verison 4. In: SeaWiFS postlaunch calibration and validation analyses, part 3. SeaWiFS postlaunch technical report series. S.B. Hooker and E.R. Firestone (eds). NASA/TM-2000-206892, **11**, pp. 9-23.

27. PATT, F.S., BARNES, R.A., EPLEE JR, R.E., FRANZ, B.A., ROBINSON, W.D., FELDMAN, G.C., BAILEY, S.W., GALES, J., WERDELL, P.J., WANG, M., FROUIN, R., STUMPF, R.P., ARNONE, R.A., GOULD JR, R.W., MARTINOLICH, P.M., RANSIBRAHMANAKUL, V., O'REILLY, J.E. and YODER, J.A., 2003, Algorithm updates for the fourth SeaWiFS data reprocessing. SeaWiFS postlaunch technical report series. S.B. Hooker and E.R. Firestone (eds). NASA/TM-2003-206892, **22**, p. 74.

28. SANCAK, S., BESIKTEPE, S. T., YILMAZ, A., LEE, M. and FROUIN, R, 2005, Evaluation of SeaWiFS chlorophyll-a in the Black and Mediterranean Seas. *International Journal of Remote Sensing*, **26**, pp. 2045-2060.

29. SIEGEL, D., WANG, M., MARITORENA, S. and ROBINSON, W., 2003, Atmospheric correction of satellite ocean color imagery: the black pixel assumption. *Applied Optics*, **39**, pp. 3582-3591.

30. SIGNORINI, S.R., HOOKER, S.B. AND MCCLAIN, C.R., 2003, Bio-optical and geochemical properties of the south Atlantic subtropical gyre. NASA/TM-2003-212253, NASA Goddard Space Flight Center, Greenbelt, Maryland, 43 pp.

31. SMITH, R.C. and BAKER, K.S. 1984, Analysis of ocean optical data. *Ocean optics VII*, M. Blizard (ed.), *SPIE*, 478, pp. 119-126.

32. SMITH, R.C. and BAKER, K.S. 1986, Analysis of ocean optical data. *Ocean optics VIII*, P.N. Slater (ed.), *SPIE*, **637**, pp. 95-107.

33. Smith, R.C. and Baker, K.S., 1981, Optical properties of the clearest natural waters (200-800 nm). *Applied Optics*, **20**, pp. 177-184.

34. SOROKIN, Y.I., 2002, The Black Sea, ecology and oceanography. Backhuys Publishers, Leiden, Niederlande, 875 pp.

35. STANICHNY, S. 2004. Comparison between MODIS and SeaWiFS satellite retrieved chlorophyll a concentration in the Black Sea. Report MHI UNOPS GEF 2004, (in Russian).

36. SUETIN, V.S., KOROLEV, S.N., SUSLIN, V.V. and KUCHERYAVYJ, A.A., 2004, Manifestation of specific features of the optical properties of atmospheric aerosol over the Black Sea in the interpretation of SeaWiFS data. *Morsk. Gidrofiz. Zh.*, **1**, pp. 69-79, (In Russian).

37. SUETIN, V.S., SUSLIN, V.V., KOROLEV, S.N. and KUCHERYAVYJ, A.A., 2002. Estimation of the variability of sea water optical properties in the Black Sea in summer 1998 from satellite remote sensing SeaWiFS data. *Morsk. Gidrofiz. Zh.*, **6**, 44-54, (In Russian).

38. SUETIN, V.S., SUSLIN, V.V., KUCHERYAVYJ, A.A., KOROLEV, S.N. and BERSENEVA, G.P., 2001, Peculiarities of data interpretation of the Black Sea remote optical observations using the SeaWiFS instrument. Morsk. Gidrofiz. Zh. **2**, pp. 71-80. 2001, (In Russian).

39. TREES, C.C., BIDIGARE, R.R., KARL, D.M., HEUKELEM L.V. and DORE, J., 2003, Fluorometric chlorophyll a: Sampling, laboratory methods, and data analysis protocols. In: Ocean Optics Protocols for Satellite Sensor Validation, Revision 4, Volume V: Biogeochemical and Bio-optical Measurements and Data Analysis Protocols. Mueller, J.L., Fargion G.S. and McClain, C.R. (eds.), NASA/TM-2003-211621, pp. 15-25.

40. THUILLIER, G., HERSÉ, M., SIMON, P.C., LABS, D., MANDEL, H., GILLOTAY, D. AND FOUJOLS, T., 2003, The solar spectral irradiance from 200 to 2400 nm as measured by the SOLSPEC spectrometer from the ATLAS 1-2-3 and EURECA missions, Solar Physics, **214**(**1**), pp. 1-22.

41. WANG, M., 2000, The SeaWiFS atmospheric correction updates. In: SeaWiFS postlaunch calibration and validation analyses, Part 1. NASA/TM-2000-206892, Hooker, S.B. and Firestone, E.R. (eds), **9**, pp. 57-63.

42. WELSCHMEYER, N.A., 1994, Fluorometric analysis of chlorophyll *a* in the presence of chlorophyll *b* and pheopigments. *Limnology and Oceanography,* **39**, pp. 1985-1992.

43. YUNEV, O.A., VEDERNIKOV, V.I., BASTURK, O., YILMAZ, A., KIDEYS, A.E., MONCHEVA, S. and KONOVALOV, S.K., 2002, Long-term variations of surface chlorophyll *a* and primary production in the open Black Sea. *Mar. Ecol. Prog. Ser.*, **230**, pp. 11-28.

Tables wih captions

Table 1. In situ dataset used for the validation.

Dataset	Period of investigation	Investigated area	Stations	Matching-up sat. images
IBSS	26.02.1998 - 20.09.1999	Central and north-eastern part of western Black Sea	22	19
NIMRD	13.03.2001 - 21.11.2003	In front of Danube river delta and western shelf	55	13
Sep2002	5-9.09.2002	North-western part of the western Black Sea	46	4
Sep2004	2-6.09.2004		22	5

Table 2. Number of in situ samples available per month for the period 1998-2004.

Month	Jan	Feb	Mar	Apr	May	Jun	Jul	Aug	Sep	Oct	Nov	Dec
No. of samples	-	1	9	9	9	6	15	9	72	10	4	-

Table 3. Pixels with positive and negative values of Lwn(λ) in the SeaWiFS image of Sep.9, 2002 from the western Black Sea as derived from two different atmospheric correction methods.

Atmospheric correction	412 nm		443 nm		490 nm		510 nm		555 nm	
	+	-	+	-	+	-	+	-	+	-
'Coastal 70'	69967	66	70008	25	70030	3	70032	1	70033	0
Operational	62237	2308	64057	496	64518	38	64532	24	64554	2
Total pixel number	206051		206051		206051		206051		206051	

Table 4. Summary of the error analysis and linear correlation for the SeaWiFS bio-optical algorithms and *in situ* data from Sep2002 and Sep2004 datasets.

Algorithm	n	RMS_{log}	MNB	RMS	r	r^2	slope	intercept	Min	Max
OC4v4	68	0.32	30	77	0.93	0.86	0.577	0.137	0.67	24.44
OC2v4	68	0.35	22	75	0.92	0.85	0.506	0.106	0.68	13.64
Clark	68	0.40	23	82	0.87	0.75	0.463	0.100	0.67	21.00
GSM01	65	0.32	-11	46	0.91	0.82	0.666	-0.049	0.29	50.12

Figures with captions

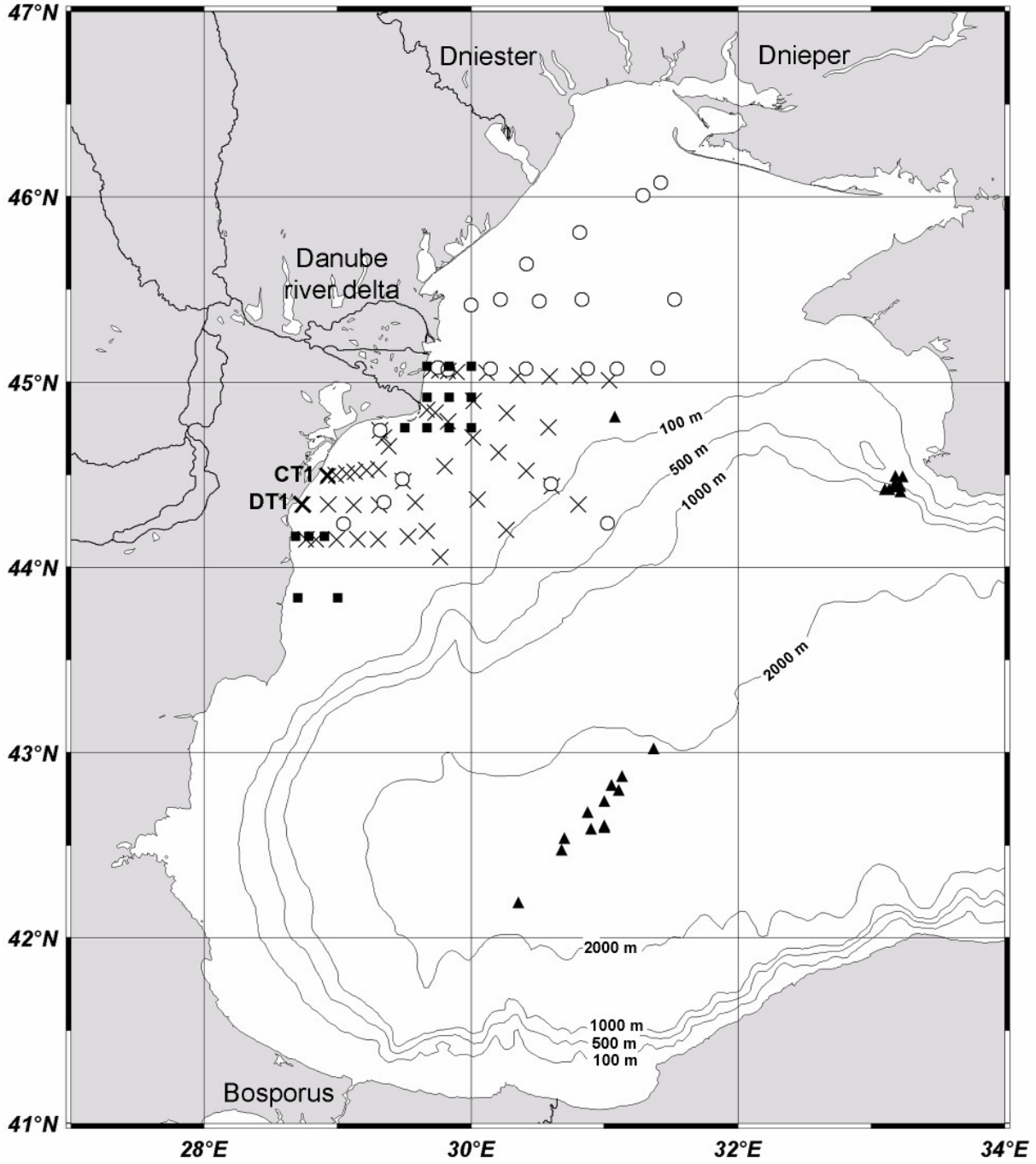

Figure 1. Map of the western Black Sea with sampling stations for Chl_{insitu} analysis within four datasets [Sep2002 (X), Sep2004 (O), IBSS (▲) and NIMRD (■)], which were used for the validation of the SeaWiFS derived Chl_{sat}. Additionally, on stations CT1 and DT1 matching up radiometrical measurements were accomplished.

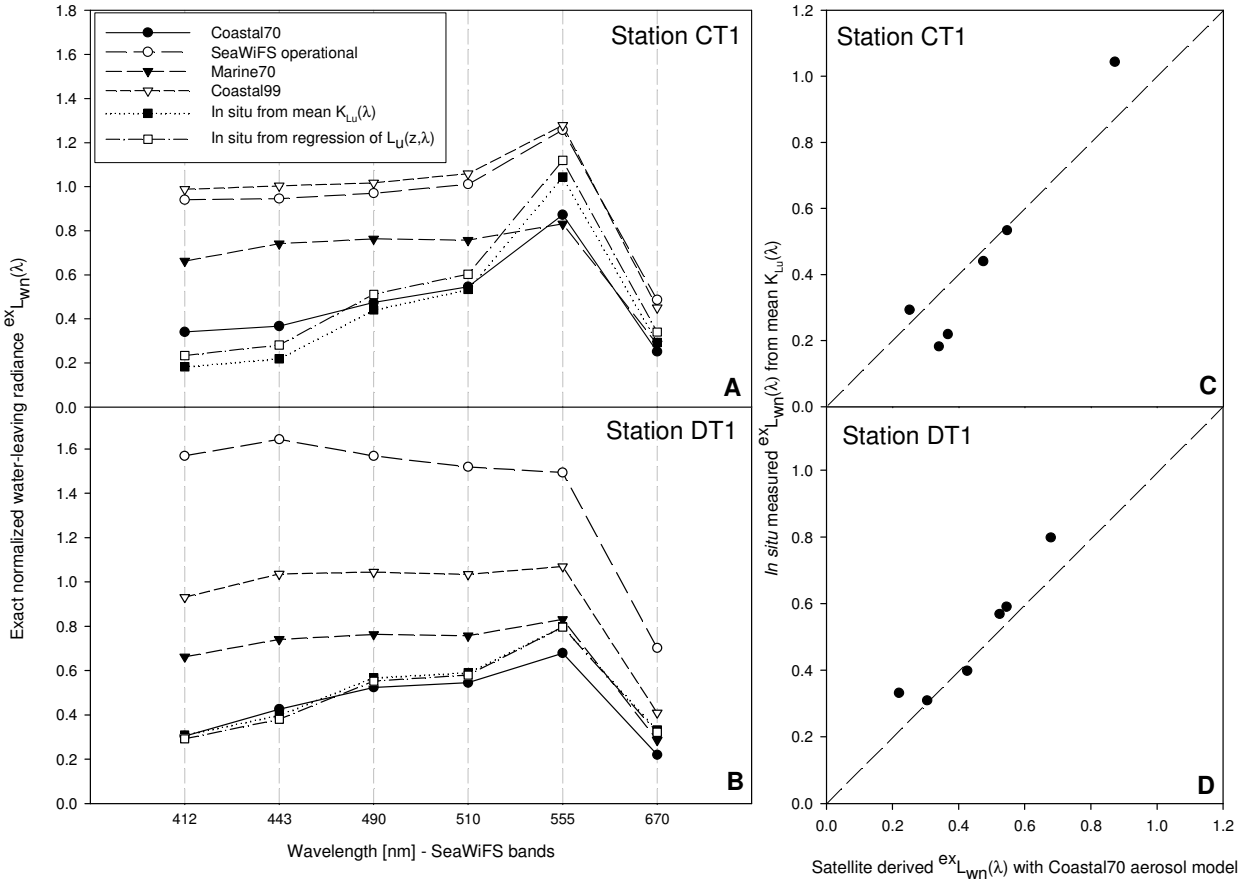

Figure 2. Comparison of *in situ* measured $^{ex}L_{wn}(\lambda)$ calculated from mean $K_{Lu}(\lambda)$ and regression of $L_u(z, \lambda)$ with the four satellite derived $^{ex}L_{wn}(\lambda)$, calculated with the operational SeaWiFS atmospheric correction algorithm as well as with the atmospheric correction algorithm implementing three different fixed aerosol models on stations CT1 and DT1 (A,B). Comparison between the satellite $^{ex}L_{wn}(\lambda)$ derived with Coastal70 aerosol model and *in situ* measured $^{ex}L_{wn}(\lambda)$ from mean $K_{Lu}(\lambda)$ on stations CT1 and DT1 (C,D).

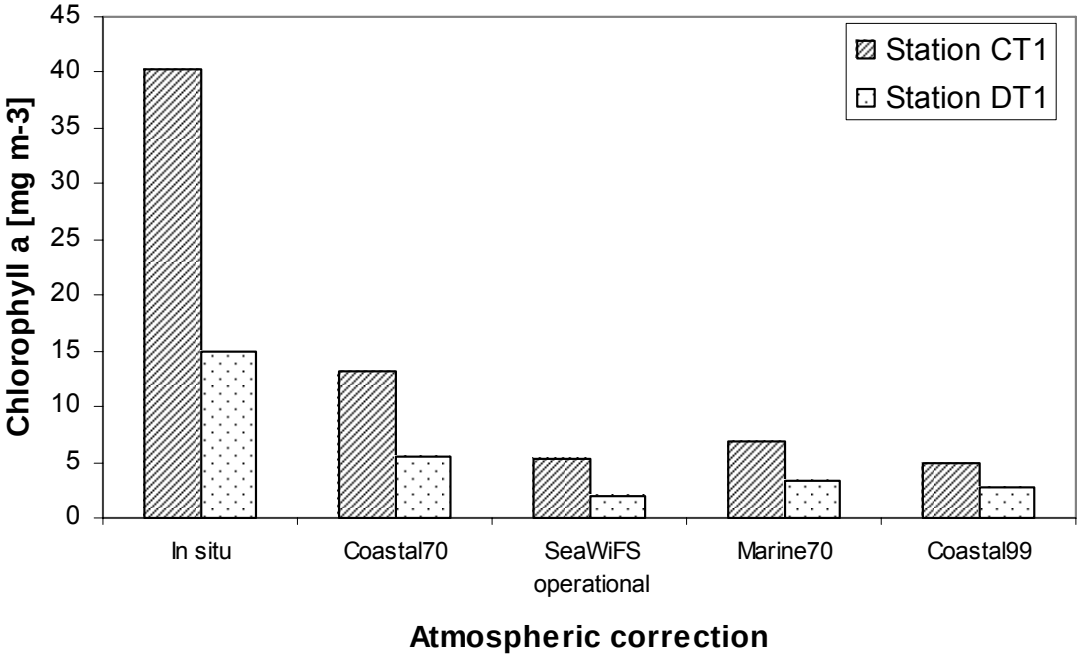

Figure 3. Comparison of OC4v4 Chl_{sat} calculated by means of four different atmospheric correction models with $\overline{Chl}_{insitu}$.

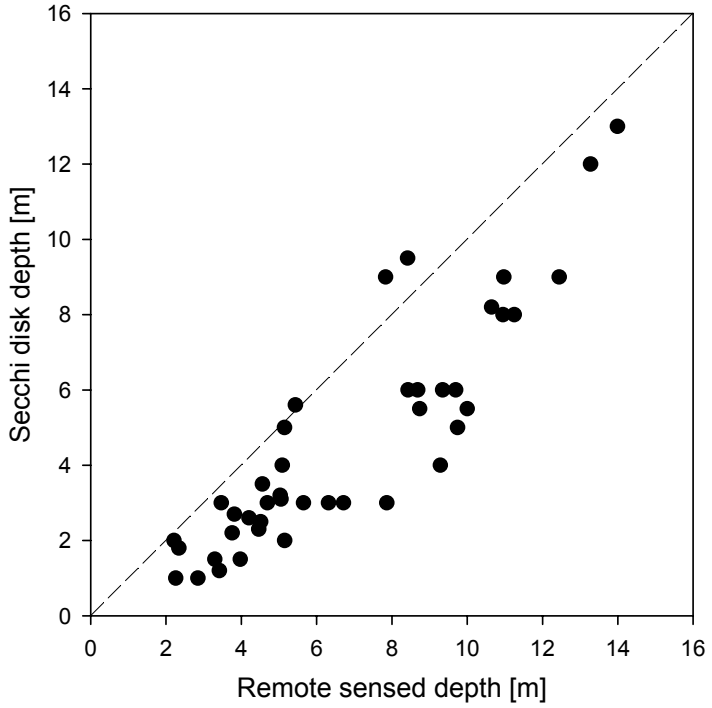

Figure 4. Comparison between satellite derived remote sensed depth and *in situ* measured Secchi disc depth in Sep2004, Sep2004 and NIMRD datasets.

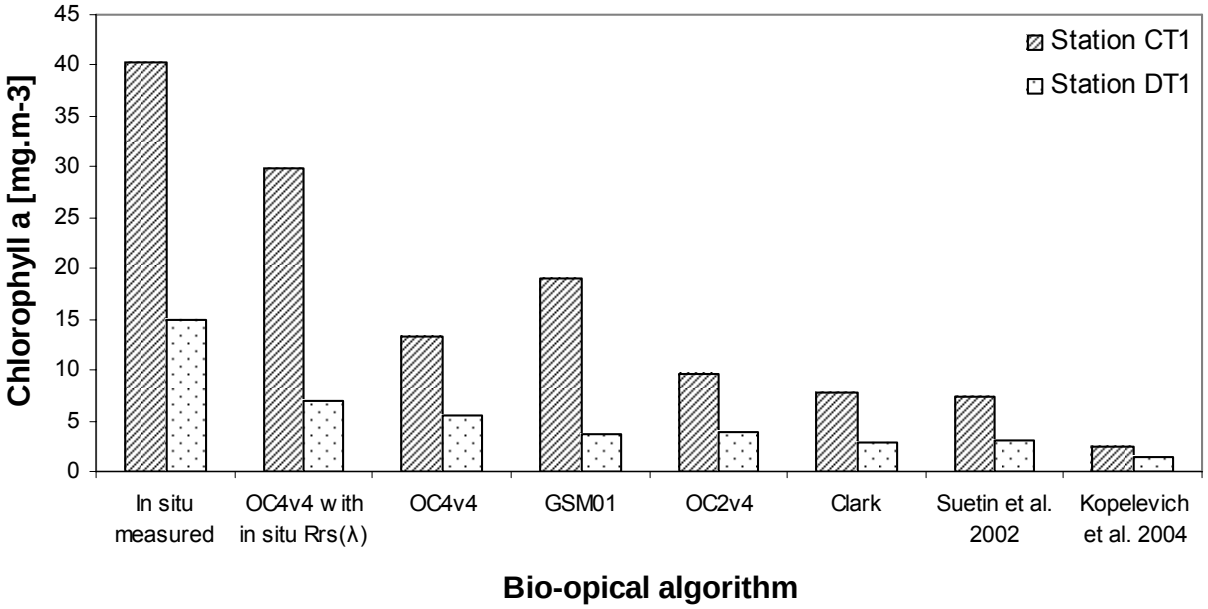

Figure 5. Comparison of Chl_{sat} calculated by means of 6 bio-optical algorithms, $\overline{Chl}_{insitu}$ and Chl_{sat} derived from the *in situ* measured $R_{rs}(\lambda)$ for the station CT1 and DT1.

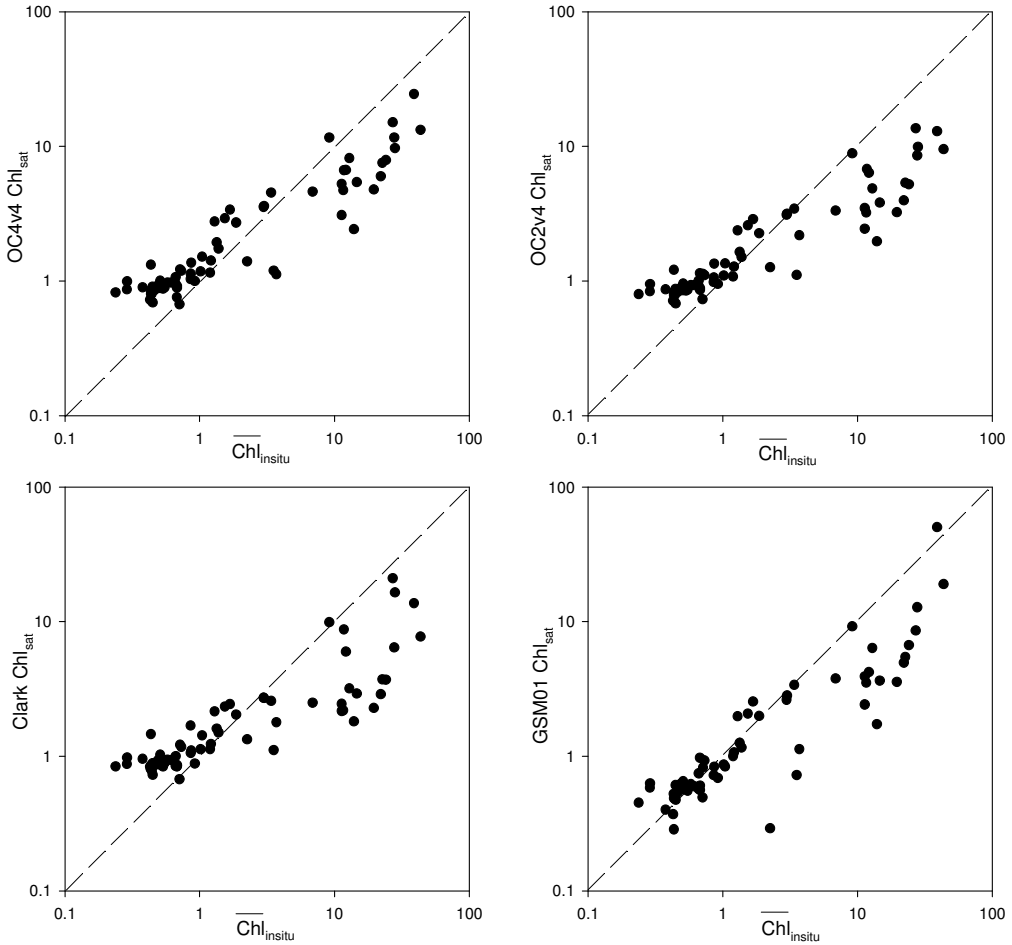

Figure 6. Comparison of Chl_{sat} calculated with four different SeaWiFS bio-optical algorithms (OC4v4, OC2v4, Clark and GSM01) with $\overline{Chl}_{insitu}$ from the Sep2002 and Sep2004 datasets in the western Black Sea.

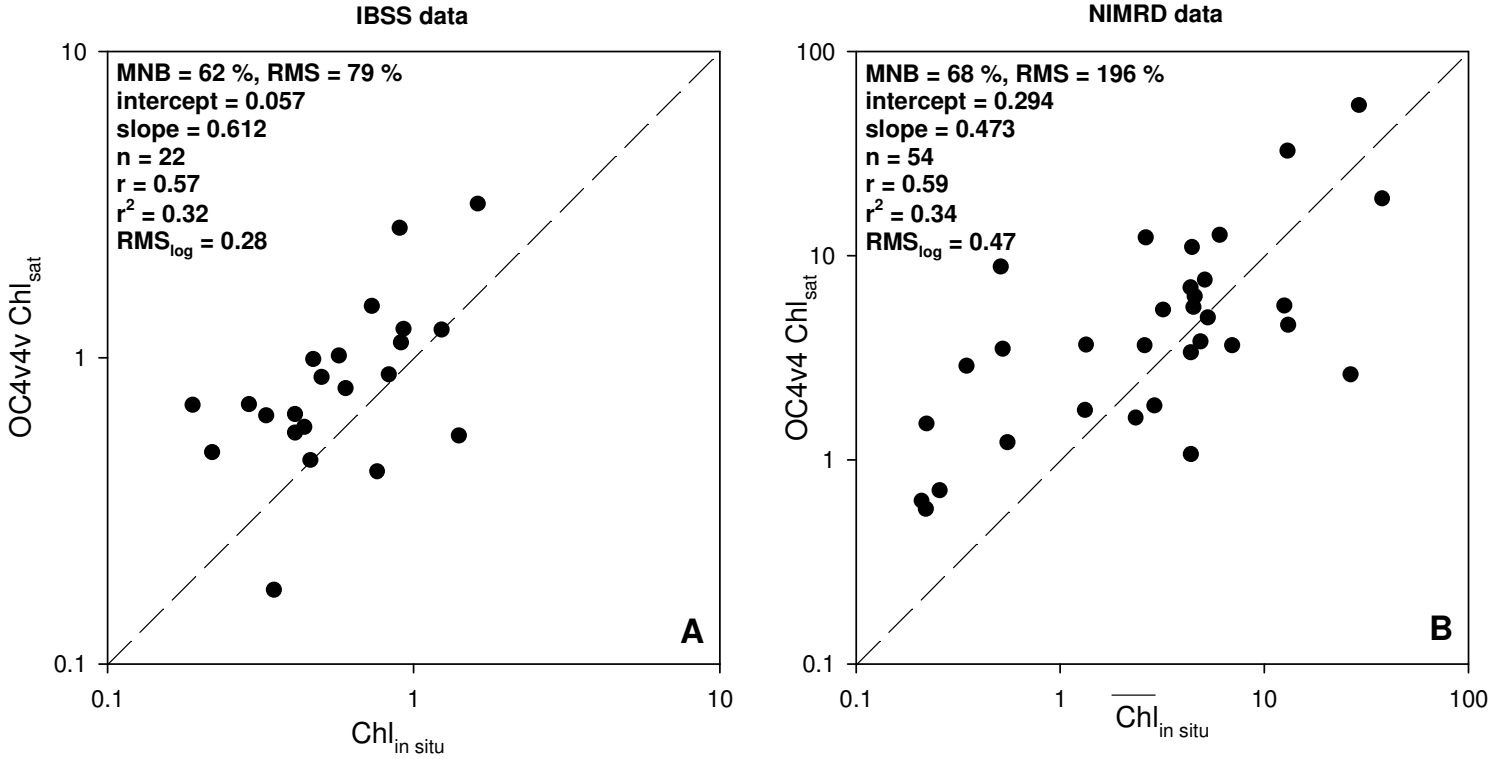

Figure 7 A,B. Comparison of the concurrent measurements of OC4v4 Chl_{sat} and Chl_{insitu} / $\overline{Chl}_{insitu}$ in:

A) Central and north-eastern part of the western Black Sea - IBSS dataset.

B) North-western part of the western Black Sea - NIMRD dataset.

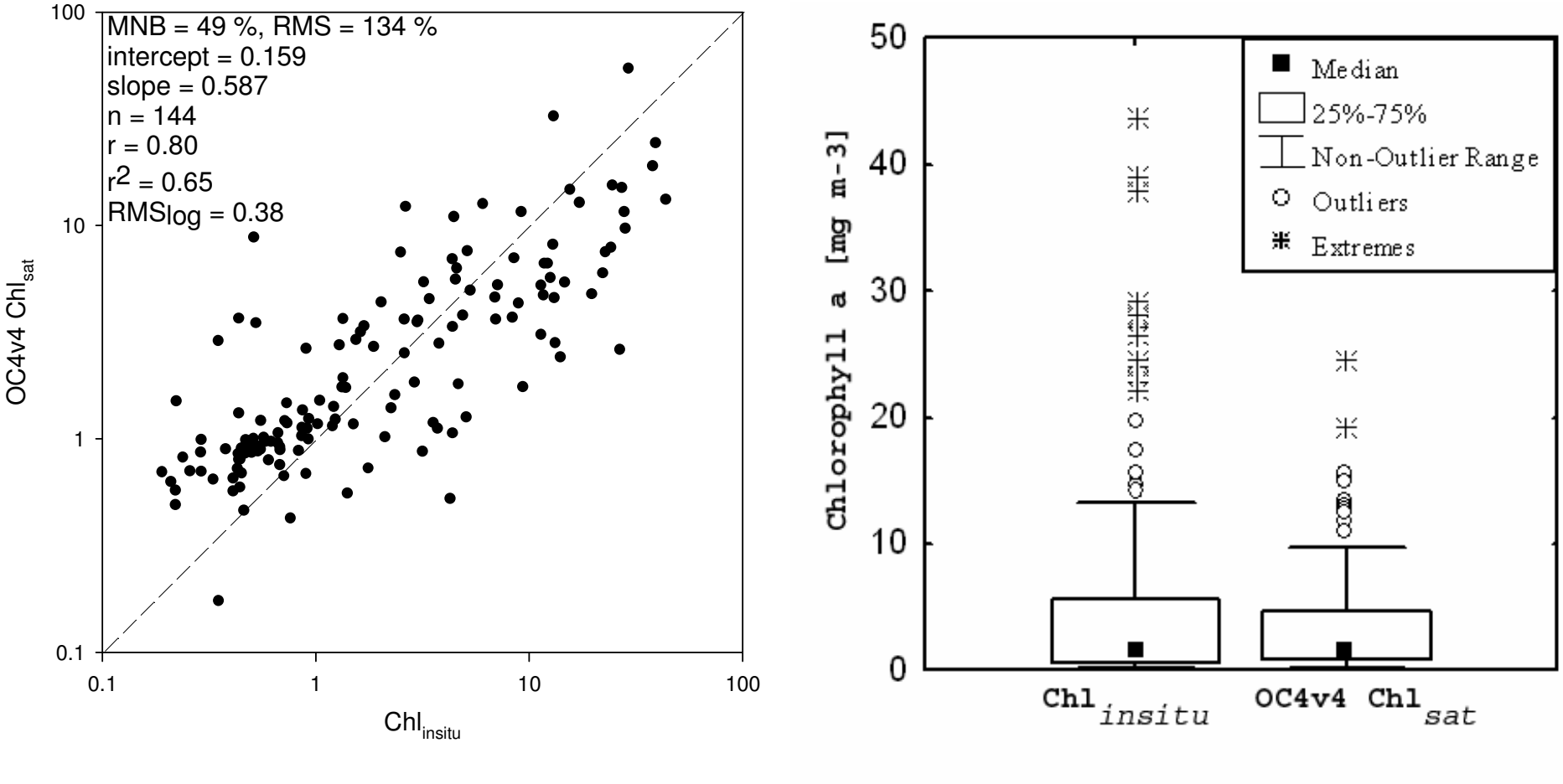

Figure 8 A,B. Performance of the satellite OC4v4 Chl_{sat} compared to $Chl_{insitu} / \overline{Chl}_{insitu}$ from the all four datasets. A) scatterplot and B) boxplot of the descriptive statistics.

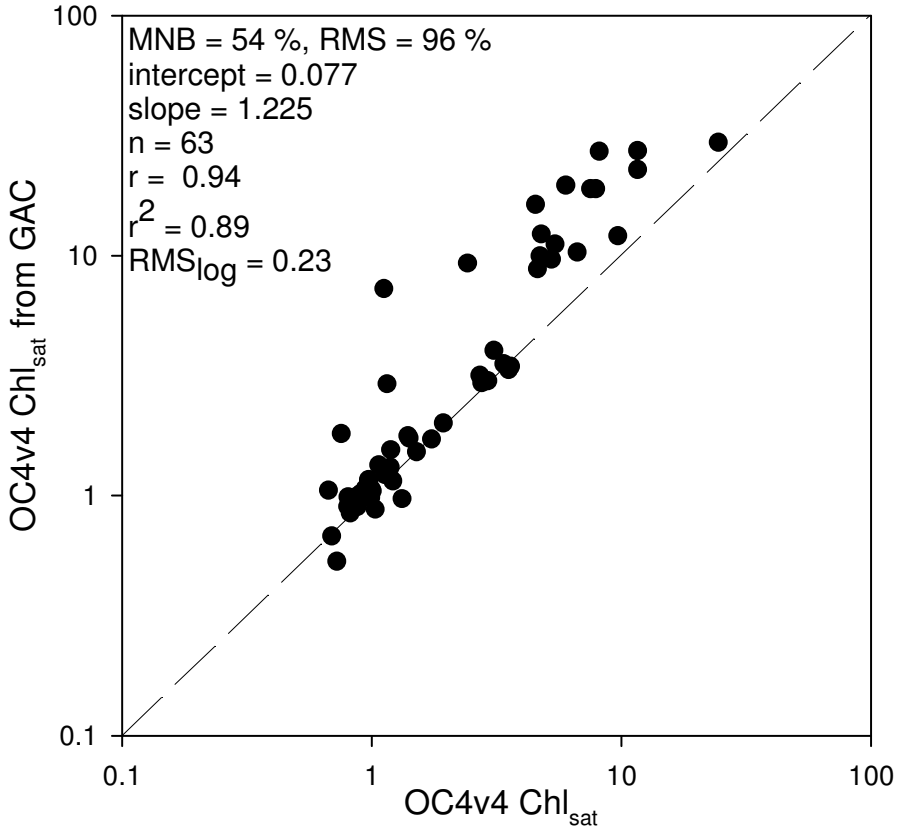

Figure 9. Comparison of the Chl_{sat} retrieved by the OC4v4 algorithm from full-resolution (1 km^2) and GAC (16 km^2 - global NASA ocean colour product) data.

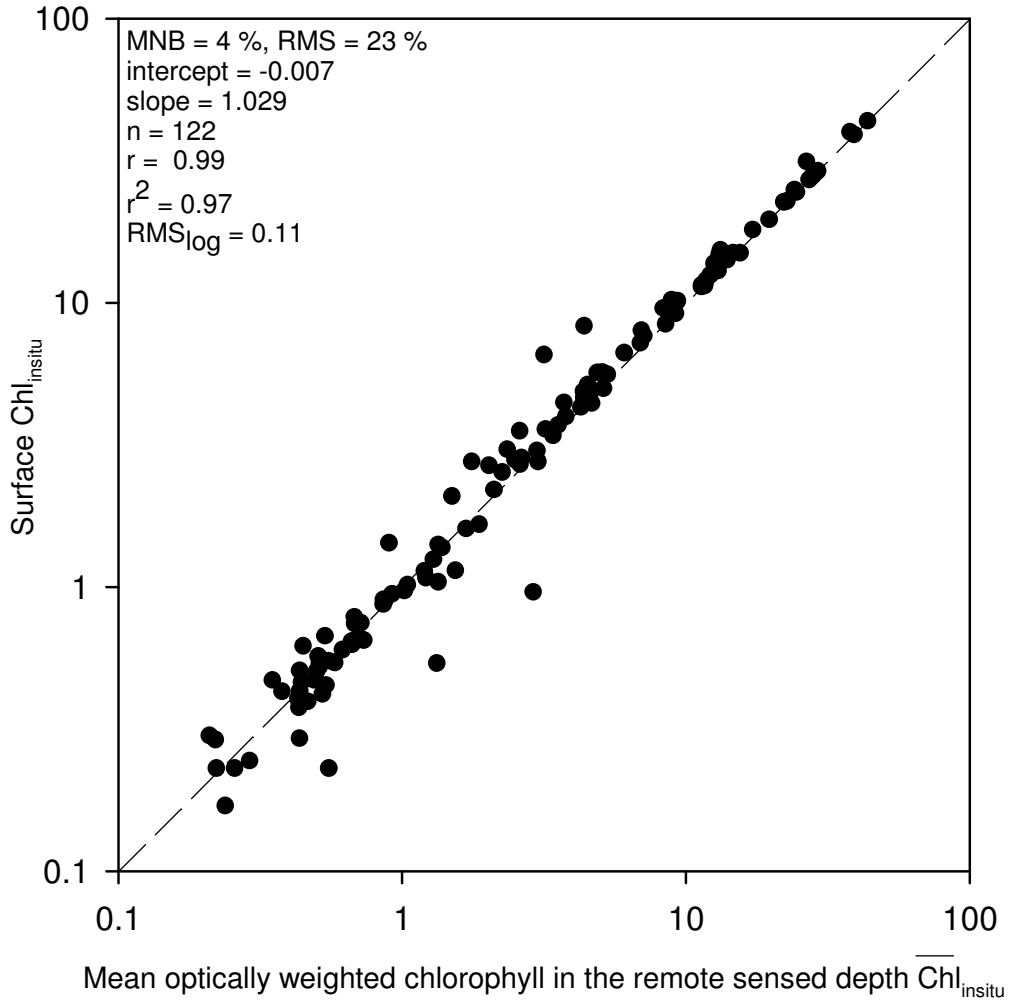

Figure 10. Comparison between $\overline{\mathrm{Chl}}_{\mathrm{insitu}}$ and $\mathrm{Chl}_{\mathrm{insitu}}$ in the western Black Sea.

List of figure captions

Figure 1. Map of the western Black Sea with sampling stations for Chl_{insitu} analysis within four datasets [Sep2002 (X), Sep2004 (O), IBSS (▲) and NIMRD (■)], which were used for the validation of the SeaWiFS derived Chl_{sat}. Additionally, on stations CT1 and DT1 matching up radiometrical measurements were accomplished.

Figure 2. Comparison of *in situ* measured $^{ex}L_{wn}(\lambda)$ calculated from mean $K_{Lu}(\lambda)$ and regression of $L_u(z, \lambda)$ with the four satellite derived $^{ex}L_{wn}(\lambda)$, calculated with the operational SeaWiFS atmospheric correction algorithm as well as with the atmospheric correction algorithm implementing three different fixed aerosol models on stations CT1 and DT1 (A,B). Comparison between the satellite $^{ex}L_{wn}(\lambda)$ derived with Coastal70 aerosol model and *in situ* measured $^{ex}L_{wn}(\lambda)$ from mean $K_{Lu}(\lambda)$ on stations CT1 and DT1 (C,D).

Figure 3. Comparison of OC4v4 Chl_{sat} calculated by means of four different atmospheric correction models with $\overline{Chl}_{insitu}$.

Figure 4. Comparison between satellite derived remote sensed depth and *in situ* measured Secchi disc depth in Sep2004, Sep2004 and NIMRD datasets.

Figure 5. Comparison of Chl_{sat} calculated by means of 6 bio-optical algorithms, $\overline{Chl}_{insitu}$ and Chl_{sat} derived from the *in situ* measured $R_{rs}(\lambda)$ for the station CT1 and DT1.

Figure 6. Comparison of Chl_{sat} calculated with four different SeaWiFS bio-optical algorithms (OC4v4, OC2v4, Clark and GSM01) with $\overline{Chl}_{insitu}$ from the Sep2002 and Sep2004 datasets in the western Black Sea.

Figure 7 A,B. Comparison of the concurrent measurements of OC4v4 Chl_{sat} and $Chl_{insitu} / \overline{Chl}_{insitu}$ in:

A) Central and north-eastern part of the western Black Sea - IBSS dataset.

B) North-western part of the western Black Sea - NIMRD dataset.

Figure 8 A,B. Performance of the satellite OC4v4 Chl_{sat} compared to $Chl_{insitu} / \overline{Chl}_{insitu}$ from the all four datasets. A) scatterplot and B) boxplot of the descriptive statistics.

Figure 9. Comparison of the Chl_{sat} retrieved by the OC4v4 algorithm from full-resolution (1 km^2) and GAC (16 km^2 - global NASA ocean colour product) data.

Figure 10. Comparison between $\overline{\mathrm{Chl}}_{\mathrm{insitu}}$ and $\mathrm{Chl}_{\mathrm{insitu}}$ in the western Black Sea.

List of abbreviations used

Abbreviation	***Full name***	***Units***
SeaWiFS	Sea-viewing Wide Field-of-view Sensor	
Chl_{sat}	satellite derived chlorophyll *a* concentration	[mg m^{-3}]
NIR	near-infrared radiation	[nm]
CDOM	coloured dissolved organic matter	
$L_w(\lambda)$	water-leaving radiance	[mW μm^{-1} sr^{-1}]
$L_{wn}(\lambda)$	normalized water-leaving radiance	[mW cm^2 μm^{-1} sr^{-1}]
Chl_{insitu}	*In situ* measured chlorophyll *a* concentration	[mg m^{-3}]
GAC	global area coverage	
${}^{ex}L_{wn}(\lambda)$	exact normalized water-leaving radiance	[mW cm^2 μm^{-1} sr^{-1}]
$\overline{Chl}_{insitu}$	*in situ* measured mean optically weighted chlorophyll *a* concentration in the remotely sensed depth	[mg m^{-3}]
$K_{Lu}(\lambda)$	vertical attenuation coefficient	[m^{-1}]
$E_s(0^+,\lambda)$	Above-water downwelling irradiance	[mW cm^{-2} nm^{-1}]
$L_u(z,\lambda)$	In-water upwelling radiance	[mW μm^{-1} sr^{-1}]
$R_{rs}(\lambda)$	remote sensing reflectance	[sr^{-1}]
F_0	sun irradiation on the top of the atmosphere	[μW cm^{-2} nm^{-1}]
SeaDAS	SeaWiFS Data Analysis System version 4.6 software	
coastal70	'coastal with 70% humidity'	
coastal99	'coastal with 99% humidity'	
marine70	'marine with 70% humidity'	
tropospheric70	'tropospheric with 70% humidity'	
NCEP	National Center for Environmental Prediction	
TOMS	Total Ozone Mapping Spectrometer	

$K_d(490)$	vertical attenuation coefficient at 490 nm	$[m^{-1}]$
MNB	mean normalized bias	
RMS	normalized root mean square	

Chapter III

Temporal and spatial variability of satellite-derived chlorophyll-a and primary production and their relation to physical factors in the western Black Sea

Alexander Davidov

Leibniz-Institute of Marine Sciences – IFM-Geomar, Kiel, Germany
Düsternbrooker Weg 20, 24105 Kiel, Germany
Email: adavidov@ifm-geomar.de

To be submitted to Marine Ecology Progress Series in June 2007 (manuscript).

Temporal and spatial variability of satellite-derived chlorophyll-a and primary production and their relation to physical factors in the western Black Sea

Alexander Davidov
Leibniz-Institut für Meereswissenschaften IFM-GEOMAR Kiel
Düsternbrooker Weg 20, 24105 Kiel, Germany
adavidov@ifm-geomar.de

Abstract

Nine years (Sep. 1997 – Oct. 2006) of SeaWiFS and MODIS ocean colour data are used to study the near-surface chlorophyll-a variability on seasonal and interannual timescales in the western Black Sea. The results suggest a classification of the western Black Sea into four different regions according to the amount and the variability of the surface chlorophyll-a: (1) waters directly influenced by the Danube river, (2) the north-western shelf, (3) the western and south-western shelf area and (4) the central part of the western Black Sea.

Two basic approaches (multiple linear correlation and empirical orthogonal function) are used for time-series analysis of satellite-derived chlorophyll-a, wind stress, sea surface temperature, photosynthetic available radiation, North-Atlantic Oscillation index and net primary production in four regions of the western Black Sea. The temporal and the spatial variability of satellite derived chlorophyll-a are high in all parts of the western Black Sea. Comparisons of the temporal pattern of chlorophyll-a to those of wind stress, SST, PAR and NAO anomalies display a distinct seasonal signal but also a significant amount of independent variability.

Furthermore, the results suggest that the interannual variability of chlorophyll-a is not related to a single factor, but to a bundle of factors, which impact varies in the different regions of the western Black Sea. The spatial analysis of chlorophyll-a in the four regions shows three EOF modes, which represent a rather independent variability in the central part and in the Danube influenced area as well as a coherent pattern in the shelf zones.

Between 26% and 65% of the entire western Black Sea area - depending on the seasons and river water discharge - can be considered as chlorophyll-rich waters (>1 mg m^{-3}). Very high chlorophyll *a* concentrations (>5 mg m^{-3}) were found only in the coastal regions close to the Danube river delta.

The mean annual succession of satellite derived chlorophyll-a in the central western Black Sea waters shows high values in autumn and spring, a moderate reduction of chlorophyll-a during winter and a late spring/ early summer increase (May-June). The late spring/ early

summer increase was more pronounced in the Danube influenced area and along the western and southern shelf compared to the central part.

KEY WORDS: Black Sea, chlorophyll, phytoplankton, remote sensing, SeaWiFS, primary production, time series

1. Introduction

The Black Sea is a semi-enclosed basin that receives a significant amount of nutrients mostly in its north-western part by the discharge of the rivers Danube (200 km^3 y^{-1}; about 60 % of the total river discharge into the Black Sea), Dnieper (43 km^3 y^{-1}) and Dniester (9.1 km^3 y^{-1}) (Jaoshvili 2002).

Considering the topography and its surface current system the Black Sea can be divided into an eastern and a western part. The circulation in the western Black Sea is dominated by the Rim Current, which is a cyclonic system with baroclinic and frontal instabilities, generating considerable short-term variability as well as seasonally varying mesoscale hydrographic structures (Oguz & Besiktepe 1999). The water exchange between shallow regions and the central deep part of the western Black Sea is complex mainly due to the instabilities of the frontal zone of the meandering Rim Current (Oguz at al. 1993).

The chlorophyll-a concentration is considered a main estimator of phytoplankton biomass and has been discussed in a variety of aspects including pattern of spatial distribution, seasonal and interannual variability in the Black Sea (Vedernikov and Demidov 1993, Yunev et al. 2002, Yunev et al. 2005). The biomass abundance and hence the concentration of chlorophyll-a is controlled by the availability of light and nutrients as well as the zooplankton grazing pressure. While the zooplankton grazing cannot be observed by satellite remote sensing, there are useful satellite-based estimations of light and some indicators for the nutrients availability. The satellite derived photosynthetic available radiation is a good estimation of the light conditions for primary productivity. The nutrients concentration cannot be measured by the satellite remote sensing, but its availability is also a function of the vertical water convection, which is determined by sea water temperature changes and/or wind stress.

The distribution of satellite-derived chlorophyll-a in the western Black Sea is rather heterogeneous. However, there are regions, which appear to have characteristic patterns. Therefore, the investigated area was divided into four regions of characteristic concentration, distribution and variability of Chl_{sat} (one central, two coastal and one river influenced) (Figure 1B). In the central western Black Sea (CWBS) the satellite-derived chlorophyll-a concentration is lower and the nutrients in the surface layer are made available mainly through seasonal, temperature-driven vertical water convection (Mashtakova and Roukhiyainen 1979, Mikaelyan 1997) as well as through remineralization and atmospheric input. The Danube river-load is the main supplier of nutrients in the Danube influenced area of the Black Sea (DA) (Cociasu et al. 1997). The North-Western Shelf (NWS) with its shallow water (depth less than 30 m in average) is supplied with nutrients by the rivers

Danube, Dnieper and Dniester as well as by temperature and wind induced vertical convection (Tolmazin 1985). The Western Shelf (WS) receives its nutrients from the vertical convection, land-based sources as well as from the Danube river water discharge.

The aim of this study is to describe the spatial pattern as well as the annual and the interannual variability of the surface chlorophyll-a between 1997 and 2006 in the western Black Sea and to examine its relation to the physical factors like sea surface temperature, light availability, surface winds and Danube river water discharge as well as the NOA index.

Furthermore, the aim is to describe the primary productivity of the western Black Sea as derived from satellite data and models, its magnitude and variability.

2. Data and Methods

2.1. Data

This study is based on satellite ocean colour data from Sea Wide-Field-of-view Sensor (SeaWiFS: McClain *et al.* 2004) and Moderate Resolution Imaging Spectroradiometer (MODIS-Aqua: Esaias *et al.* 1998). Both sensors have a spatial resolution of about 1.1 km at nadir and record images from the Black Sea between 09:00 and 12:00 GMT (11:00 and 14:00 local time) once per day. The ocean colour Level-1A data were obtained from the Ocean Colour Web of Goddard Space Flight Center at NASA (Feldman and McClain 2006).

2251 SeaWiFS (October 1997 - December 2004) and 435 MODIS (December 2004 – November 2006) full-resolution, daily images for the period between October 1997 and November 2006 have been processed and analyzed for the determination of satellite derived chlorophyll-a concentration (Chl_{sat}, mg m^{-3}).

For the estimation of the quality and availability of the SeaWiFS satellite data, the detection of the regions with characteristic pattern as well as the extension of the high-chlorophyll-a waters in the western Black Sea a preliminary study with SeaWiFS data collected between 1998 and 2003 was completed.

The SeaWiFS and MODIS data were processed and analysed using the SeaWiFS Data Analysis Software (SeaDAS: Fu *et al.* 1998) version 5.05 with MSL12 version 5.5.9.

The remotely sensed reflectance was calculated after applying the atmospheric correction (multi-scattering mode including coastal aerosols and 70% humidity) scheme according to Gordon and Wang (1994) and Wang (2000), which was found to perform best in the western Black Sea (Davidov submitted). For the calculation of the Chl_{sat} from the remotely sensed reflectance, the maximum band ratio (OC4v4) algorithm, as described by O'Reilly *et al.* (2000), was used for SeaWiFS data. The OC4v4 algorithm was found to retrieve *in situ* measured chlorophyll-a concentrations on the 68 stations measured in 2002 and 2004 in the western Black Sea with a mean systematic error (MNB) of 30% and a random error (RMS) of 77% (Davidov submitted). The MODIS Chl_{sat} was calculated with the maximum band ratio OC3M algorithm (O'Reilly *et al.* 2000).

Daily composite images were created when more than one scene for a single day was available. In order to reduce gaps in the time series the full-resolution data were binned into 9x9 km grids and the monthly mean value was calculated from all existing daily images for the corresponding month of the year. Because most of the approaches for time series analysis require evenly spaced data without gaps, the median value for each of the four predefined

regions was calculated from all valid pixels in the region. It was observed (Davidov submitted) that the chlorophyll-a values (*in situ* measured as well as satellite retrieved) in the western Black Sea exhibit a lognormal distribution. For this reason the median instead of the mean have to be used to represent the spatially and temporally averaged Chl_{sat} values as well as for statistical analysis (Campbell *et al.* 1995). Therefore, for the description of the annual and interannual variability in the four different regions of the western Black Sea, monthly median Chl_{sat} time series were used. Even after this pre-processing no useful Chl_{sat} data were available for January 1998 and August 1999. The missing datapoints were therefore filled in by means of simple interpolation.

The averaging of Chl_{sat} by calendar months over the 9-year period produced a "climatological" cycle of mean annual succession.

For the retrieval of the area occupied by the eutrophic (> 1 mg m^{-3}) and very high-chlorophyll (> 5 mg m^{-3}) waters in different seasons only images with more than 75 % of the total area visible were used in order to avoid uncertainties caused by the partly cloud-covered images.

The monthly AVHRR (1997-2002) and MODIS 11-µm (2003-2006) sea surface temperature (SST, °C) time series produced by the Ocean Productivity group at Oregon State University was used.

Wind data at 1° spatial resolution from the National Center for Environmental Prediction (NOAA), USA were obtained from Goddard Space Flight Center. The wind velocity (m s^{-1}) was calculated from the zonal and meridional component of the 10 m wind at the spatial centers of the four regions. The neutral wind stress (N m^{-2}) was calculated according to Large and Pond (1981).

A 9-year time series of monthly ocean net primary production (NPP, mg C m^{-2} day^{-1}) data calculated with the Vertically Generalized Production Model (VGPM) (Behrenfeld and Falkowski, 1997) was provided by Robert O'Malley, Oregon State University, USA, (http://web.science.oregonstate.edu/ocean.productivity/). The VGPM is a „chlorophyll-a based" model that estimates net primary production as a function of chlorophyll-a, available light, and the photosynthetic efficiency. Monthly NPP time series data were calculated from Chl_{sat}, SST, and SeaWiFS cloud-corrected incident daily photosynthetic active radiation (PAR, Einstein m^{-2} day^{-1}). Euphotic depths were calculated from Chl_{sat} according to Morel and Berthon (1989).

PAR monthly fields were calculated by NASA from SeaWiFS data with the Frouin algorithm (http://oceancolor.gsfc.nasa.gov/DOCS/seawifs_par_wfigs.pdf).

The North Atlantic Oscillation (NAO) index is one of the most prominent teleconnection patterns in all seasons (Barnston and Livezey, 1987). The NAO consists of a north-south dipole of anomalies, with one center located over Greenland and the other center of opposite sign spanning the central latitudes of the North Atlantic Ocean between 35°N and 40°N.

NAO is associated with temperature and precipitation patterns in the Black Sea area (Oguz 2005). Strong positive phases of the NAO are associated with below-average temperatures and below-average precipitation. Opposite patterns of temperature and precipitation anomalies are typically observed during strong negative phases of the NAO. Monthly NAO time series were obtained from the Climate Prediction Center, National Center for Environmental Prediction (NOAA)

(ftp://ftp.cpc.ncep.noaa.gov/wd52dg/data/indices/tele_index.nh).

Monthly Danube river water discharge data [km^3 $month^{-1}$] for the period October 1997 – December 2003, measured by the National Marine Institute for Research and Development in Constanta, Romania were obtained from the EU-Project "Nutrient Management in the Danube Basin and its Impact on the Black Sea" (*daNUbs).*

2.2. Temporal analysis

A multiple linear correlation of all variables of each single region was applied in attempt to retrieve the relation between the variables and their temporal variability.

The "long term" of Chl_{sat} was displayed by calculating a mean annual value for each region.

On every single time series of Chl_{sat}, SST, PAR and wind stress, a temporal normalization (1) of the data was applied. The temporal normalisation includes the subtractions of the mean time series value from each time series element (anomaly) and the division by the standard deviation of the time series (Fuentes-Yaco et al. 1997).

(1) $$x_{i\_norm} = \frac{(x_i - \bar{x})}{s}$$

This transformation reduces the prevailing seasonal signal as well as the high variability in some time series without completely damping out the anomalies. Furthermore, the normalisation allows to combine different time series like Chl_{sat}, SST, PAR and wind stress, which normally have a different order of magnitude. The temporal variability was analysed by means of empirical orthogonal function (EOF), which was first applied to geophysical data by Lorenz (1956). EOF analysis is a useful technique for reducing the spatial and temporal variability of time series data to the most energetic statistical modes. While statistical modes do not necessarily correspond to direct physical forcing mechanism (Dommenget and Latif, 2002), partitioning the spatial and temporal variance into modes reveals spatial functions

which have time-varying amplitudes that can be interpreted in relation to physical processes (Yoder 2002). Eigenvalues can be considered as the portion of the total variance explained by EOF, where the sum of the variances in the data equals the sum of the variance in the eigenvalues. EOF analysis requires equally distributed measurements in the time series and does not tolerate missing data.

For the detection of periodicities in the CWBS Chl_{sat} time series, we use fast Fourier transformation (periodogram). For separation of the dominating cycle, the Chl_{sat} time series were log-transformed and median-filtered.

2.3. Spatial analysis

For the analysis of the spatial variability, a multiple linear correlation was applied to the 9-year Chl_{sat} time series of the four regions.

For the analysis of the spatial variability by means of EOFs, following pre-treatment [spatial normalization - (2)] was applied.

$$(2)\quad x_{i\_norm} = \frac{(x_i - \overline{x}_{i\_mean})}{s_i}$$

The time interval mean (spatial - calculated from all regional values of corresponding month) was subtracted from each time series element and then divided by the standard deviation of the time interval before computing eigenvectors and amplitude time series (Fuentes-Yaco et al. 1997). This normalisation allows combination of regions with very different variance in statistical analysis.

3. Results

3.1 Quality of the SeaWiFS (1998-2003) data

From the daily SeaWiFS overpasses over the western Black Sea, only 42 % of the data (in average 155 days per year) were usable, due mainly to cloud-cover.

The usable daily data were not equally distributed over the year (Table 1). On average 40 % of the images used were recorded during summer months (June, July and August), 27 % in springtime (March, April and May) and 20 % in autumn (September, October and November). Only 13 % of the satellite images used were recorded during winter (December, January and February). However, there is a strong variation in different years. In 1998 about 51 % of the images used were recorded during the three summer months, while in 2002 all four seasons were more equally represented with a coverage between 20 % in winter and 31 % in summer.

[insert table 1 about here]

The quality of the daily satellite images used depends strongly on the cloud-cover, but also on the marine aerosols, haze and disturbances of the radiometer. The quality of the Chl_{sat} from any particular image cannot be estimated as very few *in situ* data synchronous to the satellite images were available. The quality of the satellite images is hereafter defined only by the size of the area, where the surface pattern is visible. During the summer months about 55 % of the images were of good quality (more than 67 % of the western Black Sea surface pattern visible), 31 % were of moderate quality (between 33 % and 67 % of the area visible) and only 14 % were of poor quality (less than 33 % of the area visible) (Table 1). In spring and autumn the number of images of good, moderate and poor quality is almost equal. In wintertime, when only a few satellite images (13 %) were useable, 8 % of them were of good, 29 % of moderate and 63 % of poor quality.

3.2 Regions with characteristic pattern of the SeaWiFS Chl_{sat} in the western Black Sea

The analysis of Chl_{sat} in the western Black Sea shows, that its concentration, distribution and variability exhibit different characteristic patterns in different areas. The mean Chl_{sat} for the period 1998-2003 show a significant difference in the pattern between the central deep part of the western Black Sea and the coastal area (Figure 1A). A pronounced gradient between coastal and offshore waters was found at 1 mg m^{-3} Chl_{sat}, which to a large extend coincide well with the 200 m depth line.

[insert figure 1 about here]

Within the coastal area a characteristic Chl_{sat} pattern was found in the following regions: 1) over the north-western shelf, 2) in the Danube influenced Black Sea waters and 3) over the western and southern shelf. The boundaries of these areas were defined mainly according to the coefficient of variation of Chl_{sat}. In the Danube influenced area, the coefficient of variation exceeds 80 % due to the considerably higher variance compared to the remaining shelf area resulting from the temporal and spatial variation of the Danube river plume (Figure 1A). The north-western shelf is also stronger affected by river-water and therefore has a higher variance and higher Chl_{sat} than the western and the southern shelf.

Considering these criteria the western Black Sea was divided into four characteristic regions (Figure 1B):

1. North-western shelf (NWS) - (approx. 26 000 km^2) north of 45° N covering the north-western shallow shelf area which is influenced by the Danube river plume at southerly winds/ northern currents as well as by the rivers Dniester and Dnieper. In this region, high Chl_{sat} values can be observed almost throughout the year.

2. Danube influenced area (DA) - (approx. 34 000 km^2) covering the area off the Danube delta, which is directly affected by the river water and which is defined as an area with coefficient of variation higher than 80%. Phytoplankton production processes in this region are strongly determined by the inflow and advection of nutrient-rich river waters.

3. Western and southern shelf (WS) - (approx. 36 000 km^2) including the coastal waters of the narrow shelf belt along the western and south-western Black Sea coast. The phytoplankton productivity in this region is characterized by smaller freshwater inlets and vertical mixing processes.

4. Central western Black Sea (CWBS) - (approx. 104 000 km^2) covering the central area of the western Black Sea including the Rim Current and part of the Crimea-induced eddy strait in its northern and north-western part. The central part of the western Black Sea exhibits generally low Chl_{sat} with exception of the areas of instability, which are partly affected by pigment-rich waters from the north-western shelf and the Danube influenced area and partly by vertical nutrient transport as a consequence of fronts and eddy formation.

Due to strong advection in the western Black Sea, an overlapping of these regions must be considered.

3.3 Spatial distribution of the Chl_{sat} in the western Black Sea (1998-2003)

The size of the area covered by high-chlorophyll waters (>1 mg m^{-3}) varies between 26 % (August) and 65 % (November) of the western Black Sea area (Figure 2). The area in front of the Danube delta as well as most of the north-western shelf and parts of the western shelf can be considered as continuously eutrophied. In May, June, October and November more than 40 % of the western Black Sea can be classified as high-chlorophyll waters. Lower values are observed in March, July and August. The areas with frequent phytoplankton blooms (>5 mg m^{-3}) were found close to the coast in front of the rivers Danube, Dnieper and Dniester throughout the year.

[insert figure 2 about here]

3.4. Temporal variability in the CWBS area

The variability of Chl_{sat} in the CWBS is characterized by high annual and interannual variations (Figure 3A). Within a year, the prevailing pattern is dominated by higher values in fall and winter (0.8 – 1.5 mg m^{-3} in different years) and rather a slight or absent increase (0.4 – 0.5 mg m^{-3}) in summer. However, the patterns in the years 1999, 2000 and 2001 are characterized by a more or less strong increase in early summer (May-June), when also the highest Chl_{sat} values are observed (0.9 – 1.8 mg m^{-3}). The interannual variability is determined not only by different annual patterns but also by the magnitude of Chl_{sat}. Mean annual Chl_{sat} is higher in the beginning (1998-2001) of the investigated period with a considerable reduction between 2002 and 2005. In 2006, there are signs of a slight increase. Therefore, the long-term changes may rather be an oscillation than a trend with a half-period of 4-5 years.

[insert figure 3 about here]

The SST time series shows a distinct seasonal variability but the temporal pattern has a slight shift in the phase ($^1/_4$ month) and significant differences in the winter SST magnitude (8.5 °C in Feb. 2001 and 5.2 °C in Feb. 2003) are obvious from year to year (Figure 3B). The wind stress time series shows a very high variability but without recognizable seasonal pattern. There is one unusual long period of low wind stress between Nov. 2000 and May 2001.

There is a significant negative correlation coefficient (-0.31) between Chl_{sat} and PAR (Table 2C) and a positive correlation (0.69) between PAR and SST (seasonality). There are also significant correlations between SST and wind stress (0.33) as well as SST and NAO (-0.22). The time series of NPP shows a negative significant correlation to the NAO (-0.23).

[insert table 2 about here]

The eigenvalues resulting from the EOF analysis of temporal normalized Chl_{sat}, SST, PAR and wind stress time series show that mode 1 explains 47.5 %, mode 2 - 25 % and mode 3 - 21.5 % of the variability in the CWBS (Table 2A). The first mode despite the pre-treatment (normalization) of the time series is obviously explaining the seasonality (Figure 3G), and is determined mostly by the SST and PAR time series (Table 2B). The second and the third mode (Figure 3EF) consider more the variability of Chl_{sat} and the wind stress time series, where mode 2 has several inverse peaks corresponding to those of the wind stress time series, while mode 3 coincides with the summer Chl_{sat} peaks in 2000 and 2001 and the fall peak in 2002 (weighting factors in Table 2B).

The time series of NPP displays an obvious seasonal pattern with high values between May and October and a maximum of about 1500 mg C m^{-2} day^{-1} in June (Figure 3D). A distinct peak is observed in June 2001 (3475 mg C m^{-2} day^{-1}), and to a lesser extend in May 2000 (2253 mg C m^{-2} day^{-1}), where the unusual high Chl_{sat} complements to the PAR availability.

The results show no evidence for a direct link between the NAO and the Chl_{sat} time series.

3.5. Temporal variability in the NWS area

There is a very high annual and interannual variability of Chl_{sat} in the NWS region (Figure 4A). No distinct annual pattern typical for the whole 9-year period can be recognized. Low values between January and May and high values between June and December are found in 1998, 2004 and 2006. In 1999, 2000 and 2003 there are high values in summer (with the 9-year maximum of 4.5 mg m^{-3} in June 2000) and lower in fall, winter and spring. In 2001 and 2002, the Chl_{sat} time series show two increases. The magnitude of the Chl_{sat} differs also significantly from year to year. In 2000 the concentration does not decrease under 1.5-1.9 mg m^{-3} during the whole year, while in 2002 1.8 mg m^{-3} is the maximum observed in February.

Mean annual Chl_{sat} in the NWS was higher in the beginning (1998-2000) of the investigated period with a significant reduction between 2001 and 2003. In 2004 and 2005, there is an increase.

The SST time series shows a distinct seasonal variability and the winter SST differs significantly from as high as 7.5 °C in February 2001 to as low as 2.8 °C in February 2006 (Figure 4B). The wind stress time series shows a very high variability but without seasonal pattern. There are two longer periods of relative high wind stress in winter 1999 to 2000 and summer 2000.

[insert figure 4 about here]

There is significant correlation (0.22) between Chl_{sat} and SST (Table 3C) as well as positive correlation (0.69) between PAR and SST (seasonality). There is also significant correlation

between SST and NAO (-0.22). The time series of NPP correlate significant with NAO (-0.19).

[insert table 3 about here]

The eigenvalues resulting from the EOF analysis of temporal normalized Chl_{sat}, SST, PAR and wind stress time series show that mode 1 explains 43.5 %, mode 2 – 27.7 % and mode 3 - 21.9 % of the variability in the NWS (Table 3A). The first mode is reflecting the seasonal pattern (Figure 4G) and is determined mostly by the SST and PAR time series (Table 3B). Second and third mode (Figure 4EF) are determined mostly by the variability of Chl_{sat} and wind stress time series. Similar to the CWBS area, mode 2 is defined by the negative weighting factors of Chl_{sat} and wind stress therefore shows inversed peaks of time series (Figure 4F). The mode 3 is determined by the negative factors for Chl_{sat} and the positive for wind stress.

The time series of NPP display obvious seasonal patterns with high values between May and October and a maximum of about 4000 mg C m^{-2} day^{-1} in June (Figure 4D). A distinct peak is observed in June 2000 (6496 mg C m^{-2} day^{-1}), where the unusual high Chl_{sat} complements the PAR availability. Lowest values in the high productive seasons are observed in June 2002 (3272 mg C m^{-2} day^{-1}).

3.6. Temporal variability in the WS area

The annual variability of the Chl_{sat} in the WS area is characterized by two increases: spring/summer (April – June) and autumn/winter (September – February) (Figure 5A). The interannual variability is distinct and in the years 1998, 2001, 2004 and 2006 the spring/summer increase is stronger than the autumn/winter one, while in 1999, 2002 and 2005 the latter predominate. The highest value is observed in May 2001 (2.65 mg m^{-3}) and the lowest in August 2003 (0.5 mg m^{-3}). The differences in the mean annual Chl_{sat} are observed with higher values (1.6 – 1.9 mg m^{-3}) in the beginning of the period (1998-2001) and with lower values (1.1 mg m^{-3}) at the end of the period (2002-2005).

[insert figure 5 about here]

The variation of the SST time series is most evident in the winter months (Figure 5B). The warmest winter month is February 2001 (9 °C) and the coldest winter month is February 2003 (4.3 °C).

The wind stress time series shows higher values in winter (December – February) and rather calm summers (Figure 5B). Distinct maxima are observed in the winters of the years 1999, 2002, 2003 and 2006.

Appart from the positive correlation between PAR and SST (0.68), there is a significant but lower negative correlation between PAR and Chl_{sat} (-0.19), PAR and wind stress (-0.28) and NAO and NPP (-0.21)(Table 4C).

[insert table 4 about here]

The eigenvalues calculated with EOF analysis of the time series show that mode 1 explains 46.7 %, mode 2 – 23.6 % and mode 3 - 22.2 % of the variability in the WS (Table 4A). The first mode is clearly reflecting the seasonal pattern despite the pre-treatment (Figure 5G) and is determined mostly by the SST and PAR time series (Table 4B). The second mode is positively determined by the Chl_{sat} and the third mode is determined mostly by the variability of wind stress time series (Figure 5EF, Table 4B). The mode 2, although by definition complete uncorrelated to the mode 1 also shows seasonal pattern and high interannual variation. On the mode 3 amplitudes, one can recognise many features of the wind stress time series. There is a rather independent variability of PAR-SST, Chl_{sat} and wind stress in the WS region.

The time series of NPP in the WS region (Figure 5D) shows a clear seasonal pattern but different to the other three regions there is a distinct double peak with a slight decrease in-between, which is due to the decrease in Chl_{sat} in July-August and also to photosynthetic efficiency suppression by high SST. The most productive month is June 2001 (4160 mg C m^{-2} day^{-1}) and the least productive year is 2003, where the maximum in June reaches only 2360 mg C m^{-2} day^{-1}.

3.7. Temporal variability in the DA area

The time series of Chl_{sat} in the DA region is characterized by higher values than the other three regions (Figure 6A). The maximum observed in June 2000 is 5.96 mg m^{-3} and the minimum in January 2004 is 0.5 mg m^{-3}. The annual succession is characterised by between one (2003) and four (2000) increases per year with the most pronounced one in May – June. The interannual variation is high considering both, the single annual successions and the mean annual Chl_{sat}. Still the trend is similar to those in the other regions of the western Black Sea.

The SST time series shows a distinct seasonality (Figure 6B). The wind stress displays generally high values in winter and lower values in summer, but some exceptions are observed in 1999, 2000 and 2005.

[insert figure 6 about here]

The Danube river water discharge (Figure 6C) has a distinct seasonality but varies in magnitude from year to year. Both years 1999 and 2000, which have the highest discharge coincide with the years with the highest values of Chl_{sat}.

The Chl_{sat} time series correlates significantly to the PAR (0.3) and the Danube river water discharge (0.33) and correlate negatively to the wind stress (-0.19) (Table 5C). The wind stress time series also correlates to NAO (0.21) as well as negatively but significant to SST (-0.29), PAR (-0.41) and NPP (-0.35).

[insert table 5 about here]

The eigenvalues from the EOF analysis of the time series show that mode 1 explains 51.6 %, mode 2 – 23.1 % and mode 3 - 18.5 % of the variability in the WS (Table 5A). The first mode shows the seasonal pattern (Figure 6G) and is determined (negatively) mostly by the SST and PAR time series (Table 5B). The second mode is positively determinated by the Chl_{sat} and the third mode – negatively by the wind stress variability (Figure 6EF, Table 5B).

The time series of NPP in the DA region (Figure 6D) shows clear seasonal pattern with pronounced peaks in June. The most productive month is June 2000 (6981 mg C m^{-2} day^{-1}) but in all years the NPP is the highest (> 4200 mg C m^{-2} day^{-1}) in the western Black Sea.

3.8. Mean annual succession of Chl_{sat} and NPP in the western Black Sea

The annual succession of Chl_{sat} in CWBS and WS is characterized by high values (approximately 0.9 mg m^{-3} in CWBS and 1.5 mg m^{-3} in WS) in autumn/winter (October to March), decreases in April (0.6 in CWBS and 1.2 in WS) and August (0.59 in CWBS and 1.0 in WS) and a single increase in May-June (0.8 in CWBS and 1.7 in WS) (Figure 7A). In the DA region, the increase in May-June (up to 3.3 mg m^{-3}) is more pronounced than during the remaining year (between 1.5 and 1.9 mg m^{-3}). In the NWS the annual succession is similar in magnitude and course to that in the WS, except that the values from June throughout September remain high (1.66 -1.8) and the summer decrease is absent.

[insert figure 7 about here]

The variation of the "climatological" NPP in the western Black Sea shows that despite the winter Chl_{sat} maximum, increased primary production takes place between May and October in all four regions (Figure 7B). The distinct peak is observed in June in all four regions and reaches as much as 1924 mg C m^{-2} day^{-1} in CWBS, 3296 mg C m^{-2} day^{-1} in WS, 4342 mg C m^{-2} day^{-1} in NWS and 5680 mg C m^{-2} day^{-1} in DA. This is also the ranking of the regions according to their productivity rates.

3.9. Spatial variability of Chl_{sat} in the western Black Sea

There is a significant positive correlation of the Chl_{sat} time series between neighbouring regions of the western Black Sea (Table 6). The highest correlation coefficient is found between CWBS and WS (0.54), and also NWS and DA (0.48) show significant correlation. Weaker are the correlations between CWBS and NWS (0.33) as well as WS and DA (0.32).

The weakest but still significant (n=110, $p<0.05$) is the correlation between CWBS and DA (0.27). There is no correlation between the region NWS and WS, which also do not have a common border.

[insert table 6 about here]

[insert table 7 about here]

The spatial normalized Chl_{sat} time series analysis with EOF show that there are three modes that explain 100 % of the variability (Table 7). Mode 1 explains 42 % of the variability and is mainly determined by the variability of NWS and WS but with opposite sign. Mode 2, which explains 33 % of the variability is determined by the DA (weighting factor of 0.96) and partly by the NWS (weighting factor of -0.58), while mode 3 (25%) is determined by the CWBS (0.95).

The periodogram of the Chl_{sat} time series of the CWBS area shows several peaks, but the maximum is at 12 months, which shows that the annual cycle is the dominant period of variability (Figure 8).

[insert figure 8 about here]

4. Discussion and conclusions

4.1. Data and methods

On average the pattern of Chl_{sat} in the western Black Sea could be observed from the SeaWiFS satellite sensor on 155 days per year. Previous descriptions of the annual succession of phytoplankton standing stock of the western Black Sea were mostly based on a temporally and spatially limited number of *in situ* measurements. The approach to retrieve the annual succession of chlorophyll *a* in the Black Sea from multi-year *in situ* datasets has been used by several authors; most recently by Yunev *et al.* 2002 and Chu *et al.* 2005. However, these approaches apparently cannot sufficiently consider the high regional, annual and interannual variability of phytoplankton standing stock in the western Black Sea, as demonstrated in this study. The reconstruction of the annual succession from synoptical satellite observations appears to be more realistic. However, with the interpretation of the annual succession derived from satellite data the following limitations should be considered:

1. Cloud-free satellite images are not equally distributed over the year and the variability of the winter Chl_{sat} in the western Black Sea is frequently underrepresented. The main reason for the missing satellite data is cloud cover. Therefore, when analysing Chl_{sat} and physical satellite derived parameters one should consider that cloud cover is a frequent weather condition in that area and not only the Chl_{sat} information, but also the (typical) physical forcing is missing during cloudy events.

2. The Chl_{sat} represents the mean optically weighted chlorophyll-a concentration in the remote sensing depth (25% of the first optical depth) and therefore deeper chlorophyll-a maxima cannot be registered. This is especially relevant for the central part of the western Black Sea in late spring and during the summer months, when deep chlorophyll-a maxima in depths up to 50 m have been observed (Vedernikov and Demidov 1997, Yunev et al. 2005). The remote sensing depth depends on the water constituents and can vary between less than 1 m and 30 m in different seasons and different parts of the western Black Sea (Davidov submitted). This is important for the calculation of the NPP which assumes vertical distribution of Chl_{sat} typical for the open ocean and is only partly valid for the Black Sea area.

The results of the Chl_{sat} calculation from SeaWiFS and MODIS sensors are widely compatible, however, due to the slightly different spectral bands and algorithms there could be a difference in the Chl_{sat} especially in more turbid waters such as DA (Werdell 2004).

The magnitude of the neutral wind stress is directly related to the vertical water convection in the CWBS. However, in the shallow coastal waters of NWS, DA and WS not only the magnitude, but also the direction of the wind is important. The wind direction influences the

advection of less dense river waters and often causes coastal upwelling (Stanichnaya et al. 2004).

The EOF method requires continuous and equidistant observations in the time series. Therefore, the full-resolution daily satellite data was spatially (over the regions) and temporally (monthly) averaged, which on the other hand results in loss of small-scale (fronts, eddies, jets) and short-term variability (day-weeks).

4.2 Classification of the western Black Sea

The classification of the western Black Sea into four regions was undertaken in order to describe areas with characteristic Chl_{sat} patterns and their variability. Strong variability of advection in the western Black Sea certainly causes an overlap of these regions. This is especially true for the north-western shelf, when mesoscale advection processes (formation of eddies and fronts) appear along the continental slope. Also long-lasting wind periods might cause unusual advection patterns in this region.

In order to describe the CZCS derived phytoplankton pigment pattern Yunev *et al.* (2002) classified the western Black Sea into nine different regions according to bathymetry, surface currents, surface chlorophyll *a* and anthropogenic impact. Kopelevich *et al.* (2002) used six regions for the description of the pigment pattern in the western Black Sea, which coincide in general with the above mentioned regions of Yunev *et al.* (2002). However, their coastal regions follow contours of the sea bottom, which in many areas are different from those of the characteristic pattern of Chl_{sat}. Certainly further subdivisions as for instance the Danube river plume or specific coastal areas (northern shelf) could lead to a more accurate description of the phytoplankton pattern but this would also unnecessarily increase the complexity of this research. One can generally conclude that the central part of the western Black Sea has a low Chl_{sat} and a specific annual succession of Chl_{sat}, while the other three regions show higher Chl_{sat} values but differences in the annual succession as the variability is concerned, especially in the river influenced areas.

4.3 Spatial distribution of high Chl_{sat} waters (1998-2003)

High Chl_{sat} (> 1 mg m^{-3}) in the western Black Sea (Fig 2) shows its widest extension (65 % of the whole area) of high-chlorophyll waters in autumn (October-November). This can be explained by a autumn phytoplankton bloom, triggered by vertical mixing of the surface layer, with additional support by the fact that in autumn the Rim Current is less pronounced (Oguz and Besiktepe, 1999) and consequently the front gradients do not prevent horizontal water advection of the high-chlorophyll coastal waters.

The areas with very high Chl_{sat} (>5 mg m^{-3}) are most extended in May and June, when the late spring/early summer increases are taking place, due to higher river water and nutrient discharge.

4.4. Temporal variability

The annual and interannual variability of the Chl_{sat} is high in all four regions of the western Black Sea. Within each region, there are both shifts in the timing of the peaks and different magnitudes of the maxima (Figure 3A-6A). In the CWBS the summer peak in 1998 is weak and occurs in May, in 1999, 2000 and 2001 it is very pronounced and occurs in June, while in 2004 and 2005 it is completely absent. The widely discussed and by several authors supported (Mashtakova and Roukhiyainen 1979, Mikaelyan 1997, Niermann et al. 1999, Daskalov 2003) theory that the interannual fluctuations are caused by the changes in the global teleconnection index NAO and its influence on the winter SST and the vertical convection is not supported by the 9-years time series. After rather warm winters of 2000 and 2001 there is high Chl_{sat} observed in these years, whereas after a cold winter of 2003 lower Chl_{sat} follows.

Oguz (2005) found significant correlation between time series of NAO and Black Sea winter SST for the 40-year period (1960-2000). However, the analysis of the time series after year 2002 shows a decoupling between NAO and winter SST. This could be result of to NAO modulation by regional atmospheric patterns, for example, the high/low pressure system over Europe and Caspian Sea region, as pointed out by Krichak et al. (2002). This decoupling deserves more detailed analyses.

There is no significant correlation between SST and Chl_{sat} time series and the variability in the EOFs modes suggest that except for the seasonality there is not much common variance (Table 2). The seasonal signal dominates in the first EOF mode of all four regions of the Black Sea and explains 43.5-51.6 % of the variability as previously reported for EOFs on SST images (Everson et al. 1997). The weighting factors of the physical parameters for the independent (after definition) EOF modes suggest that apart from the seasonality the variability of the Chl_{sat} and the physical parameters is also rather independent. Even the restored EOF mode 2 and 3 amplitudes of the time series reveal typical structures of the single parameter (Chl_{sat} and/or wind stress). The influence of the NAO on SST is confirmed by the significant correlation found in all regions. PAR and SST correlate constantly due to their seasonal determined changes. The wind stress seems to vary independenly and correlates only with SST in DA and CWBS, with PAR in DA and WS as well as with Chl_{sat} in DA. The first two correlations are due to prevailing seasonal changes, but the correlation with the Chl_{sat} supports previous observations on the advection of the Danube river water made during the

"daNUbs" project (Horstmann and Davidov 2002). This study reports that the advection and the extension of the Danube river plume in the Black Sea, which is detectable as high-chlorophyll-a surface water layer, is highly dependable on the direction of the surface winds. Other events, which coincide with specific wind stress conditions and can be related to the wind induced variability but without obvious explanation of the influencing mechanism. In the CWBS the unusual high Chl_{sat} in the summer 2001 was preceded by 5 months of low wind stress. In the NWS the wind stress was constantly high causing intense vertical mixing over a long time period prior and during the Chl_{sat} peak in June 2000.

The mean annual succession of Chl_{sat} presented in Figure 6A, agrees well with other satellite remote sensing (Nezlin, 1999) and *in situ* studies (Vedernikov and Demidov, 1993, Berseneva et al., 2004 and Chu et al., 2005), but is only a "compromise" between a few different annual successions and does not represent any of them.

The interannual variability of the Chl_{sat} is as high, that in order to recognize the 12-month cycle on the Fourier transformed data, the time series of CWBS has to be log-transformed and median-filtered in order to smooth the noise (Figure 8). The mean annual Chl_{sat} shows a general reduction in the second half of the 9-year period (Figure 3A-6A). However, it is not clear whether this reduction is becoming a trend or is a minimum and turning point of oscillation (Staneva pers. comm.).

It remains also unclear which factor or set of factors (physical: NAO, SST, river runoff, wind stress, Sahara dust or biological: zooplankton grazing, microbial remineralization) trigger the pronounced interannual variability of Chl_{sat} in the regions of the western Black Sea.

4.5. Spatial variability of Chl_{sat} in the four regions of the western Black Sea

Results of the multiple linear correlation show that all neighbouring areas are significantly correlated to each other (Table 6). However, there is no correlation between NWS and WS. The reason for this absence is the overlap of the seasonal component of the annual succession (identical in both regions) with different variability like: the advection of the Danube river water alternatively southwards or northwards (should produce negative correlation) as well as the occurrence of coastal events (upwelling, river runoff from Dnieper and Dniester).

The spatial variability of the Chl_{sat} in the western Black Sea as retrieved by the EOF analysis is characterized with an independent variability in the CWBS and DA as well as in the shelf areas. The variability in the WS shows similarities to that in CWBS and to a smaller extend to the variability of DA, while the variability in the NWS is linked only to the variability of the Danube (Table 6). These differences in the variability at relatively constant seasonal forcing reflect the different mechanisms of nutrient supply in the different regions. In the CWBS,

which is nitrogen limited the nutrients input to the surface layer results mainly from subsurface pool throughout vertical water convection (Murray et al., 2005), while the Danube river-load is the main supplier of nutrients in the DA and phosphorus appear to be limiting factor (Velikova et al., 2005). The water exchange and mutual influence between CWBS and DA is rather limited. In the NWS and WS however, the nutrient supply occur by both river waters as well as by temperature and wind induced vertical convection (Tolmazin 1985). The advection of the nutrient rich Danube river water alternately northwards (NWS) or southwards (WS) cause a temporary effect of opposing Chl_{sat} variability (high Chl_{sat} in NWS – low Chl_{sat} in WS and vice-versa).

Unfortunately, the spatial variability within our four regions was not examined, but previous studies indicate that such variability might also be important (Oguz & Besiktepe, 1999).

4.6. Variability of the net primary production

Primary production in situ measurements in the Black Sea are known to have a particularly high variability (Sorokin 2002, Vedernikov and Demidov 1993, Yunev et al. 2002), which makes detecting trends and responses to environmental factors very difficult with shipboard measurements alone. Satellite remote sensing combined with models is a powerful tool that can resolve spatial and temporal variability over large areas (Kahru et al. 2004). The Behrenfeld-Falkowski VGPM model calculates NPP from Chl_{sat}, PAR and SST. While the satellite retrieved PAR and SST parameters are assumed to be accurate, the Chl_{sat} and especially its vertical distribution in the Black Sea have a high spatial and temporal variation and might deviate significantly from the in situ measurements (Davidov 2006a). Consequently the deviations in the magnitude of the resulting calculated NPP compared to in situ data could also be significant. Despite this deviation in the absolute values the temporal trends of the NPP are of very robust nature as demonstrated in Behrenfeld et al. (2006). The NPP time series in the western Black Sea displays very pronounced seasonal signal (Figures 3-6 and Figure 7B). Different to the annual succession of Chl_{sat}, the NPP increase between April and October, when the light is not a limiting factor and SST is not significantly suppressing the photosynthetic efficiency. However, in the Behrenfeld-Falkowski VGPM model the nutrient limitation is not considered and there is still lack of validation of the model-NPP with coincident *in situ* measurements of primary productivity in the surface layer of western Black Sea.

The mean annual succession of NPP of the 9-years period (Figure 7B) is in agreement with the in situ measured depth integrated primary production during the 1986-1992 period in the central western Black Sea with maximum in June (Yunev et al. 2002). However, the

magnitude of NPP is a factor 3 to 4 lower (300-600 mg C m^{-2} day^{-1}) in the Yunev et al. (2002) data. On the other hand the magnitude of the NPP is in agreement with in situ measured primary production in Vedernikov and Demidov (1993). However, the mean annual succession suggested by Vedernikov and Demidov (1993) for the deep part of the Black sea is very different from that of NPP and exhibits a maximum in February, low values in May, June and September as well as increases in July-August and October-November. This statement however is contradicting to PAR time series data, which suggest an efficient light limitation in winter. In situ primary productivity data from Bologa (1985) support the spatial variability of satellite derived NPP and are in the same order of magnitude (400-2000 mg C m^{-2} day^{-1}).

In conclusion, the results demonstrate on the one hand the potential of the statistical analysis of time series in the western Black Sea and on the other hand the complexity of the investigated processes. Therefore, in order to clarify the spatial and temporal variability of Chl_{sat} in the western Black Sea further and especially longer time series of satellite observation are necessary.

Acknowledgements

The author would like to thank the SeaWiFS Project (Code 970.2) and the Goddard Earth Sciences Data and Information Services Center/ Distributed Active Archive Center (Code 902) at the Goddard Space Flight Center, Greenbelt, MD 20771, for the distribution of Ocean Colour Level 1A data. These activities are sponsored by NASA's Earth Science Enterprise. I would also like to thank Robert O'Malley, Oregon State University for producing and providing the primary production data. Part of the results presented stem from the project "Nutrient Management in the Danube Basin and its Impact on the Black Sea" (daNUbs) supported under contract EVK1-CT-2000-00051 by the Energy, Environment and Sustainable Development (EESD) Programme of the 5th EU Framework Programme.

References

1. Baloga, A.S., 1985. Planktonic primary productivity of the Black Sea: a review. *Thalassia Jugoslavica*, 21/22:1-22.
2. Barnston, A. G., and R. E. Livezey, 1987: Classification, seasonality and persistence of low-frequency atmospheric circulation patterns. Mon. Wea. Rev., 115, 1083-1126.
3. Behrenfeld, M.J and Falkowski, P.G, 1997. Photosynthetic rates derived from satellite-based chlorophyll-a concentration. Limnol. and Oceanogr., 42:1-20.
4. Behrenfeld, M.J, R.T. O'Malley, D.A. Siegel, C.R. McClain, J.L. Sarmiento, G.C. Feldman, A.J. Milligan, P.G. Falkowski, R.M. Letellier, E.S. Boss, 2006. Climate-driven trends in contemporary ocean productivity. *Nature*, 444:752-755.
5. Berseneva, G.P., Churilova, T.Y. and Georgieva, L.B., 2004. Seasonal variability of chlorophyll-a and phytoplankton biomass in the western part of the Black Sea. *Oceanology*, 44:211-219, (in Russian).
6. Chu, P. C., Ivanov, L. M. and Margolina, T. M., 2005. Seasonal variability of the Black Sea chlorophyll-a -a concentration. *J. Mar. Syst*., 56(3-4):243-261.
7. Cociasu A, Diaconu V, Popa L, Buga L, Nae I, Dorogan L, Malciu V (1997) The nutrient stock of the Romanian shelf of the Black Sea during the last three decades. In: Sensitivity to Change: Black Sea, Baltic Sea and North Sea, E. Özsoy and A. Mikaelyan (eds.), pp. 49-63.
8. Daskalov, G., 2003. Long-term changes in fish abundance and environmental indices in the Black Sea. *Mar. Ecol. Prog. Ser.*, 255: 259-270.
9. Davidov A., submitted. Assessment of algorithms for atmospheric correction and chlorophyll-a retrieval from SeaWiFS satellite data in the western Black Sea area. Submitted April 2006 to *International Journal of Remote Sensing*.
10. Dommenget, D. and Latif, M, 2002. Reply to a comment of Behera et al. on "A cautionary note on the interpretation of EOFs".In: *J. Climate*,16:1094-1098.
11. Esaias, W.E., Abbott, M.R., Barton, I., Brown, O.B., Campbell, J.W., Carder, K.L., Clark, D.K., Evans, R.H., Hoge, F.E., Gordon, H.R., Balch, W.M., Letelier, R., and Minnett, P.J. (1998), An overview of MODIS capabilities for ocean science

observations. *IEEE Transactions on Geoscience and Remote Sensing*, 36, 1250-1265.

12. Everson, R., Corbilson, P., Sirovich, L., and Webber, A., 1997. An empirical eigenfunction analysis of the sea surface temperature in the western North Atlantic. *J. Phys. Oceanogr.*, 27, 468-479.

13. Feldman, G. C., C. R. McClain, Ocean Color Web, SeaWiFS and MODIS Aqua data, NASA Goddard Space Flight Center. Eds. Kuring, N., Bailey, S. W., Decenber 2006. http://oceancolor.gsfc.nasa.gov/

14. Fu, G., Baith, K. S., and McClain, C. R., 1998, "SeaDAS: The SeaWiFS Data Analysis System", Proceedings of "The 4th Pacific Ocean Remote Sensing Conference", Qingdao, China, July 28-31, 1998, 73-79.

15. Gordon, H.R. and Wang, M., 1994. Retrieval of water-leaving radiance and aerosol optical thickness over the oceans with SeaWiFS: a preliminary algorithm. Appl. Opt., 33: 443-452.

16. Horstmann, U. and Davidov, A., 2002. IFM-Kiel DANUBS internal annual report 2002.

17. Jaoshvili, S., 2002. The rivers of the Black Sea. European Environmental Agency. Technical Report No.71.

    (http://reports.eea.eu.int/technical_report_2002_71/en/tab_content_RLR)

18. Kahru, M., Marinone, S.G., Lluch-Cota, S.E., Pares-Sierra, A. and Mitchell, B.G., 2004. Ocean-color variability in the Gulf of California: scales from days to ENSO, *Deep-Sea Research II,* 51(1-3):139-146.

19. Kopelevich, O.V., Sheberstov, S.V., Yunev, O., Basturk, O., Finenko, Z.Z., Nikonov, S. and Vedernikov, V.I., 2002. Surface chlorophyll in the Black Sea over 1978-1986 derived from satellite and in situ data. J. Mar. Syst. 36(3-4):145-160

20. Kopelevich, O.V., Burenkov, V.I., Ershova, S.V., Sheberstov, S.V. and Evdoshenko, M.A., 2004. Application of SeaWiFS data for studying variability of bio-optical characteristics in the Barents, Black and Caspian Seas. Deep Sea Research, 51:1063-1091.

21. Krichak, S.O., Kishcha, P. and Albert, P., 2002. Decadal trends of main Eurasian oscillations and the Eastern Mediterranean precipitation. *Theoretical and Applied Climatology*, 72:209-220.

22. Large, W. G., and S. Pond, 1981: Open ocean momentum flux measurements in moderate to strong winds. J. Phys. Oceanogr., 11, 324–336.

23. Lorenz, E.N., 1956. Empirical orthogonal functions and statistical weather prediction. Statistical Forecasting Project. Departement pf Meteorology, Science Report 1, Massachusetts Institute of Technology.

24. Mashtakova GP, Roukhiyainen MI (1979) Seasonal dynamics of phytoplankton. In: V.N. Grese, Fundamentals of biological productivity in the Black sea. Naukova Dumka, Kiew, pp. 85-88. (in Russian).

25. McClain, C.R., Feldman, G.C. and Hooker, S.B., 2004. An overview of the SeaWiFS project and strategies for producing a climate research quality global ocean bio-optical time series Deep Sea Res. (II Top. Stud. Oceanogr.) 51(1-3):5-42.

26. Mikaelyan A (1997) Long-term variability of phytoplankton communities in open Black Sea in relation to environmental changes. In: Sensitivity to Change: Black sea, Baltic Sea and North Sea. Özsoy & Mikaelyan (eds.), Kluwer Acad. Publ., pp 105-116.

27. Morel, A. and Berthon J-F., 1989, Surface Pigments, Algal Biomass Profiles, and Potential Production of the Euphotic Layer: Relationships Reinvestigated in View of Remote-Sensing Applications, *Limnol. and Oceanogr.*, 34(8): 1545-1562.

28. Murray, J.W., C. Fuchsman, J. Kirpatrick, B. Paul and Konovalov, S., 2005. Species and δ^{15} signature of nitrogen transformations in the suboxic zone of the Black Sea. *Oceanography, Vol.18,* 36-47.

29. Nezlin, N.P., Kostianoy, A.G., Gregoire, M., 1999. Patterns of seasonal and interannual changes of surface chlorophyll-a concentration in the Black Sea revealed from remote sensed data. *Remote Sens. Environ*. 69:43-55.

30. Niermann, U., Kideys, A., Kovalev, A., Melnikov, V. and Belokopitov, V., 1999. Fluctuation of pelagic species of the open Black Sea during 1980-1995 and possible teleconnections. In: Environmental Degradation of the Black Sea: Changes and Remedies. Besiktete, S., (ed.), Kluwer, Netherlands, 147-173.

31. O'Reilly, J.E., Maritorena, S., O'Brien, M.C., Siegal, D.A., Toole, D., Menzies, D., Smith, R.C., Mueller, J.L., MitchellL, B.G., Kahru, M., Chavez, F.P., Strutton, P., Cota, G.F., Hooker, S.B., Mcclain, C.R., Carder, K.L., Muller-Karger, F., Harding, L., Magnuson, A., Phinney, D., Moore, G.F., Aiken, J., Arrigo, K.R., LeTelier, R.

and Culver, M., 2000. Ocean Color Chlorophyll-a algorithms for SeaWiFS, OC2 and OC4: Verison 4. In: SeaWiFS postlaunch calibration and validation analyses, part 3. SeaWiFS postlaunch technical report series. S.B. Hooker and E.R. Firestone (eds). NASA/TM-2000-206892, 11, pp. 9-23.

32. Oguz, T. and Besiktepe, S., 1999, Observation on the Rim Current structure, CIW formation and transport in the western Black Sea. Deep-Sea Research I 46:1733-1753.

33. Oguz, T., 2005 Black sea ecosystem response to climatic teleconnection. Oceanography, 18(2):122-133.

34. Oguz, T., Latun, M., Latif, M.A., Vladimirov, V.V., Sur, H.I., Markov, A.A., Ozsoy, E., Kotovshchikov, B.B., Eremeev, V.V. and Unluata, U., 1993. Circulation in the surface and intermediate layers of the Black Sea. Deep-Sea Research, 40(8):1597-1612.

35. Sorokin, Y.I., 2002. The Black Sea, ecology and oceanography. Backhuys Publishers, Leiden, Niederlande, 875 pp.

36. Stanichnaya, R., Davidov, A., Stanichny, S., Soloviev, D., 2004. Coastal upwelling in the Black Sea as derived from satellite remote sensing. 35th COSPAR Scientific Assembly. Hold 18 - 25 July 2004, in Paris, France, p.3786.

37. Tolmazin D (1985) Changing Coastal Oceanography of the Black Sea I: NorthWestern Shelf. *Prog. Oceanog.* 15:217-276.

38. Vedernikov, V.I., and Demidov, A.B., 1993. Primary production and chlorophyll-a in deep regions of the Black Sea. *Oceanology* 33(2):193-199.

39. Vedernikov, V.I. and Demidov, A.B., 1997. The vertical distribution of the primary production and chlorophyll in the different season of the deep parts of the Black Sea. Oceanologya, 37:414–423.

40. Velikova, V., A. Cociasu, L. Popa, L. Boicenco, D. Petrova, 2005. Phytoplankton community and hydrochemical characteristics of the Western Black Sea. *J. Water Science and Technology, Vol.51,* 27-37.

41. Wang, M., 2000. The SeaWiFS atmospheric correction updates. In: SeaWiFS postlaunch calibration and validation analyses, Part 1. NASA/TM-2000-206892, Hooker, S.B. and Firestone, E.R. (eds), 9, pp. 57-63.

42. Werdell, P.J., Science Systems and Applications, Inc., 2 March 2004, modified 24 June 2004. Documentation on the OCW.

43. Yoder, J., Schollaeri, S. and O`Reilly, J., 2002. Climatological phytoplankton chlorophyll-a and sea surface temperature patterns in continental shelf and slope waters off the northeast U.S. coast. *Limnol. Oceanogr*. 47(3), 672-682.

44. Yunev OA, Vedernikov VI, Basturk O, Yilmaz A, Kideys AE, Moncheva S, Konovalov SK (2002) Long-term variations of surface chlorophyll-a and primary production in the open Black Sea. *Mar. Ecol. Prog. Ser*. 230:11-28.

45. Yunev, O.A., Moncheva, S.and Carstensen, J., 2005. Long-term variability of vertical chlorophyll-a and nitrate profiles in the open Black Sea: eutrophication and climate change. Mar. Ecol. Prog. Ser., 294:95-107.

List of figures

List of tables

Tables with captions

Table 1. Number and quality of the SeaWiFS images (1998-2003).

Percentage of usable SeaWiFS images in different seasons

averaged	*winter*	*spring*	*summer*	*autumn*
year	13 %	27 %	40 %	20 %

Quality of the SeaWiFS images

	winter	*spring*	*summer*	*autumn*	*total*
Good	8 %	33 %	55 %	23 %	36 %
Moderate	29 %	39 %	31 %	37 %	34 %
Poor	63 %	28 %	14 %	40 %	29 %

*Table 2. Eigenvalues (A) of correlation matrix and factor coordinates (B) resulting from EOF analysis of temporally normalized data as well as correlation matrix (C) from multiple linear correlation in the **CWBS** area.*

A. Eigenvalues of correlation matrix.

EOF modes	**Eigenvalue**	**% Total variance**	**Cumulative Eigenvalue**	**Cumulative %**
Mode 1	1.897006	47.42515	1.897006	47.4251
Mode 2	1.000464	25.01160	2.897470	72.4368
Mode 3	0.860346	21.50865	3.757816	93.9454
Mode 4	0.242184	6.05460	4.000000	100.0000

B. Factor coordinates of Chl_{sat}, SST, PAR and Wind stress.

Variable	**Mode 1**	**Mode 2**	**Mode 3**	**Mode 4**
Chl_{sat}	-0.441309	**-0.632555**	**0.629431**	-0.094538
SST	**0.875967**	-0.196586	0.286963	0.334197
PAR	**0.863509**	0.234750	0.302146	-0.328559
Wind stress	0.435068	**-0.711748**	**-0.539002**	-0.116653

C. Correlation matrix, n=110, p<0.05, significant r are in bold print.

	Chl_{sat}	**SST**	**PAR**	**Wind stress**	**NPP**	**NAO**
Chl_{sat}	1.00	-0.11	**-0.31**	-0.07	n.a.	-0.03
SST		1.00	**0.69**	**0.33**	n.a.	**-0.22**
PAR			1.00	0.08	n.a.	-0.11
Wind stress				1.00	0.09	0.16
NPP					1.00	**-0.23**
NAO						1.00

Table 3. Eigenvalues (A) of correlation matrix and factor coordinates (B) resulting from EOF analysis of temporally normalized data as well as correlation matrix (C) from multiple linear correlation in the **NWS** area.

A. Eigenvalues of correlation matrix.

EOF modes	Eigenvalue	% Total variance	Cumulative Eigenvalue	Cumulative %
Mode 1	1.741201	43.53002	1.741201	43.5300
Mode 2	1.106003	27.65009	2.847204	71.1801
Mode 3	0.875375	21.88437	3.722579	93.0645
Mode 4	0.277421	6.93553	4.000000	100.0000

B. Factor coordinates of Chl_{sat}, SST, PAR and Wind stress.

Variable	Mode 1	Mode 2	Mode 3	Mode 4
Chl_{sat}	-0.278991	**-0.726893**	**-0.618495**	0.106087
SST	**-0.922279**	-0.071199	0.073663	-0.372701
PAR	**-0.888044**	0.173433	0.232962	0.356409
Wind stress	0.155384	**-0.736534**	**0.658134**	0.015254

C. Correlation matrix, n=110, p<0.05, significant r are in bold print.

	Chl_{sat}	SST	PAR	Wind stress	NPP	NAO
Chl_{sat}	1.00	**0.22**	0.02	0.09	n.a.	0.05
SST		1.00	**0.69**	-0.05	n.a.	**-0.22**
PAR			1.00	-0.11	n.a.	-0.11
Wind stress				1.00	-0.05	0.16
NPP					1.00	**-0.19**
NAO						1.00

*Table 4. Eigenvalues (A) of correlation matrix and factor coordinates (B) resulting from EOF analysis of temporally normalized data as well as correlation matrix (C) from multiple linear correlation in the **WS** area.*

A. Eigenvalues of correlation matrix.

EOF modes	Eigenvalue	% Total variance	Cumulative Eigenvalue	Cumulative %
Mode 1	1.867689	46.69221	1.867689	46.6922
Mode 2	0.942573	23.56432	2.810261	70.2565
Mode 3	0.889950	22.24876	3.700212	92.5053
Mode 4	0.299788	7.49470	4.000000	100.0000

B. Factor coordinates of Chl_{sat}, SST, PAR and Wind stress.

Variable	Mode 1	Mode 2	Mode 3	Mode 4
Chl_{sat}	0.371512	**0.841885**	-0.390266	0.030021
SST	**-0.837584**	0.337822	0.224577	-0.365915
PAR	**-0.895526**	0.187635	0.066834	0.397944
Wind stress	0.475556	0.290642	**0.826281**	0.081445

C. Correlation matrix, n=110, p<0.05, significant r are in bold print.

	Chl_{sat}	SST	PAR	Wind stress	NPP	NAO
Chl_{sat}	1.00	-0.13	**-0.19**	0.10	n.a.	-0.11
SST		1.00	**0.68**	-0.14	n.a.	**-0.21**
PAR			1.00	**-0.28**	n.a.	-0.11
Wind stress				1.00	**-0.22**	0.17
NPP					1.00	**-0.21**
NAO						1.00

Table 5. Eigenvalues (A) of correlation matrix and factor coordinates (B) resulting from EOF analysis of temporally normalized data as well as correlation matrix (C) from multiple linear correlation in the **DA** area.

A. Eigenvalues of correlation matrix.

EOF modes	Eigenvalue	% Total variance	Cumulative Eigenvalue	Cumulative %
Mode 1	2.065667	51.64168	2.065667	51.6417
Mode 2	0.924151	23.10377	2.989818	74.7454
Mode 3	0.740694	18.51736	3.730512	93.2628
Mode 4	0.269488	6.73719	4.000000	100.0000

B. Factor coordinates of Chl_{sat}, SST, PAR and Wind stress.

Variable	Mode 1	Mode 2	Mode 3	Mode 4
Chl_{sat}	-0.450088	**0.856477**	-0.233605	0.096416
SST	**-0.802556**	-0.411137	-0.282312	0.327369
PAR	**-0.897794**	-0.121199	-0.173851	-0.386073
Wind stress	0.642617	-0.082914	**-0.759078**	-0.063003

C. Correlation matrix, n=110, p<0.05, significant r are in bold print.

**Danube river water discharge is correlated to other time-series for period 1997 – 2003, n=76, p<0.05.*

	Chl_{sat}	SST	PAR	Wind stress	NPP	NAO	Danube*
Chl_{sat}	1.00	0.11	**0.30**	**-0.19**	n.a.	0.03	**0.33**
SST		1.00	**0.69**	**-0.29**	n.a.	**-0.23**	**-0.32**
PAR			1.00	**-0.41**	n.a.	-0.10	0.07
Wind stress				1.00	**-0.35**	**0.21**	-0.07
NPP					1.00	-0.14	0.12
NAO						1.00	0.16
Danube*							1.00

Table 6. Correlation coefficent matrix of the Chl_{sat} from the four regions. The significant correlations are in bold print. The number of observation n=110, $p < 0.05$.

	CWBS	NWS	WS	DA
CWBS	1.000	**0.333**	**0.536**	**0.272**
NWS		1.000	-0.009	**0.475**
WS			1.000	**0.324**
DA				1.000

Table 7. Eigenvalues (upper) of correlation matrix and factor coordinates (lower) of Chl_{sat} in CWBS, NWS, WS and DA areas retrieved by EOF of the spatial normalized data.

EOF modes	Eigenvalue	% Total variance	Cumulative Eigenvalue	Cumulative %
Mode 1	1.680061	42.00152	1.680061	42.0015
Mode 2	1.318114	32.95285	2.998175	74.9544
Mode 3	1.001825	25.04564	4.000000	100.0000

	Mode 1	Mode 2	Mode 3
CWBS	0.290573	0.073651	**0.954014**
NWS	**-0.81198**	-0.58037	0.062105
WS	**0.928243**	-0.24932	-0.27605
DA	-0.27328	**0.955875**	-0.1078

Figures with captions

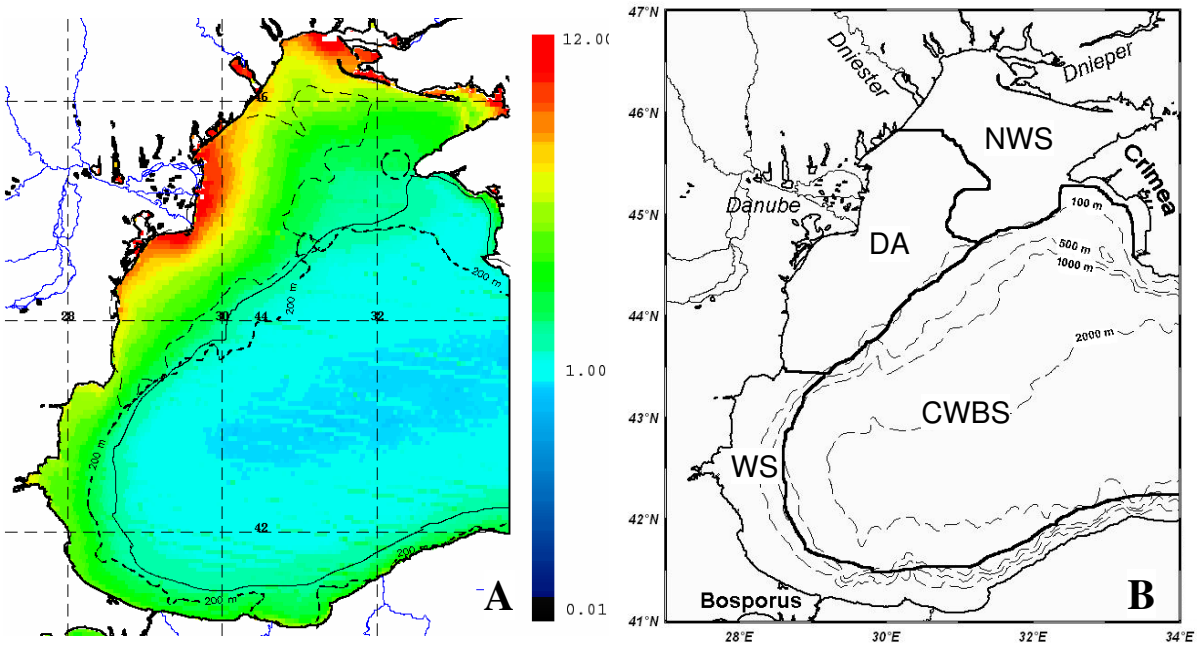

Figure 1 AB.

A. 6-years mean chlorophyll a with criteria, which were used for the definition of the regions: Chl_{sat} of 1 mg m^{-3} (solid line), depth of 200 m (dashed line) and variability coefficient of 80% (long-dashed line).

B. Western Black Sea with four regions of characteristic surface chlorophyll a pattern (chlorophyll a concentration, variability and coefficient of variance). North-western shelf (NWS), Danube influenced water (DA), Western und southern shelf (WS) and Central western Black Sea (CWBS).

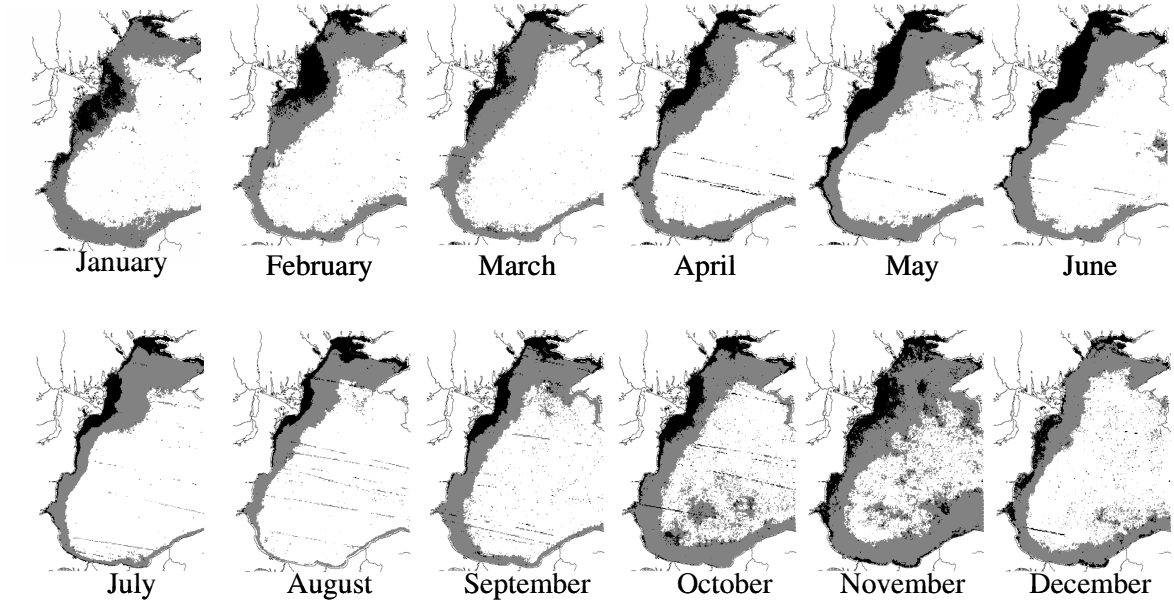

Figure 2. Area of high [> 1 mg m^{-3} (grey)] and very high [> 5 mg m^{-3} (black)] concentrations of Chl_{sat} in the western Black Sea for the time period between 1998 and 2003.

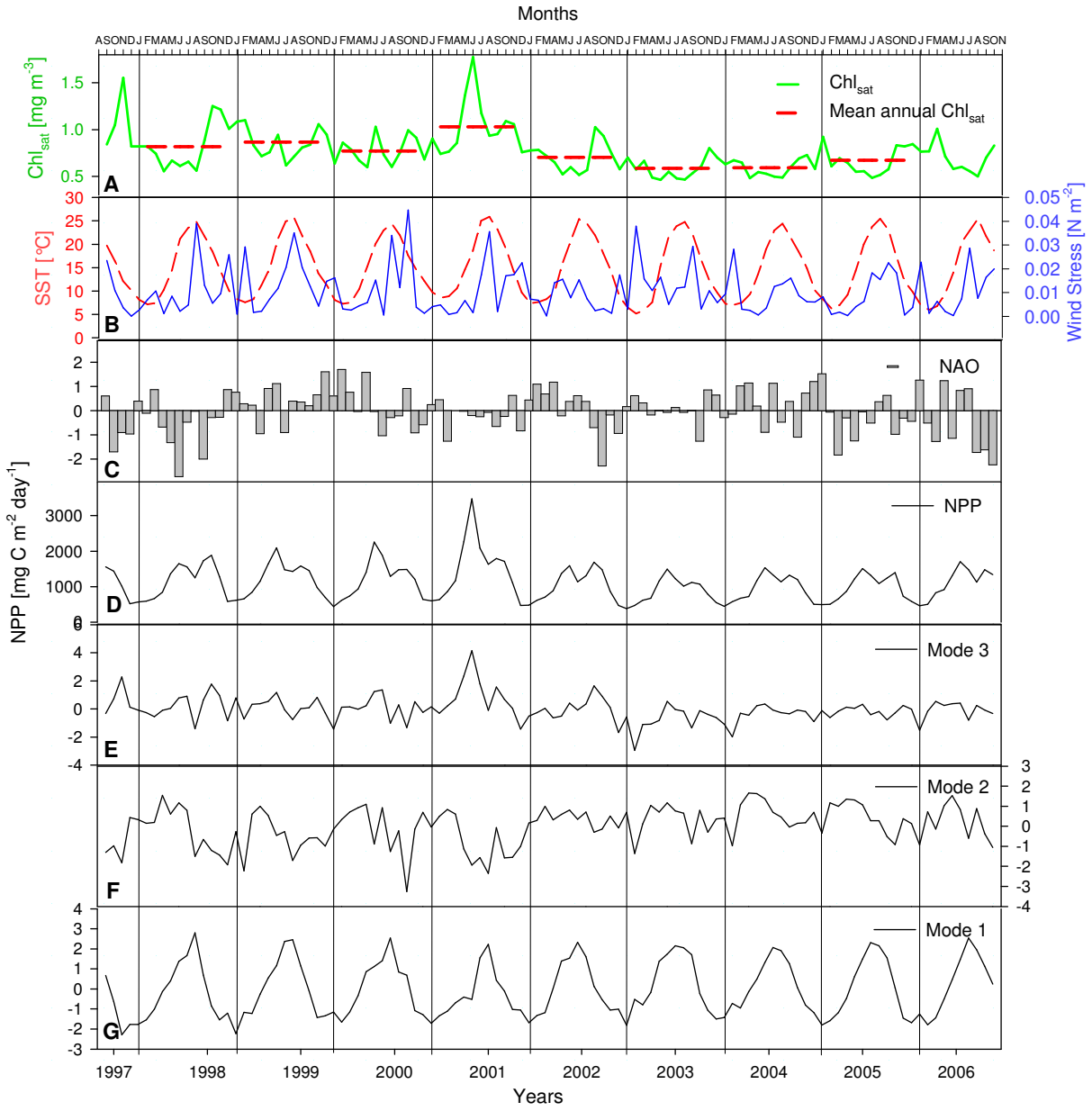

*Figure 3. Time series (1997 – 2006) of **A.** Chl_{sat} with annual mean; **B.** SST and Wind Stress; **C.** NAO index; **D.** NPP as well as **G-F-E.** Presenting the time series of the first 3 temporally normalised EOF modes in the CWBS area. See Table 2 for EOF weighting factors.*

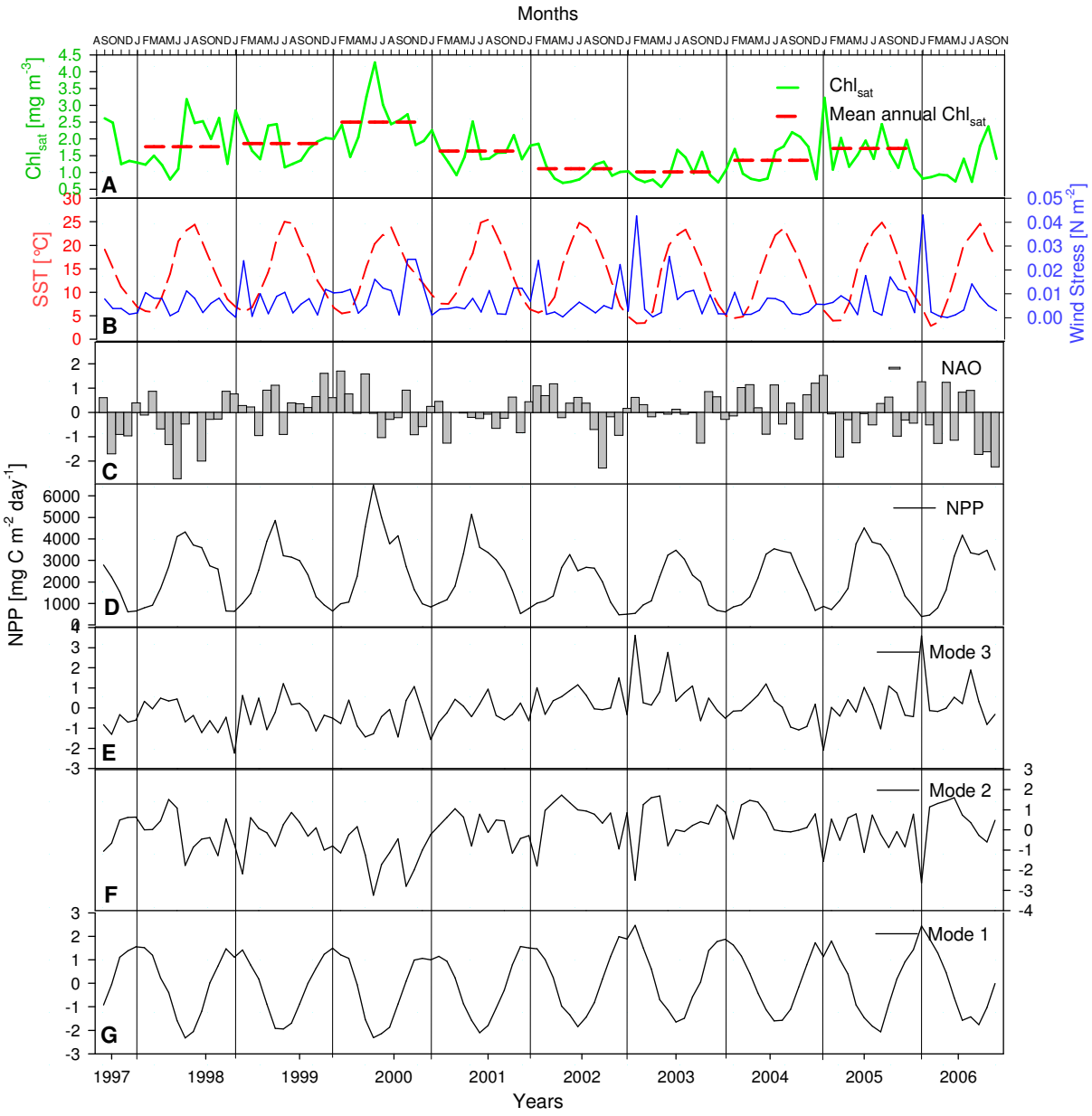

*Figure 4. Time series (1997 – 2006) of **A.** Chl_{sat} with annual mean; **B.** SST and Wind Stress; **C.** NAO index; **D.** NPP as well as **G-F-E.** Presenting the time series of the first 3 temporally normalised EOF modes in the **NWS area**. See Table 3 for EOF weighting factors.*

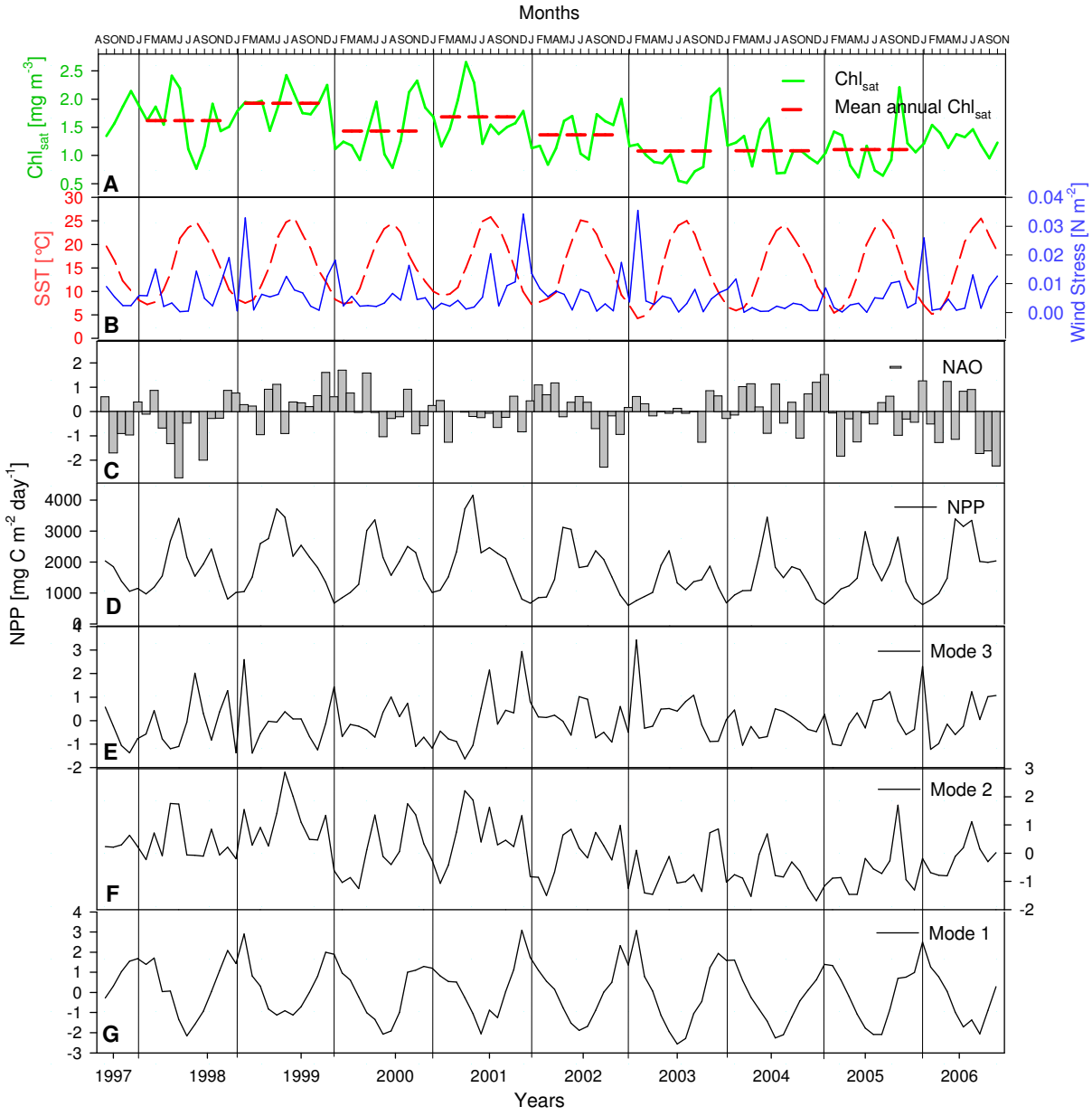

*Figure 5. Time series (1997 – 2006) of **A.** Chl_{sat} with annual mean; **B.** SST and Wind Stress; **C.** NAO index; **D.** NPP as well as **G-F-E.** Presenting the time series of the first 3 temporally normalised EOF modes in the **WS area**. See Table 4 for EOF weighting factors.*

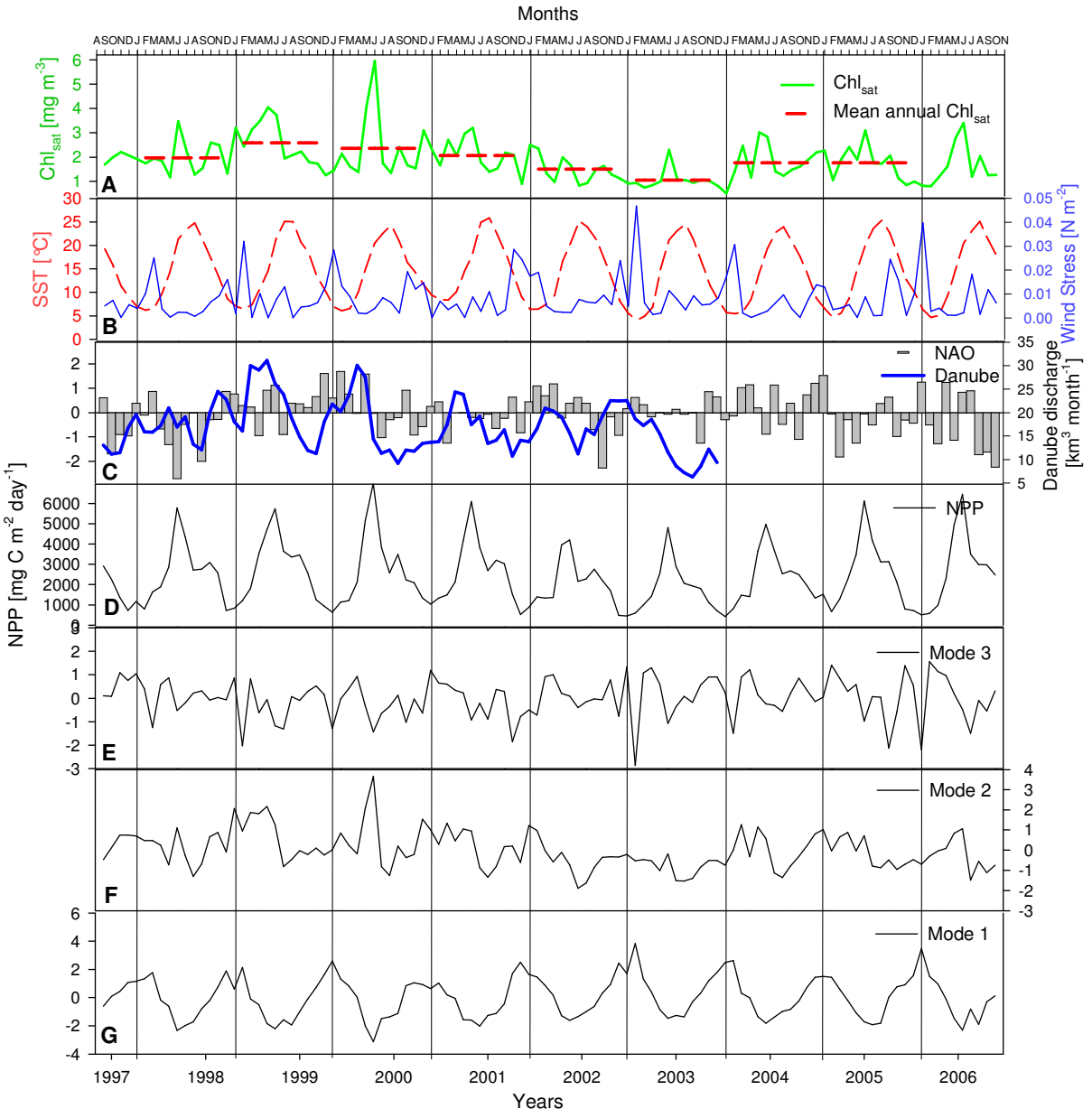

*Figure 6. Time series (1997 – 2006) of **A.** Chl_{sat} with annual mean; **B.** SST and Wind Stress; **C.** NAO index and Danube river water discharge (1997 -2003); **D.** NPP as well as **G-F-E.** Presenting the time series of the first 3 temporally normalised EOF modes in the **DA area**. See Table 5 for EOF weighting factors.*

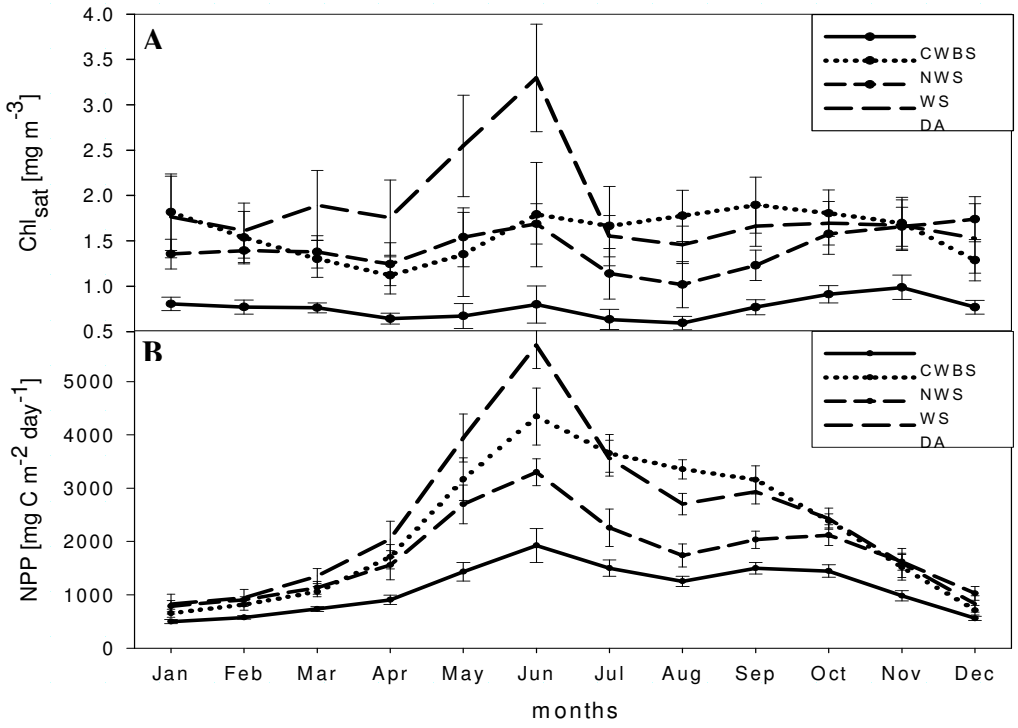

*Figure 7 AB. "Climatologically" annual succession (1997 – 2006) of **A**.) Chl$_{sat}$ and **B**.) NPP in the four different regions of the western Black Sea. Error bars represent one-half of the standard deviation.*

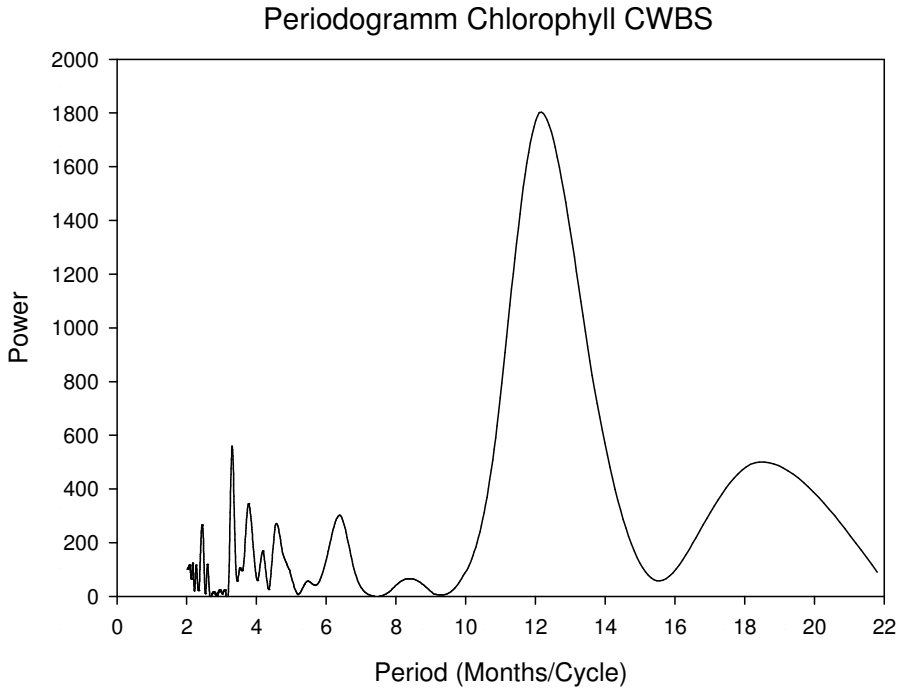

Figure 8. Periodogram of the Chl$_{sat}$ time series in CWBS area.

Chapter IV

Black Sea plankton dynamics: seasonal variability and comparison to SeaWiFS data

K. P. Tsiaras[1], V.H. Kourafalou[1,2], A. Davidov[3] and J. Staneva[4]

[1] Hellenic Center for Marine Research, Anavyssos, Greece
[2] Rosenstiel School of Marine and Atmospheric Science, Univ. of Miami, Miami, FL, U.S.A.
[3] Leibniz-Institute of Marine Sciences – IFM-Geomar, Kiel, Germany
[4] University of Oldenburg, Oldenburg, Germany

Submitted to Journal of Geophysical Research

September 2006

A three-dimensional coupled model of the western Black Sea plankton dynamics: seasonal variability and comparison to SeaWiFS data

K. P. Tsiaras[1], V.H. Kourafalou[1,2], A. Davidov[3] and J. Staneva[4]

[1] Hellenic Center for Marine Research, Anavyssos, Greece
[2]Rosenstiel School of Marine and Atmospheric Science, Univ. of Miami, Miami, FL, U.S.A.
[3]University of Kiel, Kiel, Germany
[4]University of Oldenburg, Oldenburg, Germany

Abstract: The main physical and biological processes that control the seasonal cycle of the plankton dynamics over the Western Black Sea were explored by means of a three-dimensional, 7-compartment, on-line coupled biophysical model that was developed for this study. Adopting high frequency forcing in terms of air-sea interaction and Danube river inputs, we performed a simulation of the coupled model during the 2002-2003 period. A series of 8-day Chl-a SeaWiFS images provided a validation tool that guided us, along with available in-situ measurements, to the improvement of model parameterizations and the calibration of the biological parameters. The simulation of the seasonal phytoplankton variability over the entire Western Black Sea, extending from the highly eutrophic river influenced area to the open sea area was a major challenge that made necessary the representation of both the spatial and time variability of several processes. Despite the model simplicity, the simulated Chl-a patterns presented a good agreement as compared to the SeaWiFS images. The most noticeable differences were observed in the open sea area, consisting of an overestimation during spring and an underestimation during autumn. During winter, phytoplankton in coastal areas was shown to be limited by light availability, primarily due to the increased particulate matter concentrations, as a result of resuspension from the sediment and the increased river loads. During summer, the primary production was mostly sustained by riverine nutrients and regeneration processes and thus was strongly linked to the evolution of the Danube plume. The model simulated Chl-a presented a reasonably good agreement with in-situ data in the Danube front and in the Romanian shelf areas. The limiting nutrients, however, showed significant deviations from the observed concentrations, which

suggests that certain processes need to be improved in the biological model, such as remineralization and grazing pressure.

1. Introduction

The Black Sea is a semi-enclosed basin, connected to the Mediterranean through the narrow and shallow strait of Bosporus. Its hydrodynamic and biogeochemical structure is characterized by a strong main pycnocline, imposed by the hydrological balance, that is mostly defined by the fresh river water inflow and the restricted water exchange through the Bosporus straits (outflow of light surface water and inflow of more saline Mediterranean water). The strong density stratification inhibits the ventilation of sub-pycnocline waters. As oxygen is consumed by the decomposition of sinking organic matter, the water mass below ~150 m is permanently anoxic and the distributions of essential nutrients across the oxic/anoxic interface are defined by redox processes.

The Northwestern Black Sea shelf is characterized by a broad shelf and is a highly eutrophic area, as it receives the majority of river water discharge from the rivers Dniestr, Dniepr, Bug and particularly the Danube (fig. 1), which contributes to about 70% of the Black Sea fresh water input (Tolmazin, 1985). The significant increase of nitrogen and phosphorus loads from the Danube River during the 1970's – 1980's resulted in the intensive eutrophication of the Northwestern Black Sea shelf which was characterized by the reduction of non-gelatinous zooplankton stocks, mass mortality among benthic communities and decrease of biodiversity (Zaitsev and Alexandrov, 1997; Kideys, 2002). The strong eutrophication combined with the invasion of the ctenophore *Mnemiopsis Leidyi* and other synergetic factors such as overfishing (Gucu, 2002), led to a significant deterioration of the Black Sea ecosystem and particularly that of the Northwestern shelf area. The recent decrease of nutrient river loads, along with the appearance of a predator of *Mnemiopsis*, the ctenophore *Beroe* (Finenko et al. 2003), have contributed to the gradual recovery of the Black Sea ecosystem (Kideys, 2002).

Over the last decade the Black Sea ecosystem functioning has been explored by several studies, employing models of various complexity levels and spatial resolutions. A 1-D vertically coupled low-trophic model was developed by Oguz et al. (1996) to study the open Black Sea plankton dynamics and was also used by Staneva et al. (1998) to examine the effect of different meteorological conditions. This model was further elaborated by including additional trophic levels (Oguz et al., 1998; Oguz et al., 2001a), in order to study food web

trophic interactions, resolving redox cycles (Oguz et al., 2001b) and oxygen dynamics (Oguz et al., 2000). Oguz and Salihoglu (2000) using the biological model in Oguz et al. (1999) developed a three-dimensional, three-layer model to assess the impact of eddy-dominated horizontal circulation on the open Black Sea plankton dynamics. Eeckout and Lancelot (1997) developed a high trophic resolution 0-D box model to study the functioning of the Northwestern Black Sea shelf ecosystem. The same model was later coupled to a one-dimensional mixed layered model and a three-dimensional hydrodynamic model (Lancelot et al., 2002; Stanev et al., 2002). Cokasar and Ozsoy (1998) investigated the factors that determine the dynamics of different Black Sea regions by implementing variations of the Fasham et al. (1990) nitrogen based model. Lebedeva and Sushkina (1994) employed a two-layer model to study the effect of *Mnemiopsis* on the Black Sea plankton community. Gregoire et al. (1998) developed a three-dimensional coupled biophysical model comprising several size classes of phytoplankton and zooplankton as well as different potentially limiting nutrients (nitrogen, phosporus, silicate). A somehow simpler nitrogen-based, 6-compartment, three-dimensional coupled model was implemented by Gregoire et al. (2004) to study the seasonal variability of plankton and circulation dynamics. The same model was also used to estimate the nitrogen budget of the Northwestern Black Sea shelf (Gregoire and Friedrich, 2004).

In the present study we investigate the main physical and biological processes that control the seasonal cycle of the plankton dynamics over the Western Black Sea, by means of a three-dimensional, low-trophic, coupled biophysical model that was developed in the framework of the EU daNUbs (DAnube NUtrient management and its impact on the Black Sea, http://danubs.tuwien.ac.at) project. The uncertainties related to the parameterization of several biological processes along with the limitations on temporal and spatial coverage of observations are the main challenges regarding the calibration and validation of a biological model. The satellite-derived chlorophyll-a images by the Sea Wide-Field-of-view Sensor (SeaWiFS: McClain et al. 2004) which cover the entire area of interest almost continuously, prove an extremely valuable tool for this purpose. SeaWiFS has a spatial resolution of about 1.1 km at nadir and records images from the Black Sea between 09:00 and 11:00 GMT (11:00 and 13:00 local time) once per day. The ocean colour Level-1A data were obtained from the Ocean Colour Web of Goddard Space Flight Center at NASA (Feldman and McClain 2006). 169 SeaWiFS full-resolution, daily images for the year 2003 have been processed and analyzed for the determination of satellite derived chlorophyll-a concentration (Chl-a mg m^{-3}). The SeaWiFS data were processed and analysed using the SeaWiFS Data Analysis Software

(SeaDAS: Fu *et al.* 1998) version 4.8 with MSL12 version 5.2. The Chl-a was calculated with the maximum band ratio (OC4v4) algorithm, as described by O'Reilly *et al.* (2000). The OC4v4 algorithm was found to retrieve *in situ* measured chlorophyll-a concentrations on the 68 stations measured in 2002 and 2004 in the western Black Sea with a mean systematic error (MNB) of 30% and a random error (RMS) of 77% (Davidov submitted). An overestimation of chlorophyll *a* in the range of less than 1 mg m^{-3} and an underestimation in the range of more than 10 mg m^{-3} was found by applying the OC4v4 algorithm. Daily composite images were created when more than one scene for a single day was available. The 8-day mean value was calculated from all existing daily images for the corresponding period.

Adopting high frequency forcing in terms of air-sea interaction and of the Danube River inputs, we performed a simulation of the coupled model during the 2002-2003 period. Using a series of 8-day average Chl-a SeaWiFS images over the entire year 2003 period as a validation tool, we tried to improve and assess the model ability to reproduce the observed seasonal primary production variation over the western Black Sea. For model validation, we have also taken into account available in-situ measurements (Chl-a, nutrients, inorganic suspended matter, light attenuation) that were obtained during the 2002-2003 period in the Romanian and Bulgarian shelf areas (Velikova et al., 2005).

The description of the coupled model and the adopted biological formulations are provided in section 2. In section 3, we present the simulation setup in terms of the employed initial/boundary conditions and forcing. The model results are discussed in section 4.

2. Model Description

Hydrodynamic model

The hydrodynamic model is based on the Princeton Ocean Model which evolved from Blumberg and Mellor, (1983) and is a three-dimensional, sigma-coordinate, primitive equation and free-surface model with a 2.5 turbulence closure submodel (Mellor and Yamada, 1982), which calculates the vertical eddy viscosity / diffusivity taking into account the wind stirring and the stratification of the water column. The model has been modified to include river plume dynamics, following the approach developed by Kourafalou et. al. (1996). This is a key model modification that allows the detailed description of the development and evolution of the Danube River plume. A high resolution (~5km) hydrodynamic model of the Western Black Sea is nested to a lower resolution (~10km) basin scale model, which provides

the necessary open boundary conditions (Kourafalou et al., 2004). The model domain is shown in figure 1. Sixteen sigma levels are resolved in the vertical with logarithmic distribution approaching the surface. In order to increase the vertical resolution in the open Black Sea area, permitting a better simulation of the mixed layer dynamics and the entrainment from the subsurface nutrient pool, we employed a maximum water depth of 500 m. We, therefore, define the "open sea area" as the deepest area over the 500m flat bottom depth. The simulated hydrodynamic fields did not show significant differences from those simulated using the hydrodynamic model's initial "realistic" bathymetry (with Hmax~2200m). Therefore, since the current study does not concentrate on circulation details and vertical processes are particularly important for plankton dynamics in the open sea area, we choose the above approximation until we are able to employ a higher vertical resolution.

Biological model

The biological model is a low-trophic level, Fasham type (Fasham et al, 1990), 7-compartment model which is on-line coupled with the hydrodynamic model of the Western Black Sea. The model compartments consist of: Phytoplankton biomass (*P*), Zooplankton biomass (*Z*), Nitrates (*N*), Ammonium (*A*), Phosphates (*PO4*), Nitrogen and Phosphorus parts of biogenic Detritus (*DN, DP*).

The initial model formulation and parameter set was taken by the studies of Oguz et al. (1996) and Staneva et al. (1998) where a 1-D vertically coupled model was calibrated and tested for the open Black Sea area. In the latter studies nitrogen was considered to be the major limiting nutrient. This is a fair approximation for the open Black Sea area where productivity is mostly controlled by the subsurface nutrient pool which is characterized by low N/P ratios due to the removal of Nitrogen through the denitrification process that takes place in the suboxic layer (Murray et al., 1989; Murray et al., 2005). However, the observed N/P ratios (Ragueneau et al., 2002; Velikova et al., 2005) in the Danube influenced waters and river nutrient loads imply a P-limitation and therefore the model was extended to include PO4 and the Phosphorus part of detritus as 2 additional state variables. This was accomplished by adding a Phosphorus limitation on the phytoplankton growth function while maintaining Nitrogen as the model currency and assuming a fixed N/P stoichiometry (16:1) for phytoplankton and zooplankton biomass. Another model upgrade that was proved necessary was the inclusion of a simple benthic model describing the interaction with the sediment in terms of resuspension and deposition of biogenic detritus as well as the flux of

Phosphate and Ammonium resulting from benthic decomposition. Furthermore, Inorganic Suspended Matter (ISM) was included as a model prognostic variable in order to more realistically simulate the light conditions within coastal waters especially during winter where increased ISM river load and resuspension from the sediment may significantly decrease light availability.

The biological variables are treated as biophysical tracers, subjected to advection, vertical and horizontal diffusion. Therefore the local change of every variable *B* can be split into a "hydrodynamic" part resolved by the hydrodynamic model and a "biological" part resolved by the biological model interactions:

$$dB/dt=(dB/dt)_{hydro} + (dB/dt)_{bio} \quad (1)$$

Additional input parameters that are used by the biological model are the photosynthetically active radiation (PAR) at the sea surface $I(z=0)$ (which is derived as half the incoming short wave radiation), the water temperature (T), the bottom stress (BS), the inorganic suspended matter concentration (ISM), the water salinity (S) and the water column depth (H).

The local rates of change of the 7 model compartments as defined by the biological interactions within the water column are as follows:

- Phytoplankton

$$\partial P/\partial t = \Phi(I, N, A, PO4, T, P)\ P - G_P(P,DN, Z, T)\ Z - m_p(P)\ P \quad (2)$$

rate of P change = growth – grazing – mortality

- Zooplankton

$$\partial Z/\partial t = \gamma\ G(P,Z,T)\ Z - m_z(Z,T)\ Z - \mu_z(T)\ Z \quad (3)$$

rate of Z change = growth – mortality – excretion

- Detritus-N

$$\partial DN/\partial t=(1-\gamma)G(P,DN, Z, T)Z - G_d(P, DN, Z,T)Z + m_z(Z,T)Z + m_p(P)P - \varepsilon_N(P,T)DN \pm w_s(DN)\,\partial DN/\partial z \quad (4)$$

rate of DN change= sloppy feeding – Grazing + P,Z mortality – remineralisation ± sinking

- Detritus-P

$$\partial DP/\partial t=[(1-\gamma)G(P,DN,Z,T)Z - G_d(P,DN,Z,T)Z + m_z(Z,T)Z + m_p(P)P]/R_{N/P} - \varepsilon_P(P,T)DP \pm w_s(DP)\partial DN/\partial z \quad (5)$$

rate of DP change = sloppy feeding – Grazing + P,Z mortality – remineralisation ± sinking

- Nitrate

$$\partial N/\partial t = -\Phi_N(I, N, A, PO4, T, P)\,P + \Omega A \quad (6)$$

rate of N change = – uptake by P + oxidation of A

- Ammonium

$$\partial A/\partial t = -\Phi_A(I, N, A, PO4, T, P)\,P + \mu_z(T)\,Z + \varepsilon_N(P,T)\,DN - \Omega A \quad (7)$$

rate of A change = – uptake by P + Z excretion + remineralisation – oxidation

- Phosphate

$$\partial PO4/\partial t = [-\Phi(I, N, A, PO4, T, P)\,P + \mu_z(T)\,Z\,]/R_{N/P} + \varepsilon_P(P,T)\,DP \quad (8)$$

rate of PO4 change = – uptake by P + Z excretion + remineralisation

The following equations represent the benthic model interactions between the last water column layer (indexed as b-1) and the bottom layer (indexed as b):

- Phosphate

$$\partial PO4_{b-1}/\partial t = d_{po4}(T, DP_b) \quad (9)$$

rate of $PO4_{b-1}$ change = diffusion from the sediment

- Ammonium

$$\partial A_{b-1}/\partial t = d_A(T, DN_b) \quad (10)$$

rate of A_{b-1} change = diffusion from the sediment

- Detritus-N

$$\partial DN_{b-1} / \partial t = (w_{res}(BS)\, DN_b - w_{dep}(BS)\, DN_{b-1})/dz \quad (11)$$

rate of DN_{b-1} change = *resuspension* – *deposition*

$$\partial DN_b / \partial t = -(w_{res}(BS)\, DN_b + w_{dep}(BS)\, DN_{b-1})/dz_b - d_A(T, DN_b) - b\, DN_b \quad (12)$$

rate of DN_b change = – *resuspension* + *deposition* – *diffusion of NH4* – burial

- Detritus-P

$$\partial DP_{b-1} / \partial t = (w_{res}(BS)\, DP_b - w_{dep}(BS)\, DP_{b-1})/dz \quad (13)$$

rate of DP_{b-1} change = *resuspension* – *deposition*

$$\partial DP_b / \partial t = (-w_{res}(BS)\, DP_b + w_{dep}(BS)\, DP_{b-1})/dz_b - d_{PO4}(T, DP_b) - b\, DP_b \quad (14)$$

rate of DP_{b-1} change = – *resuspension* + *deposition* –- *diffusion of PO4* –- *burial*

The mathematical expressions for the above used functions are described in Table 1 while all the employed parameters are given in Table 2 and temperature dependence of different processes in Table 3. The adopted functions and the choice of the parameter values are briefly discussed below. It should be noted that, as the phytoplankton variability depends both on grazing pressure and phytoplankton growth limitation functions -each one depending on several different processes- the model parameter set can not be regarded as unique. The parameter values were chosen so as to achieve the best possible fit to the observed phytoplankton seasonal variability, while keeping parameter values as close as possible to those obtained from the available literature. Furthermore, variable parameters were chosen so as to roughly converge to Oguz et al. (1996) values towards the open sea area.

Phytoplankton

The function *Φ(I, N, A, PO4, T, P)* denotes the phytoplankton growth rate and is parameterized according to the Liebig's law of the minimum, assuming that either light or nutrient limitation (but not both) controls phytoplankton growth (Oguz et al., 1996). A temperature dependence is assigned to the maximum growth rate following Eppley (1972).

The light limitation $L_I(I)$ is parameterized according to Jassby and Platt (1976), assuming that the photosynthesis efficiency parameter a is constant.

Photosynthetically available radiation $I(z)$ is assumed to decrease exponentially with depth. The total attenuation coefficient $k_{tot}(z)$ is split into contributions by clear water (k_w), phytoplankton shelf-shading (k_c), organic (k_d) and inorganic (k_s) particulate matter. In Oguz et al. (1996) the values for the attenuation of water k_w=0.08 and phytoplankton k_c=0.07 were chosen in order to fit light attenuation observations in the open sea during spring and summer (Vidal, 1995; Vladimirov et al., 1996). Since inorganic particulate matter is now a model variable, we used lower attenuation values for k_w=0.04 and k_c=0.03 according to Fasham et al. (1990) and Lorenzen (1972). We chose the values for organic (k_d) and inorganic (k_s) particulate matter to k_d=0.01, k_s=0.06, based on a best fit to the observed Chl-a patterns during winter light limited periods, while keeping simulated k_{tot} values in the open sea close to those from Oguz et al. (1996) (see also discussion later). In that way we tried to provide a more realistic description of the seasonal variability for light conditions within coastal waters, which are expected to be more turbid during winter, due to the increased resuspension and river load of particulate matter.

The Nitrogen limitation function is based on Wroblewski (1977) and accounts for the inhibition of Nitrate uptake in the presence of Ammonium.

A present study innovation is the adoption of a variable half-saturation function (rather than constant) for nutrient uptake, as well as for zooplankton grazing that will be discussed later. The most frequently used formulation, along with internal storage formulations (e.g Droop, 1968), is the one introduced by Monod (1942) which has the form:

$$V = V_{\max} * \frac{NUT}{NUT + K} \qquad (15)$$

where NUT is the nutrient concentration and K is the half-saturation constant representing the nutrient concentration where the uptake rate V reduces to half its maximum value V_{max}. This formulation was confirmed for monospecific cultures under steady state conditions and is a generally accepted model describing a single-species nutrient uptake mechanism (Button, 1978). The half-saturation constant has been calculated for many different species (e.g MacIsaac and Dugdale, 1967; Eppley et al., 1969) and may vary significantly according to the nutrient environment to which they are adapted. Different (V_{max}, K) values are a way to explain resource competition amongst species (Dugdale, 1967; Tilman, 1981). In oligotrophic environments, for example, a low K value adaptation (usually with the cost of having a lower

V_{max}) permits the cell to grow faster under lower nutrient concentrations and thus to dominate against other species with higher K values. A natural system that is characterized by significant spacial and/or time variability in terms of nutrient conditions and subsequently of species composition cannot be described by a single K value Monod equation. Deviations from the Monod kinetics have been shown for mixed populations with different K values (Williams, 1973; Turapchak and Herche, 1986), especially when the relative species abundances are significantly different (Turapchak and Herche, 1986).

An alternative formulation adopting a variable half-saturation function, rather than constant, was introduced by Contois (1959):

$$V = V_{\max} * \frac{NUT / P}{NUT / P + b} = V_{\max} * \frac{NUT}{NUT + b * P} = V_{\max} * \frac{NUT}{NUT + K(P)} \qquad (16)$$

The nutrient uptake rate in this case depends rather on the ratio of available nutrients per unit phytoplankton biomass *NUT/P* or equivalently, the half-saturation function increases linearly with biomass. The Contois formulation was shown to better describe nutrient uptake in mixed cultures while its predicted negative dependence of growth rate on biomass concentration was attributed to the accumulation of inhibitory metabolic byproducts (review in Jost, 2000). In the present study context, the Contois formulation provides a means of adjusting nutrient uptake according to the actual nutrient conditions assuming an adaptation of the dominant species to these conditions. As pointed out by Morrisson et al. (1987), this formulation seems to be more suitable than the Monod expression for non-homogenous systems (many species, nutrient gradients etc). In the present study an intermediate function $K(P)=a+b*P$ (which reduces to Monod for $P=0$) was adopted, that is similar to Roques et al. (1982). Setting a lower limit for the half-saturation function signifies some kind of threshold for nutrient uptake.

The phytoplankton mortality is parameterized using a sigmoid function according to Ryabchenko et al. (1997) in order to increase the model stability.

Zooplankton

The equivalent of the Monod formulation was introduced by Holling (1959) to describe the variability of zooplankton grazing rate on phytoplankton concentration:

$$G = G_{\max} * \frac{P}{P + K_Z} \tag{17}$$

K_Z is the half-saturation constant where the grazing rate G reduces to half of its maximum value G_{max}. This formulation reflects the saturation of the attack rate as phytoplankton concentration increases, because of the finite number of preys the predator can handle. The above formulation has been criticized because it predicts an increase of only the herbivore biomass (of two trophic levels in our case) in response to an increase of phytoplankton growth rates, while in natural systems abundances of all trophic levels are expected to vary proportionally (review in Ginzburg and Akcakaya, 1992). Arditi and Ginzburg (1989) and Arditi and Akcakaya (1990) proposed that a way to resolve this paradox is to describe the predator attack rate as a function of the prey/predator concentration ratio *P/Z* (which is equivalent in form to the Contois function for nutrient uptake) as a result of predator mutual interference. This concept of decreasing grazing efficiency in higher predator densities was also earlier introduced by De'Angelis et al. (1975). Using such a "ratio dependent" function prevents the occurrence of limit cycles that are a symptom of using the Holling formulation. During our preliminary simulations, using the Holling formulation resulted in a significant underestimation of phytoplankton concentration and the occurrence of unrealistically large amplitude oscillations that were prevented only after a significant reduction of the maximum grazing rate. Gregoire et al. (2004) also mentioned that a 10-fold increase in phytoplankton growth rates was reflected by only a zooplankton stock increase, which also sounds like a symptom of using the Holling formulation. Trying to avoid such an unrealistic variability lead us to the adoption of a formulation that is similar to the one proposed by De'Angelis (the equivalent of Roques et al., 1982 for nutrient uptake) which is an intermediate model reducing to Holling for low zooplankton values:

$$G = G_{\max} * \frac{P}{P + a_z + b_z * Z} \tag{18}$$

The above function has been generalized in order to include zooplankton grazing on both phytoplankton and detritus. The zooplankton preference functions are assumed to depend on the relative phytoplankton and detritus concentrations following Fasham et al. (1990).

Steele and Henderson (1992) revealed the importance of the zooplankton mortality (as a closure term of an NPZ model) parameterization on the overall ecosystem dynamics. The

zooplankton mortality can be expected to increase with increasing zooplankton density, as a result of a higher predator whose biomass may be assumed to vary proportionally to its prey (Steele and Henderson, 1981) or as cannibalism, including predation between different species that comprise the same aggregated zooplankton compartment (Kohlmeier and Ebenhoh, 1995). The "s-shaped" function that we have adopted for zooplankton mortality rate may be interpreted to represent a satiable higher-predator that reduces its searching efforts for low prey concentrations (Edwards and Yool, 2000). A temperature dependence (Q_{10} =2.2) was also assigned in our formulation permitting the representation of the "higher predator's" seasonal cycle. The choice of zooplankton mortality parameters (m_z, K_{mz}, Q_{10}) was based on the best fit of the phytoplankton seasonal variability as deduced by our model and SeaWiFS observations.

Given the strong control exerted by higher predators on zooplankton communities (e.g. Oguz et al. 2001a; Lebedeva and Shushkina, 1994), particularly in the eutrophic Northwestern shelf area, the parameterization of zooplankton mortality plays a significant role in simulating the phytoplankton variability. The adopted parameterization, even though unable to capture the time variability that arises from the trophic interactions and the different physiology (temperature dependence, functional response, reproduction patterns) of the different groups that comprise the assumed "higher predator", provides a reasonable first approximation in the context of the present model simplicity.

Adopting a variable mortality rate provides a means to prevent the occurrence of unrealistic limit cycles (Steele and Henderson, 1992; Edwards and Yool, 2000) while keeping the Holling formulation for zooplankton grazing. In fact, the choice of the grazing formulation has no significant impact on phytoplankton biomass in the productive river influenced waters, where the increased zooplankton predation mortality results in a quite low grazing pressure. However, zooplankton mortality is a "top-down" control defined by the biomass of higher predators that may depend on external factors (such as top-predation, temperature, anoxia etc). Adopting the "ratio-dependent" grazing formulation which introduces a "bottom-up" negative feedback mechanism increased the model stability and robustness even under lower zooplankton mortality rates (see discussion of model results later).

Detritus

Microbial decomposition of particulate and dissolved organic matter (comprising the detritus compartment) is likely to proceed at much higher rates within coastal eutrophic areas. The detritus decomposition rate therefore is assumed to increase with increasing phytoplankton concentration, since the bacteria biomass, which is not explicitly represented, can be expected to follow an algal biomass increase and the subsequent production of Particulate Organic Matter (POM). A similar model formulation was proposed by Di'Toro and Matystic (1980); the difference in our model formulation is that we set a lower limit in the remineralisation rate for low phytoplankton concentrations. Significant correlation between decomposition rates and photosynthesis has also been recorded in in-situ measurements (e.g. Harrisson, 1978). We chose using phytoplankton rather than detritus as the depending variable, because fresh organic matter is expected to decompose at much faster rates. Garber (1984) indicates decomposition rates of 0.02-0.2 day^{-1} for the more labile fraction of POM. A maximum rate of 0.2 day^{-1} was assigned for Nitrogen (in the open sea the nitrogen remineralization rate reduces to ~0.05 day^{-1} on average as in Oguz et al. (1996) while a higher value of 0.3 day^{-1} was fitted for phosphorus (see discussion later). Higher decomposition rates for Phosphorus have been shown to occur at least during the initial phase of decomposition (Garber, 1984; Grill and Richards, 1964) and are also suggested by the increase of dissolved and particulate organic matter N/P stoichiometry over depth (Hopkinson et al., 2002, Knauer et al. 1979).

The detritus sinking velocity can be expected to increase at higher concentrations as a result of flocculation. Therefore a hyperbolic function is adopted as in Oguz et al. (2001a).

Benthic model

An initial organic matter benthic pool ($DP_{b0}(S,H)$, $DN_{b0}(S,H)$) was assumed to vary as a function of the annual mean surface salinity and water column depth (therefore, higher values to river influenced coastal areas were assigned). The deposition and resuspension rates of biogenic detritus from this sediment pool are thus calculated as functions of the bottom stress, which is provided by the hydrodynamic model (Guan et al., 2001). The employed function for erosion is based on Partheniades (1965) while the deposition formulation is based on Krone (1962).

Benthic decomposition is parameterized assuming a temperature dependent diffusional flux of phosphate and ammonium from the sediment pool. The maximum benthic fluxes (0.15 mmol P m^{-2} day^{-1} for phosphate and 1 mmol N m^{-2} day^{-1} for ammonium) were assigned taking

into account the Friedrich et al. (2002) estimates from in situ measurements within the Danube front area (fig. 8 of Friedrich et al., 2002) during summer 1995 and spring 1997 (see also discussion later).

The assigned values for the maximum benthic pool concentrations (100 mmol N/m^{-2} ; 6.25 mmol P $/m^{-2}$) were chosen so as to achieve a reasonable seasonal variability of the benthic pool and the associated benthic fluxes in response to the deposition/resuspension variability. Assigning much higher values would make the benthic pool practically constant, while lower values would result in unrealistic short term variability.

Inorganic Suspended Matter

The ISM is subjected to resuspension and deposition using the same formulation as for biogenic detritus. The assumed initial sediment pool however, is defined assigning a smaller weight on salinity and a larger weight on water column depth. The dependence of the ISM settling velocity on flocculation was parameterized using a function of only ISM concentration of the form $w = a * (ISM)^b$ (Krone, 1962; Dyer, 1989; Shi and Zhou, 2004). Additional dependencies on shear stress (Burban et al. 1989) and salinity would be probably necessary for a more accurate sediment transport model that is beyond the scope of this study.

3. Simulation setup

Forcing

The air-sea interaction for the 2002-2003 period was based on 6-hourly meteorological forcing with ~10Km horizontal resolution, provided by the operational atmospheric model of the Hellenic Center for Marine Research POSEIDON Project (Papadopoulos et al., 2002; http://www.poseidon.ncmr.gr/). Such high-frequency and high-resolution atmospheric forcing was particularly valuable for the simulation needs, as it permitted the capture of the high variability in the Danube plume transport pathways. The provided meteorological data included 10m wind speed, 2m air temperature, 2m relative humidity, precipitation, incoming long-wave radiation and incoming short-wave radiation. These data were used by the hydrodynamic model to evaluate the surface heat, water and momentum fluxes using the bulk formulas that are adopted by the POSEIDON operational hydrodynamic model (Nittis et al., 2006). The incoming short wave radiation was also used as an input parameter in the biological model. In figure 2 we can see the wind variability in the Danube front area and the variability of the average wind speed over the Western Black Sea area.

Daily Danube discharge rates and nutrient inputs (figure 3) were calculated by a model of the Danube Delta (Constantinescu et al., 2000; Gils et al., 2005) based on estimated nutrient emissions by a model of the Danube catchment area (Schreiber et al., 2005) and measurements. The N/P ratio of the Danube input for 2003 (not shown) has a lower value of 30 during summer 2003 and a maximum above 100 during winter. Therefore Phosphate is expected to be the most limiting nutrient in river influenced waters. For the other major Western Black Sea rivers (Dniepr, Bug, Dniestr) we employed constant values of discharge rates based on climatology by Kourafalou and Stanev (2001). The dissolved inorganic nitrogen and phosphate concentrations were assigned to 1/10 and 1/5 of the respective Danube concentrations, giving a total load of about 3% for nitrogen and 7% for phosphorus of the Danube inputs as suggested by Friedl et al. (1998).

Initial and Boundary Conditions

The initial conditions (temperature, salinity and biological variables) for the 2002-2003 simulation were provided by a 1-year long “climatological” type simulation of the coupled model under perpetual year daily mean air-sea fluxes with high frequency anomalies superimposed. These air-sea fluxes as well as the initial density field were provided by a long-

term climatological run of a basin scale hydrodynamic model (Staneva et al., 1997). On the other hand, the Danube discharge rates and nutrient inputs were assigned to their 2001-2002 year period values in order to approximate the actual nutrient conditions in the beginning of the 2002-2003 simulation.

For this "climatological" simulation the initial conditions of the biological state variables were obtained by simulating the vertical profiles with a 1-D version of the coupled model that was based on Oguz et al. (1996) and then adopting a density dependent intepolation on our 3-D coupled model grid. Using density rather than depth for the interpolation into the model grid is aiming at the exclusion of the horizontal variability due to dynamical effects (Tugrul et al,. 1992; Saydam et al., 1993). The nutrients horizontal distributions were further increased along the low salinity gradient in order to provide an initial representation of the eutrophic riverine waters. In proportion, a combined function of salinity and water column depth was used to describe the initial sediment nutrient pool. The initial nitrate and phosphate vertical profiles in the open sea were fitted to the data obtained by the Knorr campaign on April 2003 (www.ocean.washington.edu/cruises/Knorr2003), that revealed a value of ~4μM for the nitrate subsurface maximum concentration. The subsurface nitrate pool has been shown to exhibit a significant inter-annual variability in response to the variation of primary production and the subsequent fluxes of organic matter in the water column (Konovalov et al., 2005). Nitrate maximum values of ~6μM, ~12μM and ~3μM have been recorded during 2001, 1991 and 1969 respectively.

Since the model vertical resolution does not permit a proper representation of the subsurface nitrate maximum, a constant value was assigned below this maximum in order to prevent the establishment of artificial horizontal variability. Consequently, the removal of nitrates through denitrification has not been taken into account.

The values of biological variables along the open eastern boundary are relaxed to an area average over the open sea along isopycnal surfaces. In that way we avoided a simulation of the coupled model over the entire Black Sea that would significantly increase the computational time.

4. Discussion of Results

Seasonal variability of phytoplankton growth

We first examine the seasonal variability of the phytoplankton growth rate as an average for the open sea (deepest area over the 500m flat bottom depth) and the coastal Danube influenced area (defined as bounded by the 17 psu isohaline). In the next section, we will discuss the simulated horizontal patters in comparison with SeaWiFS images for the same periods in 2003.

The phytoplankton concentration that is captured by the SeaWiFS images may be assumed to be representative of the relatively homogeneous zone that is actively mixed from the surface, due to wind stirring and convective overturning in the winter. The so-called "MiXing Layer" (Gregoire et al., 2004) Depth (MXLD) depends on the mixing conditions, represented in the model by the vertical eddy diffusivity. For the purposes of our analysis, we define the bottom of the mixing layer at the depth where eddy diffusivity reduces to 10 cm^2/s.

The MXLD variability, averaged over the open sea and over the coastal river influenced waters is shown in figure 4 together with the total attenuation coefficient k_{tot}, the ISM concentration, the phytoplankton growth rate, as well as the light and nutrient limitation functions as averages over the MXLD again for the open sea and coastal areas. For the total attenuation coefficient, our formulation, which includes an ISM contribution and has used the parameters (k_w=0.04; k_c=0.03), is plotted against the formulation in Oguz et al. (1996), which does not include ISM and has values (k_w=0.08; k_c=0.07).

During winter, the primary production is mostly limited by light availability, due to the reduced incoming solar radiation and the increased vertical mixing. The light limitation in the open sea area (fig. 4a) is as expected stronger (indicated by lower values of the light limitation function, that takes values from 0 to 1 with 1 signifying no limitation, fig.4a) than in coastal waters (fig. 4b) due to the higher mixing layer depth (reaching 40-50m during the stronger wind periods in December and February, fig. 4c; see also fig. 2b). In coastal waters shallow depths and stratification induced by low salinity limit the mixing layer depth to 5-10m (fig. 4d) and light limitation is mostly due to the increased particulate matter concentrations as a result of resuspension from the sediment and increased river loads. The peaks on k_{tot} for coastal waters (reaching ~1 m^{-1}, fig. 4f) coincide with storm events during December and February which result in significant resuspension from the sediment (fig.4h). An increase on k_{tot} in the open sea (fig. 4e) is also observed in correlation with increased

suspended matter concentrations (fig.4g) that slowly decrease after spring as ISM supply from river load and coastal erosion is diminishing. While the open sea k_{tot} is roughly the same to the one calculated using the Oguz et al. (1996) formulation (with differences not exceeding ~0.015 m^{-1}), in the coastal area the differences are noticeable. The Oguz et al. (1996) formulation produces lower light attenuation values during winter, since the particulate matter contribution is not represented, and slightly higher values during summer, which arise from assigning a higher value to the phytoplankton contribution k_c. The simulated k_{tot} values using either formulation were in agreement with available coastal secchi disk observations in the spring to autumn seasons 2002 (A. Cociasu, personal communication). Unfortunately no observations were available during winter, that would permit us to confirm the much higher simulated attenuation coefficient values. However, our representation of the resuspension processes and the correlation with the winter storm events is encouraging and will allow a more realistic parameterization of the light attenuation variability once data become available.

In the beginning of March the mixing layer depth significantly decreases both in coastal and open sea areas (fig. 4c,d) as winds get weaker (fig.2) and the seasonal thermocline begins to develop. In response, the light limitation function is sharply increased (1 signifies no limitation, fig. 4a,b). A more moderate increase is however encountered in phytoplankton growth rate (red line fig. 4i,j) due to the low temperatures in both coastal and open sea areas. In order to investigate the effect of temperature on phytoplankton growth we have calculated the average growth rate assuming no temperature dependence (i.e. Q10=1, blue line in figures 4i,j). As clearly shown in figure 4i,j, a much stronger spring bloom is encountered if no temperature dependence is assigned. One should also notice that, surprisingly, a higher impact of temperature in both coastal and open sea areas is observed during the spring period (March-May) rather than the colder, on average, winter period (December-February); lowest temperatures are observed in mid-February for the coastal area and mid-March for the open sea. This is because during the lowest available light period in winter, the phytoplankton growth rate lies in the beginning of the light limitation curve (also known as the P-I curve), where the variation of the maximum growth rate $P_{max}=\sigma_m L_T(T)$ with temperature has a minor effect, since the photosynthesis efficiency parameter a (representing the initial slope of the P-I curve) is assumed constant. As the light limitation function increases during spring, the impact of the variation of P_{max} with temperature is much higher.

In the open sea area the late winter-spring bloom is fueled by the nitrates (as nitrogen is the most limiting nutrient) that were brought to the surface from the subsurface deposit during winter and particularly in the December and February stronger mixing periods. As the nitrates

are gradually exhausted (not shown), the growth rate (fig. 4i) drops to very low values after May. The vertical mixing increases again after October (fig. 4c) giving rise to an autumn bloom (fig. 4a,i). In the river influenced area the nutrient limitation function (fig. 4b) and the associated growth rate (fig. 4j) sharply decrease after the first bloom in the beginning of March. The increase of nutrient river load (fig.3) and the enhancement of vertical mixing in the autumn period can be accounted for the respective increase of phytoplankton growth rate.

In figure 5 we present the model simulated vertical structure of the phytoplankton and zooplankton biomass seasonal variability, averaged over the open sea area. A subsurface chlorophyll maximum (~0.6 mmol N/ m^3 ~1.2 mgr Chl-a /m^3) is simulated during summer at a depth of ~30m (fig. 5a) where available light is combined with nutrients diffused from below (fig. 5b). The zooplankton biomass (fig. 5c) follows the phytoplankton biomass variation attaining maximum values of ~0.3 mmol N/ m^3 during the spring of 2003.

Comparison with SeaWiFS

In figure 6 we present the model simulated surface phytoplankton patterns against the SeaWiFS Chl-a images for the same time periods covering the entire year 2003. Conversion from nitrogen model units to Chl-a units was made assuming the Redfield ratio C/N=6.625 and C/Chl-a=40 (Ragueneau et al., 2002), giving a factor of ~2 (mgr Chl-a / mmol N).

The spatial and temporal coverage of the satellite images provided a valuable tool for the evaluation of model results. As seen in figure 6, there is an overall very good agreement on the horizontal chlorophyll patterns, over different periods in the yearlong simulation. Both computed and observed horizontal patterns are closely linked to the transport pathways of the Danube inputs that are mostly determined by the amount of river discharge and the wind variability. During winter and until the early spring of 2003, the prevailing winds were strong and mostly downwelling-favorable (from the North, Northeast - which is typical for this season) in the Danube area (fig. 2a). Therefore, the Danube plume was constrained near the coast and directed to the South. During summer, the prevailing winds were mostly upwelling favorable (from the South, Southwest), resulting in the offshore expansion of the Danube plume toward the East and Northeast.

During winter, phytoplankton growth is limited by light availability as mentioned above. Within coastal areas both model simulated patterns and SeaWiFS images (fig. 6a,b) in January 2003 present a relatively low phytoplankton concentration (as compared to the

summer season), which can be attributed to the reduced incoming short wave radiation (minimized in early January 2003, not shown) combined to the increased vertical mixing (fig. 4d) and high light attenuation due to increased ISM concentration. In the river plume area average time series shown in figure 4, light attenuation and ISM concentration do not present particularly high values in January 2003 because they are mostly correlated to water column depth, while the low-salinity plume (that defines the averaging area) is extended offshore due to occasional westerly winds (fig.2a). In December and February periods, as the river plume is confined near the coast due to strong northerly winds (fig.2a), light attenuation and ISM concentration present particularly high values. The model simulated Chl-a is a bit underestimated in the southwestern coastal area possibly due to an overestimation of the ISM concentration. Another probably additional cause, is that model bathymetry over the Bulgarian and Turkish shelf areas is a bit deeper than in reality due to model smoothing toward the much deeper open sea areas. In the northwestern coastal areas, shallow water column depths result in a lower light limitation despite the even higher ISM concentrations. A model calculated patch of low-salinity and high-chlorophyll water at around (30^o E, 42^o N) is not observed in the SeaWiFS image.

A phytoplankton bloom in the Danube area (in front and in the south) is observed in the SeaWiFS image of 14-21 March (fig. 6d). As there was no available image for early March we can not identify the exact bloom initiation period. A similar although weaker, bloom is simulated by the model slightly earlier in 3-10 March (fig. 6c), as phosphorus is later on quickly exhausted (see nutrient limitation in fig. 4b) leading to a higher underestimation of phytoplankton concentration (as compared with the SeaWiFS image of 14-21 March 2003). This could be attributed to an underestimation of the phosphorus river load or a weak remineralization rate in the model. A higher maximum remineralization rate has already been assigned for phosphorus (0.3 day^{-1} vs 0.2 day^{-1} for nitrogen) but we are reluctant to further increase remineralization rates, since a better understanding of the decomposition process would require at least an explicit representation of bacterial biomass (see also comparison with in-situ data discussion). The simulated phytoplankton concentration along the Turkish coast is overestimated as compared to the SeaWiFS image probably due to an overestimation of the Nitrogen river load during winter since open sea Phosphorus, in contact with the southern Turkish coast, is always not limiting. The model simulated phytoplankton in the open sea area (~1.5 mgr Chl-a/m^3) is slightly higher than in the SeaWiFS image (~0.8 mgr Chl-a/m^3). One possible reason is the insufficient model vertical resolution that results in

excessive vertical mixing from the subsurface nutrient pool, particularly in areas of sharp bathymetric variation (which coincide with the areas of higher phytoplankton concentration).

During summer, primary production is mostly sustained by riverine nutrients and regeneration processes and thus is confined to river influenced waters and coastal areas where nutrient fluxes from the sediment provide an additional source. During most of the summer period winds are southerly or southeasterly in the Danube area, thus leading the Danube plume toward the North, Northeast. As the river supply is cut off, the productivity along the Romanian shelf gradually decreases from May until July. Along the Turkish coast, the primary production is occasionally enhanced due to upwelling (Oguz et al., 2002). Such an enhancement is observed during June (fig. 6h), as winds are easterly (upwelling favorable) along the Turkish coast. The model simulated phytoplankton is underestimated along the Turkish coast even though coastal upwelling can be tracked from the simulated temperature patterns. In fact the simulated Chl-a concentrations are comparable to SeaWiFS at a depth of ~15m which may be an indication of the fact that the SeaWiFS image is representing an integrated part of the water column according to its "reflecting" properties. The Chl-a concentration is slightly higher as compared to the SeaWiFS image, in the coastal area between rivers Dniestr and Danube in mid July 2003. However, the overall agreement is remarkable, for both coastal and open sea areas.

The high-chlorophyll waters follow the evolution of the Danube plume and are subjected to the wind variability. It is interesting to notice how the high-chlorophyll plume evolves under abrupt changes in wind direction. After a period of persistent southerlies during June 2003 (fig. 2a), the plume, that was spread to the East and Northeast (fig. 6e,f and fig. 6g,h), is subjected to an extended anticyclonic turn offshore and to the South (fig. 6i,j and 6k,l), as the winds are turning west in mid July 2003. Subsequently, in late July and in the beginning of August, as the winds change to northerlies the chlorophyll plume that was widely spread over the Ukrainian shelf gradually diminishes (fig. 6k,l and 6m,n) due to the cut of supply from Danube.

During autumn, the onset of cold fronts and northerly winds elongated the plume along the western Black Sea coast (fig. 6o,p). As the increased wind stirring enhances the resuspension of organic matter from the sediments and the vertical diffusion from the subsurface nutrient pool, primary production is increased over the shelf and open sea areas. The simulated autumn bloom in the open sea area is not as strong, as compared to SeaWiFS, and shifted towards November probably due to an underestimation of vertical mixing, possibly arising again from the insufficient vertical resolution. Another possible cause for the

observed more intense autumn bloom could be an increased higher predator zooplankton mortality as suggested by Oguz et al. (2002). It is possible that the inverse situation (lower zooplankton mortality) occurs in the spring, which could explain the model overestimation of the spring bloom. In the river influenced waters a decrease of Chl-a is revealed by both model simulated and SeaWiFS October and November 2003 patterns, which can be attributed to the light limitation related to increased ISM concentration (fig. 4f,h). The underestimation of model simulated Chl-a for November 2003 in the western coastal areas most likely arise from the inaccurate simulation of ISM, similar to the January 2003 results, mentioned above.

In the above discussion we attempted to evaluate the model simulated Chl-a patterns employing SeaWiFS images that offered good spatial and temporal coverage. However, we should note that satellite derived Chlorophyll-a patterns are subject to certain accuracy limitations, resulting from sensor capabilities, calibration procedures, choice of bio-optical algorithms etc. (McClain et al. 2006, for a review on SeaWiFS validation).

Benthic fluxes and N/P limitation

In figure 7 we present the seasonal variability of the Nitrogen and Phosphorus fluxes at the sediment interface that result from resuspension/deposition of organic matter and diffusion of Phosphate and Ammonium from the sediment. The averaging area is the Danube front area, of about 2400 Km^2 (fig.1), so as to be comparable with the estimates of Friedrich et al. (2002, see their figure 8). During winter, the net deposition (deposition minus resuspension) of POM is minimum, since primary production (which is the main source of POM) is reduced due to the light limiting conditions, while the increased vertical mixing enhances resuspension from the sediment and/or prevents the POM deposition. However, a little proportion of the resuspended organic matter is decomposed, as the remineralization rate is a function of temperature and phytoplankton biomass (both reducing during winter). The POM net deposition attains maximum values during summer (May-August), as wind stirring is weak and primary production is high. During short periods of stronger wind stirring, resuspension from the sediment is enhanced, resulting in the nutrient enrichment of surface waters. The variation of the diffusional flux of Phosphate and Ammonium from the sediment is defined by the temperature seasonal variability, as well as the variability of the sediment pool concentration according to the deposition/resuspension history. The Phosphates benthic flux roughly balances net sedimentation, representing an important nutrient source that is

comparable to the Phosphorus river load, particularly during summer. The adopted benthic fluxes of Ammonium and Phosphates are characterized, by a N/P molar ratio of about 7:1 accounting for the losses of Nitrogen through denitrification in the sediment. Therefore, the sediment fluxes are expected to contribute to a Nitrogen limitation of primary production in coastal areas that are outside the immediate influence of river inputs.

The annual and seasonal mean benthic fluxes for the Danube front area (fig.1) are presented in Table 4. The simulated phosphate flux for spring 2003 (8.2 tons/day) is rather close to the estimate of Friedrich et al. (2002) for spring 1997 (7 tons/day), while the simulated flux for summer 2003 (10.1 tons/day) is considerably lower than the estimated flux for summer 1995 (17 tons/day). The model simulated ammonium flux was fitted to lower values (26 tons/day for spring and 31 tons/day for summer) than Friedrich et al. (2002) estimates (43 tons/day for spring 1997 and 66 tons/day for summer 1995), because adopting a higher ammonium flux was shown to produce an overestimation of phytoplankton during the summer to autumn period, mostly along the Ukrainian coastal areas. The simulated ammonium fluxes represent about 49% of the Nitrogen net sedimentation, which is similar to the budget calculation (37%) of Gregoire and Friedrich (2004) for the 1995/1997 period. Therefore, it seems that the simulated decrease of ammonium benthic fluxes, as compared to the 1995-1997 period, is consistent with a similar decrease of Nitrogen net sedimentation (model simulated ~3 mmol N/m^2, compared to ~5 mmol N/m^2 from Gregoire and Friedrich, 2004). Such a decrease of the net sedimentation rates and subsequently of the phosphate and ammonium fluxes is probably expected, considering the phosphate river load reduction (~50%) since the 1995/1997 period.

In figure 8 we can see the lines where the dissolved inorganic nitrogen to phosphorus ratio equals the Redfield ratio N/P=16:1, thus setting the boundaries between the N and P limitation areas. During winter (December-February) the P-limitation extends from the Danube area to the Turkish coast, as river loads are characterized by very high N/P ratios. In spring (March-May) the P-limitation area is a bit confined to the south as the river load N/P ratio is decreasing. It is also spread toward the northern Danube area due to the advection of the river plume that results from the southern winds prevailing during May (fig. 2a, fig.6e,f). During summer and autumn the extent of the P-limited domain gradually diminishes in the Danube front area as the N river load is greatly reduced (fig. 3), while benthic fluxes (characterized by N/P ratio of ~7:1) also contribute to N-limitation.

Simulations with an earlier version of our model that considered Nitrogen to be the only limiting nutrient, presented a significant overestimation (~2-fold) of the phytoplankton March

bloom in the Danube influenced area, resulting from the quite high N/P ratios of nutrient river loads. As the N/P ratio of nutrient loads decreases toward the summer and autumn periods, the Nitrogen based 5-compartment model showed similar results with the current 7-compartment model that includes Phosphorus.

Comparison with in-situ data

In figure 9 we can see the model simulated Chl-a, nitrate and phosphate in the Danube front area and the Romanian shelf area against in-situ data that were collected during 2003 (A. Cociasu, personal communication). The two averaging areas together with the measurements locations are shown in figure 1. The significant horizontal variability that all variables exhibit along the productivity gradient makes such a comparison a bit difficult but also beneficial particularly regarding the dissolved nutrients variability.

In the Romanian shelf area there is a remarkably good agreement between model simulated and observed Chl-a values during all seasons. Despite this agreement in chlorophyll values, the model simulated nutrient concentrations exhibit certain periods with significant discrepancies from the observed. Both model results and in-situ measurements exhibit a drop in nitrate and phosphate following the early March 2003 spring bloom, but the model phosphate drops too fast, as already mentioned. During May, phosphate, which is the limiting nutrient, is practically exhausted. From late June and later on, where nitrogen is the limiting nutrient, the situation reverses and nitrate is exhausted. A possible cause could be the overestimation of the nutrient uptake rates that results in the diminution of limiting nutrients concentrations. Maximum photosynthesis rate and phytoplankton internal nutrient pools are known to vary depending on the actual nutrient conditions. The explicit simulation of such a variation, however, would require a much more sophisticated phytoplankton growth model such as Geider et al. (1998). Another possible parameterization that would prevent the underestimation of the limiting nutrients concentrations could also be the employment of a higher remineralization rate, combined with a higher grazing pressure, in order to maintain the correctly simulated Chl-a variability. This approach seems reasonable since during summer, when diminishing nutrient concentrations occur, the river nutrient supply is cut off due to the prevailing southerly winds and therefore, primary production in the Romanian shelf can only be sustained by regeneration processes. Assigning a higher remineralization rate would also sustain a stronger March bloom in the Danube prodelta area that was shown to be

underestimated (fig. 6c). Some experiments with our model that employ the above procedure show encouraging results. However, further tuning of the remineralization rate would require the addition of bacteria as a model compartment. Bacteria are usually characterized by a higher nitrogen and phosphorus content than phytoplankton (Goldman et al., 1987) and take up inorganic nutrient forms in order to meet their stoichiometric demands. The net remineralization rate depends on the above stoichiometric differences as well as the organic matter and nutrient availability (Goldman et al., 1987; Tanguy and Loreau, 2001; Fasham et al. 1990) and therefore its dynamic variability cannot be properly represented by the simplified formulation in the current study.

In the Danube frontal area, the model simulated Chl-a values agree fairly well with the observed, in May and August 2003. Perhaps an overestimation is suggested by the fact that the observed values lie at the lower limits of the model simulated Chl-a variability. However some discrepancies would be anticipated in the Danube frontal area, due to the model uncertainties related to the initial dispersion of the river outflow and also because the effect of low salinity on phytoplankton (Ragueneau et al., 2002) has not been taken into account. In September 2003, in-situ Chl-a values are curiously very low (below 1mgr/m^3 for most stations) which can be possibly attributed to some short event of diminished river plume, that cannot be tracked from the SeaWiFS (or the model simulated) patterns. In November 2003, the model simulated Chl-a is lower than the observed, resulting from the small scale differences between the model and SeaWiFS Chl-a horizontal distributions (fig.6s,t), which were attributed to an overestimation of the ISM related light limitation. The model simulated nitrate concentration presents a good agreement with the observed values, except in the spring period where the model prediction is too high, probably due to an overestimation of the Nitrogen river input during winter as already mentioned. Phosphate, which represents the limiting nutrient throughout the year, is underestimated in May and particularly in August probably following a similar reasoning as with the Romanian shelf case. In November, higher model simulated phosphate can be attributed to the underestimation of phytoplankton, explained above. The excess of phosphate in the Danube front area also contributes to the overestimation of phosphate that is encountered in the Romanian shelf area.

Impact of ratio-dependent formulations for nutrient uptake and zooplankton grazing

A variable half-saturation function was adopted for the nutrient uptake rate in order to account for the significant time and particularly space variability of nutrient conditions.

Nitrate concentration for example may vary 100-fold from the Danube river mouth to the open sea area. The adopted formulation depends on the resource/consumer ratio and reflects the adaptation of different species nutrient demands according to the actual conditions. On the other hand, adopting a varying half-saturation function for zooplankton grazing can be attributed to the decrease of predation efficiency due to consumer mutual interference. In order to demonstrate the effect of using a variable half-saturation function -rather than constant- for nutrient uptake and zooplankton grazing, we performed two additional simulations using constant values for K_N=0.8 mmol N/m^3 (Run 2) and K_Z =0.5 mmol N/m^3 (Run 3), which represent the annual mean values of the adopted varying $K_N=f(P)$ and $K_Z=f(Z)$ functions over the open sea area. Major differences from the reference simulation (Run 1) would thus be expected within coastal / Danube influenced waters that are characterized by much higher values.

In figure 10 we can see the phytoplankton patterns as simulated for Run 2, during July 2003 (compare with fig. 6i), where an overestimation of phytoplankton concentration is evident in river influenced waters for Run 2. Assigning a constant value of K_N=0.8 mmol N/m^3, which is much lower than the one assigned by the variable $K_N=f(P)$ in the eutrophic waters (~3 mmol N/m^3 on average), results in an increasing overestimation of phytoplankton growth rate along the productivity gradient. Since the nutrient river loads are the same for the two cases, one would expect a decrease of the high-chlorophyll plume area, as an increased phytoplankton concentration in one area would produce a stronger nutrient limitation in an adjacent less eutrophic area. However, this is not exactly the case because an increased phytoplankton growth results in the increase of the remineralization rate, which is a function of phytoplankton concentration, and thus leads to an overall increased primary production.

Since the grazing pressure in the eutrophic waters is rather low due to the increased zooplankton mortality induced by higher-predators, the impact of using a different grazing formulation on phytoplankton dynamics would be rather small, as already mentioned. Therefore, in order to reveal the behavioral difference between the Holling formulation and the adopted “ratio-dependent” formulation, the zooplankton mortality rate was decreased to a low level as for phytoplankton and the reference simulation was repeated adopting the same low mortality rate (Run 4). While changing the nutrient uptake formulation has an effect mostly on horizontal variability, changing the zooplankton grazing rate - which is a top-down control - results in a significant change of time variability in the phytoplankton dynamics. In figure 11 we can see the phytoplankton and zooplankton biomass variability for the two cases (Run 3, Run 4) and our reference simulation (Run 1) within river influenced waters (SSS<16

psu, which was slightly decreased from the earlier SSS limit of 17 psu (fig. 4), because the differences between the model runs are more apparent toward to the more productive areas). Assigning a constant value for K_Z=0.5 mmol N/m^3 results in the appearance of a zooplankton biomass oscillation that brings phytoplankton biomass to almost extinction (prevented only by the assigned threshold concentration for grazing). This type of pathological behavior is prevented in Run 4 where K_Z increases with zooplankton concentration. Notice that in Run 3, even though a stronger grazing pressure is assigned (resulting from the lower K_Z=0.5 mmol N/m^3), the zooplankton biomass attains lower values than Run 4 after August, due to the suppressed phytoplankton biomass. The phytoplankton extinction in Run 3 naturally would be prevented by choosing a much higher value for K_Z, which however would result in an underestimation of grazing rate in the open sea area. One should also notice that the effect of using a lower zooplankton mortality rate by about 10 times results in an about 2-fold reduction of phytoplankton biomass (compare Run 4 to Run 1 in fig. 11). Even though the impact of the zooplankton grazing formulation is rather small under the adopted high zooplankton mortality rates, the "ratio dependent" grazing formulation seems more robust and provides an additional "bottom-up" stabilizing mechanism even for a decreased zooplankton mortality rate.

Conclusions

A three-dimensional coupled model of the Western Black Sea plankton dynamics was developed and implemented for the 2003 period using high-resolution/high-frequency forcing, in terms of air-sea interactions and Danube river inputs. A series of 8-day Chl-a SeaWiFS images provided a valuable validation tool that guided us to the improvement of model parameterizations and the calibration of the biological parameters. The simulation of the seasonal phytoplankton variability over the entire Western Black Sea, extending from the highly eutrophic river influenced area to the open sea area, was a major challenge that made necessary the representation of both the spatial and time variability of several processes. Including Phosphorus as a model compartment permitted a more realistic simulation of the P-limited river influenced waters. Adopting a variable function for the zooplankton mortality rate induced from higher predators pressure, resulted in a more realistic variability of the grazing pressure across the productivity gradient. The adoption of a variable function for remineralization rate, as well as the parameterized interaction with the sediment by means of a

simple benthic model, permitted the simulation of the observed increased production in coastal areas. The adoption of a variable half-saturation function for nutrient uptake was shown to better describe phytoplankton growth across the significant nutrient gradients. A "ratio-dependent" formulation was adopted for zooplankton grazing, which even though it has no significant impact under the adopted high zooplankton mortality rates, seems more robust and provides an additional "bottom-up" stabilizing mechanism. The inclusion of ISM as a state variable permitted a more realistic simulation of the light conditions in coastal areas during winter.

Despite the model simplicity, the simulated Chl-a patterns presented a good agreement as compared to the SeaWiFS images. The most noticeable differences were observed in the open sea area, consisting of an overestimation during spring and an underestimation during autumn periods. One possible cause is the insufficient vertical resolution in deep areas that results in an overestimation of vertical mixing during spring and an underestimation during autumn. An additional cause could be the over simplistic seasonal variability of zooplankton mortality induced by higher predators. Agreement between model and observations was best in the coastal areas that were the focus of this study. During winter, phytoplankton in coastal areas was shown to be limited by light availability mostly due to the increased particulate matter concentrations, as a result of resuspension from the sediment and the increased river loads. During summer, the primary production was mostly sustained by riverine nutrients and regeneration processes and thus was strongly linked to the evolution of the Danube plume. Using high-frequency atmospheric forcing and a comprehensive, three-dimensional hydrodynamic model with river plume dynamics permitted the capture of the variability of the Danube waters transport pathways under the wind variability. A subsurface chlorophyll maximum was also simulated at a depth of ~30m.

Phosphorus limited areas were shown to extend from the Danube prodelta to the Turkish coast during the winter and spring periods, according to the river pathways and the high N/P ratio of river loads. During summer and autumn periods, the P-limited area was confined in the Danube frontal area as the river load N/P ratio was greatly reduced and the benthic fluxes of dissolved nutrients favored N-limitation.

The model simulated Chl-a presented a reasonably good agreement with in-situ data in the Danube front and the Romanian shelf area. The limiting nutrients, however, showed significant deviations from the observed concentrations, which motivates us to further calibrate the biological model, particularly with regard to remineralization processes and grazing pressure.

Acknowledgments:

The study was funded by the CEC Contract EU Fifth Framework Programme – Energy, environment and sustainable development, Contract No. EVK1-CT-2000-00051: NUtrient management in the DAnube basin and its impact on the Black Sea (DANUBS). We are grateful to Anastasios Papadopoulos of the Hellenic Center for Marine Research, who provided the 2002-2003 POSEIDON atmospheric fields, as well as, to Adrianna Cociacu of the National Institute for Marine Research and Development "Grigore Antipa", Romania and Violeta Velikova of the Institute of Fisheries and Aquaculture, Varna, Bulgaria, who provided us with in situ data. Danube daily discharge rates and nutrient loads were kindly provided by Adrian Constantinescu of the Danube Delta National Institute for Research and Development, Tulcea, Romania. The SeaWiFS ocean color data were obtained from NASA's Goddard Space Flight Centre (GSFC-DAAC).

References

Arditi, R. and L.R. Ginzburg (1989). Coupling in predator-prey dynamics: ratio-dependence. *J. Theor. Biol., 139*, 311-326.

Arditi, R. and H.R. Akcakaya (1990). Underestimation of mutual interference of predators. *Oecologia, 83,* 358-361

Blumberg, A.F. and G.L. Mellor (1983). Diagnostic and prognostic numerical circulation studies of the South Atlantic Bight. *J. Geophys. Res*., *88(C8)*, 4579-4592.

Burban, P.Y., Lick W, Lick J. (1989). The flocculation of fine-grained sediments in estuarine waters.. *J. Geophys. Res*., *94*, 8323-8330.

Button, D.K. (1978). On the theory of microbial growth kinetics by limiting nutrient concentrations, *Deep-Sea Res., 25,* 1163-1177.

Cokasar, T., and E. Ozsoy (1998). Comparative analyses and modelling for regional ecosystems of the Black Sea, in *Ecosystem Modelling as a Management tool for the Black Sea, NATO Sci. Ser. 2, vol.47*, edited by L. Ivanov and T. Oguz, pp. 323-358, Kluwer Acad., Norwell, Mass.

Contois, D.E. (1959). Kinetics of bacterial growth: relationship between population density and specific growth rate of continuous cultures. *J. Gen. Microbiol*. 21, 40-50.

Constantinescu, A. and G.A.M. Menting (2000). Ecological gradients in the Danube Delta lakes, Present state and man-induced changes, chapter 3: Hydrology, DDNI and RIZA, Report 2000.015, ISBN 90.369.5309x, The Netherlands.

Davidov A., submitted. Assessment of algorithms for atmospheric correction and chlorophyll-a retrieval from SeaWiFS satellite data in the western Black Sea area. Submitted April 2006 to *International Journal of Remote Sensing*.

DeAngelis, D. L., R.A., Goldstein and R.V. O'Neill (1975). A model for trophic interactions. *Ecology, 56,* 881-892.

Di Toro, D.M. and W.F. Matystik (1980). Mathematical Models of Water Quality in Large Lakes, Part 1: Lake Huron and Saginaw Bay. EPA-600/3-80-056. pp. 28-30.

Droop, M.R. (1968). Vitamin B12 and marine ecology. IV. The kinetics of uptake, growth and inhibition in Monochrysis lutheri. *J. Mar. Biol. Assoc. U.K., 48,* 469-733.

Dugdale, R.C (1967). Nutrient limitation in the sea: dynamics, identification and significance. *Limnol. Oceanog*., 12, 685-695.

Dyer KR. (1989). Sediment processes in estuaries: future research requirements. *J. Geophys. Res.,*94 *(C10)*, 14327-14339.

Edwards, A.M. and A. Yool (2000). The role of higher predation in plankton population models. *J. Plankton Res*. 22, 1085-1112.

Eeckhout, D.V., and C. Lancelot (1997). Modeling the functioning of the northwestern Black Sea ecosystem from 1960 to present, in *Sensitivity to change: Black Sea, Baltic Sea and North Sea, NATO Sci. Ser. Partnership Sub-ser. 2, vol. 27,* edited by E. Ozsoy and A. Mikaelyan, pp. 455-469, Kluwer Acad., Norwell, Mass.

Eppley, R.W. (1972). Temperature and phytoplankton growth in the sea. *Fish. Bull., 70,* 1063-1085.

Eppley, R.W., J.N. Rogers and J.J. McMarthy (1969). Half-saturation constants for uptake of nitrate and ammonium by marine phytoplankton, *Limnol. Oceanogr., 14,* 912-920.

Fasham, M., H. Ducklow and S. McKelvie (1990). A nitrogen-based model of plankton dynamics in the oceanic mixed layer. *J. Mar. Res., 48,* 591-639.

Feldman, G. C., C. R. McClain, Ocean Color Web, SeaWiFS and MODIS Aqua data, NASA Goddard Space Flight Center. Eds. Kuring, N., Bailey, S. W., Decenber 2006. http://oceancolor.gsfc.nasa.gov/

Finenko, G. A., A. Romanova, G. I. Abolmasova, B. E. Anninsky, L. S. Svetlichny, E. S. Hubareva, L. Bat, and A. E. Kideys (2003). Ingestion, growth and reproduction rates of the alien Beroe ovata and its impacts on the plankton community in the Black Sea, *J. Plankton Res., 25*, 539-549.

Friedl, G., C. Dinkel and B. Wehrli (1998). Benthic fluxes of nutrients in the northwestern Black Sea,.*Mar. Chem.*, 62, 77-88.

Friedrich, J., C. Dinkel, G. Friedl, N. Pimenov, J. Wijsman, M.-T. Gomoiu, A. Cociasu, L. Popa and B. Wehrli (2002). Benthic nutrient cycling and diagenetic pathways in the North Western Black Sea. *Estua. Coast and Shelf Sci*., *54,* 369-383.

Fu, G., Baith, K. S., and McClain, C. R., 1998, "SeaDAS: The SeaWiFS Data Analysis System", Proceedings of "The 4th Pacific Ocean Remote Sensing Conference", Qingdao, China, July 28-31, 1998, 73-79.

Garber, J.H. (1984). Laboratory study of nitrogen and phosphorus remineralization during the decomposition of coastal plankton and seston. *Estua. Coast and Shelf Sci*., *18,* 685-702.

Geider, R.J., H.L. MacIntyre and T.M Kana (1998). A dynamic regulatory model of phytoplanktonic acclimation to light, nutrients and temperature, *Limnol. Oceanogr., 43,* 679-694.

Gils, J.van, H. Behrendt, A. Constantinescu, K. Isermann and M. Zessner, (2005). "Future development of nutrient emissions and river loads in the Danube Basin", Proceedings of the River Basin Management Conference, pp.219-230, Budapest.

Ginzburg, L.R., and H.R. Akcakaya (1992). Consequenses of ratio-dependent predation for steady state properties of ecosystems. *Ecology, 73,* 1536-1543.

Goldman, J.C., D.A. Caron and M.R. Dennett (1987). Regulation of gross growth efficiency and ammonium regeneration in bacteria by substrate C:N ratio. *Limnol. Oceanogr., 32,* 1239-1252.

Gregoire, M., J. M. Beckers, J.C.J Nihoul and E. Stanev (1998). Reconnaissance of the main Black Sea's ecohydrodynamics by means of a 3D interdisciplinary model. *J. Mar. Syst. 16,* 85-105.

Gregoire, M. and J. Friedrich (2004). Nitrogen budget of the nortwestern Black Sea shelf inferred from modelling studies and in situ benthic measurements. *Mar. Ecol. Prog. Ser., 270,* 15-30.

Gregoire, M., K. Soetaert, N. Nezlin and A. Kostianoy (2004). Modelling the nitrogen cycling and plankton productivity in the Black Sea using a three-dimensional interdisciplinary model, *J. Geophys. Res., 109,* C05007, doi:10.1029/2001JC001014.

Grill, E.V., and F.A. Richards (1964). Nutrient regeneration from phytoplankton decomposing in seawater. *J. Mar. Res., 22,* 51-59.

Guan, W.B, L.A. Wong, D.F. Xu (2001). Modeling nitrogen and phosphorus cycles and dissolved oxygen in the Pearl River (Zhujiand) Estuary. I. Model development, *Acta Oceanologica Sinica, 20,* 71-82.

Gucu A.C. (2002). Can overfishing be responsible for the successful establishment of Mnemiopsis leidyi in the Black Sea?, *Estua. Coast and Shelf Sci*., *54*, 439-451.

Harrison, W.G. (1978). Experimental measurements of nitrogen remineralization in coastal

waters. *Limnol. Oceanogr.*, *23*, 684-694.

Holling, C. S. (1959). Some characteristics of simple types of predation and parasitism. *Can. Entomol. 91,* 385–398.

Hopkinson, C.S.Jr., J.J. Vallino and A. Nolin (2002). Decomposition of dissolved organic matter from the continental margin. *Deep-Sea Res. II*, 49, 4461-4478.

Jassby, A.D. and T. Platt (1976). Mathematical formulation of the relationship between photoshynthesis and light for phytoplankton. *Limnol. Oceanogr*., 21, 540-547.

Jost, C. (2000). Predator-prey theory : hidden twins in ecology and microbiology, *Oikos, 90,* 202-208.

Kideys, A. E. (2002). Fall and rise of the Black Sea ecosystem, *Science, 297,* 1482-1484.

Knauer, G.A, J.H. Martin and K.W Bruland (1979). Fluxes of particulate carbon, nitrogen and phosphorus in the upper water column of the northeast Pacific, *Deep-Sea Res.*, *26A,* 97-108.

Kohlmeier, C. and Ebenhoh, W. (1995). The stabilising role of cannibalism in a predator-prey system. *Bull. Math. Biol*., 57, 401-411.

Konovalov, S., J.W. Murray and G.W. Luther, III (2005). Basic processes of Black Sea biogeochemistry, *Oceanography, 8,* 25-35.

Kourafalou, V.H., L.-Y. Oey, J.D. Wang and T. N. Lee (1996). The fate of river discharge on the continental shelf. Part I: modeling the river plume and the inner-shelf coastal current. *J. Geophys. Res.*, *101(C2)*, 3415-3434.

Kourafalou, V.H. and E.V. Stanev, 2001. Modelling the impact of atmospheric and terrestrial inputs on the western Black Sea coastal dynamics. *Annales Geophysicae*, 19, 245-256.

Kourafalou, V., K. Tsiaras and J. Staneva (2004). Numerical studies on the dynamics of the Nortwestern Black Sea shelf, *Med. Mar. Sci., Vol.5/1,* 133-142.

Krone RB. (1962). Flume Studies of the Transport of Sediment in Estuarial Shoaling Processes. Report of Hydraulic Engineering Laboratory and Sanitary Engineering Research, University of California: Berkley: 110.

Lancelot, C. L., J. V. Staneva, D. Van Eeckhout, J.-M. Beckers, and E. V. Stanev (2002). Modelling the Danube-influenced North-western continental shelf of the Black Sea. Ecosystem response to changes in nutrient delivery by the Danube River after its damming in 1972, *Estua. Coast and Shelf Sci*., *54*, 473-499.

Lebedeva, L. P., and E.A. Shushkina, (1994). Modeling the effect of Mnemiopsis on the Black Sea plankton community, *Oceanology, Engl. Transl*., *34*, 72-80.

Lorenzen, C.J., (1972). Extinction of light in the ocean by phytoplankton. J. Cons., 34, 262-267.

MacIsaac, J.J, and R.C. Dugdale (1969). The kinetics of nitrate and ammonia uptake be natural populations of marine phytoplankton, *Deep-Sea Res*.,*16*, 415-422.

McClain, C., G. Feldman and S. Hooker (2004). An overview of the SeaWiFS project and strategies for producing a climate research quality global ocean bio-optical time series Deep Sea Res. (II Top. Stud. Oceanogr.) 51(1-3):5-42.

McClain, C., S. Hooker, G. Fledman and P. Bontempi (2006). Satellite data for ocean biology, biogeochemistry and Climate Research. *EOS, Transactions, American Geophysical Union, 87(34)*, 337-343.

Mellor, G. L. and Yamada, T. (1982). Development of a turbulence closure model for geophysical fluid problems, Rev. *Geophys. Space Phys., 20*, 851-875.

Monod, J. (1942). Recherches sur la croissance des cultures bacteriennes. 2nd ed. Hermann, Paris. 211p.

Morrisson, K.A., N. Therien, and B. Macros (1987). Comparison of Six Models for Nutrient Limitations on Phytoplankton Growth. *Can. J. Fish. Aquat. Sci. 44*, 1278-1288.

Murray, J.W., H.W. Jannasch, S. Honjo, R.F. Anderson, W.S. Reeburgh, Z. Top, G.E. Friedrich, L.A. Codispoti and E. Izdar (1989). Unexpected changes in the oxic/anoxic interface in the Black Sea. *Nature, 338,* 411-413.

Murray, J.W., C. Fuchsman, J. Kirpatrick, B. Paul and S. Konovalov (2005). Species and δ^{15} signature of nitrogen transformations in the suboxic zone of the Black Sea. *Oceanography, Vol.18,* 36-47.

Nittis, K., L. Perivoliotis, G. Korres, C. Tziavos, I. Thanos (2006). Operational monitoring and forecasting for marine environmental applications in the Aegean Sea. *Environmental modelling & Software*, *21,* 243-257.

Oguz, T. and B. Salihoglou (2000). Simulation of eddy-driven phytoplankton production in the Black Sea. *Geophys. Res. Lett., 27,* 2125-2128.

Oguz, T., H. Ducklow, P. Malanote-Rizzoli, S. Turgul, N. Nezlin and U. Unluata (1996). Simulation of annual plankton cycle in the Black Sea by a one-dimensional physical

biological model. *J. Geoph. Res*., *101*, 16551-16569.

Oguz, T., H. Ducklow, E.A. Shushkina, P. Malanote-Rizzoli, S. Turgul and L.P. Lebedeva (1998). Simulation of upper layer biogeochemical structure in the Black Sea, in *Ecosystem Modelling as a Management tool for the Black Sea, NATO Sci. Ser. 2, vol.47*, edited by L. Ivanov and T. Oguz, pp. 323-358, Kluwer Acad., Norwell, Mass.

Oguz, T., H. Ducklow, P. Malanotte-Rizzoli, J.W. Murray, V.I. Vedernikov and U. Unluata (1999). A physical-biochemical model of plankton productivity and nitrogen cycling in the Black Sea. *Deep Sea Res., I, 46,* 597-636.

Oguz,T., H.W. Ducklow and P. Malanotte-Rizzoli (2000). Modeling distinct vertical biogeochemical structure of the Black Sea: Dynamical coupling of the oxic, suboxic and anoxic layers. *Global Biogeochem. Cycles., 14*, 1331–1352.

Oguz,T.,Ducklow,H.W.,Purcell,J.E.,Malanotte-Rizzoli,P (2001a). Modelling the response of top-down control exerted by gelatinous carnivores on the Black Sea pelagic food web. *J. Geoph. Res*., *106*, 4543-4564.

Oguz, T., J. W. Murray, and A.E. Callahan (2001b). Modeling redox cycling across the suboxic-anoxic interface zone in the Black Sea. *Deep-Sea Res. I., 48*, 761-787.

Oguz, T., A. G. Deshpande, and P. Malanotte-Rizzoli (2002). On the role of mesoscale processes controlling biological variability in the Black Sea: Inferences from SeaWiFS-derived surface chlorophyll field*, Cont. Shelf Res., 22,* 1477-1492.

O'Reilly, J.E., Maritorena, S., O'Brien, M.C., Siegal, D.A., Toole, D., Menzies, D., Smith, R.C., Mueller, J.L., MitchellL, B.G., Kahru, M., Chavez, F.P., Strutton, P., Cota, G.F., Hooker, S.B., Mcclain, C.R., Carder, K.L., Muller-Karger, F., Harding, L., Magnuson, A., Phinney, D., Moore, G.F., Aiken, J., Arrigo, K.R., LeTelier, R. and Culver, M., 2000. Ocean Color Chlorophyll-a algorithms for SeaWiFS, OC2 and OC4: Verison 4. In: SeaWiFS postlaunch calibration and validation analyses, part 3. SeaWiFS postlaunch technical report series. S.B. Hooker and E.R. Firestone (eds). NASA/TM-2000-206892, 11, pp. 9-23.

Papadopoulos, A., G. Kallos, P. Katsafados, and S. Nickovic (2002). The Poseidon weather forecasting system: An overview. *The Global Atmosphere and Ocean Systems* (retitled *Journal of Atmospheric and Ocean sciences)*, *8,* No.2-3, 219-237.

Partheniades, E. (1965). Erosion and deposition of cohesive soils. *Journal of the Hydrology Division,* ASCE 91, No. HY1, 105–139.

Ragueneau, O., C. Lancelot, V. Egorov, J. Vervlimmeren, A. Cociasu, G. Deliat, A. Krastev, N. Daoud, V. Rousseau, V. Popovintchev, N. Brion, L. Popa and G. Cauwet (2002). Biogeochemical Transformations of Inorganic Nutrients in the Mixing Zone between the Danube River and the North-western Black Sea. *Estua. Coast and Shelf Sci., 54,* 321-336.

Roques, H., H. Yue, S. Saipanich and B. Capdeville (1982). Faut-il abandonner le formalisme de monod pour la modelisation des processus de de´pollution par voie biologique? *Water Res. 16*, 839–847.

Ryabchenko, V.A., M.J.R Fasham, B.A Kagan, E.E. Popova (1997). What causes short-term oscillations in ecosystem models of the ocean mixed layer? *J. Mar. Syst*., *13,* 33-50.

Saydam, C., S. Tugrul, O. Basturk and T. Oguz (1993). Identification of the oxic/anoxic interface by isopycnal surfaces in the Black Sea, *Deep-Sea Res., 40,* 1405-1412.

Schreiber, H., H. Behrendt, L.T. Constantinescu, I. Critevic, D. Drumea, D. Jabucar, S. Juran, B. Pataki, S. Snishko and M. Zessner (2005). Point and diffuse nutrient emissions and loads in the transboundary Danube River basin. A modelling approach. *Arch. Hydrobiol. Suppl. Large Rivers,* (in print).

Shi Z., and H.J. Zhou (2004). Controls on effective settling of mud flocs in the Changjiang Estuary, China. *Hydrol. Process.*, *18,* 2877-2892.

Stanev, E.V., J.M. Beckers, C. Lancelot, J.V. Staneva, P.Y. Le Traon, E.L. Peneva and M. Gregoire (2002). Coastal-open Ocean Exchange in the Black Sea: Observations and Modelling. *Estua. Coast and Shelf Sci*., *54,* 601-620.

Staneva, J.V. and E.V. Stanev (1997). Cold water mass formation in the Black Sea and its sensitivity to horizontal resolution in numerical models. E. Ozsoy and A. Mikaelyan (eds.): *Sensitivity of North Sea, Baltic Sea and Black Sea to anthropogenic and climatic changes*, NATO Series, Kluwer academic publisher; 375-393.

Staneva J. V. and E. V. Stanev and T. Oguz (1998). The Impact of Atmospheric Forcing and Water Column Stratification on the Yearly Plankton Cycle, In: T. Oguz and L. Ivanov (eds.) NATO-ASI Kluwer academic publisher, 301-323.

Shushkina, E. A., E. I. Musaeva, L. L. Anokhina, and T. A. Lukasheva (2000). The role of gelatinous macroplankton, jellyfish Aurelia and ctenophores Mnemiopsis and Beroe in the planktonic communities of the Black Sea, *Oceanology, Engl. Transl., 40*, 809-815.

Steele, J.H. and E.W. Henderson (1981). A simple plankton model. *Am. Nat., 117*, 676-691.

Steele, J.H. and E.W. Henderson, (1992). The role of predation in plankton models. *J. Plankton Res., 14,* 157-172.

Tarapchak, S.J., and L.R. Herche (1986). Phosphate uptake by microorganisms in lake water: deviations from simple Michaelis-Menten kinetics. *Can. J. Fish. Aquat. Sci*., *43*, 319-328.

Tanguy, D. and M. Loreau (2001). Ecological stoichiometry, primary producer-decomposer interactions and ecosystem persistence. *Ecology, 82*, 3069-3082.

Tilman, D. (1981). Tests of resource competition theory using four species of Lake Michigan algae. *Ecology, 62(3*), 802-815.

Tolmazin, D. (1985). Changing coastal oceanography of the Black Sea. I: Northwestern Shelf. *Progress in Oceanography, 15,* 217-276.

Tugrul, S., O. Basturk, C. Saydam, and A. Yilmaz (1992). Changes in the hydrochemistry of the Black Sea inferred from water density profiles, *Nature, 359,* 137-139.

Velikova, V., A. Cociasu, L. Popa, L. Boicenco, D. Petrova (2005). Phytoplankton community and hydrochemical characteristics of the Western Black Sea. *J. Water Science and Technology, Vol.51,* 27-37.

Vidal, C.V. (1995), Bio-optical characteristics of the Mediterranean and the Black Sea. M.S. Thesis, 134pp., Inst. Of Mar. Sci., Middle East Tech. Univ., Endemli, Icel, Turkey.

Vladimirov, V.L., V.I. Mankovsky, M.V. Solokev and A.V. Mishonov (1996). Seasonal and long term variability of the Black Sea optical parameters, in *Sensitivity of North Sea, Baltic Sea and Black Sea to Anthropogenic and Climatic Changes, NATO ASI Ser. 2*, edited by E. Ozsoy and A. Mikaelyan, Kluwer Acad., Norwell, Mass.

Williams, P.J. (1973). The validity of the application of simple kinetic analysis to heterogeneous microbial populations. *Limnol. Oceanogr*., *18,* 159-165.

Wroblewski, J. (1977). A model of phytoplankton plume formation during variable Oregon upwelling, *J. Mar. Res., 35,* 357-394.

Zaitsev, Yu. P., B.G. Alexandrov (1997). Recent man-made changes in the Black Sea ecosystem, in *Sensitivity of North Sea, Baltic Sea and Black Sea to Anthropogenic and Climatic Changes, NATO ASI Ser. 2*, edited by E. Ozsoy and A. Mikaelyan, Kluwer Acad., Norwell, Mass.

Tables with captions

Table 1: Biological processes formulation

Function	Description	Formula
$\Phi(I,N,A,PO4,T,P)$	*Phytoplankton growth rate*	$\sigma_m L_T(T)$ *min [* $L_L(I)$, $L_{NT}(N,A,P)$, $L_{PO4}(PO4,P)$*]*
$L_T(T)$	*temperature dependence*	$Q_{10}^{(T-20)/10}$
$L_I(I)$	*light limitation*	$\tanh[\frac{aI(z,t)}{\sigma_m L_T(T)}]$
$I(z,t)$	*PAR at depth z*	$I(z=0,t)\exp[-\int k_{tot}(z)dz]$
$k_{tot}(z)$	*Total attenuation coefficient*	$k_w + k_p\ P + k_d\ D + k_s\ ISM$
$L_{NT}(N,A,P)$	*Nitrogen limitation*	$L_N(N,A,P) + L_A(A,P)$
$L_N(N,A,P)$	*Nitrate Nitrogen limitation*	$\frac{N}{N+K_N(P)}\exp(-\Psi A)$
$L_A(A,P)$	*Ammonium Nitrogen limitation*	$\frac{A}{A+K_A(P)}$
$\Phi_N(I,N,A,PO4,T,P)$	*Nitrate uptake rate*	$\Phi(I,N,A,PO4,T,P)\frac{L_N(N,A,P)}{L_{NT}(N,A,P)}$
$\Phi_A(I,N,A,PO4,T,P)$	*Ammonium uptake rate*	$\Phi(I,N,A,PO4,T,P)\frac{L_A(A,P)}{L_{NT}(N,A,P)}$
$K_N(P)$	*Nitrate uptake half-saturation*	$a_N + b_N\ P$
$K_A(P)$	*Ammonium uptake half-saturation*	$0.1\ K_N(P)$
$L_{PO4}(PO4,P)$	*Phosphorus limitation*	$\frac{PO4}{PO4+K_{PO4}(P)}$
$K_{PO4}(P)$	*Phosphate uptake half-saturation*	$K_N(P)\ /\ 16$
$m_p(P)$	*Phytoplankton mortality*	$m_{p\max}\frac{P^2}{P^2+K_{mp}}$
G(P, DN, Z, T)	*Zooplankton grazing rate*	$\sigma_g L_T(T)\frac{F(P,DN)-F_{th}}{F(P,DN)-F_{th}+K_Z(Z)}, F > F_{th}$
F(P,DN)	*Total available food for grazing*	$p_p(P,DN)\ (\ P-P_{th}(P,DN)\ ) +$ $p_d(P,DN)\ (\ DN-D_{th}((P,DN)\ )$
$p_p\ (P,DN),\ p_d\ (P,DN)$	*Zooplankton preferences for grazing on phytoplankton and detritus*	$\frac{P}{P+DN},\ 1-p_p\ (P,\ DN)$

$G_p(P, DN, Z, T)$	*Zooplankton grazing rate on phytoplankton*	$G(P,DN,Z,T)\frac{p_p(P,DN)\cdot(P-P_{th}(P,DN))}{F}$
$G_d(P, Z, T)$	*Zooplankton grazing rate on detritus*	$G(P,DN,Z,T)\frac{p_d(P,DN)\cdot(DN-DN_{th}(P,DN))}{F}$
$P_{th}(P,DN)$, $DN_{th}(P,DN)$	*Phytoplankton and detritus grazing thresholds*	$F_{th}\ p_p\ (P,DN)$, $F_{th}\ p_d\ (P,DN)$
$K_Z(Z)$	*Zooplankton grazing half-saturation*	$a_Z + b_Z Z$
$m_z(Z,T)$	*Zooplankton mortality rate*	$m_{z\max} L_T(T)\frac{Z^2}{Z^2+K_{mz}}$
$\mu_z(T)$	*Zooplankton excretion rate*	$\mu_z\ L_{Tz}(T)$
$\varepsilon_N(P,T)$	*Nitrogen remineralization rate*	$\varepsilon_N\ L_T(T)\ f_R(P)$
$\varepsilon_P(P,T)$	*Phosphorus remineralization rate*	$\varepsilon_P\ L_T(T)\ f_R(P)$
$f_R(P)$	*Remineralization phytopl. dependence*	$\frac{0.5+P}{2+P}$
$w_s(DN)$	*Detritus sinking rate*	$-w_{s\max}\frac{DN}{DN+K_{sd}}$
$w_{res}(BS)$	*Resuspension rate*	$w_{res\max}(1-\frac{\tau_{res}}{BS}), BS>\tau_{res}$
$w_{dep}(BS)$	*Deposition rate*	$w_{s\max}(1-\frac{BS}{\tau_{dep}}), BS<\tau_{dep}$
$d_A\ (T, DN_b)$	*Ammonium benthic flux*	$d_{A\max}L_T(T)\frac{DN_b(S,H)}{DN_{b\max}}$
$d_{PO4}\ (T, DP_b)$	*phosphate benthic flux*	$d_{PO4\max}L_T(T)\frac{DP_b(S,H)}{DP_{b\max}}$
$w_s(ISM)$	*ISM settling velocity*	$0.15\ (ISM+0.2)^2$

Table 2: Biological model parameter values

Parameter	Symbol	Value
Phytoplankton maximum growth rate at 20°C	σ_m	3 (day^{-1})
Photoshynthesis efficiency parameter	A	0.02 ($(W/m^2)^{-1}$ day^{-1})
Clear water light attenuation coefficient	k_w	0.04 (m^{-1})
Phytoplankton shelf shading coefficient	k_c	0.03 (m^2/mmolN)
Particulate organic matter attenuation coefficient	k_d	0.01 (m^2/mmolN)
Particulate inorganic matter attenuation coefficient	k_s	0.06 (m^2/gr)
NH_4 inhibition parameter	Ψ	3 $(mmol\ N)^{-1}$
Nitrate uptake half-saturation 1st constant	a_N	0.5 (mmol N/m^3)
Nitrate uptake half-saturation 2nd constant	b_N	0.5
Phytoplankton maximum mortality rate	m_p	0.04 (day^{-1})
Phytoplankton mortality half-saturation constant	K_{mp}	0.1 $(mmol\ N/m^3)^2$
Herbivore maximum grazing rate at 20°C	σ_g	0.8 (day^{-1})
Phytoplankton threshold conc. for grazing	P_{th}	0.2 (mmol N/m^3)
Grazing half-saturation 1st constant	a_Z	0.2 (mmol N/m^3)
Grazing half-saturation 2nd constant	b_Z	1.3
Herbivore maximum mortality rate at 20°C	m_z	0.45 (day^{-1})
Herbivore mortality half-saturation constant	K_{mz}	0.08 $(mmol\ N/m^3)^2$
Herbivore excretion rate at 20°C	μ_z	0.07 (day^{-1})
Herbivore assimilation efficiency	Γ	0.75
Nitrogen maximum remineralisation rate at 20°C	ε_N	0.2 (day^{-1})
Phosphorus maximum remineralisation rate at 20°C	ε_P	0.3 (day^{-1})
Oxidation rate	Ω	0.05 (day^{-1}) , σ_t <15,4
		0, σ_t >15.4
Detrital maximum sinking rate	w_{smax}	4 (m/s)
Half-saturation for detritus sinking	K_d	0.2 (mmol N / m^3)
Detrital maximum resuspension rate	W_{resmax}	0.006 (day^{-1})
Critical shear stress for resuspension	τ_{res}	0.01 (Nt / m^2)
Critical shear stress for deposition	τ_{dep}	0.4 (Nt / m^2)
Maximum ammonium benthic flux	d_{Amax}	1 (mmol N m^{-2} day^{-1})
Maximum phosphate benthic flux	d_{PO4max}	0.15 (mmol P m^{-2} day^{-1})
Initial benthic pool maximum nitrogen conc.	DN_{bmax}	(100 mmol N m^{-2})
Initial benthic pool maximum phosphorus conc.	DP_{bmax}	(6.25 mmol P m^{-2})
Sediment burial rate	B	0.007 (day^{-1})
Phytoplankton and zooplankton N/P stoichiometry	$R_{N/P}$	16

Table 3: Temperature dependence (Q_{10}) of biological processes

Biological process	Q_{10} **value**
Phytoplankton growth	1.88
Zooplankton growth	1.88
Zooplankton mortality	2.2
Zooplankton excretion	1.88
Remineralization	1.2
Benthic flux of phosphate, ammonium	1.2

Table 4: Model simulated annual and seasonal nitrogen and phosphorus mean sediment fluxes in the Danube front area (2400 Km^2), along with Danube river loads

Period	**Net deposition (tons/day)**		**Benthic flux (tons/day)**		**River load (tons/day)**	
	Nitrogen (Detritus-N)	Phosphorus (Detritus-P)	Nitrogen (NH4)	Phosphorus (PO4)	Nitrogen (NH4+NO3)	Phosphorus (PO4)
Winter	12.9	2.2	23.4	6.6	1147	22
Spring	67.7	8.8	26.1	8.2	1215	22
Summer	92.1	11.8	30.7	10.2	297	11
Autumn	48.1	6.6	29.6	9.5	327	15
Annual	55.3	7.3	27.4	8.6	745	17

Figure captions

Figure 1: Model domain and bathymetry. The Boxes A and B enclose the areas around in-situ measurements (indicated as dots) that are compared with area averaged model results (A: Danube front and B: Romanian Shelf) while box C represents the Danube front area (~2400Km^2) where model simulated area averaged sediment fluxes are compared to estimates based on in-situ data.

Figure 2: a) wind (10m) variability in the Danube front area (29.8^o E, 45.1^o N) and b) wind speed (m/s) variability averaged over the Western Black sea, for the 2002-2003 period (the fields are provided by the POSEIDON operational atmospheric forecast model).

Figure 3: a) Danube discharge variability over 2003 (blue line). The black line represents a long term average over the 1994-2003 period (A. Constantinescu, personal communication), b) dissolved inorganic Nitrogen and Phosphorus Danube loads (ktons/year) variability. Notice that the scaling on Y-axis is fitted to N/P molar ratios of 16:1 (i.e. the two lines coincide when N/P ratio equals 16:1), c) Inorganic suspended matter Danube load (ktons/year)

Figure 4: Open sea (left) area and Danube river plume (right) averages of: a),b) light and nutrient limitation functions (1 signifies no limitation), c),d) the mixing layer depth (m) e),f) total attenuation coefficient (m^{-1}), g),h) ISM concentration (mgr/lt), i),j) phytoplankton growth rate (day^{-1}), vertically averaged over the mixing layer depth (defined as the depth where the diffusivity coefficient reduces to 10 cm^2/s).

Figure 5: vertical profile seasonal variability of a) phytoplankton (mmol N/m^3), b) minimum of the light and nutrient limitation function (1 signifies no limitation), c) zooplankton (mmol N/m^3), averaged over the open sea (H>500m) area.

Figure 6: Model simulated (left) and SeaWiFS (right) Chlorophyll-a (mgr/m^3) for a,b) 9-16 January, c) 3-10 March, d)14-21 March, e,f) 9-16 May, g,h) 2-9 June, i,j) 12-19 July, k,l) 20-27 July, m,n) 5-12 August, o,p) 14-21 September, q,r) 8-15 October and s,t) 17-24 November of year 2003.

Figure 7: Model computed seasonal variability of a) Nitrogen and b) Phosphorus sediment fluxes (tons/day) in the Danube front area (~2400 Km^2, shown as box C in figure 1). The blue lines represent the net deposition (deposition minus resuspension) of nitrogen and phosphorus parts of detritus respectively for a) and b). The red lines represent the ammonium and phosphate benthic flux respectively for (a) and (b).

Figure 8: Contours where the model simulated dissolved inorganic N/P molar ratios, equal to 16:1, averaged over seasons.

Figure 9: Model simulated (continuous line), from top to bottom: Chlorophyll-a (mgr/m^3), nitrates (mmol N/m^3) and phosphates (mmol P/ m^3) against in-situ measurements (dots) in a),b),c) averaged over the Danube front area and d),e),f) averaged over the Romanian shelf area (sea area boxes A and B in figure 1).

Figure 10: Chlorophyll-a (mgr/m^3) as simulated by Run2, adopting a half-saturation constant value of Kn=0.8 (mmol N/m^3), for 12-19 July 2003 (compare with figure 6i).

Figure 11: a) Phytoplankton (mmol N/m^3) and b) Zooplankton (mmol N/m^3) biomass variability, averaged within the Danube plume area (*SSS*<16 psu) and over the mixing layer depth, as simulated by Run3 that adopts the parameters (K_Z =0.5, m_z=0.04) (red line), Run4 that adopts the parameters (K_Z =0.2+1.3 *Z*, m_z=0.04) (green line) and the reference simulation (Run1, blue line).

Figures with captions

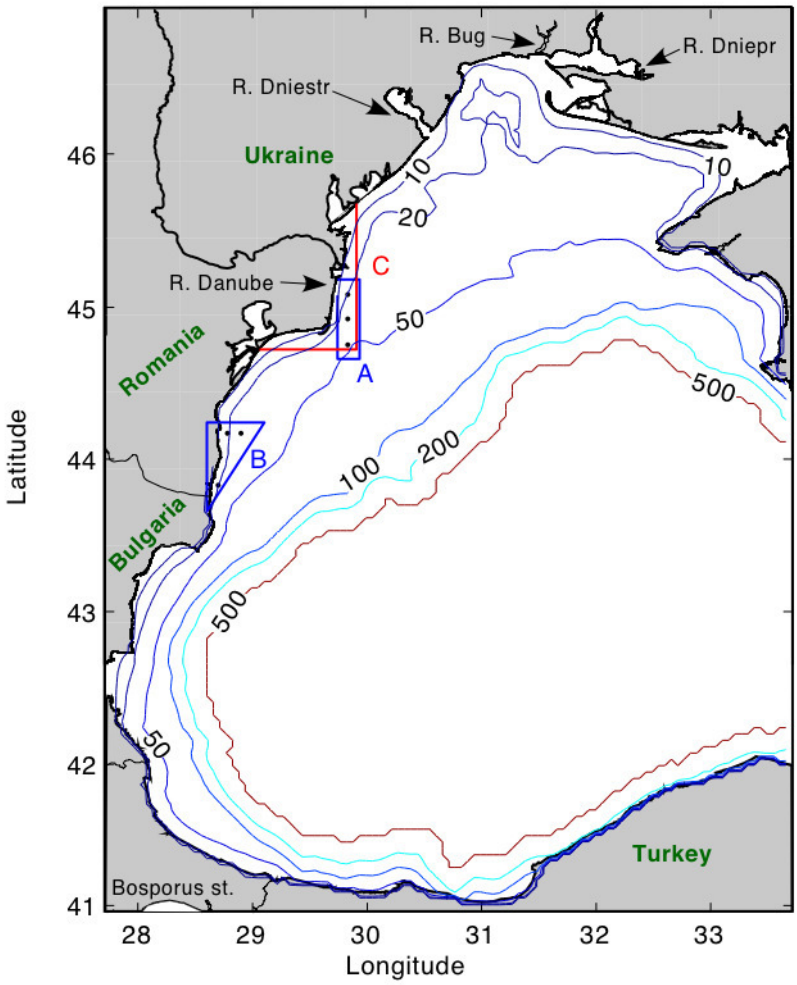

Figure 1: Model domain and bathymetry. The Boxes A and B enclose the areas around in-situ measurements (indicated as dots) that are compared with area averaged model results (A: Danube front and B: Romanian Shelf) while box C represents the Danube front area (~2400Km^2) where model simulated area averaged sediment fluxes are compared to estimates based on in-situ data.

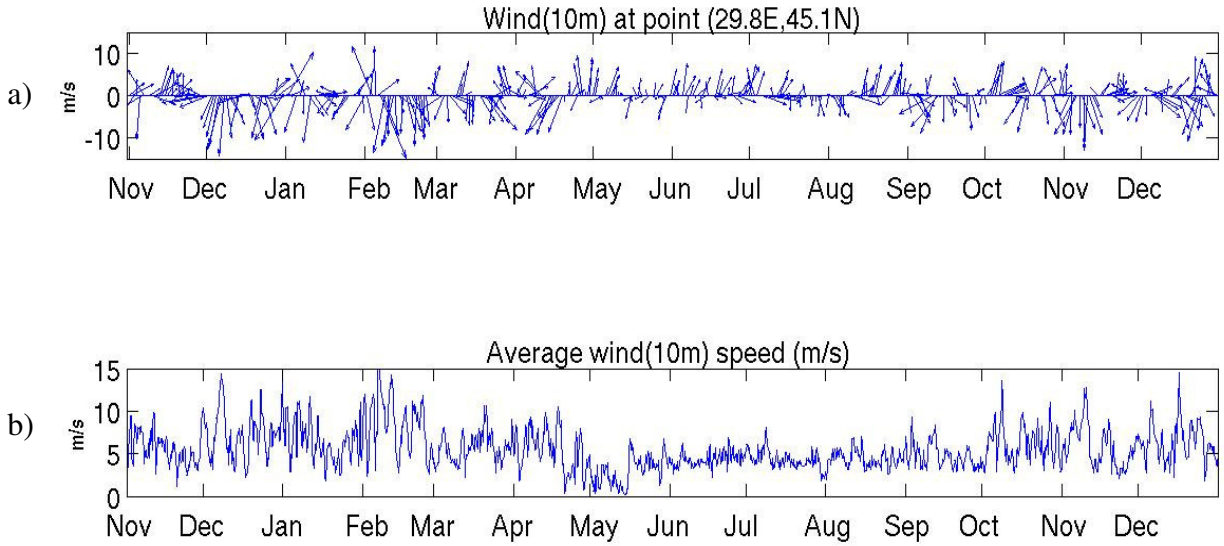

Figure 2: a) wind (10m) variability in the Danube front area (29.8^{o} E, 45.1^{o} N) and b) wind speed (m/s) variability averaged over the Western Black sea, for the 2002-2003 period (the fields are provided by the POSEIDON operational atmospheric forecast model).

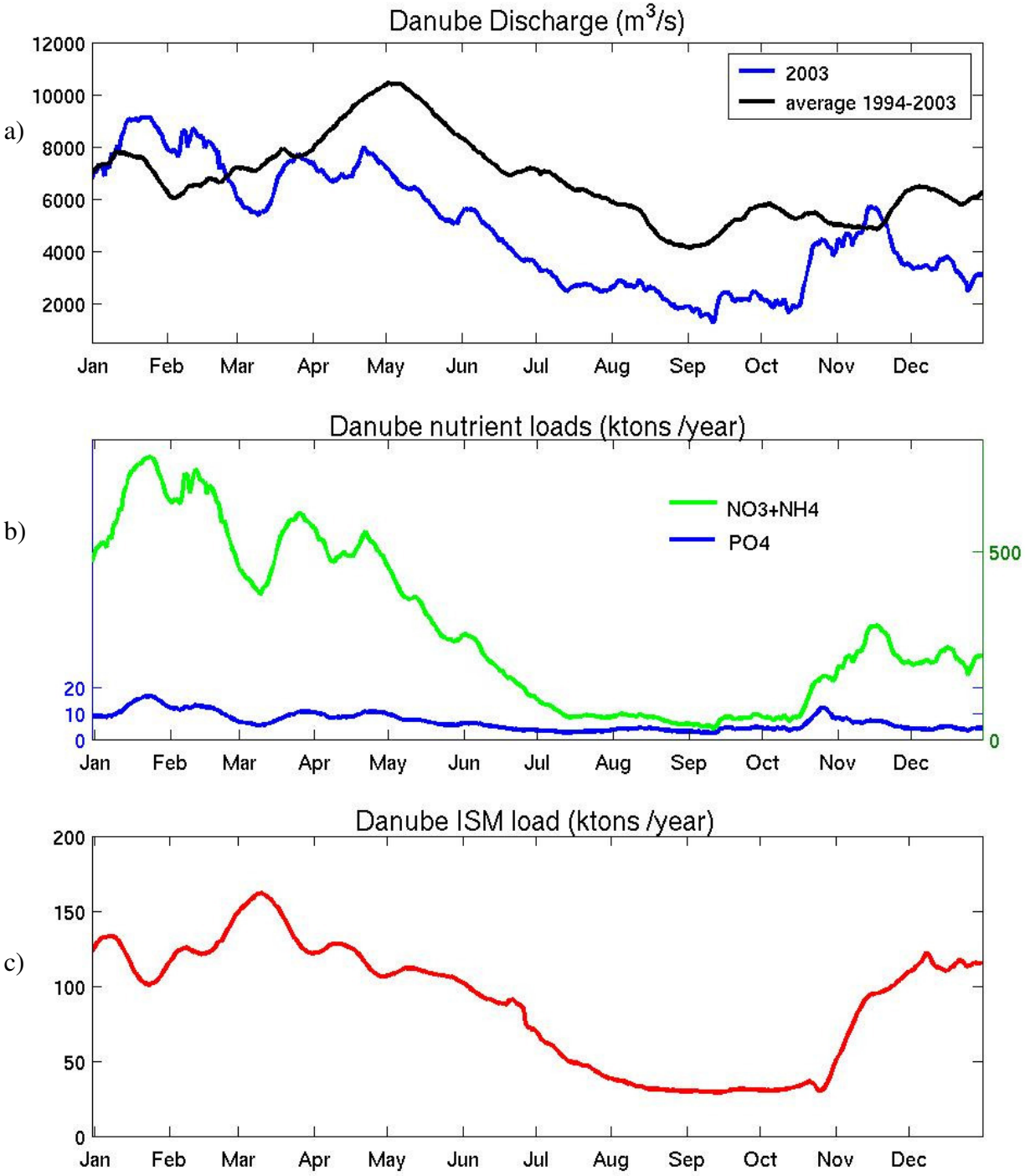

Figure 3: a) Danube discharge variability over 2003 (blue line). The black line represents a long term average over the 1994-2003 period (A. Constantinescu, personal communication), b) dissolved inorganic Nitrogen and Phosphorus Danube loads (ktons/year) variability. Notice that the scaling on Y-axis is fitted to N/P molar ratios of 16:1 (i.e. the two lines coincide when N/P ratio equals 16:1), c) Inorganic suspended matter Danube load (ktons/year).

OPEN SEA AREA DANUBE AREA

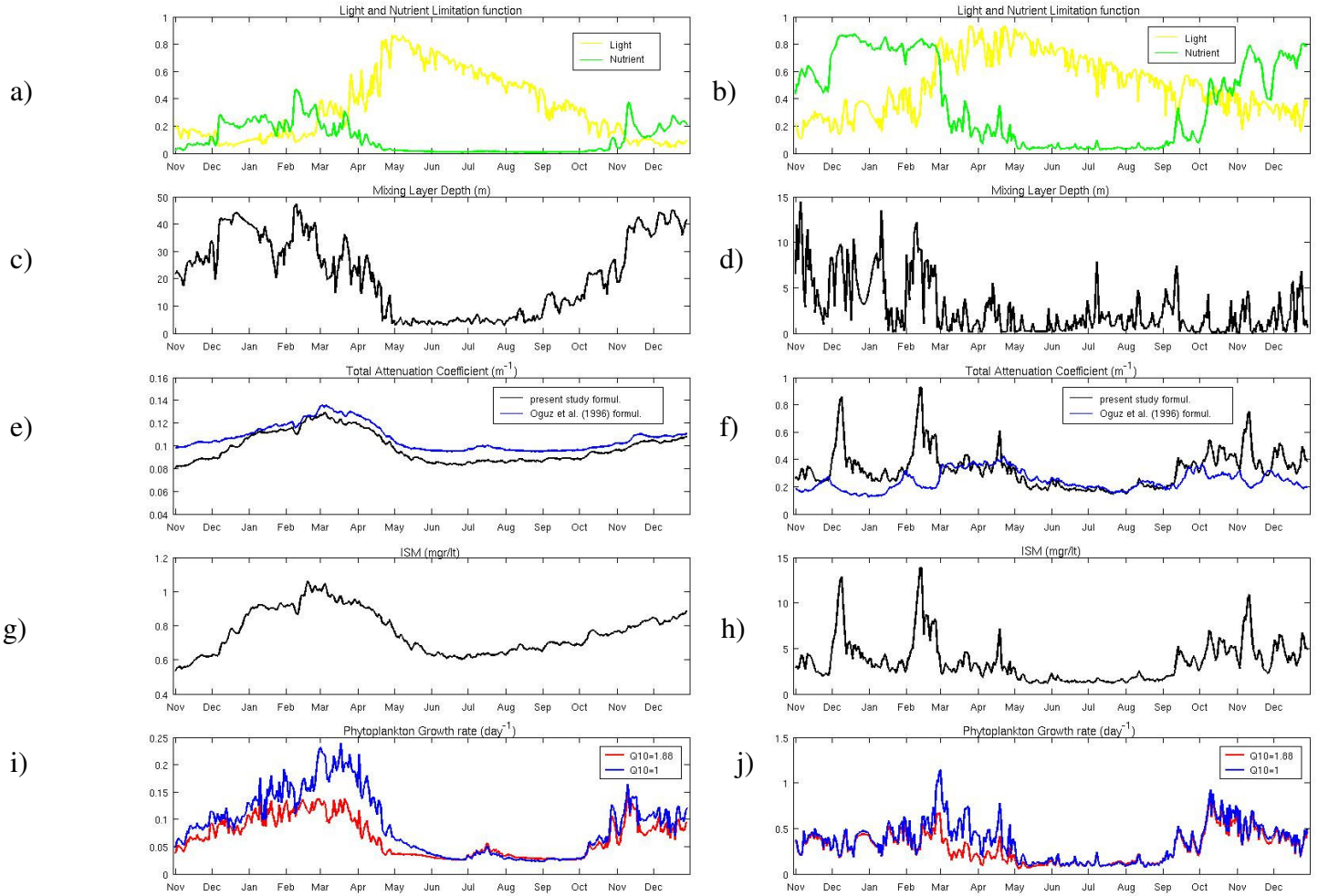

Figure 4: Open sea (left) and Danube River plume (right) area averages of: a),b) light and nutrient limitation functions (1 signifies no limitation), c),d) the mixing layer depth (m) e),f) total attenuation coefficient (m^{-1}), g),h) ISM concentration (mgr/lt), i),j) phytoplankton growth rate (day^{-1}), vertically averaged over the mixing layer depth (defined as the depth where the diffusivity coefficient reduces to 10 cm^2/s).

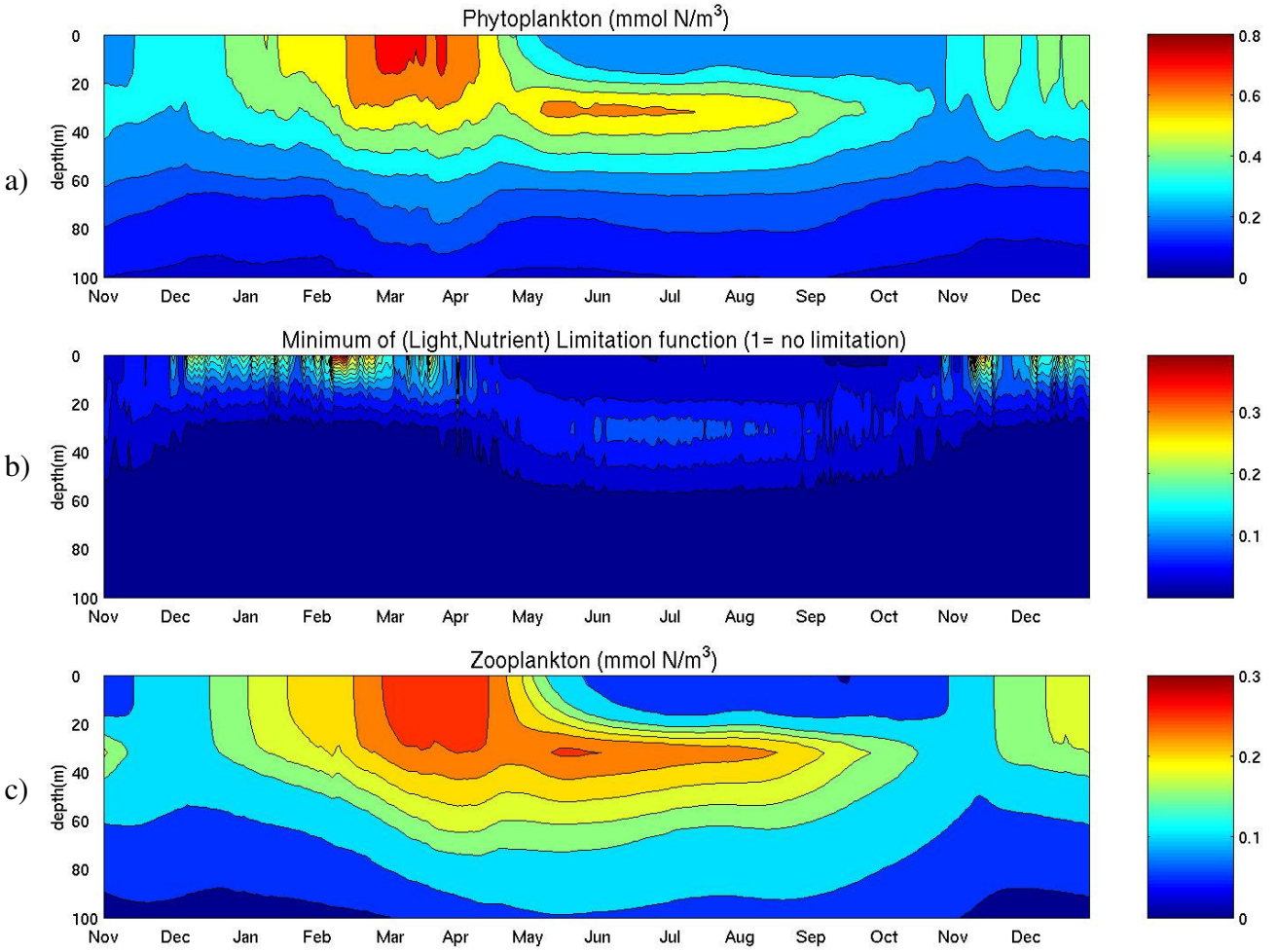

Figure 5: vertical profile seasonal variability of a) Phytoplankton (mmol N/m^3), b) minimum of the light and nutrient limitation function (1 signifies no limitation), c) Zooplankton (mmol N/m^3), averaged over the open sea area.

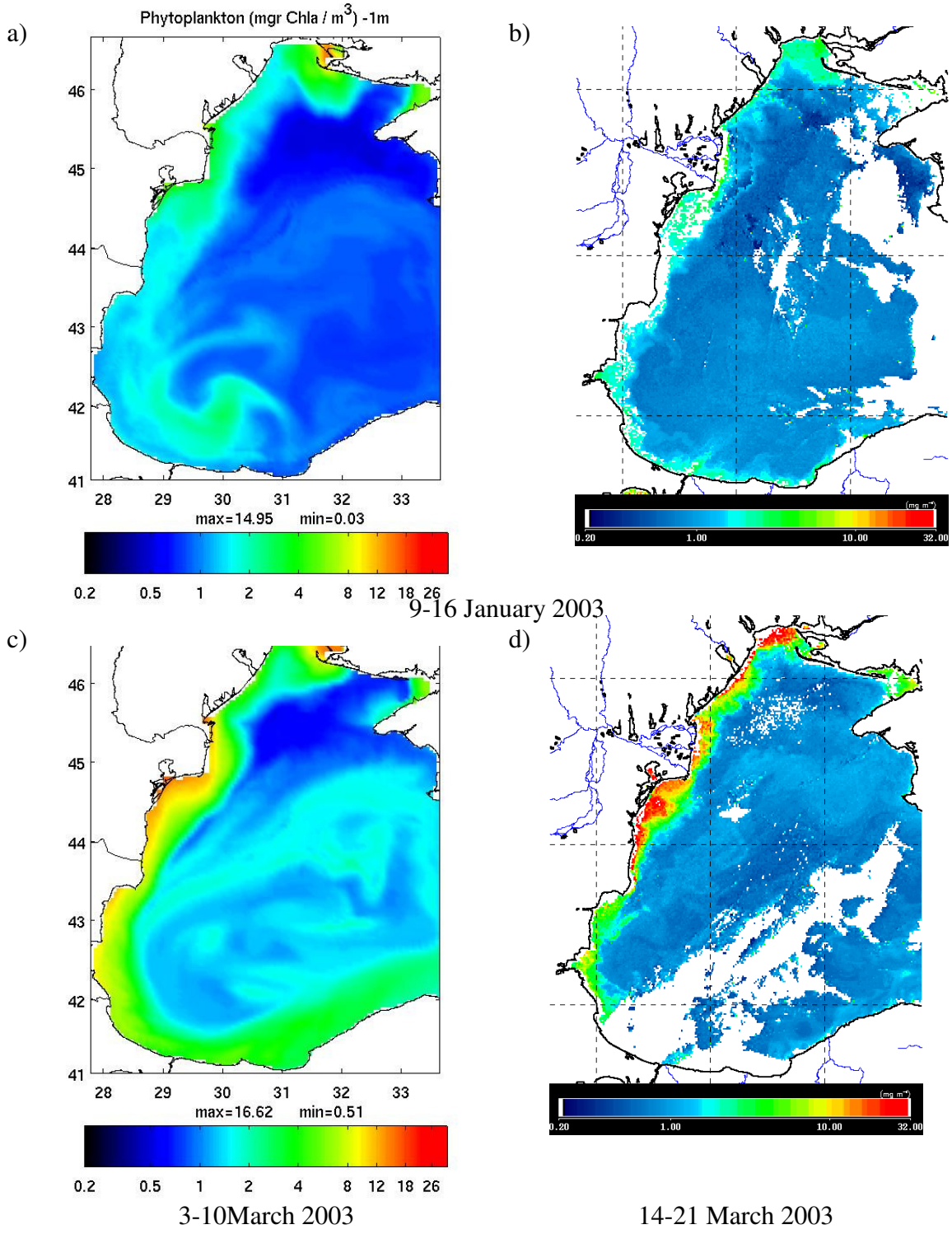

Figure 6: Model simulated (left) and SeaWiFS (right) Chlorophyll-a (mgr/m^3) for a),b) 9-16 January, c) 3-10 March, d)14-21 March, e),f) 9-16 May, g),h) 2-9 June, i),j) 12-19 July, k),l) 20-27 July, m),n) 5-12 August, o),p) 14-21 September, q),r) 8-15 October and s),t) 17-24 November of year 2003.

e)

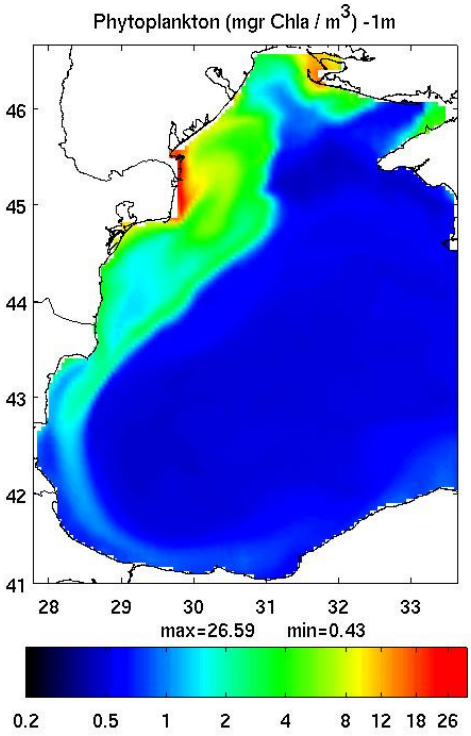

f)

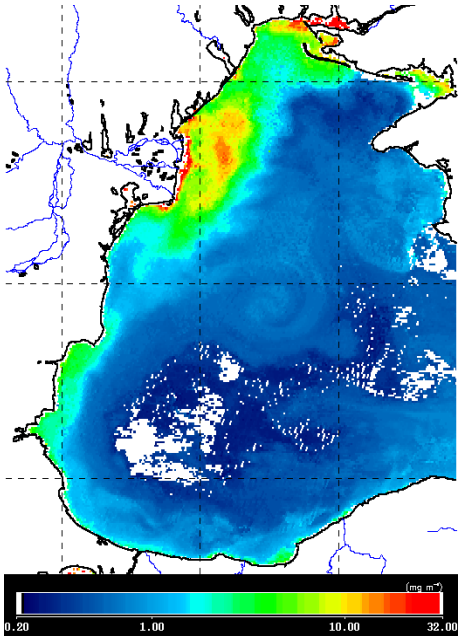

9-16 May 2003

g)

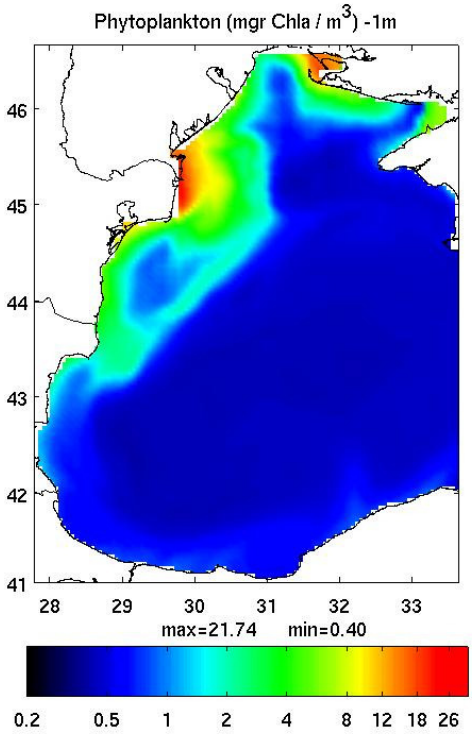

h)

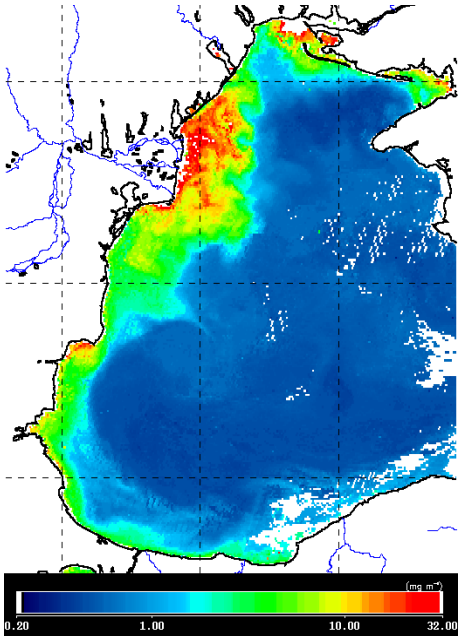

2-9 June 2003

figure 6 (continued)

i)

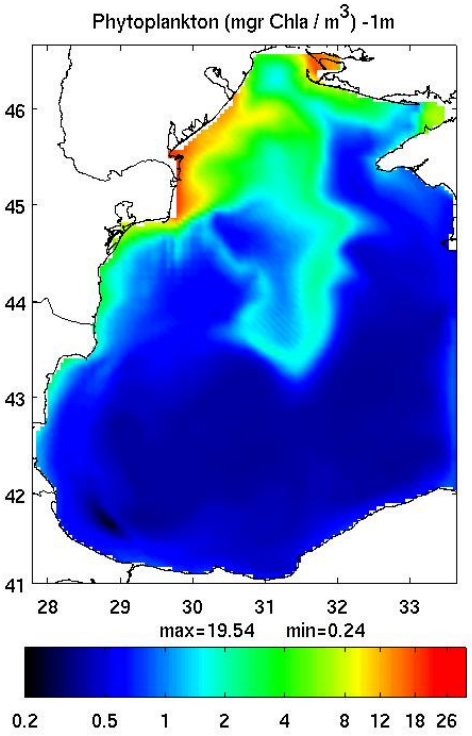

j)

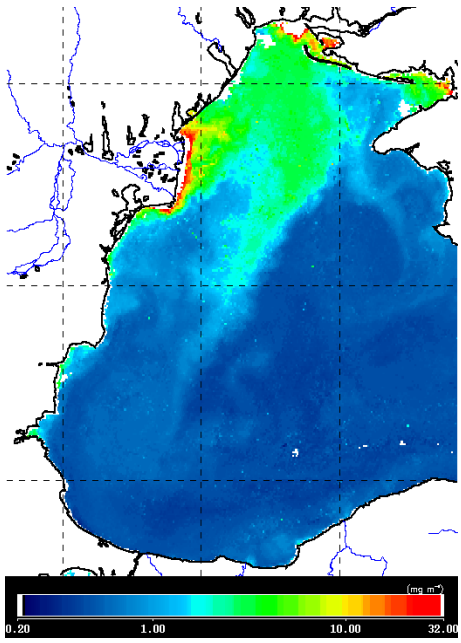

12-19 July 2003

k)

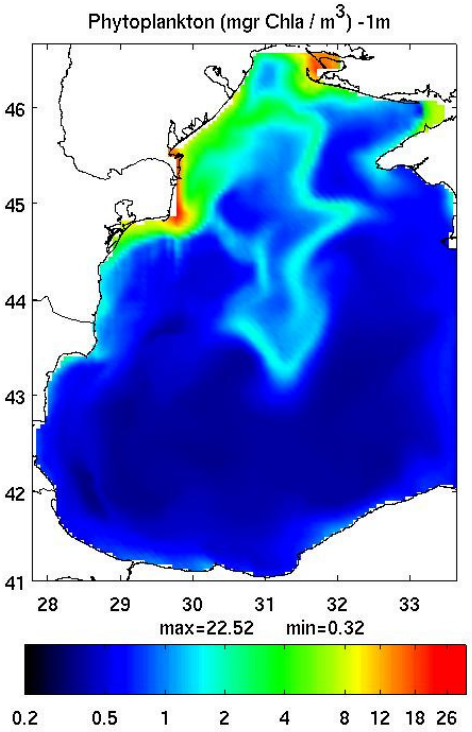

l)

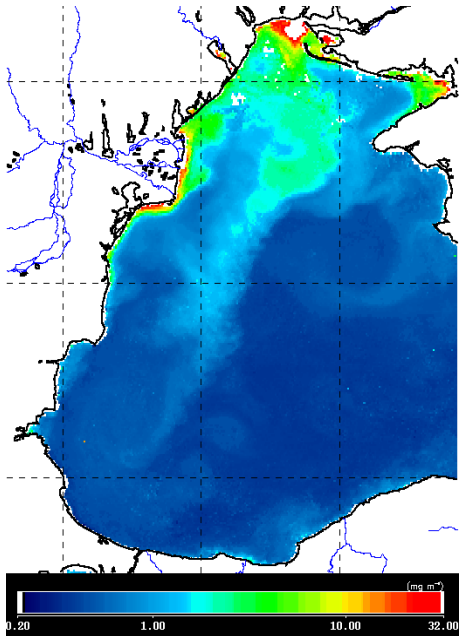

20-27 July 2003

figure 6 (continued)

m)

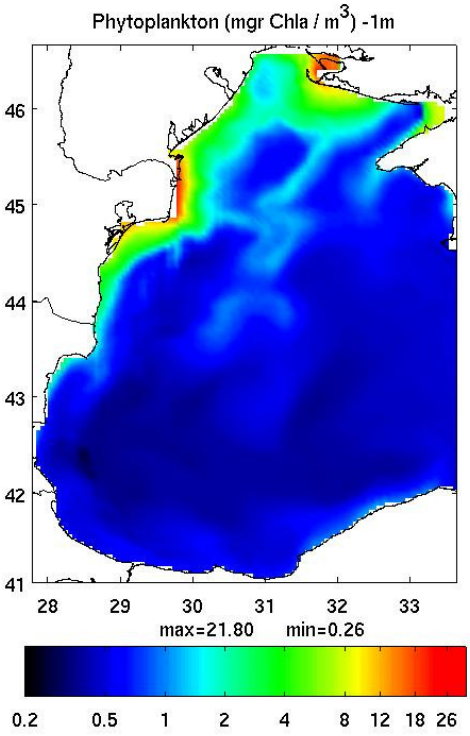

n)

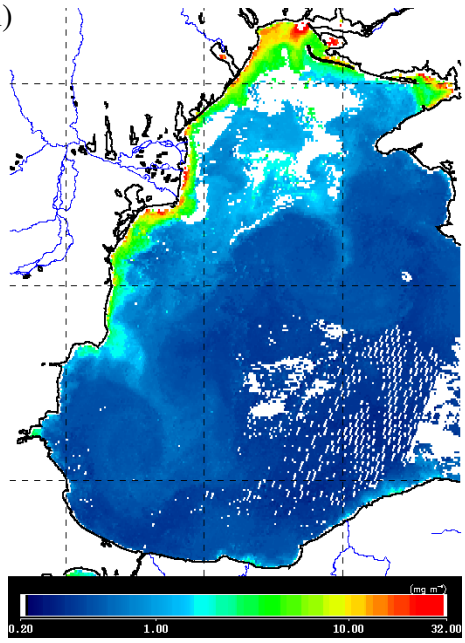

5-12 August 2003

o)

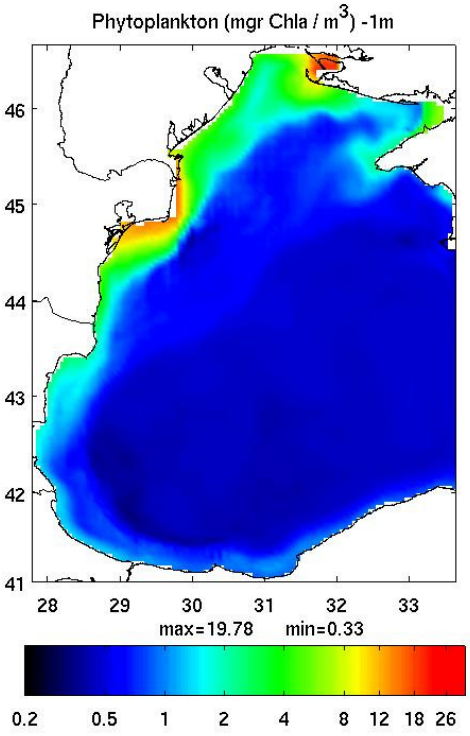

p)

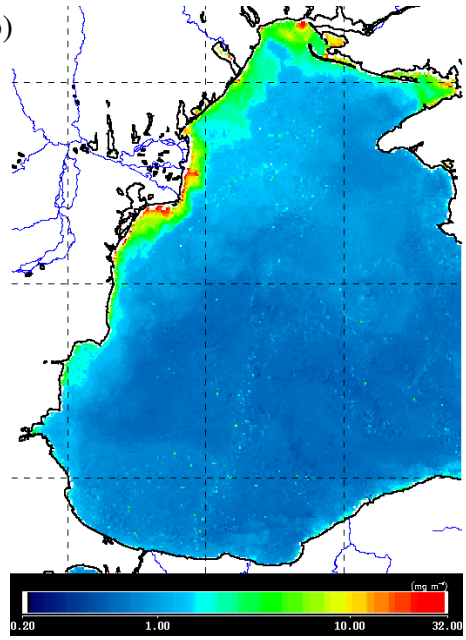

14-21 September 2003

figure 6 (continued)

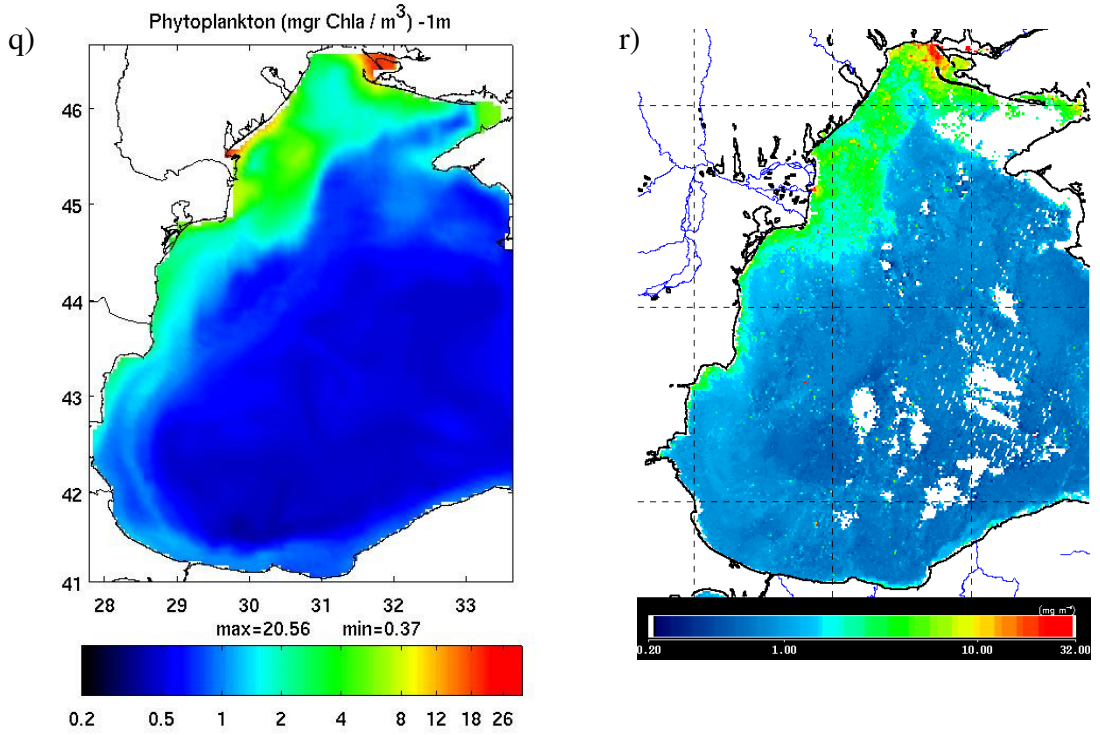

8-15 October 2003

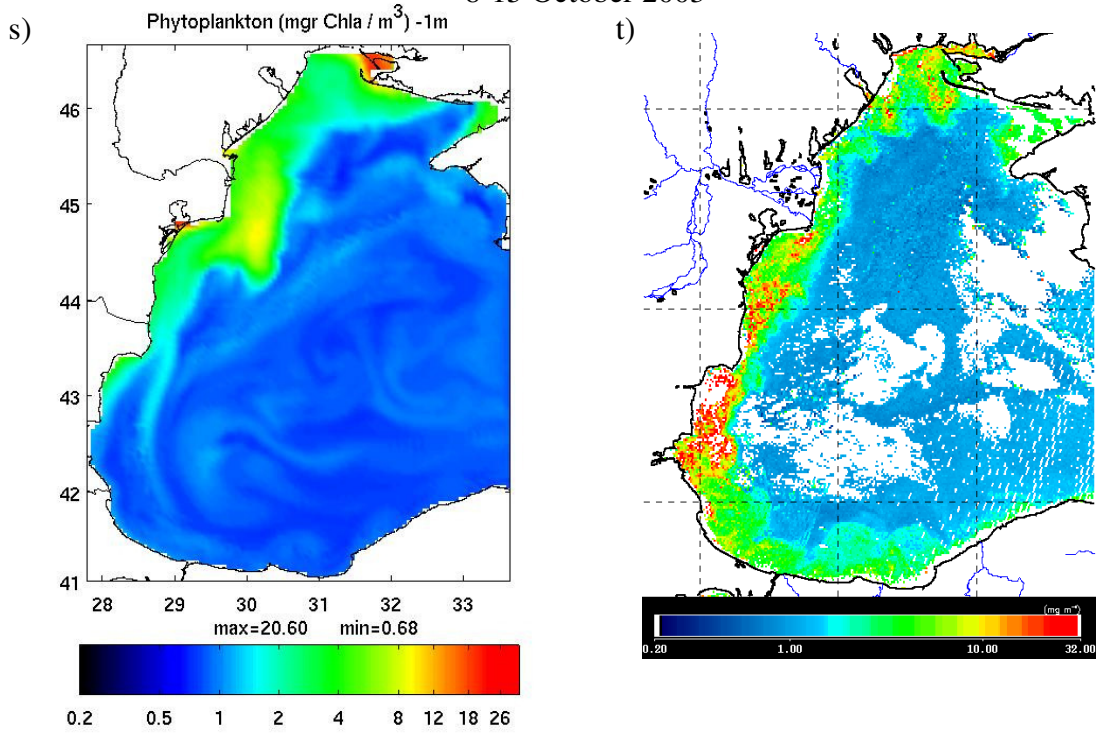

17-24 November 2003

figure 6 (continued)

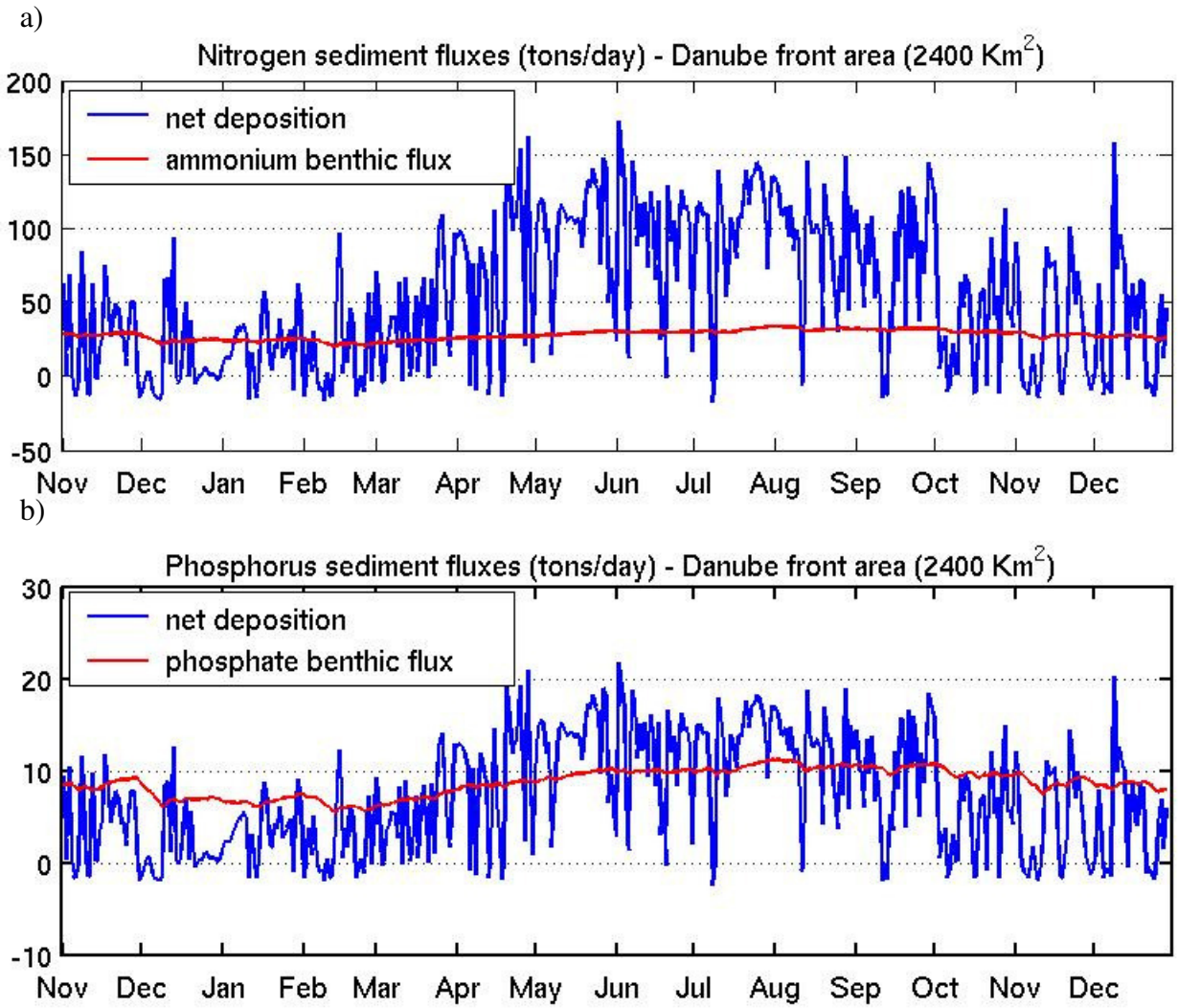

Figure 7: Model computed seasonal variability of a) Nitrogen and b) Phosphorus sediment fluxes (tons/day) in the Danube front area (~2400 Km^2, shown as box C in figure 1). The blue lines represent the net deposition (deposition minus resuspension) of nitrogen and phosphorus parts of detritus respectively for a) and b). The red lines represent the ammonium and phosphate benthic flux respectively for a) and b).

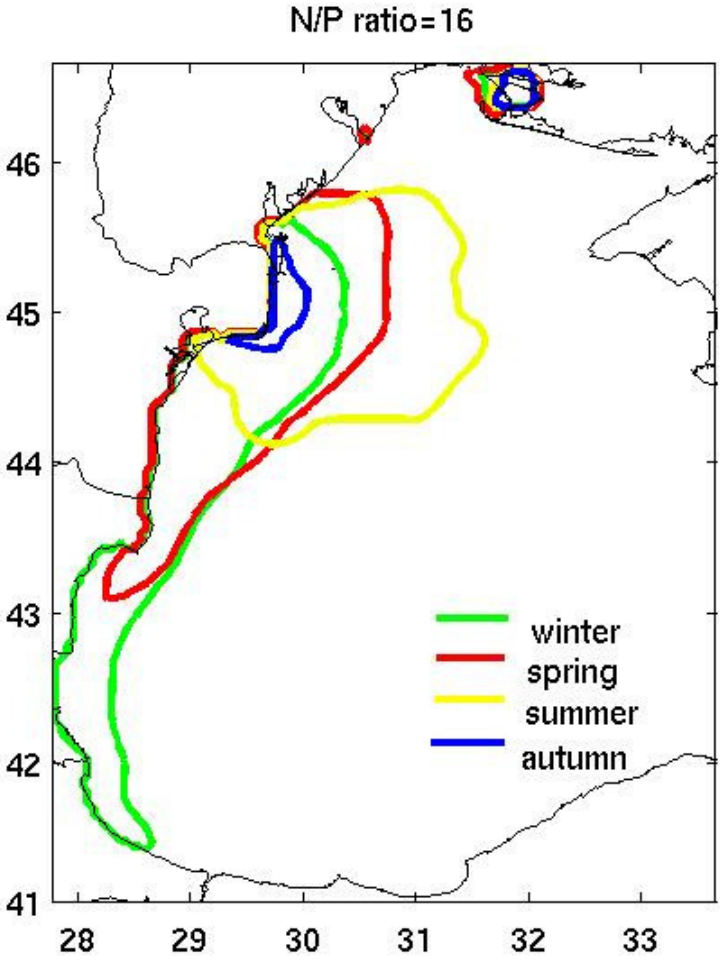

Figure 8: Contours where the model simulated dissolved inorganic N/P molar ratios equal to 16:1, averaged over seasons.

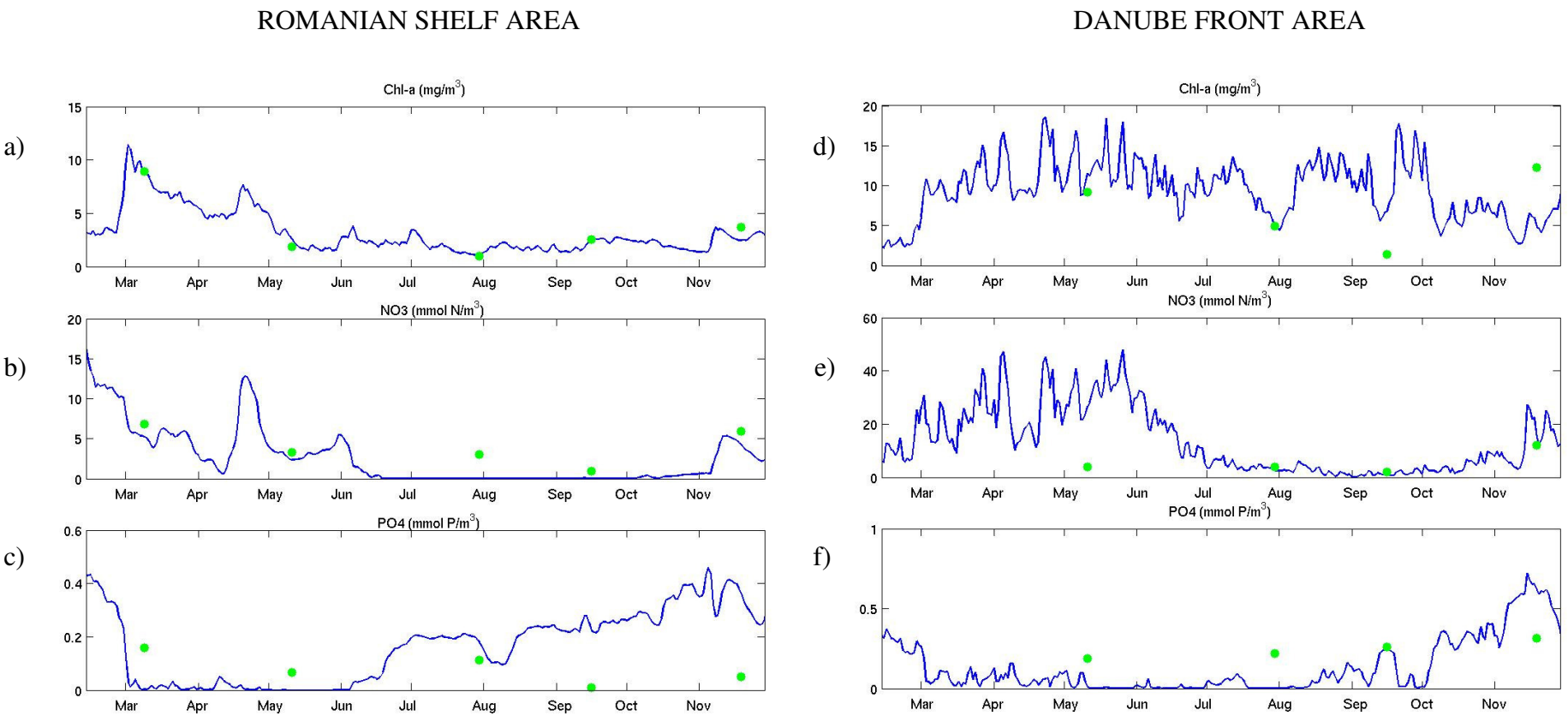

Figure 9: Model simulated (continuous line), from top to bottom: Chlorophyll-a (mgr/m^3), nitrates (mmol N/m^3) and phosphates (mmol P/ m^3) against in-situ measurements (dots) in a,b,c) averaged over the Danube front area and d,e,f) averaged over the Romanian shelf area (sea area boxes A and B in figure 1).

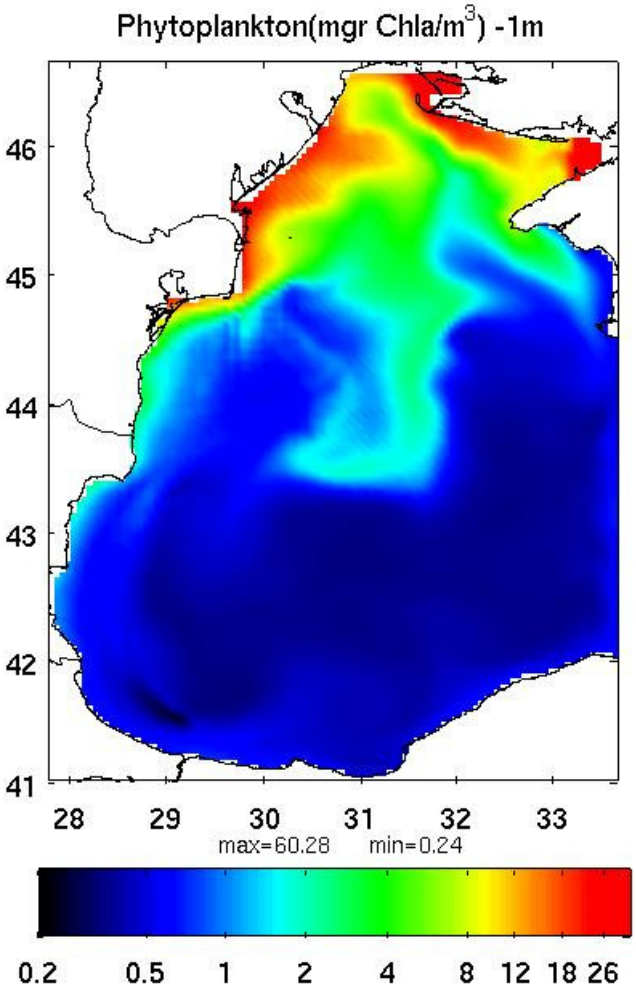

Figure 10: Chlorophyll-a (mgr/m^3) as simulated by Run2, adopting a half-saturation constant value of K_N =0.8 (mmol N/m^3), for 12-19 July 2003 (compare with figure 6i).

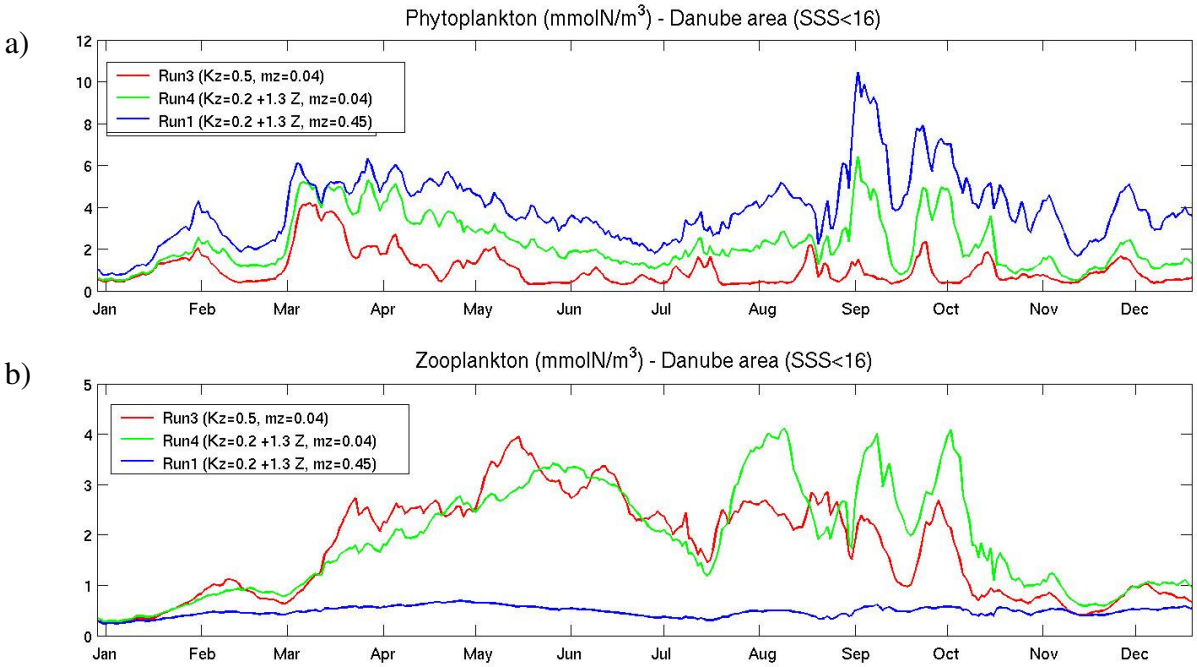

Figure 11: a)Phytoplankton (mmol N/m^3) and b)Zooplankton (mmol N/m^3) biomass variability, averaged within the Danube plume area (*SSS*<16 psu) and over the mixing layer depth, as simulated by Run3 that adopts the parameters (K_Z =0.5, m_z=0.04) (red line), Run4 that adopts the parameters (K_Z =0.2+1.3 Z, m_z=0.04) (green line) and the reference simulation (Run1, blue line).

3. Conclusions and Outlook

3.1. Conclusions

Since the launching of SeaWiFS (1997), MODIS-Terra (2000) and MODIS-Aqua (2002) satellite sensors, ocean colour data with high radiometric resolution (8-36 bands) and accuracy, medium spatial resolution (250–1100 m) and frequent observation (3-5 per day) are freely available to the scientific community covering all seasons and the entire Black Sea area. The missing observations, mainly due to cloud cover occur during all seasons. However, especially during the winter months frequent cloud cover conditions lead to some under-representation of the chlorophyll-a variability during this season (as demonstrated in Chapter III) and should be considered in the analysis of the phytoplankton annual succession. It is also not possible to estimate the physical forcing during the cloudy situation and its influence over the phytoplankton standing stock.

The results in Chapter II show that the existing atmospheric correction and bio-optical algorithms represent the phytoplankton standing stock in the surface layer of the western Black Sea quite acurately. However, there are some limitations to the method. It is not possible to detect chlorophyll-a maxima below the remotely sensed depth, which varies between 1 and 30 m in the western Black Sea. This is especially a problem in the central part of the western Black Sea during summer, when such deep chlorophyll-a maxima exist. The river waters in the north-western part of the sea, which are rich of coloured dissolved organic matter causing enhanced absroption as well as sediments initiating enhanced backscattering will need separate attention and adapted algorithms.

The time series analysis of the pattern of chlorophyll-a concentration in the surface layer of the western Black Sea (see Chapter III) shows very high spatial and temporal variability. During the investigated period, no general or typical annual succession of phytoplankton standing stock was detected but rather specific successions for each year and each region was found. Satellite remote sensing compared to *in situ* monitoring benefits from the high frequency of observations (several per day) recorded over the entire Black Sea area. This enables the detection of short-term and small-scale events as well as their advection. However, even after time series analysis of 9-year ocean colour observation it remains unclear whether the observed general reduction in the satellite-derived chlorophyll-a concentration for the period 1997-2006 is part of a trend or represents a minimum and turning point of oscillation. The results of this study also do not provide a definite explanation which factor or set of factors (physical: North Atlantic Oscillation, sea surface temperature, river runoff, wind stress, Sahara dust or biological: zooplankton grazing, microbial remineralization) trigger the

pronounced interannual variability of the satellite-derived chlorophyll-a concentration in the regions of the western Black Sea. The analysis of the time series after the year 2002 shows signs of decoupling between North Atlantic Oscillation and winter sea surface temperature, which will require more detailed analyses in future studies.

The spatial and temporal variability of the net primary production calculated with the Behrenfeld-Falkowski vertically generalized production model from the satellite remote sensing data in the western Black Sea should be regarded with attention since the nutrient concentrations are not considered in this model. However, the magnitude and annual succession of model-calculated net primary production conforms to *in situ* measured data.

It is not reasonable to the make an assessment of the productivity and state of the western Black Sea ecosystem using only satellite remote sensing data without reliable information on the nutrient concentration and grazing pressure. It is difficult to decide whether the observed decrease in the mean annual satellite derived chlorophyll-a concentration is caused by the reduced nutrient loads, changes in the food web or regime shift. However, the satellite data analysis shows that long-lasting extensive summer phytoplankton blooms, which were reported regularly over the north-western and western shelf in the 1980s were observed only once (June 2000) within the previous 9 years. This data support other *in situ* observations of the wide recovery of the benthic community in recent years.

In conclusion, it can be stated that despite some limitations the satellite remote sensing of ocean colour is an essential tool for understanding the recent state of the western Black Sea ecosystem.

3.2. Outlook

Despite of the good results demonstrated by the above studies, there is enormous demand for further investigation in the Black Sea. The validation and calibration of the satellite remote sensing data with synchronous *in situ* optical, radiometrical and biological measurements is required in order to improve the quality of the existing atmospheric correction algorithm and the bio-optical algorithms for the Black Sea. The collection of the *in situ* data should consider all different seasons, trophic states and regions of the Black Sea. Special attention should be paid to the optically complex waters in front of the Danube delta. Methods for reliable recognition of the Danube river plume should be developed in order to describe its high variability and advection. It is also important to reveal the role of the small-scale phenomena (eddies, fronts and jets) in the Black Sea ecosystem. The short-term variability (days to weeks) should be considered as contributing significantly to the productivity of the coastal areas. It is also important to analyse longer time series of satellite data, in order to define their

evolution in both the spatial and temporal domains. The satellite data could be used not only for validation of the models, but their assimilation into biological-physical models will improve significantly our understanding of the Black Sea ecosystem.

There is a number of new satellite sensors coming (planned as well as already operating), with enhanced spectral sensitivity as well as spatial and temporal resolution. The next generation remote sensing data combined with the rapid increasing computing power and newly developed processing techniques will possibly allow to separate dominant phytoplankton groups in the near future.

Acknowledgements

I would like to thank Dr. Ulrich Horstmann, who helped me to obtain a grant from the German Academic Exchange Service (DAAD) and thus made my stay and research at the IFM-Geomar in Kiel possible. Furthermore, I would like to thank Dr. Ulrich Horstmann for his support and scientific supervision throughout all these years in Kiel.

I would also like to thank Dr. Verena Dauben, Siggi Podewski and Petra Schmidt for their support, fruitful discussions and inspiring ideas as well as for correcting my scientific texts.

Furthermore, I would like to thank Prof. Dr. Karin Lochte, who accepted to be my scientific supervisor and gave me the opportunity to complete my research and to finish my PhD.

I am also indebted to many other people – friends and colleagues, who helped me with my work at different stages. They are too numerous to name them all.

The German Academic Exchange Service (DAAD) as well as The EU project "Nutrient Management in the Danube Basin its Impact on the Black Sea" (daNUbs) supported under contract EVK1-CT-2000-00051 by the Energy, Environment and Sustainable Development (EESD) Programme of the 5th EU Framework Programme provided the financial support for this work.

The SeaWiFS Project (Code 970.2) and the Goddard Earth Sciences Data and Information Services Center / Distributed Active Archive Center (Code 902) at the Goddard Space Flight Center, Greenbelt, MD 20771, provided the satellite data used in this work.

Erklärung

Hiermit erkläre ich, dass ich die vorliegende Arbeit selbstständig und ohne unerlaubte Hilfe angefertigt habe und dass sie nach Form und Inhalt meine eigene Arbeit ist. Wörtlich und inhaltlich aus anderen Quellen entnommene Textstellen sind als solche kenntlich gemacht. Diese Arbeit wurde weder ganz noch in Auszügen an einer anderen Stelle im Rahmen eines Prüfungsverfahrens vorgelegt. Ferner erkläre ich hiermit, dass dies mein einziges und bisher erstes Promotionsverfahren ist. Der Zulassung von Zuhörern/Zuhörerinnen bei der Disputation wird nicht widersprochen.

Kiel, den 30. Mai 2007

_____

Alexander Davidov